# Yucca Mountain Coupled Hydrothermal-Ventilation Study
# Annual Report for April 2004 through March 2005

NWRPO-2005-02

*Prepared for*
Nuclear Waste Repository Project Office
Grant No. DE-FC28-02RW12163

*Prepared by*
George Danko and Davood Bahrami
University of Nevada, Reno

November 2005

## DISCLAIMER

This report was prepared by the Nye County Nuclear Waste Repository Project Office, pursuant to a Cooperative Agreement funded by the U.S. Department of Energy, and neither Nye County nor any of its contractors or subcontractors nor the U.S. Department of Energy, nor any person acting on behalf of either, assumes any liabilities with respect to the use of, or for damages resulting from the use of, any information, apparatus, method, or process disclosed in this report. Reference herein to any specific commercial product, process, or service by trade name, trademark, manufacturer, or otherwise, does not necessarily constitute or imply its endorsement, recommendation, or favoring by the U.S. Department of Energy or Nye County. The views and opinions of authors expressed herein do not necessarily state or reflect those of the U.S. Department of Energy.

## EXECUTIVE SUMMARY

Since the mid-1990s, the Nye County Nuclear Waste Repository Project Office (NWRPO) has conducted independent modeling studies to analyze the feasibility and potential benefit of long-term ventilation at the U.S. Department of Energy (DOE) high-level radioactive waste repository at Yucca Mountain, Nevada. From April 2004 to March 2005, the NWRPO contracted the University of Nevada, Reno, to conduct coupled hydrothermal-ventilation modeling to support the evaluation of the design and performance of the repository. One major NWRPO interest is the use of ventilation in the repository design to enhance performance and thereby minimize long-term health and environmental impacts to southern Nye County. The NWRPO is specifically interested in the potential use of ventilation to keep repository temperatures below 100 degrees centigrade (ºC) and relative humidity (RH) below 100 percent, as well as to identify the safest, smallest portion of the mountain for long-term isolation of the nuclear waste.

The NWRPO, other stakeholders, and numerous independent reviewers believe that keeping repository temperatures and RH at these levels can reduce uncertainties in performance assessment models, improve safety, and ultimately benefit citizens living downgradient of Yucca Mountain. Many of these entities believe that minimizing the total storage area will help ensure the emplacement of waste in the most stable, and therefore safest, area available.

This annual report describes the tasks performed for this study, with the exception of Task 6, “Attend Technical Meetings,” which is self-explanatory.

### TASK 1: Model Update and Baseline Case Simulation

All model elements were revised to reflect the most recent repository design configuration used by the DOE during its license application work. A base case simulation of temperature, humidity, and condensation was conducted in emplacement drifts, with forced ventilation for a 50-year pre-closure period, followed by a 5,000-year post-closure period of natural ventilation.

### Conclusion

Temperature, RH, and condensation distribution in the emplacement drift can be established relatively quickly and easily if barometric pressure variation with time is disregarded, as done in DOE reports. It is difficult to compare the results of Task 1 to those in DOE reports because of the differences in model conditions, assumptions, and simplifications (DOE, 2004a). Clearly, a thorough comparison and evaluation of differences between Nye County and DOE models will be needed in the future, especially regarding condensation distribution. Another example of model differences is the DOE assumption that the dispersion coefficient is a constant. Task 1 modeling showed that the dispersion coefficient cannot be regarded as a universal constant and reasonable variations in its magnitude can have a significant influence on condensation distribution along an emplacement drift.

### TASK 2: Pre-Closure Time Study

The Task 1 simulation was repeated using pre-closure forced ventilation periods of 100, 200, and 300 years to simulate a cooler repository; the changes in temperature, humidity, and condensation in the emplacement drifts as a function of the forced ventilation time period were studied.

### Conclusion

Based on a perhaps oversimplified study model, an extended pre-closure ventilation period carries some hydrothermal advantages as well as disadvantages. Lower temperatures with longer pre-closure ventilation result in diminished condensation at focused locations; however, RH may actually increase due to lower temperatures. In addition, the longer maximum temperature evolution time of 750 years, with 300 years of pre-closure ventilation, is a potential liability regarding monitoring and performance confirmation.

## TASK 3: Barometric Pressure Pumping Study

The effects of barometric pumping on the temperature and moisture histories for the waste packages modeled in Tasks 1 and 2 were simulated.

### Conclusion

The always-present barometric pressure variation will have a major effect on RH and condensation distribution in the emplacement drifts during the few thousands of years when at least part of the emplacement drift is above boiling. It should be noted that the average barometric pressure used in DOE modeling to date as well as in Task 1 of this study is hypothetical as opposed to actual barometric pressure, which is variable.

## TASK 4: Fate of Condensation Study

The fate of condensation previously shown to develop on rock surfaces in the emplacement drifts was simulated. Water saturations and flux in the rock around the drift, including beneath the drift where it may have the greatest influence on radionuclide transport, were presented.

### Conclusion

More studies are needed with the numerical model to understand condensation distribution and the amount of condensation at a specific location that may cause drippage. This phenomenon has not been well understood or reported in the literature.

## TASK 5: Laboratory Test Preparation

Progress was made in preparing a numerical simulation of a future laboratory condensation experiment in a large welded tuff boulder. The simulation will help design the laboratory experiment, including the selection of measurement parameters and procedures, to physically verify condensation processes shown in modeling results from Tasks 1 through 5.

### Conclusion

Careful planning of the laboratory experiments on condensation imbibition is necessary before conducting laboratory measurements. The rock currently in the laboratory is at an ambient air-dry condition that will be altered by the measurement; it will be difficult to repeat the experiment without a lengthy initialization.

## CONTENTS

## TABLES

## FIGURES

## FIGURES (CONTINUED)

## FIGURES (CONTINUED)

## FIGURES (CONTINUED)

## FIGURES (CONTINUED)

## APPENDICES

## ACRONYMS AND ABBREVIATIONS

| | |
|---|---|
| ºC | degree centigrade |
| 2-D | two-dimensional |
| 3-D | three-dimensional |
| BWR | boiling water reactor |
| CFD | computational fluid dynamics |
| DOE | U.S. Department of Energy |
| DSNF | defense spent nuclear fuel |
| HLW | high-level waste |
| kg/s | kilogram per second |
| m | meter |
| $m^2/s$ | square meter per second |
| $m^3/s$ | cubic meter per second |
| MF | Multiflux |
| NTCF | numerical transport code functionalization |
| NUFT | non-equilibrium unsaturated-saturated flow and transport |
| NWRPO | Nuclear Waste Repository Project Office |
| Pa | pascal |
| $Pbar_{av}$ | average barometric pressure |
| σ(Pbar) | standard deviation of barometric pressure |
| PWR | pressurized water reactor |
| RH | relative humidity |
| UNR | University of Nevada, Reno |
| YM | Yucca Mountain |
| $W/(m^2K)$ | watts per square meter degree Kelvin |

# 1.0 INTRODUCTION

The Nye County Nuclear Waste Repository Project Office (NWRPO) is independently evaluating the conceptual design of the Yucca Mountain (YM) high-level radioactive waste repository currently being developed by the U.S. Department of Energy (DOE). One major NWRPO interest is the use of ventilation in the repository design to enhance performance and thereby minimize long-term health and environmental impacts to southern Nye County. The NWRPO is specifically interested in the potential use of ventilation to keep repository temperatures below 100 degrees centigrade (ºC) and relative humidity (RH) below 100 percent, and to identify the safest, smallest portion of the mountain for long-term isolation of the nuclear waste.

The NWRPO, other stakeholders, and numerous independent reviewers believe that keeping repository temperatures below 100 ºC and RH below 100 percent can reduce uncertainties in performance assessment models, improve safety, and ultimately benefit citizens living downgradient of YM. Many of these same entities believe that minimizing the total storage area will help ensure that waste is emplaced in the most stable, and therefore safest, area available.

Since the mid-1990s, the NWRPO has conducted independent modeling studies to analyze the feasibility and potential benefit of long-term ventilation (NWRPO, 2003). From April 2004 to March 2005, Nye County contracted the University of Nevada, Reno (UNR) to conduct hydrothermal-ventilation modeling using a code called Multiflux (MF) (Multiflux, 2003). This annual report describes the work performed.

MF was developed at UNR and applies the non-equilibrium, unsaturated-saturated, flow and transport (NUFT) model as a module for simulating heat and moisture flows in the rock domain (NUFT, 2000), and a computational fluid dynamics (CFD) module for the simulation of transport processes in the airway system, including the waste packages. The two modules are coupled on the rock-air interface until the heat and moisture flows are balanced at the common surface temperature and partial vapor pressure at each surface node and time instant. In the case of natural ventilation, MF also takes into account the air movement in the drift. For integrated pre- and post-closure hydrothermal simulations, MF applies a three-dimensional (3-D), combined canister- and mountain-scale rock mass model based on NUFT.

Studies with the MF model have given important insight into thermally driven hydrologic processes, including in-drift convection and condensation during post-closure. The studies have increased the understanding of the coupled in-drift and near-field rock process interactions. Preliminary modeling results indicate that repository-scale water drainage through the emplacement area is strongly affected by the in-drift, passive ventilation process during the first few thousand years of underground storage (Danko and Bahrami, 2004a).

The MF code has been designed to avoid many of the limitations of the DOE hydrothermal ventilation modeling approach. For example, the DOE pre-closure ventilation model includes dry, conduction-only processes (DOE, 2002 and 2004b). In addition, the model can assume only line-averaged heat load during pre-closure and therefore cannot be used to study localized hot spots from individual, high-heat-load waste containers.

The DOE post-closure, multiscale, thermal-hydrologic model (DOE, 2004b) also has many limitations listed as model assumptions. One of these assumptions is that the barometric pressure is constant with time. The DOE model based on this assumption is not applicable for studying the effects of barometric pressure pumping (i.e., Task 3 herein). The MF model and code, on the other hand, can be used to simulate complex processes, such as barometric pressure pumping, that are likely to be present in the real-world situation at YM.

# 2.0 MODEL UPDATE AND BASELINE CASE SIMULATION (TASK 1)

## 2.1 Introduction

The psychometric conditions and environment (i.e., temperature, humidity, and condensation) surrounding the waste package are of great importance in meeting the primary goal of safe long-term storage of high-level nuclear waste. The modeling described in this report addresses this issue and attempts to simulate a complete storage environment for the waste packages in a representative emplacement drift. MF is used herein to model the flow of heat, moisture, superheated steam, and condensation in the emplacement drift.

MF applies a universal coupler that connects the heat and moisture transport models in two different domains: 1) the rockmass and 2) the airway with heat-generating nuclear waste packages. MF uses NUFT in the 3-D rockmass, the results of which are reprocessed using the numerical transport code functionalization (NTCF) modeling technique (Danko, 2004). In the emplacement drift, MF uses a lumped-parameter CFD model (Danko and Bahrami, 2004b).

## 2.2 Assumptions

The Task 1 model is configured to be closely equivalent to the model that will likely be included in the DOE license application (DOE, 2004b). The following summarizes the assumptions used in Task 1:

1. The pre-closure model assumes forced ventilation of fresh air at 15 cubic meters per second ($m^3/s$) for a period of 50 years, removing heat and moisture according to a hydrothermal transport simulation. Variable heat and moisture removal rates are determined along the emplacement drift versus time. The desaturation in the rockmass is also modeled.
2. Heat and mass transport due to natural convection are modeled during the post-closure period of 5,000 years. The thermal and hydrologic effects caused by pre-closure ventilation are used as initial conditions for the post-closure simulation. The pre- and post-closure models are integrated into one system.
3. The emplacement drift is assumed to be an open system regarding barometric (i.e., total) pressure. The effect of barometric pressure pumping is the subject of Task 3 and is not modeled in Task 1.
4. The barometric pressure is assumed to be the hydrostatic air pressure at the average drift level that is a function of the air temperature affecting air density.
5. Hydrothermal properties of the surrounding rockmass are taken from the DOE ventilation model report (DOE, 2002). The rock stratigraphy is varied with depth but constant in lateral (i.e., x and y) directions.
6. The heat-generating waste package arrangement follows the sequence of the arrangement in DOE (2002).
7. The unheated edge effect is included in the mountain-scale model. This subtask applies a mountain-scale, 3-D NUFT model, which includes an entire drift and two unheated edge areas.

## 2.3 Description of the Multiscale Thermohydrologic Model

### 2.3.1 Integrated Pre- and Post-Closure Cycles

Temperature and RH variations are analyzed from the beginning of waste emplacement for a 5,050-year period that includes two distinct thermal cycles: during pre- and post-closure. During pre-closure, the drift is mechanically ventilated with a forced (i.e., powered), constant airflow rate of 15 $m^3$/s for 50 years. After pre-closure, the access shafts and connecting tunnels are backfilled and sealed, and the emplacement drifts are exposed only to natural air movement. It is assumed that the emplacement drifts are not backfilled, and that the gradual collapse of the drifts over time will not prevent natural air movement around the waste packages.

### 2.3.2 Conceptual Repository Arrangement and Model

The conceptual repository arrangement follows the conceptual design developed by DOE, using five emplacement panels at YM (Figure 2-1). One emplacement drift at the center location of Panel 2, previously referred to as Panel 5 (Danko and Bahrami, 2004c), has been selected for the analysis herein. Panel 2 is surrounded on three sides by unheated edges and will therefore develop a temperature field that is colder around the edges than in the center. The transport of moist air along the length of the drift may give rise to moisture condensation along the relatively cold edge sections. This edge-cooling phenomenon will affect all the panels shown on Figure 2-1, but Panel 2 has been selected for its modeling simplicity.

During post-closure, natural airflow in the drift will develop due to the temperature differences between the waste package surfaces and the drift wall. The large eddies caused by vertical air movement will effectively establish an axial transport of heat and moisture along the drift by dispersion (Webb and Itamura, 2004). Although other axial transport mechanisms may also be present during post-closure, such as axial, buoyancy-pressure-driven air infiltration (Danko and Bahrami, 2004a, 2004b, 2004c), these effects are disregarded in the analysis. Under certain conditions in the emplacement drift, condensation may occur, generating liquid-phase water on the drift rock or waste package surfaces, or in the air. The hydrothermal model configured in the lumped-parameter CFD of MF includes model elements that describe the natural, small-scale air movement and related psychrometric processes in the emplacement drift.

The geometry of the rockmass surrounding the center drift in Panel 2 is shown on Figure 2-2. Two peripheral drifts are perpendicular to emplacement drifts with two vertical shafts, an intake and exhaust that are typically used to connect the peripheral drifts to the atmosphere in a panel for pre-closure ventilation. The peripheral drifts and the shafts, however, are assumed to be backfilled and completely sealed during the assumed repository closure at Year 50.

## 2.4 Models of the Rock Domain

The NTCF heat and moisture flow models of the rock domain are generated in MF using NUFT. The geometrical domain shown on Figure 2-2 is simplified for the NUFT runs to reduce the computational capacity and run time. First, it is halved by the vertical symmetry plane along the drift centerline. Second, the rockmass is further halved along the length of the drift. A symmetry is assumed between NTCF cells (i.e., “i”) 4 and 5, along an adiabatic surface that divides the entire rock domain into two mirrored halves: entrance and exit drift section areas. These simplifications reduce the computational rock domain to a quarter of that on Figure 2-2; however, two consecutive NUFT models are needed to deal with asymmetries in the temperature field, caused by the pre-closure forced air ventilation that occurs from left to right. The reduced rock cell with its internal grids is shown on Figure 2-3. Each NUFT domain includes four rock cells along the drift and another four cells in the edge regime, all fully connected with respect to heat and moisture flows. The number of nodes in each 3-D NUFT domain provides adequate discretization and acceptable grid independence. The grid in the x and z direction is identical to the two-dimensional (2-D) discretization that was applied and verified by the DOE (2002).

The entire drift is surrounded by four sections in the first NUFT rock domain and four sections in the second, giving eight 3-D mountain-scale cells (i.e., i = 1 through 8). The two planes of symmetry included in the rock model, but not in the model of the airway, result in only a small model error, while reducing the computer memory requirements to a quarter.

The numerical model assumes a porous, moist, but unsaturated rock formation, in which both heat and moisture transport are present and affect the thermal and psychrometric waste container environment. The rock properties with dual-porosity elements, required as NUFT input parameters, were identical to those used by the DOE (2002) for a representative stratigraphic block at YM.

### 2.4.1 Initial and Boundary Conditions

The atmospheric climate boundary conditions on the surface were varied according to the modern-time, monsoon, and glacial-transition cycles with time. The known, constant, virgin rock temperature and 100-percent water saturation were applied at the bottom of the rock domain, representing the water table. On the other outside vertical planes, the rock domain is assumed to be adiabatic. Boundary conditions on the drift surface are defined and discussed later in this section.

The initial temperature and moisture saturation conditions in the rockmass at the time of waste emplacement were initialized by simulating 10 complete climate cycles of 74,000 years each as the likely prehistory for the current conditions at YM (DOE, 2004c).

### 2.4.2 Numerical Transport Code Functionalization Model of the Rock Domain

NTCF is used in all versions of MF to reprocess the time-dependent heat and moisture responses from the thermohydrologic NUFT model into matrix equations (Danko, 2004). A linear NTCF processor is applied herein, using first-order matrix polynomial equations for modeling heat and moisture fluxes on the drift surface boundaries with constant-coefficient matrices. During the NUFT runs, the input boundary conditions on the drift surface are temperature and partial vapor pressure functions, varying with time and location. In addition, the total barometric pressure is prescribed as a boundary condition for the NUFT runs. The output variables from NUFT are spatial and temporal heat and moisture flux variations on the drift wall. The NTCF procedure determines dynamic admittance matrices from the NUFT input and output functions. The NTCF model matrices represent connections between input and output. Within the useful application regime of the NTCF model, the dependence of the matrices on the input boundary conditions used in the NUFT calculations is negligible. The NUFT input boundary conditions for which the

NTCF model is determined are called the central values of NTCF. The mountain-scale NTCF model for the rock cell along the drift length (Figure 2-2) expresses the time-dependent wall heat and moisture fluxes as follows:

$$qh_i = hh_i \cdot \left[T_i - Tinit_i\right] + hm_i \cdot [P_i - Pc_i] \tag{1-1}$$

$$qm_i = mh_i \cdot \left[T_i - Tinit_i\right] + mm_i \cdot [P_i - Pc_i] \tag{1-2}$$

where $qh_i$ and $qm_i$ are vectors composed of heat and moisture flux elements at time divisions $t_1,..,t_N$; $T_i$ and $P_i$ are wall temperature and partial vapor pressure vectors; $Tinit_i$ is the initial, constant wall temperature; $hh_i$ is a dynamic admittance matrix of heat flux, generated by the wall temperature driving force; $hm_i$ is a cross-effect dynamic admittance matrix of heat flux generated by the wall partial vapor pressure driving force; $mh_i$ and $mm_i$ are dynamic admittance matrices for the moisture flux expression; and $Pc_i$ is the partial vapor pressure variation vector for the predicted central condition around which the NTCF model is determined. Dynamic admittance matrices $hh_i$, $hm_i$, $mh_i$, and $mm_i$ are all N x N matrices, determined using the NTCF modeling method (Danko, 2004). Dependence of the NTCF model on the central values (i.e., $Tc_i$ for temperature and $Pc_i$ for partial vapor pressure) is eliminated by iteration, as discussed later in this section.

Within each 3-D mountain-scale rock cell, further divisions are made to capture the drift-scale temperature and humidity variations along the drift. While the numerical discretization points on the drift wall in each cross section are still bundled by averaging into a surface node, 420 independent nodes are generated from the 8 divisions along the drift length in the refined NTCF model. Each mountain-scale rock cell is rescaled into subdivisions (i.e., "j") (Table 2-1). The rescaling of the $hh_i$, $hm_i$, $mh_i$, and $mm_i$ mountain-scale 3-D cell matrices into drift-scale $hh_{ij}$, $hm_{ij}$, $mh_{ij}$, and $mm_{ij}$ matrices are accomplished by proportioning them by the ratio between the $i^{th}$ cell and the $ij^{th}$ drift segment surfaces, $A_i$ and $A_{ij}$, as follows:

$$hh_{ij} = hh_i \cdot \frac{A_{ij}}{A_i} \tag{1-3}$$

$$hm_{ij} = hm_i \cdot \frac{A_{ij}}{A_i} \tag{1-4}$$

$$mh_{ij} = mh_i \cdot \frac{A_{ij}}{A_i} \tag{1-5}$$

$$mm_{ij} = mm_i \cdot \frac{A_{ij}}{A_i} \tag{1-6}$$

The rescaling procedure generates 420 individual drift-scale $hh_{ij}$, $hm_{ij}$, $mh_{ij}$, and $mm_{ij}$ "daughter" matrices without any additional NUFT runs, all inheriting the mountain-scale heat and moisture transport connections from the original, mountain-scale "parent" matrices $hh_i$, $hm_i$, $mh_i$, and $mm_i$. The average size of the spatial rock domain in the axial drift direction is 1.7 meters (m), which is sufficient to generate temperature variations even along individual waste packages. The multiscale NTCF rock model defines heat and moisture flux vectors as a function of the 420 time-dependent input vectors of surface temperature and partial vapor pressure boundary conditions. It is important to emphasize that the heat and moisture fluxes, as well as the temperature and partial vapor pressure vectors, are all considered unknown at this point and subject to coupling calculations with the in-drift CFD models for the drift. The central-value dependence of the first-order NTCF model is relatively minor and dealt with by an outside iteration. The 420 nodes represent the interface boundary at selected points between rock cell and airway that include the waste packages. The NTCF rock model includes both drift- and mountain-scale heat and moisture flow components without sub-models and/or superpositions.

The axial, y-directional heat conduction in the rockmass along the length of the drift is included in the NTCF model from coarse discretization. The drift-scale daughter matrices inherit the axial heat conduction and moisture diffusion connections from their mountain-scale parent matrices during rescaling. These axial connections, however, do not account for the axial heat and moisture fluxes in the rock in the close vicinity of the drift wall, caused by axial gradients within each mountain-scale cell. In the current study, a simplified approach is used by adding axial connections to the model. For fine, drift-scale, axial heat conduction modeling, the thermal conduction connection of a 10-m-thick tubular rock layer is added to the interface nodes of the in-drift model. This connection between the neighboring wall nodes along the drift length is calculated and applied in the CFD model to “smooth” the temperature variation that is caused by the individual waste package heat load variations. However, no additional drift-scale, axial moisture/vapor diffusion connection is applied herein.

The linear NTCF model requires several update iterations. These NTCF matrices are iteratively recalculated from new NUFT run results with better and better central values obtained from the coupled model calculations. The present solution is based on the third iteration of the NTCF module with respect to the thermal model. In the third iteration, the NTCF thermal model is determined based on the output of the second iteration as central values for the NUFT runs. The moisture transport NTCF model is iterated only twice, starting with the robust model concept (Danko and Bahrami, 2004a; 2004b; and 2004c). The first iteration of the approximate model for the moisture flow across the drift wall assumes that 100 percent of water percolation flow from precipitation on the ground surface reaches the drift footprint. The NTCF sub-model for moisture is replaced by a time-dependent but temperature-independent and simplified model in the first iteration. The time-dependent moisture flux used in the first iteration is given in Table 2-2. In the second iteration, the moisture fluxes are corrected according to the first-order NTCF sub-model, determined based on NUFT results for the balanced temperature and humidity boundary conditions. These iterations in the NTCF models provide adequate model accuracy, based on previous application experiences (Danko and Bahrami, 2004a; 2004b; and 2004c and DOE, 2002).

The comparison between the robust, percolation-based water flux and the NUFT-based moisture flux distribution is useful in understanding the nature of water drainage through the emplacement drift. Section 2.9.2 discusses simulation results and whether the drift “shadows” or “attracts” water flow.

## 2.5 Model of Airway with Waste Containers

The energy balance equation in the CFD model of MF is used in a simplified form, as follows, for an *x*-directional flow with velocity ($v_i$) in a flow channel of cross section *dy* by *dz*:

$$\rho c \frac{\partial T}{\partial t} + \rho c v_i \frac{\partial T}{\partial x} = \rho c a \frac{\partial^2 T}{\partial x^2} + \rho c a \frac{\partial^2 T}{\partial y^2} + \rho c a \frac{\partial^2 T}{\partial z^2} + \dot{q}_h \tag{1-7}$$

In Equation 1-7, $\rho$ is the density of moist air; $c$ is the specific heat of moist air; $a$ is the molecular or eddy thermal diffusivity for laminar or turbulent flow, respectively; and $\dot{q}_h$ is the latent heat source or sink for condensation or evaporation, respectively. Equation 1-7 is discretized and solved numerically and simultaneously along all parallel flow channels for the temperature field $T$ in MF. The parallel flow channels represent the natural coordinate system of the flow field that must be known for the calculations. A few typical flow velocity profiles are built-in functions in MF. Various boundary conditions, such as given wall temperature, heat flux, or convective coupling with a given heat transport coefficient across a boundary layer or sub-layer, may be applied for the solution of the energy equation.

An example of the solution to Equation 1-7 was published and compared with CFD software (FLUENT, 1997), as well as with experimental, published results for turbulent flow (Danko and Bahrami, 2002). A 150-m-long drift section was discretized into 50 segments along the airflow with heat-generating waste packages along the length according to the conceptual design for YM. In the annulus between the waste packages and the drift wall, 60 unequally spaced segments were used along the radius. The flow was assumed to be fully developed hydraulically when entering the drift section. The eddy diffusivity and the velocity profiles were obtained from the dimensionless equations published by Kays and Leung (1963) and built into MF. The results showed excellent agreement among MF, FLUENT, and the experimental results.

The simplified moisture transport convection-diffusion equation in the CFD model of MF is similar to Equation 1-7, as follows:

$$\rho \frac{\partial \rho_v}{\partial t} + \rho v_i \frac{\partial \rho_v}{\partial x} = \rho D \frac{\partial^2 \rho_v}{\partial x^2} + \rho D \frac{\partial^2 \rho_v}{\partial y^2} + \rho D \frac{\partial^2 \rho_v}{\partial z^2} + \dot{q}_{cm} + \dot{q}_{sm} \tag{1-8}$$

In Equation 1-8, $\rho_v$ is the partial density of water vapor; D is the molecular or eddy diffusivity for vapor for laminar or turbulent flow, respectively; $\dot{q}_{cm}$ is the moisture source or sink due to condensation or evaporation, respectively; and $\dot{q}_{sm}$ is the vapor flux in superheated steam form.

It is possible to reduce the number of discretized elements in the computational domain by lumping nodes. MF allows for defining connections between lumped volumes, applying direct heat and moisture transport relations between them. A large selection of transport coefficient-based models is available for laminar and turbulent flows, as well as for natural convection. When only a few flow channels are used in the model configuration, such as in the present study, a lumped-parameter CFD model is configured.

In this example, the entire emplacement drift is 710-m-long, housing 140 waste packages. The current lumped-parameter CFD model for heat transport in the airway applies 2,544 nodes for the entire drift. Each waste package is represented by two nodes, with one additional node for the gap between neighboring containers. CFD nodes are in the airway along the following three longitudinal lines: 1) close to the waste package, 2) close to the wall above the waste package, and 3) close to the sidewall, with 424 nodes on each line. The drift inside wall is assumed to be separated from the rock wall with a $1.0 \times 10^{-5}$-m-thick immobile air layer; both walls are also represented by 424 nodes each. Of these numbers, some nodes represent a short, unheated section at both ends, as well as the incoming air connections for the pre-closure ventilation task. The same number of nodes is used in the CFD model for moisture.

In the CFD domain, a sequence of eight (i.e., two half and six full) waste packages, shown on Figure 2-4a, is first mirrored to form a 16-package sequence, and second, repeated 10 times in the emplacement drift. Drip shields are not included in this analysis. The heat and moisture transport CFD models of the emplacement drift are integral, continuous 3-D models.

In the pre-closure models, heat and moisture transport by turbulent convection are applied on the drift wall and waste package surface. The heat and moisture transport coefficients in the annulus between the waste containers and drift wall are calculated in MF using transport coefficients in the lumped-parameter CFD during pre-closure. Thermal radiation between the waste packages and the drift wall, between waste packages, and between drift wall segments are incorporated into the CFD models. The axial convection connections along the three airlines are modeled according to the convective terms in Equations 1-7 and 1-8.

In the post-closure CFD models, natural secondary flow is considered to be due to local temperature differences in the drift. The average of the axial airflow is assumed to be zero in this case, unlike previous studies (Danko and Bahrami, 2004a; 2004b; and 2004c), with various in-drift air infiltration assumptions. In each half-waste-package-long drift segment, the re-circulating mass flow rate in the vertical plane is assumed to be 0.04 kilograms per second (kg/s), a constant value for the study time period between 60 and 5,000 years, based on FLUENT simulation results of natural convection (Webb and Itamura, 2004). The axial connection between the air nodes is bi-directional, representing dispersion. A constant dispersion coefficient of 0.1 square m per second ($m^2/s$) is used, from Webb and Itamura (2004). The dominantly natural heat transport coefficient on the drift and waste package walls during post-closure are all set to a constant value of 1.85 watts per square meter degree Kelvin ($W/[m^2K]$), a value consistent with the results of more detailed numerical modeling published by Webb and others (2003).

The two CFD model configurations used in the calculations for pre- and post-closure are shown on Figures 2-4b and 2-4c. The pre-closure configuration on Figure 2-4b is a convective model, assuming that the air moves along the drift caused by forced ventilation, removing heat and moisture from the drift wall surfaces. The flowpath in this model assumes shear turbulent flow along the drift. The post-closure configuration on Figure 2-4c is a natural convection model with directional airflow patterns separating the drift wall nodes from the waste package surface nodes in each cross section. Therefore, the moving air, shown in the cross-sectional view of Figure 2-4c, orients the convective heat and moisture transport connections between the drift wall and the waste packages.

## 2.6 Condensation Modeling

The condensation model is based on partial vapor pressure trimming in the moisture transport CFD sub-model solution in MF (Danko and Bahrami, 2004a; 2004b; and 2004c). Trimming is a process that effectively enforces partial pressure to be within its physical boundaries, notably, to be less than both barometric pressure and saturated pressure. An example is shown on Figure 2-5, showing the saturated vapor pressure, trimmed and untrimmed partial vapor pressures and barometric (i.e., total) pressure on the drift wall. The results on Figure 2-5 were obtained for demonstration purposes by stopping the MF run at the end of the balancing iterations at Year 1500, and accessing the internal variables. The untrimmed partial vapor pressure curve section above the barometric pressure limit is hypothetical, since the moisture CFD model in MF forces the partial vapor pressure to stay between physical limits. The pressure-trimming process is accomplished by iteratively and numerically adjusting the $\dot{q}_{sm}(i)$ and $\dot{q}_{cm}(i)$ terms in Equation 1-8 for each grid in the CFD model domain until the following conditions are met:

a. Superheated steam removal:

$$increase\ (-)\dot{q}_{sm}(i): \quad if\ P_v(i) > P_b(i)\ and\ P_s(i) > P_b(i) \tag{1-9}$$

b. Condensation removal:

$$increase\ (-)\dot{q}_{cm}(i): \quad if\ P_v(i) > P_s(i)\ and\ P_s(i) \le P_b(i) \tag{1-10}$$

where $P_v(i)$ is the partial vapor pressure, $P_s(i)$ is the saturated vapor pressure, and $P_b(i)$ is the total barometric pressure at node $i$.

Initially, flux terms $\dot{q}_{sm}$ and $\dot{q}_{cm}$ are set to zero for all nodes. Condensation or superheated steam fluxes are identified implicitly and numerically from the correct mass balance equations represented by the CFD model. The identification is simultaneously performed during the balancing iterations between the CFD and NTCF models. Condensation may be detected at surface nodes or at nodes assigned to air; in the latter case, the condensation is assumed to be mist. The fate of the condensation by drainage or imbibing into the rock wall is currently not modeled, but this effect is likely to be important and the subject of future studies with MF. The current model assumes that the condensation drains through the rock. The terms $\dot{q}_h$ and $\dot{q}_{cm}$ in Equations 1-7 and 1-8 are linked through the latent heat of water evaporation in MF.

## 2.7 Total System Model

The NTCF and CFD models are coupled on the rock/air interface by MF until the heat and moisture flows are balanced at the common surface temperature and partial vapor pressure at each surface node and time instant. The solution of the coupled hydrothermal-ventilation model includes heat and moisture balance iteration loops between the NTCF and airway CFD models for each time division.

As explained in the NTCF model description, three model iterations were completed during the solution incorporating NTCF re-functionalizations. In previous studies (Danko and Bahrami, 2004a; 2004b; and 2004c), a small air infiltration was assumed across the emplacement drift, driven by a natural buoyancy pressure difference in the air between the hot emplacement area and the unheated environment. During these previous studies, it became apparent that the fractured and porous rock at YM allows for some airflow and that it may be reasonable to assume an open system regarding the total barometric pressure in the emplacement drift. Based on this observation, it is hypothesized herein that the total pressure in the drift equals that of the hydrostatic barometric pressure in an open system kept at the same temperature and humidity conditions. This "open system" model concept was verified in a previous study (Danko and Bahrami, 2004b).

## 2.8 Input Data

The input data used in Task 1 calculations essentially agree with those used by the DOE (2002). The main input parameters are given in Table 2-3. Other input data used in MF and NUFT are documented in a report submitted by Danko and others (2003). The input files used in the calculations are presented in Appendix A. It should be noted that the input data and design configuration applied in the calculations might not agree exactly with those used in the most current DOE design version.

## 2.9 Results and Discussions

### 2.9.1 Temperature and Relative Humidity Distributions

Pre- and post-closure spatial and temporal variations in temperature and RH from MF calculations are shown for the representative emplacement drift on Figure 2-6. Figures 2-6a and 2-6b show temperature and RH values, respectively, on the drift wall as a function of time and drift length. Figures 2-7 and 2-8 show similar scenarios for drift air and centerline. The drift centerline includes the waste packages.

Figures 2-9 through 2-11 show 2-D spatial distributions for temperature and RH along the drift for selected post-closure periods for drift wall, air, and centerline, respectively.

The evolution of two thermal peaks is shown in the temperature variations for the drift wall (Figure 2-6a), a minor peak around Year 5 during pre-closure and a major one between Years 75 and 100 during post-closure, depending on drift location. The second peak is reached more rapidly due to the young age of the waste and the short pre-closure ventilation than in a previous study (Danko and Bahrami, 2003), in which the time for peak temperature evolution during post-closure was approximately 1,000 years, following a 300-year pre-closure ventilation. The much higher second thermal peak underlines the importance of post-closure analysis for both the maximum temperature evolution as well as the threshold limitation for localized corrosion. Waste package temperatures exceed 140 ºC, a temperature perfectly compatible with a low-alloy steel, such as CORTEN, but could be a critical value for localized corrosion for Alloy 22 (Farmer, 2003). This condition is predicted for an extended period of time and for a large section of emplacement drift containing more than 100 waste packages. If drip shields were included in the calculation, the predicted temperatures of the waste package surface would rise even higher. The longitudinal, sawtooth-like fluctuations in both temperature and RH values on Figures 2-9 through 2-11 are caused by the variation of heat dissipation of the individual waste packages.

The maximum differences in temperature between the drift wall and air, as well as between waste packages and air, are only approximately 10 ºC at peak temperatures, and lower afterward. Under this condition, the buoyancy driving force for local, natural air convection in each drift cross section is moderate, with a Rayleigh number on the order of $10^9$ and with a natural heat transport coefficient of 1.85 $W/(m^2K)$ between the waste package and the air, as well as between the air and the drift wall. The convective heat transport in this case is lower than the radiant heat transport, a parallel transport mechanism in the lumped-parameter CFD model. Therefore, the sensitivity of the resultant heat transport to the heat-transport coefficient in this regime is moderate, and the lumped-parameter CFD model based on a constant transport coefficient was not seen to be in need of refinement with more elaborate heat and moisture convection elements.

The drift wall temperature variation along the drift axis is very significant, more than 32 ºC between Years 1000 and 3000 (Figure 2-9). From a few hundred to a few thousand years, the edge-cooling effect generates significant axial temperature variation within the drift, since the waste is still hot enough to heat the middle section of the drift but enough time has passed to cool the edge area. An axial temperature variation corresponding to the heat load variation in the waste packages is dominant for only a few hundred years after closure as an undulation on the mountain-scale trend. Figure 2-9 shows drift wall RH and temperature along the drift length. Similar results at drift centerline nodes that include the waste packages are shown on Figure 2-11. A small, periodic variation of approximately 3 ºC, corresponding to the emplacement sequence of the waste packages, is superimposed on the general trend of the temperature distributions over the drift length at Year 75 for the drift wall. The superimposed, periodic variation for the drift centerline temperatures is much higher, up to 10 $^{o}C$, modulating the temperature trend at Year 75 on Figure 2-11. These variations would have been much higher without using the previously discussed enhanced axial heat conduction connection in the rock model. The current temperature fields are less variable in the drift axial direction than those in previous studies (Danko and Bahrami, 2004a; 2004b; and 2004c), due to the additional axial heat conduction connections in the rock model and the increased heat flow by dispersion in the air space of the drift.

The RH distributions are somewhat higher, smoother, and more symmetric than in previous results (Danko and Bahrami, 2004a; 2004b; and 2004c), due to the lack of one-directional air infiltration in the current model. RH reaches 100-percent saturation in only a few places at the outside edges of the drift wall and waste packages (Figures 2-9 and 2-11). These results support the initial assumption that evaporation in the middle, hot drift section and cold-trap condensation in the relatively cold edge drift section will take place in the central drift of Panel 2. Other drifts in the same panel will likely follow the same trend, as will drifts in other panels.

Waste package environment information required to support the evaluation of potential container corrosion was also obtained from simulations. Figure 2-12 shows surface temperature and RH evolutions versus time for the hottest and coldest waste packages containing four types of waste: pressurized water reactor (PWR), boiling water reactor (BWR), high-level waste (HLW), and defense spent nuclear fuel (DSNF). Waste package temperatures remain below 160 ºC. The maximum RH is only slightly below 100 percent for the PWR, BWR, and DSNF packages, but reaches 100 percent for the coldest HLW package from approximately Year 750.

### 2.9.2 Cold-Trap Condensation Drippage

The MF simulation model not only indicates the condition for condensation (i.e., 100 percent RH), but also numerically quantifies the amount of liquid water condensation from the moisture transport solution.

Condensation rates per m of drift are given on Figure 2-13 for the drift centerline that includes the waste packages and on Figure 2-14 for the drift wall. As shown on Figure 2-14, condensation starts around Year 1000 at the drift wall over a few relatively cold sections. The onset of condensation, not shown, is Year 750. The condensation rate decreases with time, indicating that the total water source for condensation is thermally driven.

In a previous work (Danko and Bahrami, 2004b), a more even distribution of condensation along the drift length was obtained. The current study shows fewer condensation locations and somewhat lower condensation accumulation in each particular location. The total condensation rate for the entire drift in the previous and the current work are somewhat different, due to the differing modeling conditions, transport mechanisms, and increased heat load, as well as partially to the fact that the present study applies an iterated NTCF moisture model versus the approximate, robust model in the previous study.

Condensation directly on relatively cold waste package centerlines is shown on Figure 2-13. Although lesser in magnitude than condensation on the drift wall (Figure 2-14), direct liquid water formation on the centerlines is an important phenomenon, since it may facilitate aqueous radionuclide transport at focused locations. None of the relatively hot packages containing PWR, BWR, or DSNF waste is among the points of liquid water condensation.

Moisture fluxes into the drift from the NTCF model described herein are compared with the values predicted from the previous robust model (Danko and Bahrami, 2004b) on Figure 2-15 for four drift sections. The two halves of the drift are nearly symmetrical in temperature and humidity variations at long periods; therefore, only half of the drift is shown (i.e., i = 5 to 8). The moisture inflow to the drift, according to NUFT results, exceeds the initial values from the robust relocation flux-based model along the drift for 2,000 years in the middle portion of the drift (i.e., i = 5 and 6) while it falls below the robust model results after 2,000 years. In the cold edges of the drift (i.e., i = 7 and 8), the moisture inflow to the drift is reduced by the increasing moisture content in the drift air. Reversal of the moisture flow direction from rock-to-drift to drift-to-rock is also experienced at the coldest section (i.e., i = 8), indicating condensation drainage from the drift into rock during the first 2,000 years.

The drift flux appears to attract more moisture in vapor form than percolation flux would provide on its footprint area. The result of the example indicates that the emplacement drift cannot shadow vertical moisture flux, averaged along the length of the drift, during the first few thousand years. The question about the emplacement drift as a whole acting as a shadow or water attractor must be investigated further. More studies are needed with an even more refined model configuration that accounts for longer, unheated drift sections and variable dispersion coefficients for axial heat and moisture transports in the drift.

### 2.9.3 Open-System Model Assumption Justification

Figure 2-16a shows the amount of superheated steam influx into the emplacement drift according to the CFD balancing iterations. In-drift condensation, also shown on Figure 2-16a, removes the steam from the system. A critical period between Years 60 and 700 demonstrates excess superheated steam formation that may cause pressure buildup in the emplacement drift. A separate model was used to check the discharge of this steam flow from the system into the unheated rockmass around the edge of the repository in the horizontal direction. This separate transport mechanism is not included in the original mountain-scale transport model, due to lack of axial transport connection along the drift in the rockmass model. A 3-D NUFT model of the rock domain for the unheated edges was used with properties identical to the mountain-scale model. The boundary condition assumed gaseous steam flow in the axial direction at the drift level. The results from this model (Figure 2-16b) shows a relatively small pressure buildup between Years 60 and 700, with a peak of less than 100 pascals (Pa), which supports the working hypothesis about the open pressure system at YM.

### 2.9.4 Computational Performance

The NTCF modeling technique reduced the number of necessary NUFT runs, making it feasible to complete the complex calculations in a few months, in spite of the average estimated number of 150 balancing iterations with the MF model for the 5,000-year post-closure period. In comparison, a single NUFT run with one set of boundary condition variations for 5,000 years for the complete rock domain, with entrance and exit segments, took approximately 150 hours. Comparing run times between MF with the NTCF method and a hypothetical case without the NTCF method indicates that without using the NTCF method, but replacing it with direct NUFT runs and assuming the same number of balancing iterations, the modeling task would take a minimum of 150 times 150 hours, or 2.6 years of nonstop computation.

The NTCF modeling technique not only accelerated the calculations but also provided for rescaling of the NUFT results from mountain-scale configuration to a fine, drift-scale application. The scalability of the NTCF model makes it a unique and efficient modeling technique.

## 2.10 Effect of Lower Value Dispersion Coefficient

As shown in previous publications (Danko and Bahrami 2003; 2004a; and 2004b), the drift wall, air, and centerline temperatures all vary significantly along the drift length. Therefore, because of this significant temperature gradient, or temperature tilt, along the drift, the high dispersion coefficient of 0.1 $m^2/s$ is the appropriate choice (Webb and Itamura, 2004). However, many other factors may lower the axial dispersion coefficient, such as rock falls or partial drift collapse. For this reason, a second model was set up and run using the lower dispersion coefficient of 0.004 $m^2/s$ determined by Webb and Ituamua (2004). The results of the numerical simulation are shown on Figures 2-17 through 2-24.

Ttemperatures were found to be approximately 8 ºC colder at the drift edge and approximately 2 ºC hotter in the middle of the drift for the lower dispersion coefficient case (Figure 2-17) compared to the higher case (Figure 2-9)..   The differences are explained by the weaker heat transport along the drift length. Temperature and RH profiles along the drift were more jagged in appearance, caused by weaker heat and moisture connections in the drift along its length. The RH values increased in the middle portion of the drift after 1,000 years, with the difference between high and low dispersion coefficient models increasing to approximately 30 percent at Year 5000. This effect can be explained by the reduction of moisture transport from the center portions of the drift toward the edges. An additional effect is an increase in the length of the very humid edge sections in the lower dispersion coefficient model case. Comparing the drift wall condensation rate distributions shown on Figures 2-14 and 2-22 indicates that the lower dispersion coefficient increases the length of the condensation zone from 42 m in the base case to 148 m.

Comparing total condensation rate $\dot{q}_{cm}$ on Figures 2-16a and 2-24a shows approximately 5 times less drift condensation in the low dispersion coefficient case.

In addition, there is no condensation at the drift centerline nodes, including the waste packages, mainly due to the fact that the total moisture inflow is approximately 5 times lower in the low dispersion coefficient case.

## 2.11 Conclusions and Recommendations

1. An integrated, pre- and post-closure hydrothermal airflow study was successfully completed with both mountain- and drift-scale rockmass model elements using MF. The model applied a multiscale rockmass element without the need for solving subtasks or subsequent superposition. Heat conductivity reduction in the rockmass, due to desaturation during pre-closure, was included in post-closure calculations. The model applied open-loop powered ventilation during pre-closure and in-drift natural air movement during post-closure for one continuous 5,000-year period, thereby capturing the dynamics in temperature and humidity variation with time.
2. Figure 2-12 summarizes the surface temperature and RH evolutions versus time for the hottest and coldest packages containing PWR, BWR, HLW or DSNF waste. As shown, the waste package surface temperatures remained below 160 ºC for all waste types. RH remained significantly below 100 percent for the PWR, BWR, and DSNF waste packages, but reached 100 percent for the coldest HLW package from approximately Year 300.
3. In a previous study (Danko and Bahrami, 2004b), a more even distribution of condensation along the drift length was obtained. The study described herein shows fewer condensation locations. The total condensation rate for the entire drift in both previous and current studies differ somewhat, mainly due to differing modeling conditions and transport mechanisms, and at least partially due to the fact that the present study applies an iterated NTCF moisture model versus the approximate, robust model from the previous study.
4. Task 1 shows that condensation forms directly on relatively cold HLW waste packages on the outer edges of the emplacement drift. Although lesser in magnitude than condensation on the drift wall, direct liquid water formation on the waste packages is an important phenomenon, since it may facilitate aqueous radionuclide transport at focused locations. However, condensation did not form on any of the

relatively hot packages containing PWR, BWR, and DSNF waste. The fact that condensation was found only on the peripheral waste packages implies that the application of longer cold drift sections at both ends of the emplacement drift may eliminate condensation and wet conditions on waste packages. Since the current simulation assumes only a few short m of unheated (i.e., empty) drift sections at both ends, the arrangement is definitely less favorable than the newest DOE baseline design, which uses much longer unheated drifts. Consequently, the length of unheated drift sections will be modified according to this new design in future NWRPO studies.

5. The hydrothermal ventilation model used an open system assumption regarding the total barometric pressure in the emplacement drift. This assumption was tested by numerical simulation and found to be valid with a less than 100-Pa pressure increase during the critical period for superheated steam formation between Years 60 and 700.
6. The value of the heat and moisture dispersion coefficient has a significant impact on both the distribution and magnitude of condensation, which implies that this input parameter may not be substituted as a universal constant. It is recommended that variations in dispersion coefficients be addressed in future models by either direct temperature field-dependent CFD simulations, or by correlation equations for a given temperature distribution along an emplacement drift.

## 3.0 PRE-CLOSURE TIME STUDY (TASK 2)

Task 2 involves the effect of the length of pre-closure forced ventilation on the psychometric conditions (i.e., temperature and RH) and environment (i.e., condensation) in the emplacement drift at YM. For the sake of simplicity and to save time, a scoping calculation was made with the following assumptions:

1. Temperature and partial vapor pressures are assumed unchanged from Year 50 to the end of the extended pre-closure time within the emplacement drift. This assumption may be an oversimplification, but can certainly be met with open-loop powered ventilation by decreasing the volumetric flow rate with time.
2. The rockmass desaturation during the extended pre-closure is not modeled. The rockmass saturation conditions for post-closure simulation are assumed to remain constant and equal to conditions reached at Year 50 of pre-closure.
3. The decreased heat generation of the waste packages is the primary reason for temperature reduction when an extended pre-closure ventilation period is applied.
4. The thermally driven moisture flux component in the drift is fixed at the base case level. The NTCF moisture model used in this study responds only to partial vapor pressure variations and the variation in total barometric pressure. The moisture flux model was not iterated for temperature-dependency, which required more computational time than was possible for this report. This assumption may create excessive conservatism in the modeling results.

At the setup of the pre-closure time study, simplifying assumptions 1 to 4 were expected to be conservative but conducive to overwhelmingly positive results with respect to the benefit of longer-term pre-closure ventilation. This working hypothesis proved to be incorrect. The results were not positive, which might have been due to excessive conservatism in the simplifying assumptions.

### 3.1 Model Configuration

The 50-year pre-closure period modeled in Task 1 was used as the starting point for modeling longer pre-closure periods (i.e., 100, 200, and 300 years). Pre-closure plus post-closure periods were therefore 5050, 5150, and 5250 years, respectively. Input files for this task are presented in Appendix B.

### 3.2 Results and Discussion

This study shows the expected results; that is, as pre-closure ventilation time increases, more heat is removed and less heat becomes available for the post-closure period. Therefore, temperatures will decrease. Unexpected factors have also been found, such as the evolution of maximum temperature becoming slower and RH increasing in the emplacement drift. Figures 3-1 through 3-3 show the distribution of temperature and RH for pre- and post-closure periods at the drift wall, air, and centerline nodes, respectively, for the 300-year pre-closure ventilation case. Maximum post-closure temperatures are 100.2, 100.6, and 103.2 ºC, respectively. The maximum temperature of approximately 100 ºC occurs at Year 750. The maximum post-closure RH values at the drift wall, air, and centerline are 100, 95.5, and 99.99 percent, respectively, near the edges of the drift.

Comparing results of post-closure temperatures between the base case of Task 1 (Figures 2-6, 2-7, and 2-8) and the case of 300-year pre-closure (Figures 3-1, 3-2, and 3-3) reveals that the maximum temperature occurs much later (i.e., approximately 750 years versus 75 to 100 years after emplacement) and the maximum temperature is much lower. If monitoring the thermal peak is required and the only factor considered, the approximately 650- to 675-year difference in required monitoring makes the 300-year pre-closure period clearly less favorable than the 50-year period. The same problem will result from aging the waste, since it will likely lengthen the time required to reach the maximum temperature.

Regardless, other factors besides monitoring only during peak temperatures must be considered. For example, the reduction in uncertainty in modeling hydrothermal, thermo-chemical, and thermo-mechanical processes by significantly lowering the maximum temperature (e.g., below boiling) may far outweigh the cost of monitoring for very long periods of time. Moreover, early-time monitoring (i.e., the first 100 years) may reduce uncertainty even further, to such an extent that requirements for additional monitoring may also be significantly reduced.

The results of temperature and RH values on the surface of the hottest and coldest waste packages for each waste category are shown on Figures 3-4 through 3-6 for three pre-closure periods. The locations of these packages were determined by determining their maximum and minimum surface temperatures during post-closure. Comparing the results of waste package surface temperatures leads to the conclusion that increasing pre-closure length will decrease post-closure temperatures. As the waste package surface temperature decreases, a rise in RH relative to the base case is expected, as shown for most times on Figures 3-4 through 3-6. Although minimum RH values increase as the length of pre-closure increases, maximum RH values do not.

Figures 3-7 through 3-15 show temperature and RH distributions at the drift wall, air, and centerline nodes for various lengths of pre-closure ventilation at selected post-closure periods. These figures show spatial variations of the storage environment. Figures 3-7 through 3-9 show the 100-year pre-closure period. Overall, temperature profiles are smoother for the wall and centerline profiles than in the base case, due to a lower heat load. The temperature and RH profiles are almost symmetrical except for the first few hundred years after the pre-closure time period. Both temperature and RH are affected during the first few hundred years of the post-closure operation by pre-closure ventilation effects, notably, asymmetrical cooling and drying. The maximum temperature is reached at Year 550 and is still well above boiling at Year 1050. The lowest and highest RH values vary between 55 and 100 percent. The temperature difference between drift wall and air or drift centerline and air during post-closure remain very small, at approximately 2 to 3 ºC. This small temperature difference makes CFD modeling results quite susceptible to thermal and pressure side effects, such as local overheating due to drift collapse or air movement caused by barometric pressure variation.

Figure 3-10 shows the results of spatial distribution of drift wall temperature and RH values at Years 650, 1150, 3150, and 5150 for the case of 200 years of pre-closure ventilation. Temperatures reach a maximum at Year 650 and are well above boiling for a section of the drift at Year 1150. RH varies between 60 percent near the middle of the drift and 100 percent near the edges. Year 1150 results show that drift wall nodes along the cold waste packages reach a maximum of 100 percent RH and average around 70 percent RH along the drift wall. Figure 3.11 shows that the drift air remains below 100 percent RH for the entire drift. Similar but somewhat lower distributions are seen for the drift centerline temperature and RH, with more jagged profiles shown on Figure 3-12.

Figures 3-13 through 3-15 show the detailed results of 300-year pre-closure ventilation. Temperatures for Year 750 are above boiling; at Year 1250 they have already cooled to below boiling. RH values vary between approximately 65 and 100 percent on drift wall, centerline, and air nodes.

Figures 3-16 through 3-21 show the condensation distribution along the drift wall and centerline for the cases of 100-, 200-, and 300-year pre-closure ventilation for a selection of post-closure time divisions. A comparison of the condensation rate between these three cases shows that the condensation rate for a given post-closure time division decreases with an increase in pre-closure ventilation time. Comparing the condensation rates between drift wall and centerline shows that most of the condensation (i.e., approximately 85 percent) occurs on the drift wall, since drift wall temperatures are lower than centerline temperatures. Condensation rates are at a maximum at the drift edges, where temperatures are lowest. The variation in condensation along the drift length is caused by the variation in temperature and RH distributions. The condensation rate decreases somewhat, while the section length of the condensation zone increases with length of pre-closure ventilation.

Figure 3-22 shows the drift moisture inflow and condensation for different pre-closure ventilation periods. The results show that total inflow and condensation increase with an increase in length of pre-closure ventilation. This surprising result is due to the fact that partial vapor pressures are generally lower at lower temperatures, thereby attracting more moisture/vapor inflow into the drift. The simplifying assumptions used in this study did not allow modeling of temperature effects on moisture inflow from the rockmass.

## 3.3 Conclusions

The main conclusions are as follows:

1. Drift temperatures decrease as the length of pre-closure time increases.

2. Minimum values of drift RH increase as the length of pre-closure time increases.

3. The maximum temperature for the 50-year pre-closure base case is reached at Year 75; for the cases of 100-, 200-, and 300-year pre-closure periods, this maximum temperature is reached at Years 550, 650, and 750, respectively.

4. Monitoring the effects of maximum temperature become less practical as the length of pre-closure increases. This problem will also be encountered if peak temperature monitoring is required for waste that has been aged on surface pads.

5. Total drift moisture inflow and condensation increase with an increase in the length of pre-closure ventilation, due to lower temperatures and partial vapor pressure.

6. The condensation rate per unit drift length slightly decreases with an increase in pre-closure ventilation time, due to a more even distribution over longer and cooler drift sections.

7. Task 2 results are considered those of an oversimplified model, especially due to setting the temperature-driven moisture-flow component from or into the drift equal to that of the base case with higher temperatures. The magnitude of the temperature-driven moisture flow component is definitely higher at the higher temperature of the base case. The oversimplified model used herein tends to underestimate water removal and rock desaturation by ventilation during pre-closure, and overestimate moisture removal during post-closure. Since conflicting effects have been found, further studies are recommended to re-examine this task with a refined model eliminating excessive conservatism.

8. According to the simplified model results, 300-year pre-closure ventilation cannot quite bring the temperature below boiling. More efficient pre-closure ventilation, which cools the initial temperatures further from the values found at Year 50, may result in a solution with temperatures entirely below boiling. That, in turn, will likely reduce condensation on the edges of the emplacement drifts.

# 4.0 BAROMETRIC PRESSURE PUMPING STUDY (TASK 3)

Task 3 involved the effects of barometric pressure changes at the drift level on post-closure environmental conditions, and included the following steps.

1. Ambient barometric pressure data from various locations close to the YM site were combined to create a sufficient continuous period for determining daily barometric pressure variation (Table 4-1). A very robust barometric pressure variation was found around YM, exceeding a plus/minus 1,000-Pa regime. Variations from several borehole sensors were found to be in close agreement. Not taking into account constant additive, site-specific shifts related to the altitudes of the different locations, close correlations were found in the variations, even between data from YM and the McCarran Airport station in Las Vegas.
2. The effect of static barometric pressure alteration for 12,500 years was then studied using a small, embedded rockmass NUFT model. This embedded, 2-D model describes vertical and horizontal heat and moisture flows in the vertical plane normal to the drift centerline in the rockmass around a 1-m-long drift section in the hottest, central section of the drift at 355 m. The model domain is a vertical slice of the rockmass from surface to water table (i.e., in the z direction), from drift center to mid-pillar in the normal direction to the drift (i.e., in the x direction), and 1 m along the drift length (i.e., in the y direction). The boundary conditions of temperature and partial vapor pressure at the drift surface in the 2-D model are imported from the balanced results obtained from the 3-D model used in Task 1. This embedded model is a close approximation to the 3-D model but much faster to solve. The disadvantages of using the embedded 2-D model is the absence of y-directional heat and mass flows, assumed to be of secondary importance at this phase of the study. This assumption will be reexamined in future studies. The following constant barometric pressure values within the drift were used to study the effect of barometric pressure change upon the drift wall fluxes: 1) barometric pressure values averaged over time, 2) a value above the average, and 3) a value below the average. The results show that either a positive or negative change in the drift barometric pressure significantly changes the heat and moisture flux during the period when the temperature is above boiling.
3. MF simulations were then made using the altered moisture inflow values in the NTCF moisture model. The results showed that the effect of barometric pressure on humidity and condensation was significant. It was therefore decided to use a refined prediction method for establishing heat and moisture flux variations due to barometric pressure pumping.
4. First, the cyclic nature of the barometric pressure variation with time was identified, using a Fourier analysis of the pressure data. The barometric pressure was found to be varying, with a dominant period of 10.66 days. The amplitude of the cyclic pressure wave was evaluated as the standard deviation (i.e., a one-sigma variation) equal to 1,160.5 Pa.
5. After identifying the frequency of the variable barometric pressure at drift level, a square wave with the same frequency and one-sigma amplitude was considered for the determination of the amount of drift wall moisture flux correction due to a cyclic

barometric pressure variation. To achieve this objective, the embedded 2-D NUFT model described above in step 2 was again used. The following model solutions were completed:

a. The wall boundary condition was configured using the coupled and balanced results of Task 1. The time divisions corresponding to Years 750, 1000, 1500, and 2000 were considered, since these cover the above-boiling time period. For each time division, a direct NUFT simulation was performed, using the balanced temperature and vapor pressure history from the Task 1 results. The NUFT drift wall boundary conditions, temperature, and vapor pressure were kept constant, while the barometric pressure boundary condition was perturbed with the cyclic square wave, with one sigma as amplitude and frequency of 10.66 days for 200 cycles in order to reach quasi-steady state. Figure 4-1 shows the moisture flux deviation results of this simulation.

   The moisture flux deviation study was repeated at different times to Year 3000. Figure 4-2 shows that the moisture flux deviation values are close to zero for Year 3000, when the temperature is below boiling. Therefore, it was concluded that the effect of barometric pressure pumping was most significant during the boiling regime. These results show that the averaged values of 1.5946e-4 and -2.0114e-4 kg/s-m of drift moisture flux correction may be used, due to plus one and minus one sigma barometric pressure variation during the boiling regime. The moisture flux deviation values represent the effect of in-drift barometric pressure pumping on the drift wall moisture flux. The results indicate that changing the in-drift barometric pressure would affect the amount and distribution of condensation in the drift.

b. The moisture flux deviations were applied to the NTCF moisture-flux model element and MF balancing calculations were made in order to identify the effect of barometric pressure pumping on the humidity and condensation distribution in the emplacement drift. For the high barometric pressure case (i.e., $Pbar_{av}+\sigma[Pbar]$ where $Pbar_{av}$ is the average barometric pressure and $\sigma Pbar$ is sigma or standard deviation of barometric pressure), the moisture flow deviation of -2.0114e-4 kg/s-m was used at drift wall nodes where the temperature is at or above the boiling temperature. For the low barometric pressure case where drift wall temperature was above boiling (i.e., $Pbar_{av}-\sigma[Pbar]$), moisture flow was changed by adding 1.5946e-4 kg/s-m. Upper and lower condensation conditions were determined from the simulations with positive and negative deviations.

c. The variation in heat flux due to barometric pressure changes is noted but not entered into the MF model. The large thermal capacity of the near-field rockmass and waste package prevent any high-frequency temperature change. The enhancement in heat flux will likely lower the average temperature field somewhat. It is estimated that barometric pressure pumping enhances heat transfer in the rock, which may result in a 4 to 10 percent temperature decrease during the most critical, above-boiling regime.

The effect of barometric pressure variation upon the moisture flux is shown on Figure 4-2, with moisture fluxes given at $Pbar_{av}$, $Pbar_{av}+\sigma(Pbar)$, and $Pbar_{av}-\sigma(Pbar)$ total airway pressure histories. Figure 4-2 shows that the moisture correction value is approximately 6 to 8 times the moisture flux value at $Pbar_{av}$. After establishing the effect of barometric pressure pumping on the moisture flux as an average and plus or minus a correction per m of drift, the NTCF moisture flux model is adjusted accordingly for positive and negative bounding model calculations. Input files for this task are presented in Appendix C.

## 4.1 Results of MULTIFLUX Model Calculations

Figure 4-3 shows the results of total drift condensation and moisture inflow as a function of time for the base case and the low barometric pressure case. As expected, there is more moisture inflow during the above-boiling regime. Between Years 50 and 500, the entire drift is above boiling (Figure 4-3c) and the moisture inflow is approximately 16 times higher than in the base case. Starting from Year 750, the minimum drift wall temperature drops below boiling near the edges and the boiling zone decreases in length along which the moisture inflow is deviated by 2.0114e-4 kg/s-m per m of drift. During this time, the moisture inflow is elevated, and more condensation is seen along the below-boiling drift section. As shown on Figure 4-3 for Years 3000 and 5000, both maximum and minimum drift temperatures are below the boiling point of water, and the moisture inflow agrees with the base case, as there is no moisture inflow deviation during the below-boiling regime. The drift condensation rate shows a similar trend as more moisture inflow results in more condensation (Figure 4-3b). It can be seen that the maximum condensation rate is approximately 12 times higher than that for the base case.

Figure 4-4 shows the axial distribution of drift wall condensation and temperatures for the case of $Pbar_{av}$-$\sigma$(Pbar) during Years 75 through 5000 of post-closure. As shown, the length of the condensation zone from the drift edges reaches the maximum of approximately 80 m at Year 2000, due to the additional moisture inflow along the boiling zone of the drift wall. When the entire drift is below boiling, this length drops to approximately 21 and 18 m at Years 3000 and 5000, respectively.

Figure 4-5 shows results for the drift centerline that includes the waste packages. The condensation rate is approximately one-fourth that for the drift wall, due to the larger surface area of the drift wall and colder temperatures that allow more condensation on the wall.

Figures 4-6 through 4-8 show the results of RH and temperature profiles along the drift length during post-closure between Years 75 and 5000 for drift wall, drift air, and centerline nodes. The RH profiles show that the drift is the most humid at Year 2000.

The case of high barometric pressure results requires much more computational time to reach balanced results and is not included herein. However, it is possible to use only the low and average barometric pressure results for comparison and evaluation. It is expected that the high barometric pressure case will be somewhat drier than the low case, with lower RH and condensation rate values. Using the average barometric pressure results instead of high ones gives a conservative prediction of the changes.

Figure 4-9 shows the results of the base case and the case of $Pbar_{av}$-$\sigma$(Pbar) in terms of axial distribution of drift wall condensation rate and RH at selected post-closure time divisions. The shaded area represents the variation between upper and lower bounds due to the reduction of barometric pressure. It can be concluded that Year 2000 is a critical time in terms of RH and the length of the condensation zone. The condensation zone varies between 42 and 430 m, approximately two-thirds of the drift length, during a period of 10.66 days.

## 4.2 Effect of Low Axial Dispersion Coefficient

Since a significant sensitivity was found regarding the input value of the dispersion coefficient in Task 1, an additional exercise was conducted to evaluate barometric pressure pumping effects under the assumption of a low dispersion coefficient (Webb and Itamura, 2004).

Figure 4-10a shows that drift wall moisture flux (i.e., flow into the drift) is not affected significantly by the use of a lower dispersion coefficient. However, a comparison of Figure 4-10b with Figure 4-3b indicates that lowering the axial dispersion coefficient significantly lowers the amount of drift condensation.

A comparison of Figures 4-4 and 4-11 shows that the condensation zone at Years 3000 and 5000 is increased, but the condensation rate per m of drift is decreased by a factor of 10. On the other hand, the length of the condensation zone is not affected between Years 1000 to 2000, probably due to large amounts of moisture inflow during this 1000-year period. The value of condensation rate per m of drift has increased due to increased moisture transport resistance along the drift. However, according to Figure 4-10b, total drift condensation rate is decreased compared to the case of a high dispersion coefficient.

Figure 4-12 shows that the drift centerline experiences condensation only at Year 2000, the most critical post-closure period in terms of moisture condensation and RH.

A comparison of Figures 4-13 through 4-15 with Figures 4-6 through 4-8 shows that temperature and RH distributions are more rugged for a low dispersion coefficient than a high one.

## 4.3 Conclusions

1. Comparing average and low barometric pressure results shows that barometric pressure variation has a major effect on RH and condensation during the above-boiling operating time period.
2. RH and condensation distribution on the drift wall is strongly time variable. Results of both the average and low barometric pressures are valid, alternating within 5.33 days for low to average barometric pressure. This variation affects approximately one-third of the drift lengths for a few thousand years, which will likely be periodically dry, then wet, for 5.33 days each time.
3. According to the simulations, only a few waste packages on the drift centerline will experience alternating conditions from wet to dry, assuming a high dispersion coefficient. Nevertheless, the effects of frequent drying and rewetting warrant further investigation.
4. In the case of low dispersion coefficients, condensation is predicted only at Year 2000 for the centerline nodes that include the waste packages; however, a longer section of the emplacement drift (i.e., two-thirds of the total length) will experience periodic rewetting and drying on the wall, with a likely period of 10.66 days.

5. Temperature variations caused by barometric pressure pumping have not been included in the simulations. However, even a small temperature variation may affect corrosion. Therefore, further refinement of the model for temperature variation is recommended.

# 5.0 FATE OF CONDENSATION STUDY (TASK 4)

A NUFT numerical model was applied for Task 4 after the coupled MF simulation established the amount of condensation on the drift wall. A 1-m slice of the 3-D mountain-scale rockmass was used to study the fate of condensation placed directly on the rock surface. Heat and moisture fluxes, as well as matrix and fracture saturations, were examined with direct NUFT runs under the added load of the condensation rate determined by MF. Additional input files for this task are presented in Appendix D.

Four cases were studied, assuming: 1) condensation on the roof with a balanced condensation rate, 2) condensation on the invert with a balanced condensation rate, 3) condensation on the roof with a reduced condensation rate, and 4) condensation on the invert with a reduced condensation rate. The balanced condensation rate amount was defined based on Task 1 simulation results taken from a longitudinal drift location at 710.9 m as an example. The total condensation rate at all wall nodes, including the roof, side walls and invert, was then taken as focused condensation and applied directly to the surface sections of the roof or the invert.

The condensation rate varied along the emplacement drift. To explore sensitivity to the condensation rate, the study was repeated with a reduced amount. A reduction factor of 10.0 was applied on the balanced condensation rate.

## 5.1 Balanced Condensation on the Roof

Figure 5-1 shows the total condensation rate that accumulated on the entire drift wall surface over a 1-m drift length of the 710.9 m drift location (i.e., the 420$^{th}$ drift section) according to Task 1. The drift wall at this location is at 100 percent RH and the total condensation rate is re-entered into the model for two focused drift wall sections (i.e., the roof and invert) as study examples.

The comparison between drift wall moisture fluxes for the condensation rate examples is shown on Figure 5-2. It can be seen that placing all condensation on the invert does not affect the baseline moisture flux (i.e., condensation is removed from the system) across the drift wall. This result can be explained by capillary flow and vertical gravitational drainage towards the water table of the added condensation, which does not noticeably impact the moisture flow into the rock. Placing the condensation on the roof nodes, however, changes the moisture flux after Year 750 from an orientation into the rock to one into the drift. This orientation change indicates that at least a portion of the condensation stays on the drift surface as liquid water. Depending on surface geometry, this condensation water may run on the surface of the sidewalls until it imbibes into the rock, or drips onto the drift or drip shield.

The effect of condensation can be seen in the increase in the liquid saturation in both the matrix and fracture nodes. Figures 5-3 and 5-4 show absolute liquid saturation and an increase in saturation, respectively, at Year 5000 in the matrix nodes. Figures 5-5 and 5-6 show the absolute and the increase in liquid saturation, respectively, at Year 5000 in the fracture nodes. As a response to the condensation load from the NUFT simulation, the liquid saturation increased in both the fracture and matrix nodes.

Interpretation of these results is not straightforward or simple. The increase in the matrix saturation is probably inconclusive, due to the uncertainty associated with interpreting the meaning of non-zero matrix saturations in above-boiling rock regimes. Drippage may be indicated by the maximum increase in the fracture saturation of approximately 14 percent; from 21 percent saturation to 35 at the center of the roof may indicate drippage (Figure 5-6). Not enough information currently exists to know what triggers drippage and what threshold of fracture saturation in the model results may relate to drippage. The capillary pressure holding threshold values of the fractures need to be studied further to better understand the potential for drippage. The increase in fracture saturation must result from matrix-fracture interactions, since the entire condensation source was added to the matrix nodes in the model. The condensation process appears to deliver liquid water to the fractures or simply reduces the fracture's ability to pass vertical water transport from the percolation flux into the rock matrix.

In summary, the results imply that the roof of the drift may develop wet conditions in drift sections where condensation is present. The 14-percent change in the fracture saturation between cases with and without applying the condensation on the roof wall nodes may indicate drippage.

## 5.2 Balanced Condensation on the Invert

In the case of cooler floor drift wall than roof nodes, it is possible to have condensation on the floor nodes. Applying the total condensation amount to the invert simulates this case. Figures 5-7 through 5-10 show the saturation distribution in the rockmass. As shown, the increase in liquid saturation occurs around the floor nodes and downward within the rock matrix and fracture nodes, which might change the drift shadow concept if the condensation amount is great enough.

## 5.3 Reduced Condensation on the Roof and Invert

Figures 5-11 and 5-12 for reduced condensation are comparable to Figures 5-1 and 5-2 for balanced condensation. Moisture fluxes with added reduced condensation are equal to the no-condensation-added case for all condensation application cases, showing that the condensation can imbibe into the rock even if applied to the roof of the drift.

Figures 5-2 and 5-12 show drift wall moisture flux for balanced and reduced condensation, respectively. These results are summarized in Table 5-1, for balanced condensation and 5-2, for reduced condensation. It can be concluded that moisture flux after Year 500 is positive, into the rock, and without condensation. The moisture flux into the rock is driven by 100-percent RH in the 710.9-m drift location. After Year 750, moisture flux becomes negative and into the drift when balanced condensation is applied on the roof rock surface nodes. This result can be explained by the fact that the matrix and fracture nodes are wet and can no longer accept the amount of condensation applied. The amount of return flux is small compared to the total condensation applied to the rock.

It can also be seen that the amount of balanced condensation will imbibe into the rock if the condensation is applied to the invert nodes. The transport of water occurs mainly through fractures. Tables 5-1 and 5-2 show that net condensation is approximately equal to applied condensation, since only a small fraction of the condensation returns to the drift and most of the applied condensation will imbibe into the rock.

Figures 5-13 and 5-14 show the absolute and increase in liquid saturation, respectively, under reduced roof condensation conditions at Year 5000 in matrix nodes. Figures 5-15 and 5-16 show the same parameters for fracture nodes. Figures 5-17 through 5-20 show the same parameters as those on Figures 5-13 through 5-16, except that reduced condensation is applied to the invert.

A comparison of the saturation results for reduced condensation on Figures 5-13 through 5-20 with those for balanced condensation on Figures 5-3 through 5-10 shows that the increase in the condensation will cause an increase in liquid saturation around the drift within both matrix and fracture nodes.

## 5.4 Conclusions

1. More studies with the numerical model are needed to understand the fate of condensation and interpret the modeling results.
2. A laboratory experiment on condensation imbibition is being prepared and is discussed in Task 6. The measurements and observations from this experiment will contribute to better understanding of this important phenomenon, which has few published supporting data.

# 6.0 LABORATORY TEST PREPARATION (TASK 5)

A verification experiment of condensation imbibition was conceptually designed using a large welded tuff boulder in a UNR laboratory. In order to design the experiment and select the correct parameters and procedures, simulation of the measurement with a numerical model is necessary. It is especially critical to know, in advance, the results and time frame expected for given input conditions. The measurement is non-repeatable, since the boulder may take years to dry out after the short wetting period; it is therefore important to measure correctly the first time. Preparation of a NUFT model is still underway, based on geometry and rock properties.

A simplified geometry of the rock is shown on Figure 6-1. In order to set up the experiment, and for the sake of simplicity and computational time, a 2-D symmetrical model will be used. The NUFT rock domain of this model is shown on Figure 6-2. Room conditions are used as the outside rock boundary condition. On the symmetry planes, adiabatic boundary conditions are assumed due to assumed symmetry. A preliminary set up configuration for the steam generation apparatus is shown on Figure 6-3.

In summary, careful planning of the experiment is necessary before actual measurement. The large welded tuff boulder is at an ambient air-dry condition that will be altered by the measurement; it will be difficult to repeat the experiment without a lengthy initialization.

# 7.0 REFERENCES


Danko, G. 2004. "Numerical Transport Code Functionalization Procedure and Software Functions." Proceedings of ASME, Heat Transfer/Fluid Engineering, July 11-15, 2004, Charlotte, North Carolina.

Danko, G. and D. Bahrami. 2002. "The Application of CFD to Ventilation Calculations at Yucca Mountain." 28th Waste Management '02 Conference, Tucson, Arizona. pp 1-8.

Danko, G. and D. Bahrami. 2003. "Powered, and Natural, Passive Ventilation at Yucca Mountain." Proceedings, 10th Int. High-Level Radioactive Waste Management Conference, pp.683-689.

Danko, G. and D. Bahrami. 2004a. "Mountain-scale Moisture Transport under Thermal Influence." Devils Hole Workshop, June 2, 2004.

Danko, G. and D. Bahrami. 2004b. "Heat and Moisture Flow Simulation with MULTIFLUX", *Proceedings of HT-FED04 – ASME Heat Transfer/ Fluids Engineering Summer Conference*, (2004), Charlotte, NC.

Danko, G. and D. Bahrami. 2004c. "Coupled, Multiscale Thermohydrologic-Ventilation Modeling with MULTIFLUX" 2004 SME Annual Meeting, February 23-25, Denver, CO.

Danko, G., D. Bahrami, and S. Lanka. 2003. *Technical Support Services for the MULTIFLUX Software*. MOL.20031208.0025, Final Report, submitted to BSC, Nevada.

DOE (U.S. Department of Energy). 2002. *Ventilation Model*. Prepared by Bechtel SAIC Company, LLC. ANL-EBS-MD-000030 REV 01D draft. Yucca Mountain Project. Las Vegas, Nevada.

DOE (U.S. Department of Energy). 2004a. *In-Drift Natural Convection and Condensation*. Prepared by Bechtel SAIC Company, LLC. MDL-EBS-MD-000001 REV 00. Yucca Mountain Project. Las Vegas, Nevada.

DOE (U.S. Department of Energy). 2004b. *Multiscale Thermohydrologic Model*. Prepared by Bechtel SAIC Company, LLC. ANL-EBS-MD-000049 REV 01. Yucca Mountain Project. Las Vegas, Nevada.

DOE (U.S. Department of Energy). 2004c. *TSPA for Site Recommendation*, TDR-WIS-PA-000001 REV 00 ICN 01. Yucca Mountain Project. Las Vegas, Nevada.

Farmer, J. 2003. "Chemical Environment Evolution on Alloy 22." Presentation to the Nuclear Waste Technical Review Board, January 28, Las Vegas, Nevada.

FLUENT 5.5. 1997, copyright Fluent Inc., Lebanon, NH.

Kays, W. M. and E.Y. Leung. 1963. "Heat Transfer in Annular Passages: Hydrodynamically Developed Turbulent Flow with Arbitrarily Prescribed Heat Flux" *Int. J. Heat Mass Transfer*, Vol. 6 pp. 248-249.

MULTIFLUX. 2003. *Draft Software Qualification Documents*. Prepared for Bechtel SAIC Company, LLC (BSC) by George Danko, University of Nevada, Reno.

NUFT. 2000. *Flow and Transport Code Version 3.0s*. Software Configuration Management, Yucca Mountain Project – STN: 10088-3.0S-00. Prepared by Lawrence Livermore National Laboratory.

NWRPO (Nuclear Waste Repository Project Office). 2003. *Coupled Hydrothermal-Ventilation Studies for Yucca Mountain Annual Report For April 2002-March 2003.* NWRPO-2003-5. Nye County Department of Natural Resources and Federal Facilities. Pahrump, Nevada. December 2003.

Webb, S.W. and M.T. Itamura. 2004. "Calculation of Post-Closure Natural Convection Heat and Mass Transfer in Yucca Mountain Drifts." Proceedings of ASME, Heat Transfer/Fluid Engineering, July 11-15, 2004, Charlotte, North Carolina, USA

Webb, S.W., N.D. Francis, S. Dalvit-Dunn, and M.T. Itamura. 2003. "Pre- and Post-Closure Natural Convection Effects in Yucca Mountain Drifts." Proceedings, 10th Int. High-Level Radioactive Waste Management Conference, pp. 667-674.

Table 2-1
Drift-Scale Subdivisions in Mountain-Scale Rock Cells

| Mountain-Scale Rock Cell (i) | Number of NTCF[a] Subdivisions (j) |
|---|---|
| 1 | 21 |
| 2 | 42 |
| 3 | 63 |
| 4 | 84 |
| 5 | 84 |
| 6 | 63 |
| 7 | 42 |
| 8 | 21 |

[a]Numerical Transport Code Functionalization

Table 2-2
Rock Model Moisture Flux across Drift Wall

| Time Period per DOE Climate Model (year) | Percolation (millimeter per year) | Moisture Flux per Linear Meter of Drift (kg/s-m x $10^{+6}$) |
|---|---|---|
| 0 - 600 | 12 | 2.1127 |
| 600 - 2000 | 20 | 3.5211 |
| 2000 - 5000 | 37 | 6.4789 |

Table 2-3
Input Data[a] for Task 1 Calculations

| Parameter | Description |
|---|---|
| Rock input data | NUFT input deck specified in DOE (2002). The spatial rock domain is shown on Figures 1-3 and 1-44 in this reference. |
| Drift dimensions | 710 meters long, 5.5 meters in diameter. |
| Airflow rate | 15 $m^3$/s at 25 ºC intake temperature and 30% relative humidity until Year 50; 0 $m^3$/s afterwards and assumed velocities for natural vertical flow rates. |
| Waste packages | 140 waste packages in the emplacement drift. A mirrored repeat sequence of eight waste packages with variable heat load, two halves and six full packages in a repeating drift segment of 35.5 meters. Shown on Figure 1-4 in DOE (2002). |
| Waste mass load | 56 MTU/acre. |
| Drip shield | No drip shield is assumed in the model configuration. |

[a]Data from U.S. Department of Energy. 2002. *Ventilation Model.* Prepared by Bechtel SAIC Company, LLC. ANL-EBS-MD-000030 REV 01D draft. Yucca Mountain Project. Las Vegas, Nevada.

Table 4-1
Location, Duration, and Data Tracking Number of Extracted Barometric Pressure Data

| Number | Borehole Location | Sensor Number | Measurement Period | | Data Tracking Number (DTN) |
|---|---|---|---|---|---|
| | | | Start Date | End Date | |
| 1 | USW-NRG 7a | 452 | 10/01/98 | 12/17/01 | GS000108312232.001 |
| | | | | | GS000708312232.004 |
| | | | | | GS010908312232.001 |
| | | | | | GS021008312232.001 |
| 2 | UE25-UZ #4 | 1053 | 10/01/98 | 12/17/01 | GS000108312232.001 |
| | | | | | GS000708312232.004 |
| | | | | | GS010908312232.001 |
| | | | | | GS021008312232.001 |
| 3 | UE25-UZ #5 | 1131 | 10/01/98 | 12/17/01 | GS000108312232.001 |
| | | | | | GS000708312232.004 |
| | | | | | GS010908312232.001 |
| | | | | | GS021008312232.001 |
| 4 | USW-UZ 7a | | 10/01/98 | 03/31/99 | GS000108312232.001 |
| | | | | | GS000708312232.004 |
| 5 | USW-SD 12 | | 10/01/98 | 03/31/99 | GS000108312232.001 |
| | | | | | GS000708312232.004 |
| 6 | ZONE 2 ALCOVE 7 of ESF | | 12/08/97 | 12/12/98 | GS990108312242.005 |
| 7 | ESF NICHE3566 (NICHE 1) | | 02/01/98 | 7/31/98 | GS980908312242.021 |
| 8 | UE-25 WX Station 3 | | 10/01/94 | 09/30/95 | GS960808312111.003 |
| 9 | ALCOVE 7 of ESF | 1775 | 09/20/01 | 01/27/03 | GS020808312231.002 |
| | | | | | GS030508312231.001 |
| 10 | ECRB | 1955 | 01/30/02 | 01/27/03 | GS020808312231.002 |
| | | | | | GS030508312231.001 |

Table 5-1
Drift Wall Flux Comparison for Balanced Condensation

| Time (year) | Total Balanced Condensation[a] | Drift Wall Moisture Flux[a] | | | Net Condensation[a] |
|---|---|---|---|---|---|
| | | No Condensation | Roof Condensation | Invert Condensation | |
| 60 | 0.000000 | -22.014000 | -22.014000 | -22.014000 | 0.000000 |
| 75 | 0.000000 | -18.187600 | -18.187600 | -18.187600 | 0.000000 |
| 100 | 0.000000 | -10.804000 | -10.804000 | -10.804000 | 0.000000 |
| 150 | 0.000000 | -8.957000 | -8.957000 | -8.957000 | 0.000000 |
| 200 | 0.000000 | -3.138200 | -3.138200 | -3.138200 | 0.000000 |
| 300 | 0.000000 | -0.274960 | -0.274960 | -0.274960 | 0.000000 |
| 500 | 0.000000 | 14.107800 | 14.107800 | 14.107800 | 0.000000 |
| 750 | 149.518000 | 3.679800 | -45.254000 | 2.859600 | 104.264000 |
| 1000 | 217.300000 | 1.221500 | -103.048000 | 1.237900 | 114.252000 |
| 1500 | 159.878000 | 0.761160 | -58.266000 | 0.767760 | 101.612000 |
| 2000 | 107.740000 | 0.479020 | -19.213800 | 0.506500 | 88.526200 |
| 3000 | 62.240000 | 0.248560 | -7.827000 | 0.278200 | 54.413000 |
| 5000 | 29.962000 | 0.061148 | -2.806200 | 0.062894 | 27.155800 |

[a]Condensation unit = kg/s-m x $10^{+6}$.

Table 5-2
Drift Wall Flux Comparison for Reduced Condensation

| Time (year) | Total Reduced Condensation[a] | Drift Wall Moisture Flux[a] | | | Net Condensation[a] |
|---|---|---|---|---|---|
| | | No Condensation | Roof Condensation | Invert Condensation | |
| 60 | 0.000000 | -22.014000 | -22.014000 | -22.014000 | 0.000000 |
| 75 | 0.000000 | -18.187600 | -18.187600 | -18.187600 | 0.000000 |
| 100 | 0.000000 | -10.804000 | -10.804000 | -10.804000 | 0.000000 |
| 150 | 0.000000 | -8.957000 | -8.957000 | -8.957000 | 0.000000 |
| 200 | 0.000000 | -3.138200 | -3.138200 | -3.138200 | 0.000000 |
| 300 | 0.000000 | -0.274960 | -0.274960 | -0.274960 | 0.000000 |
| 500 | 0.000000 | 14.107800 | 14.107800 | 14.107800 | 0.000000 |
| 750 | 14.951800 | 3.679800 | 2.833200 | 3.723000 | 17.785000 |
| 1000 | 21.730000 | 1.221500 | 0.327740 | 1.221380 | 22.057740 |
| 1500 | 15.987800 | 0.761160 | 0.500420 | 1.035160 | 16.488220 |
| 2000 | 10.774000 | 0.479020 | 0.437080 | 0.498560 | 11.211080 |
| 3000 | 6.224000 | 0.248560 | 0.244140 | 0.279420 | 6.468140 |
| 5000 | 2.996200 | 0.061148 | 0.063568 | 0.062214 | 3.059768 |

[a]Condensation unit = kg/s-m x $10^{+6}$.

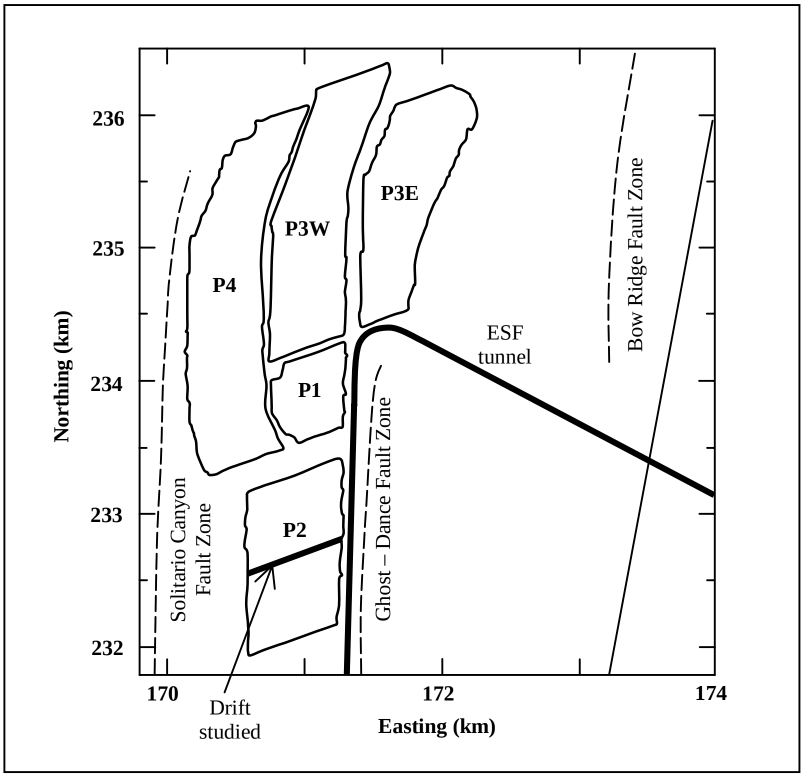


Figure 2-1
Plan of Conceptual Emplacement Panels at Yucca Mountain

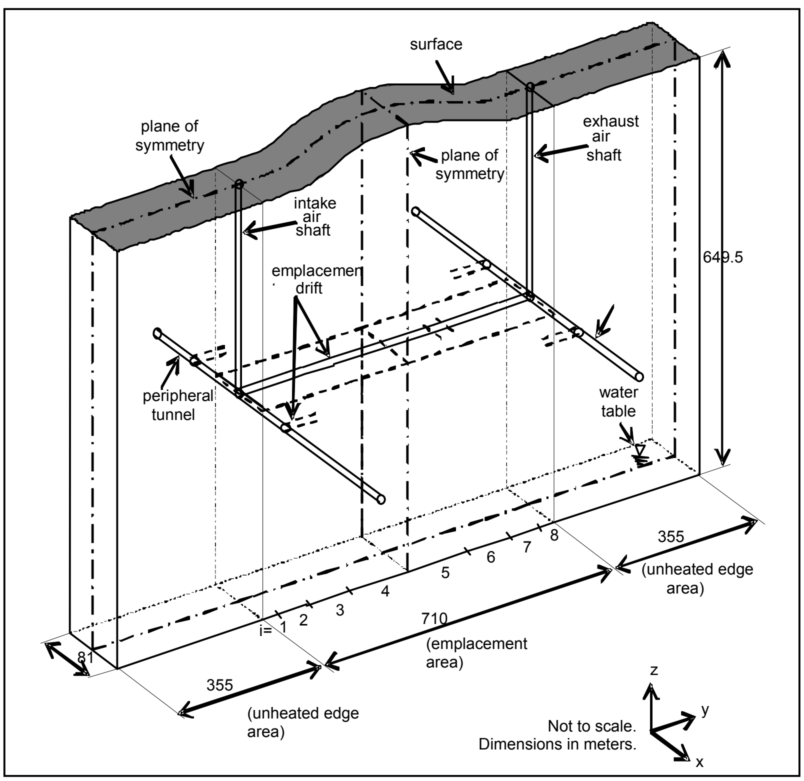


Figure 2-2
Rockmass Domain around an Emplacement Drift in Panel 2

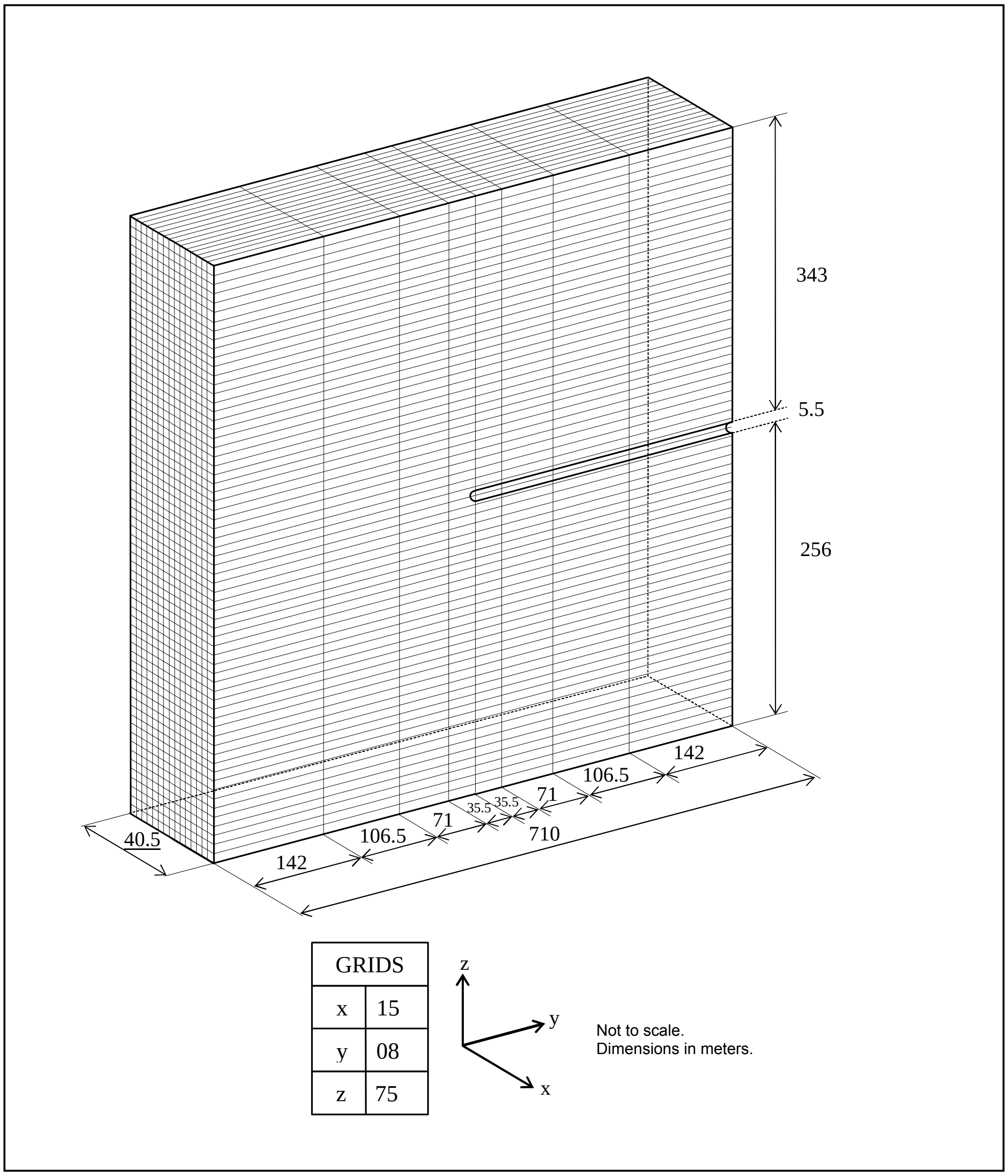


Figure 2-3
Non-Equilibrium Unsaturated-Saturated Flow and Transport
Domain Discretization Grid

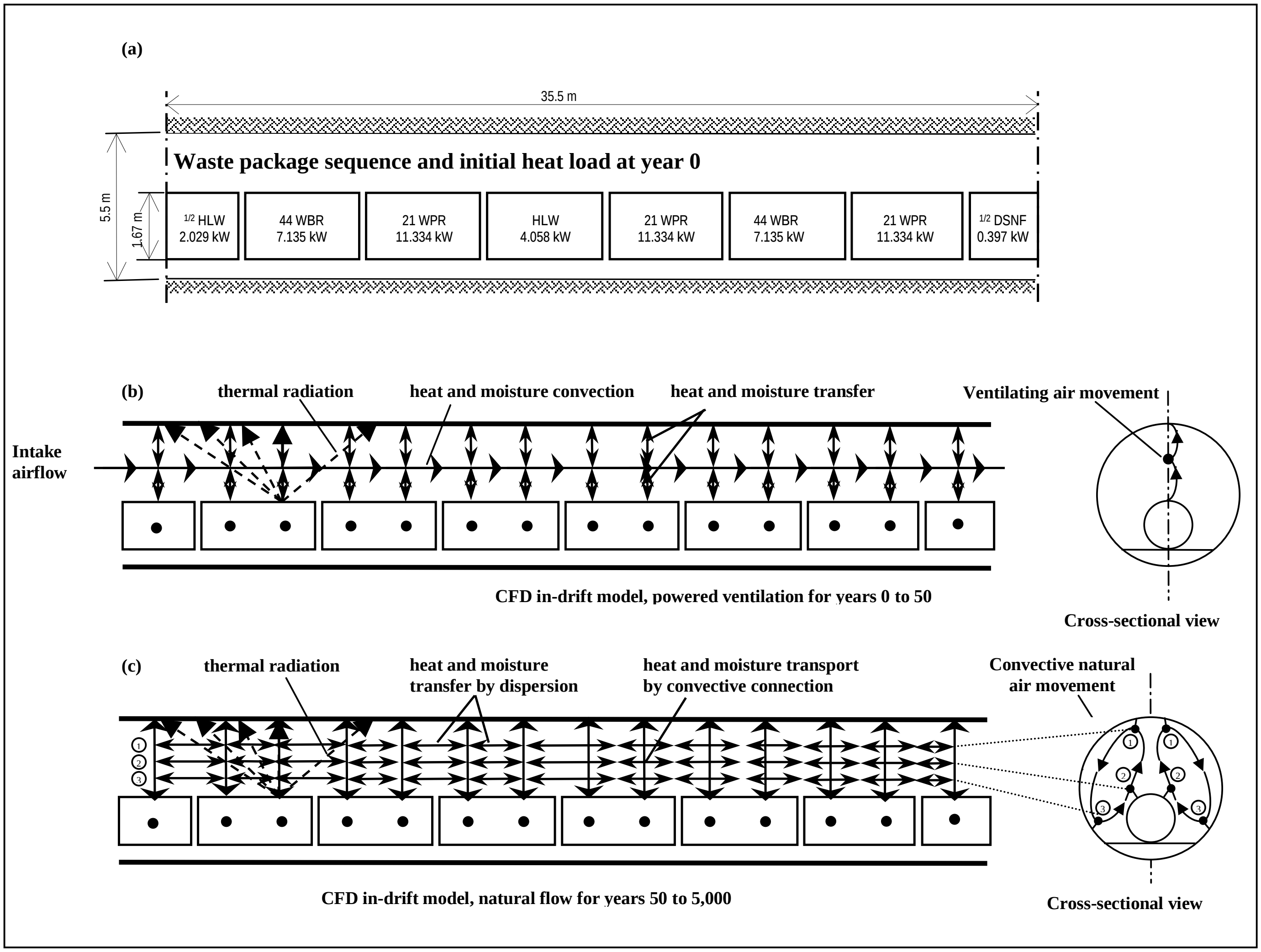


Figure 2-4
Computational Fluid Dynamics Model Configuration in the Airway Showing
Repeated Sequence of Eight Waste Packages in an Emplacement Drift (a),
Schematic Diagram of Pre-Closure Powered Ventilation (b),
and Schematic Diagram of Post-closure Natural Air Movement with Axial Dispersion (c)

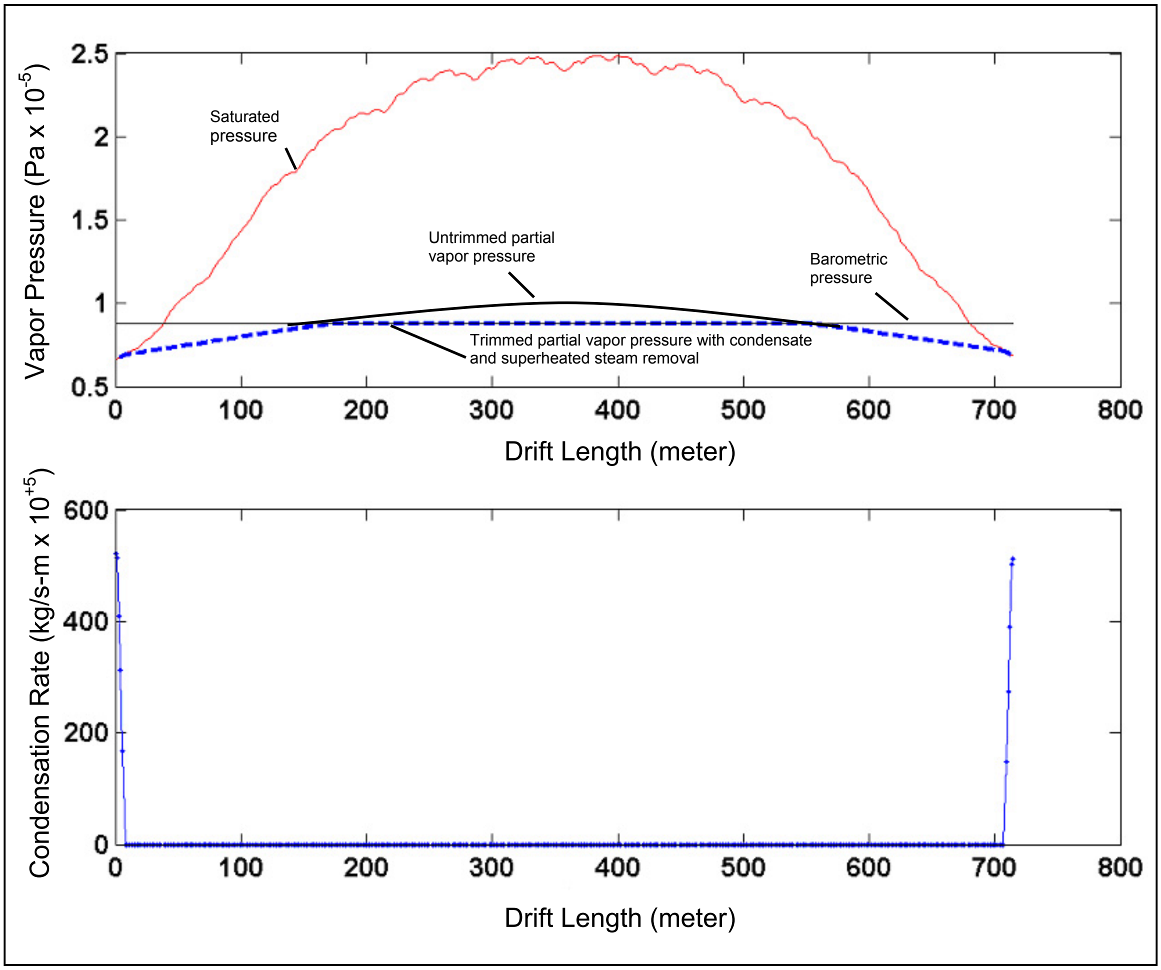


Figure 2-5
Condensation based on Partial Vapor Pressure Trimming at Year 750

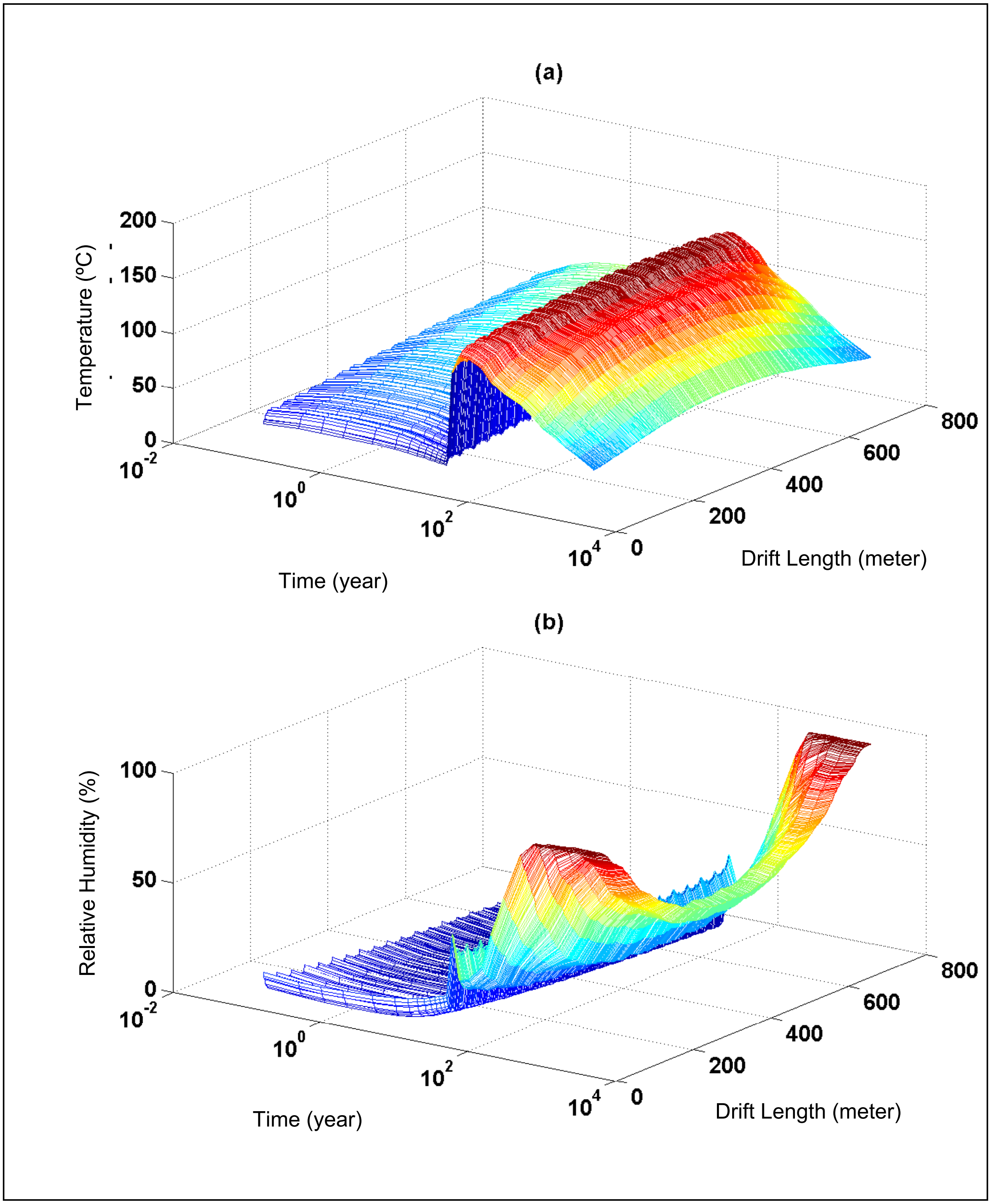


Figure 2-6
Drift Wall Temperature (a)
and Relative Humidity Distributions (b)
in Time and Space

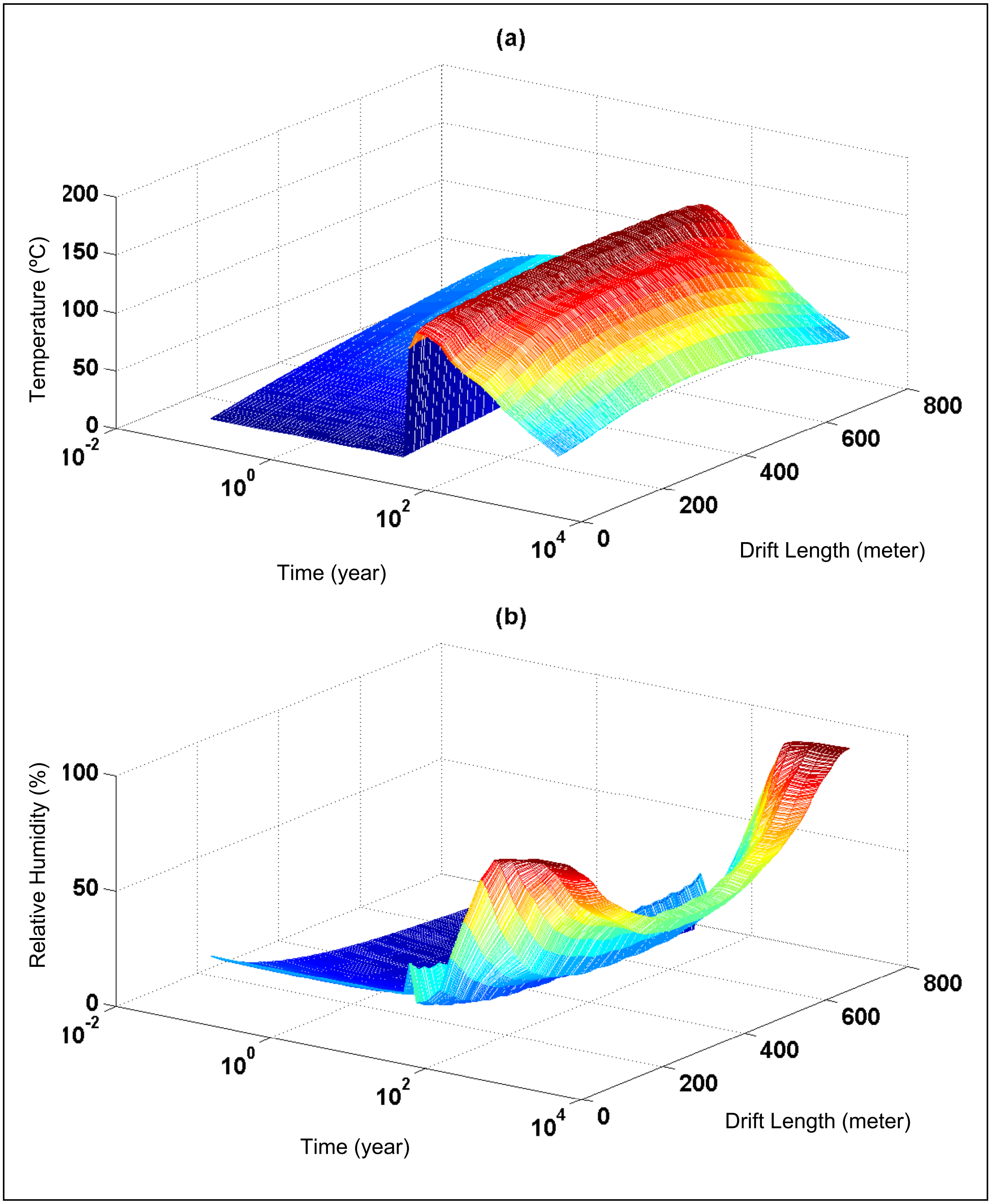


Figure 2-7
Drift Air Temperature (a)
and Relative Humidity Distributions (b)
in Time and Space

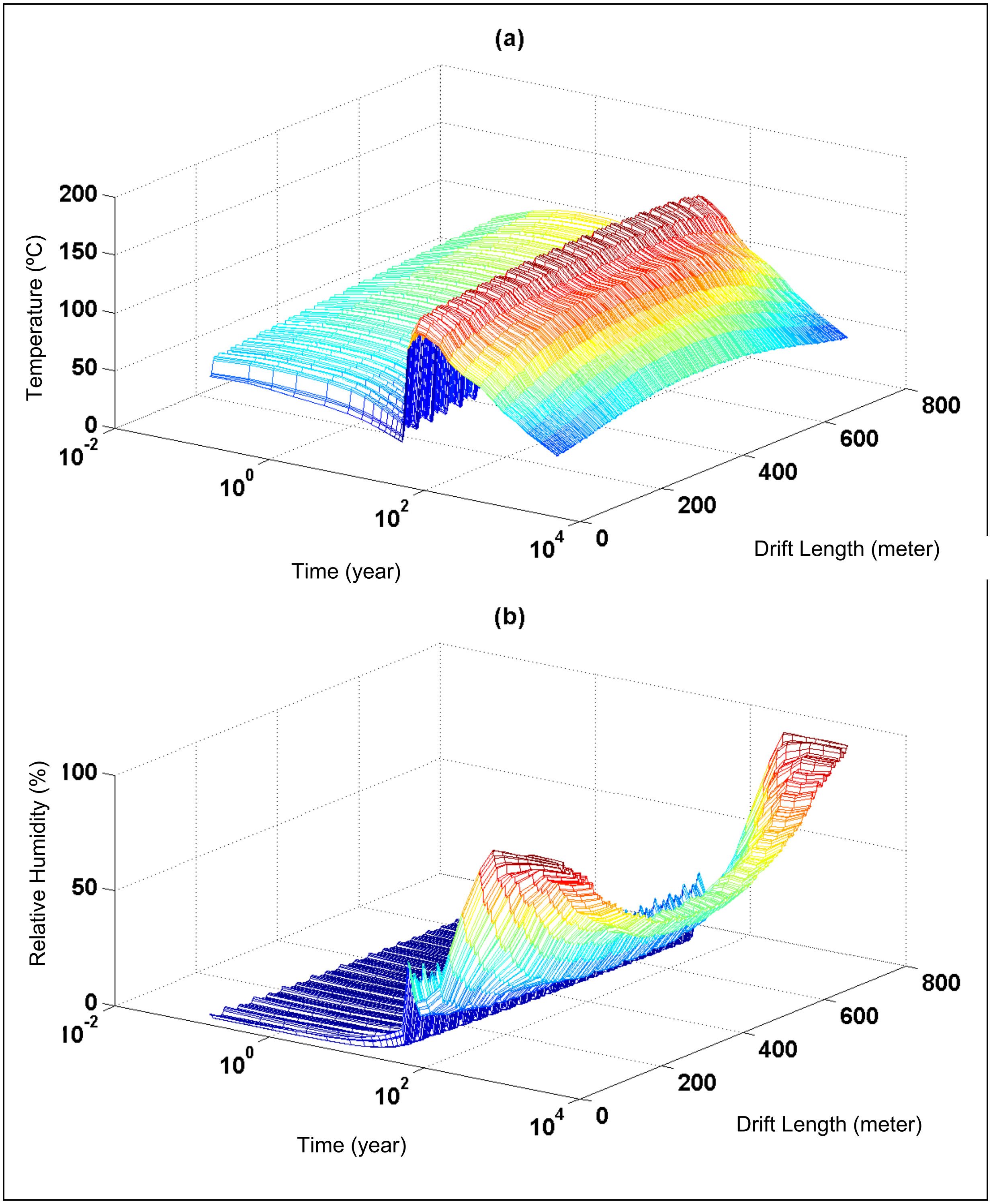


Figure 2-8
Drift Centerline Temperature (a)
and Relative Humidity Distributions (b)
in Time and Space

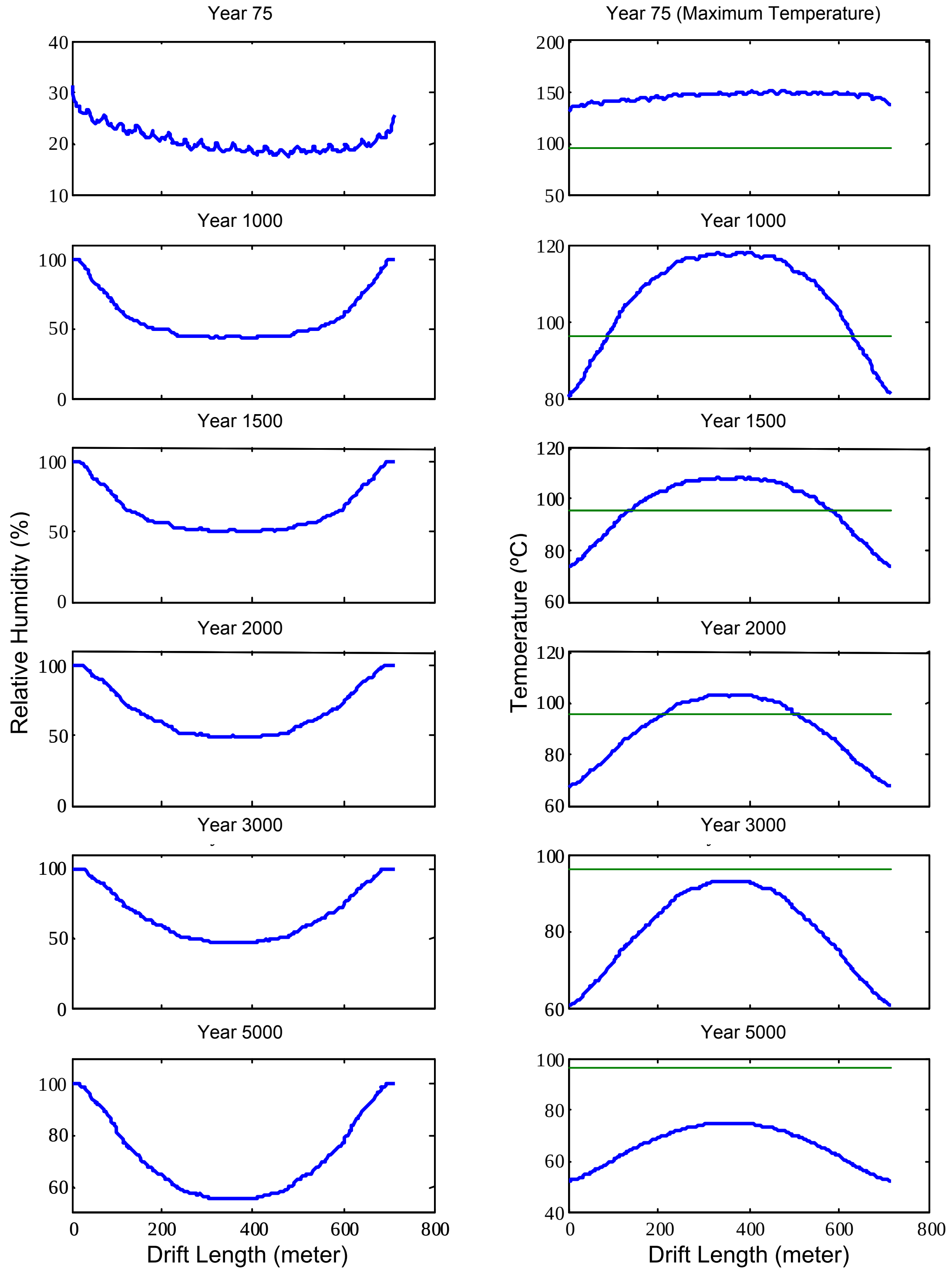


Note: Drift axial dispersion coefficient = 0.1 $m^2/s$; horizontal line in temperature profiles represents boiling temperature of water at 96 °C.

Figure 2-9
Axial Distribution of Drift Wall Relative Humidity and Temperature at Selected Post-Closure Time Divisions

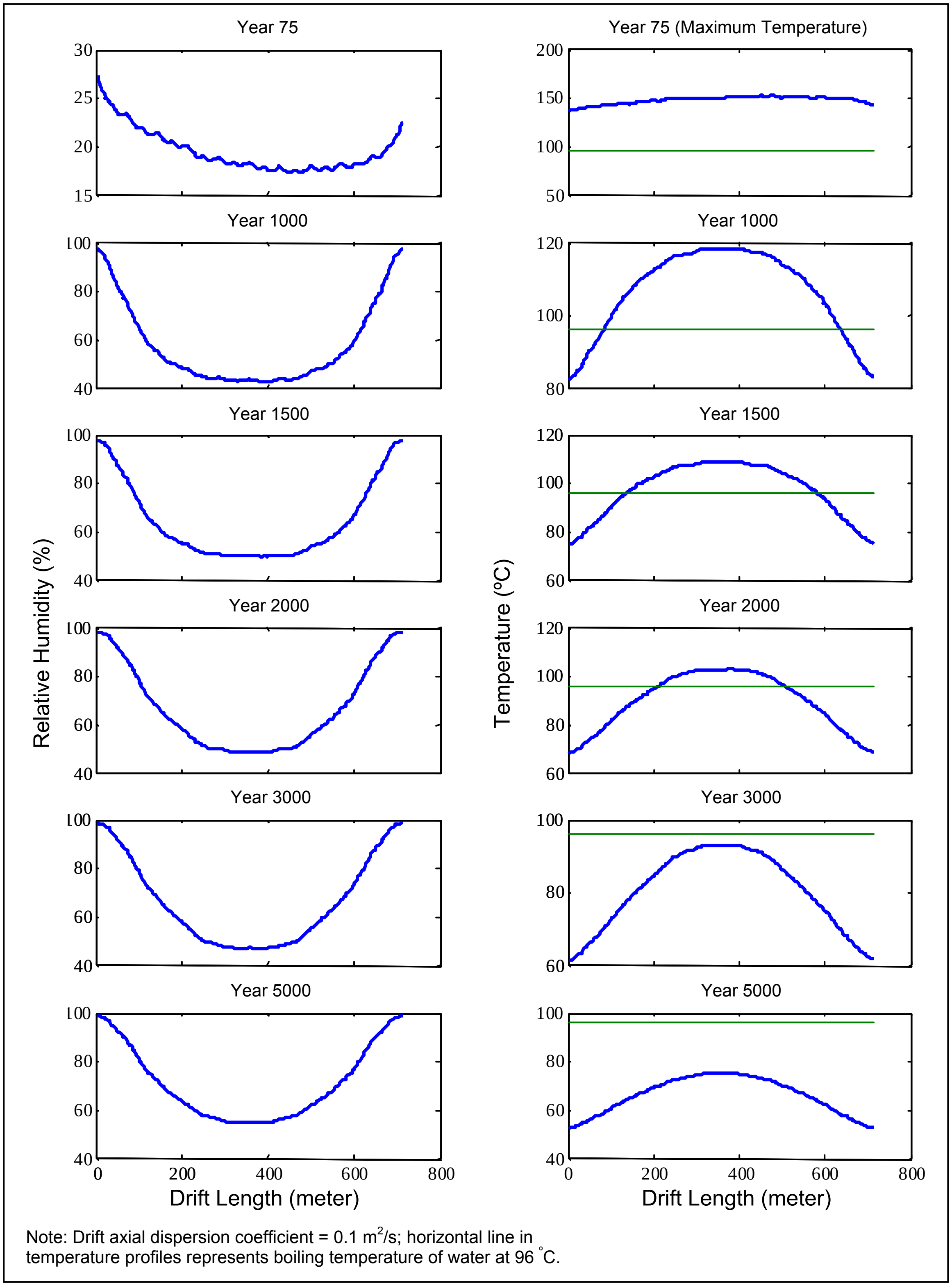


Figure 2-10
Axial Distribution of Drift Air Relative Humidity and Temperature
at Selected Post-Closure Time Divisions

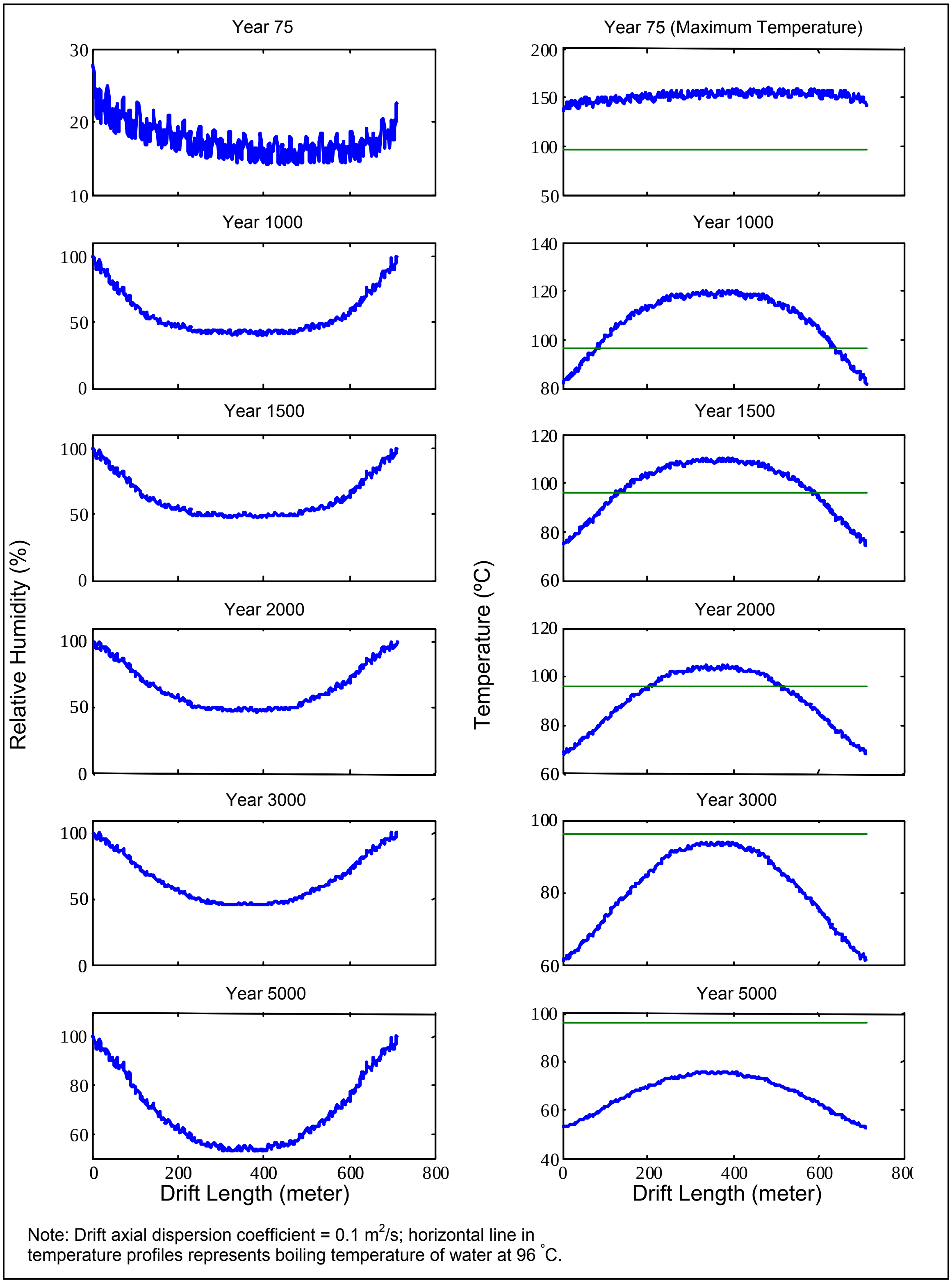


Figure 2-11
Axial Distribution of Drift Centerline Relative Humidity and Temperature
at Selected Post-Closure Time Divisions

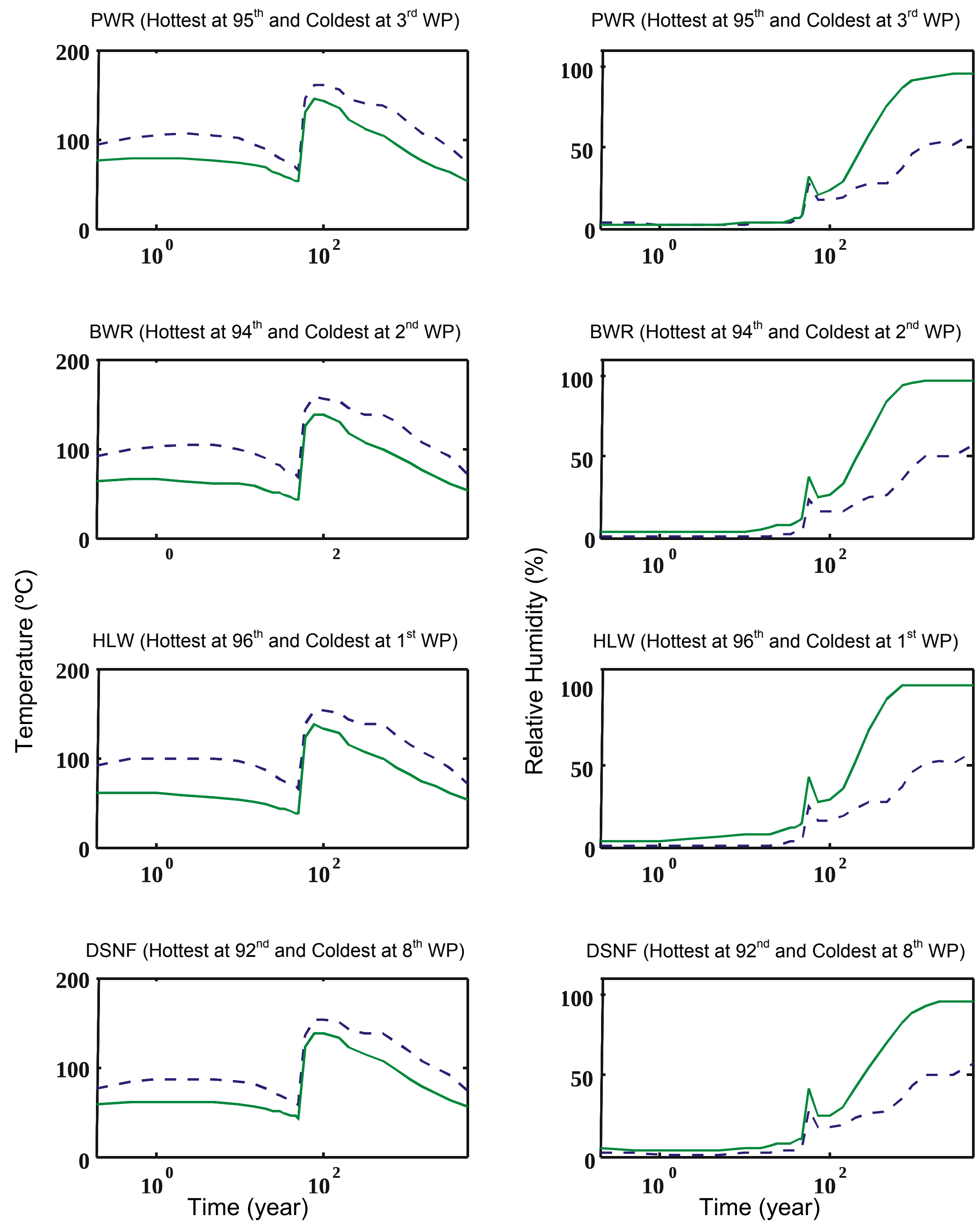


PWR = Pressurized water reactor waste.
BWR = Boiling water reactor waste.
HLW = High-level waste.
DSNF = Defense spent nuclear fuel.
WP = Waste package.

Hottest package (dashed line)
Coldest package (solid line)

Note: Drift axial dispersion coefficient = 0.1 $m^2/s$; horizontal line in temperature profiles represents boiling temperature of water at 96 °C.

Figure 2-12
Waste Package Surface Temperature and Relative Humidity versus Time

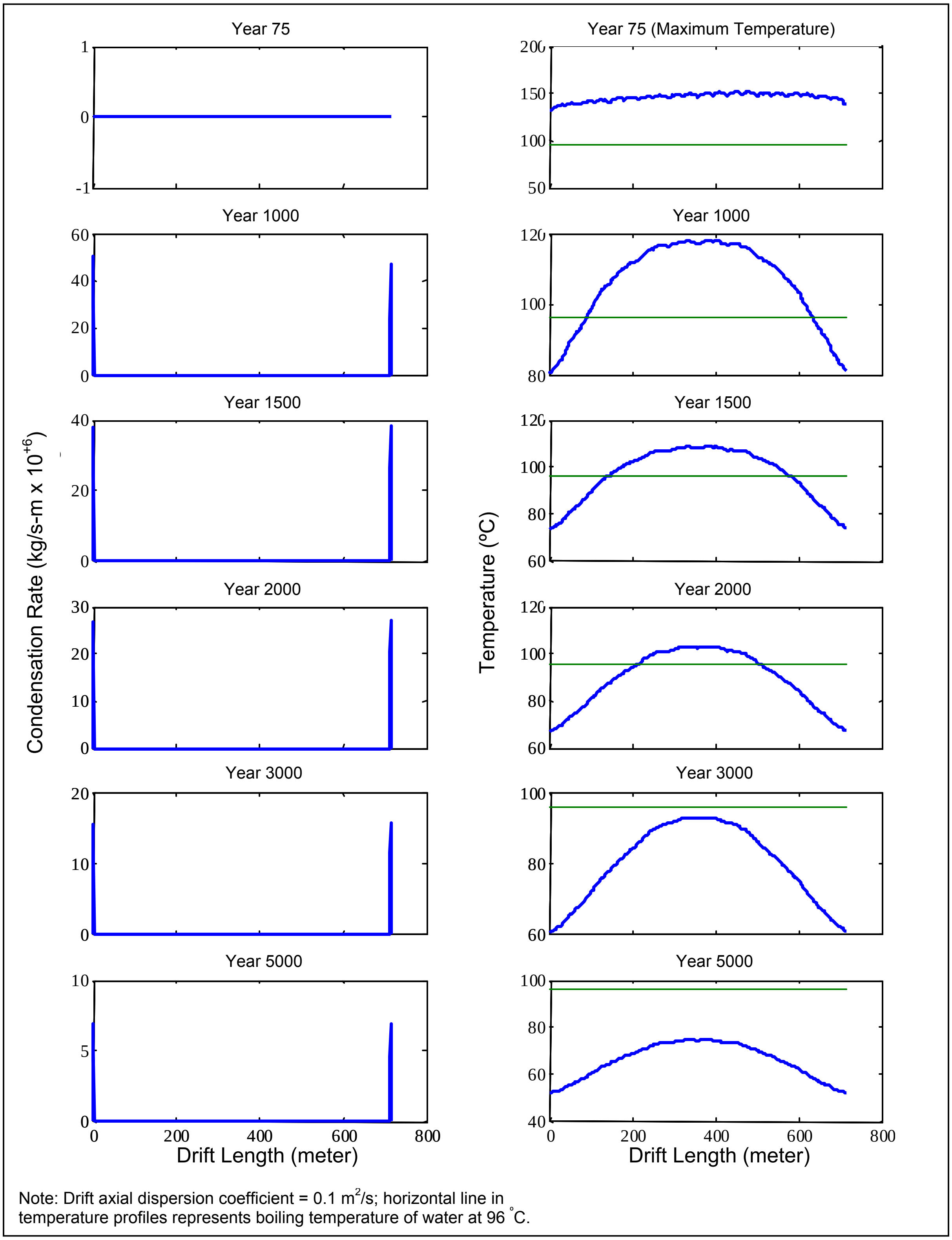


Figure 2-13
Axial Distribution of Drift Centerline Condensation Rate and Temperature
at Selected Post-Closure Time Divisions

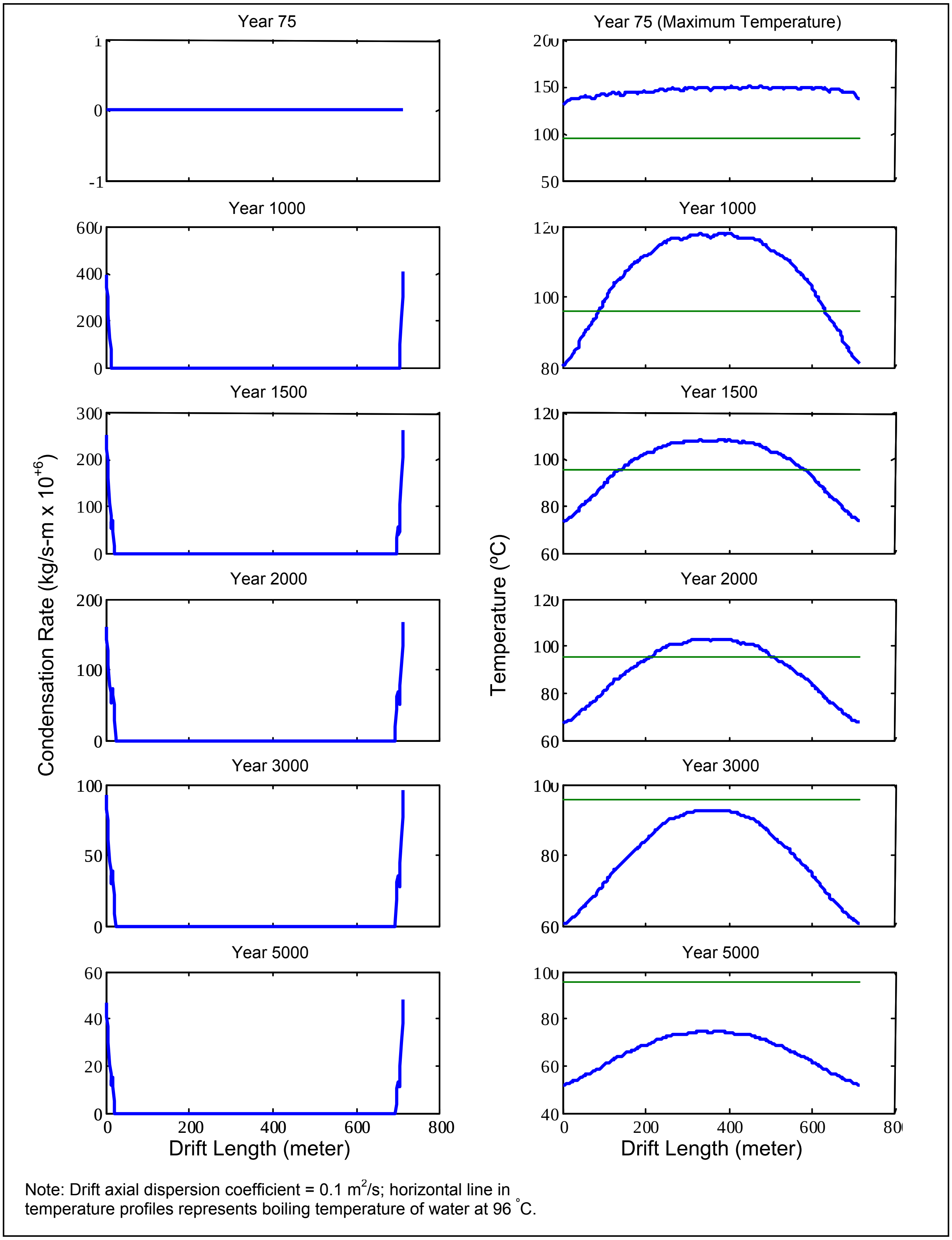


Figure 2-14
Axial Distribution of Drift Wall Condensation Rate and Temperature at Selected Post-Closure Time Divisions

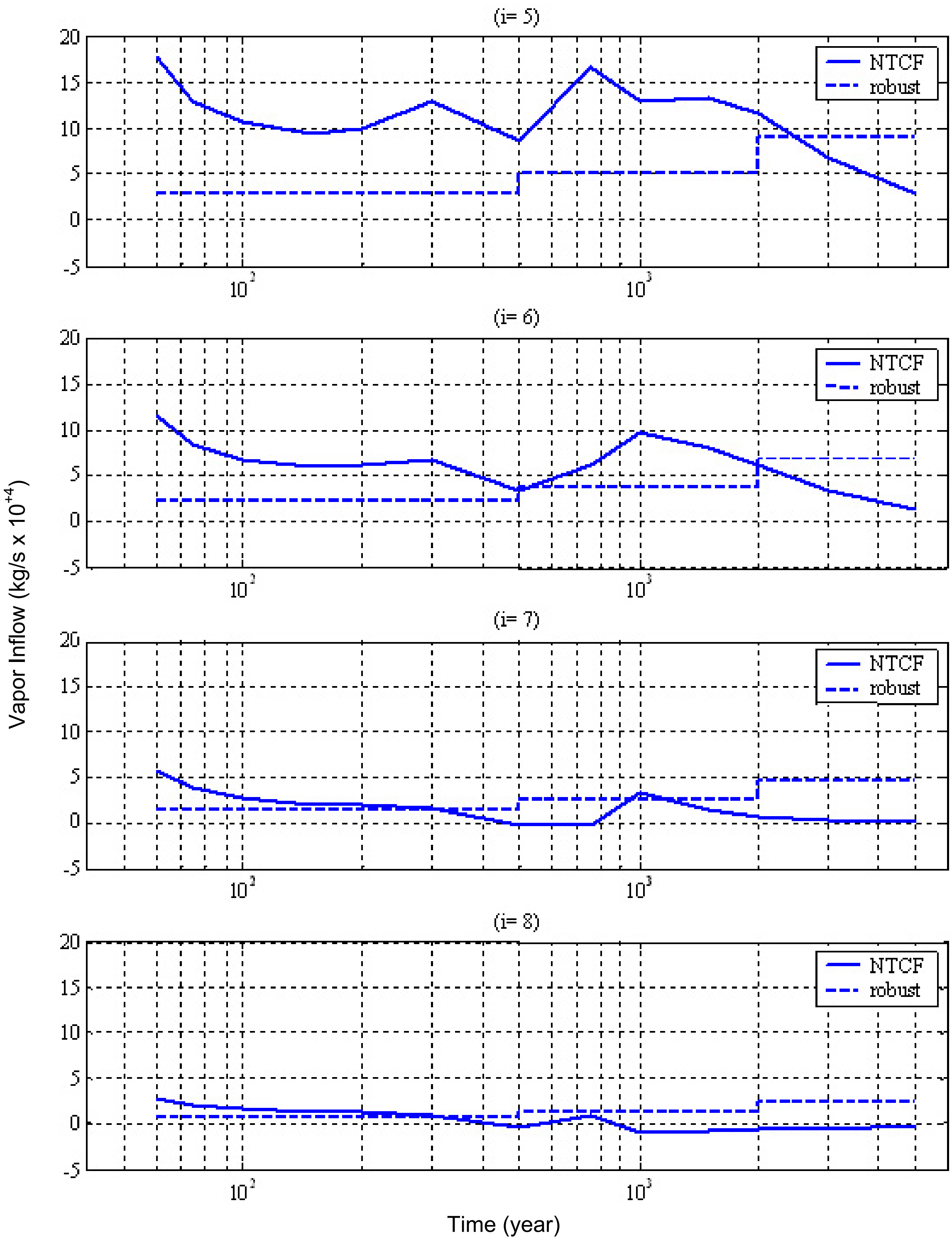


NTCF = Numerical transport code functionalization.
Note: Drift axial dispersion coefficient = 0.1 $m^2/s$.

Figure 2-15
Comparison of Vapor Inflow Rates versus Time for
Robust Moisture Transport and Numerical Transport Code Functionalization Models

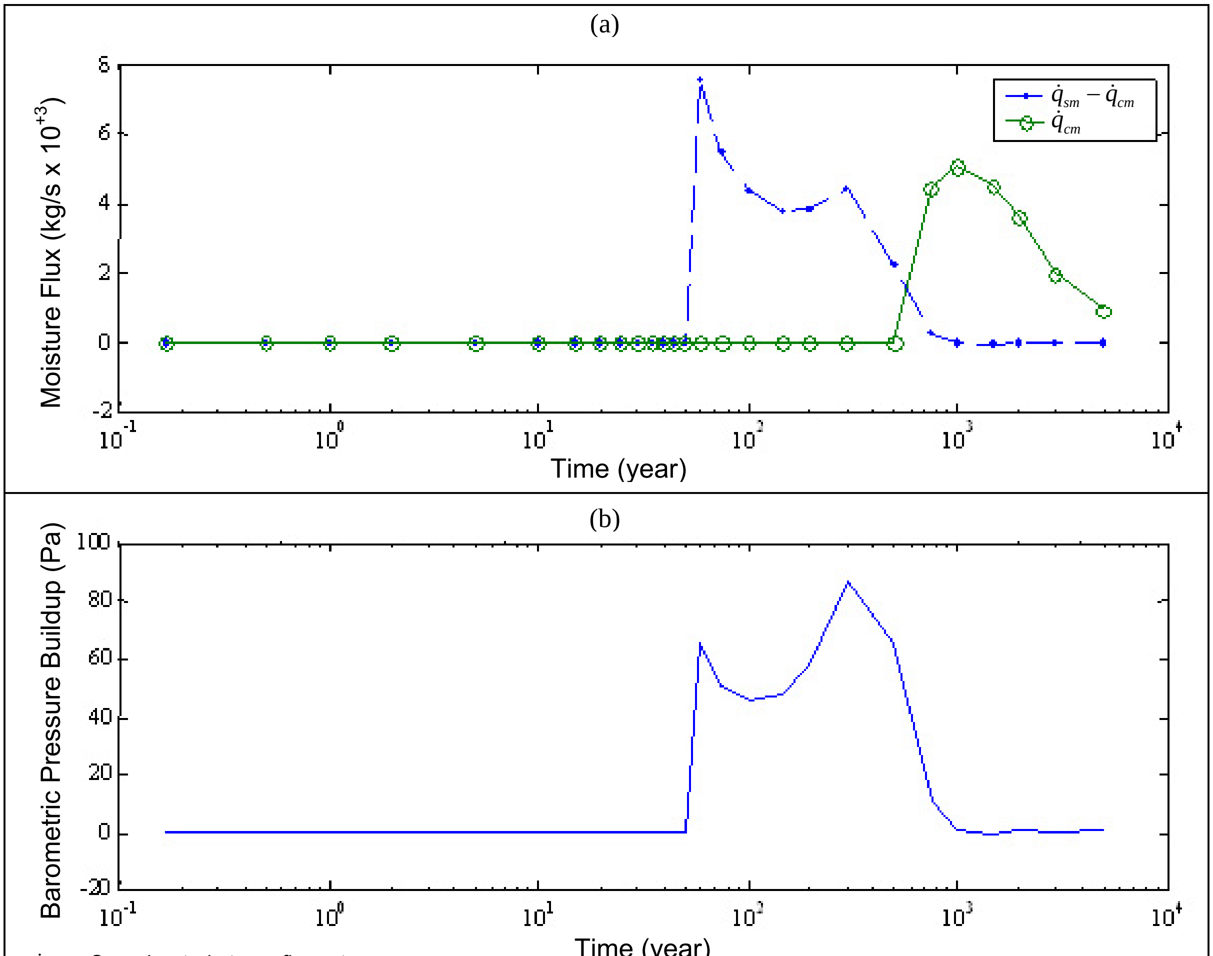


$\dot{q}_{sm}$= Superheated steam flux rate.

$\dot{q}_{cm}$ = Condensation flux rate.

Note: Drift axial dispersion coefficient = 0.1 m$^2$/s.

Figure 2-16
Superheated Steam and Condensation Flux Rates in the Emplacement Drift versus Time from the Computational Fluid Dynamics Solution (a) and Total Barometric Pressure Buildup in the Drift to Discharge the Excess Steam into the Unheated Rockmass in the Horizontal Direction (b)

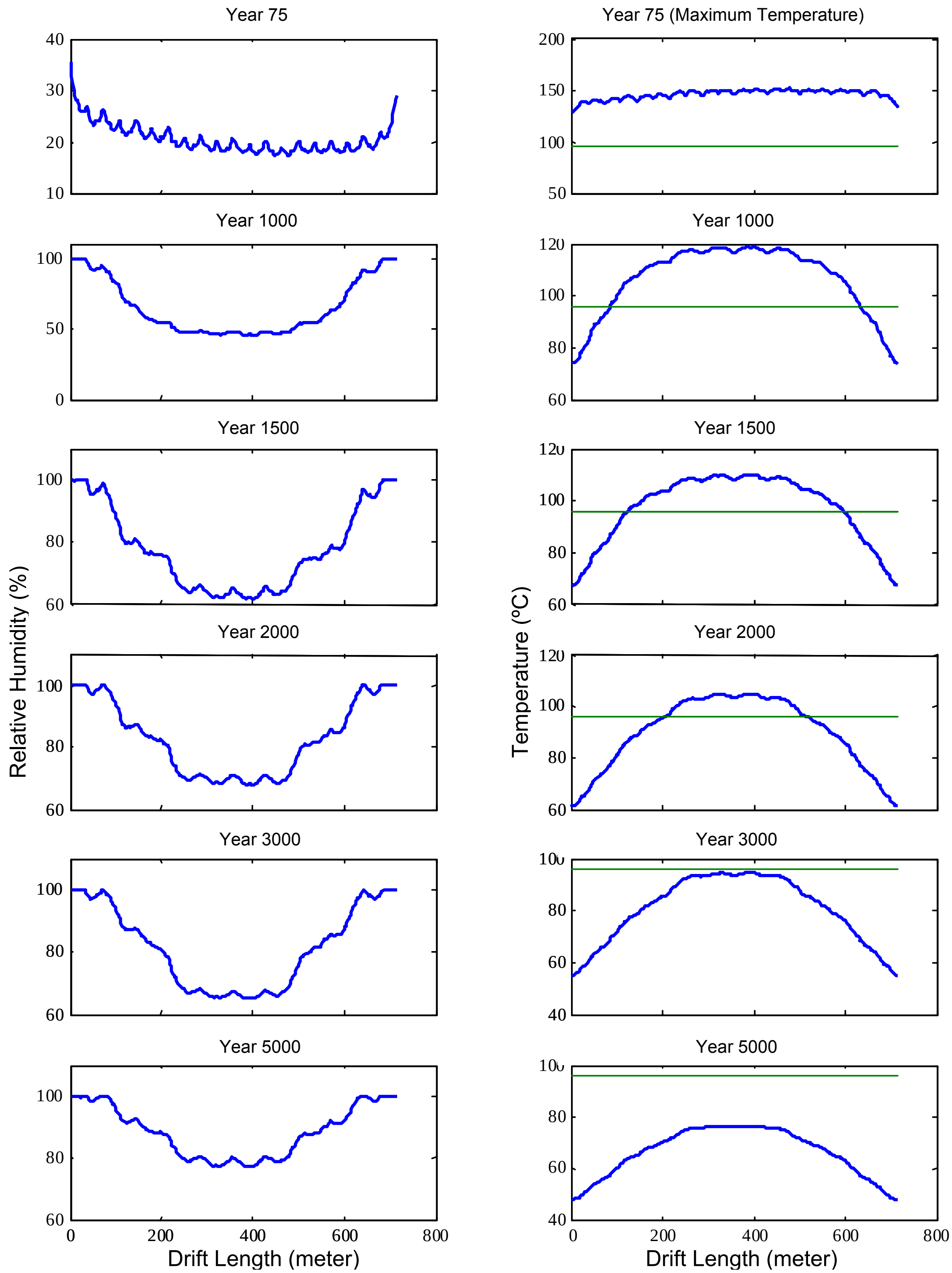


Note: Drift axial dispersion coefficient = 0.004 $m^2/s$; horizontal line in temperature profiles represents boiling temperature of water at 96 °C.

Figure 2-17
Axial Distribution of Drift Wall Relative Humidity and Temperature
at Selected Post-Closure Time Divisions

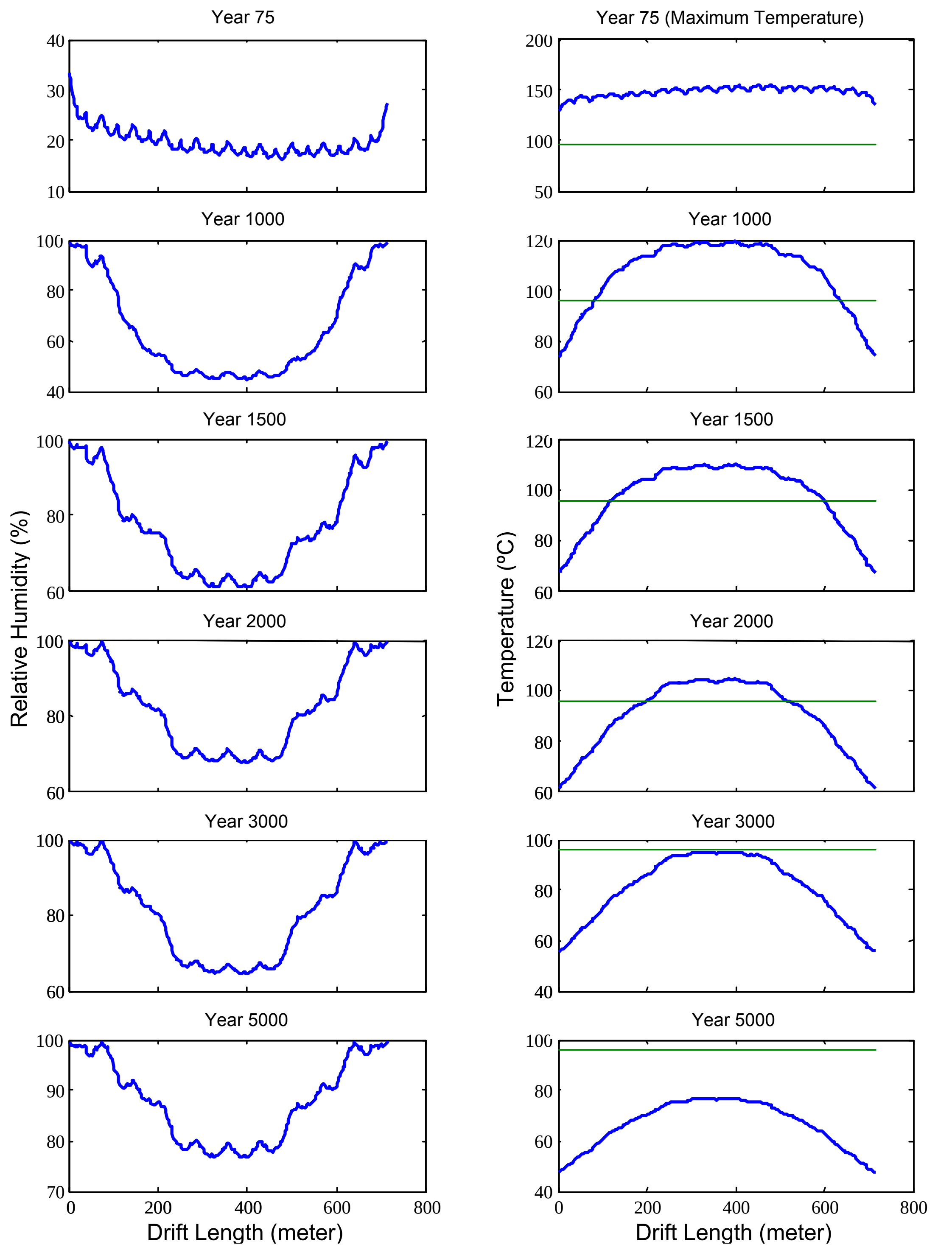


Note: Drift axial dispersion coefficient = 0.004 $m^2/s$; horizontal line in temperature profiles represents boiling temperature of water at 96 °C.

Figure 2-18
Axial Distribution of Drift Air Relative Humidity and Temperature
at Selected Post-Closure Time Divisions

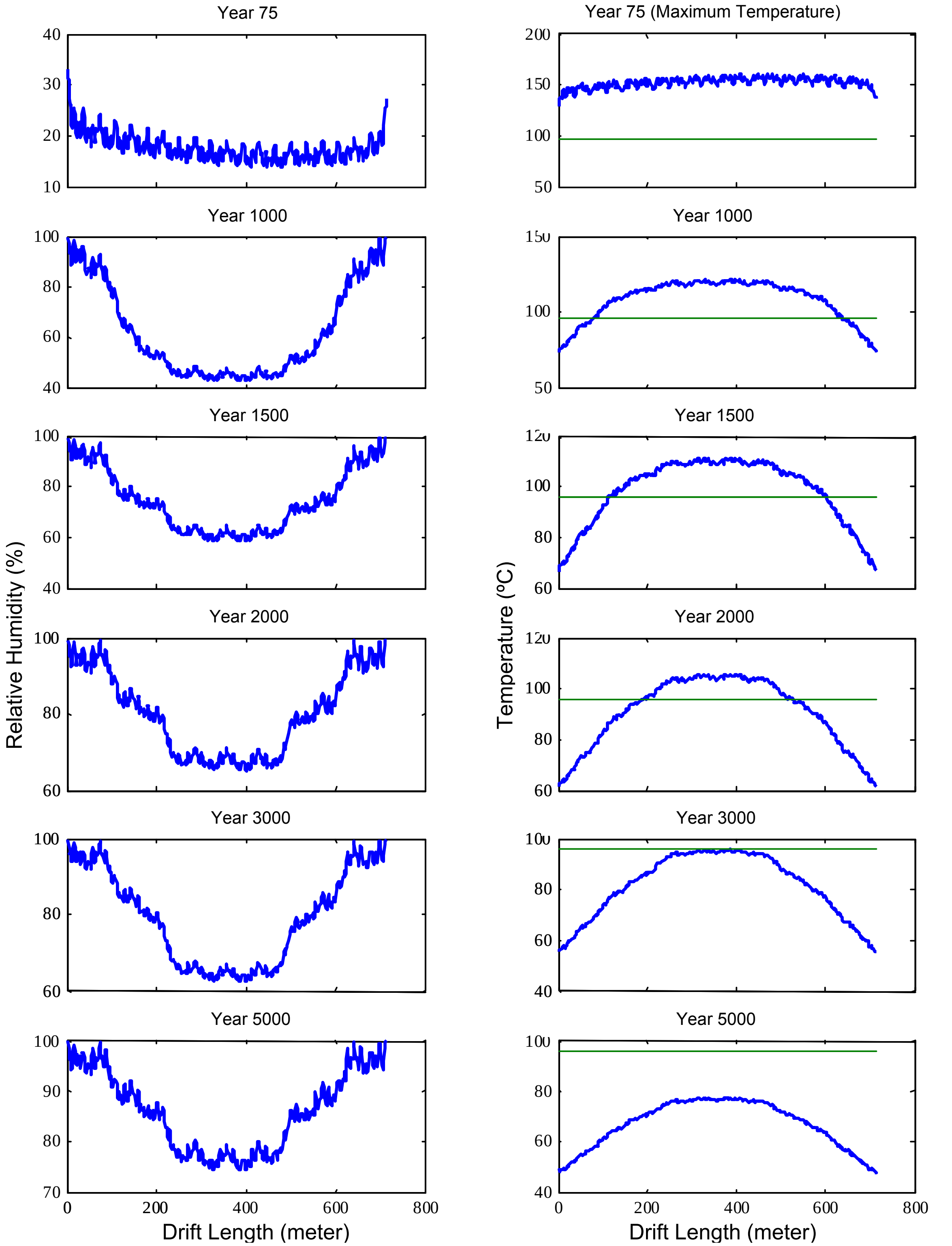


Note: Drift axial dispersion coefficient = 0.004 m²/s; horizontal line in temperature profiles represents boiling temperature of water at 96 °C.

Figure 2-19
Axial Distribution of Drift Centerline Relative Humidity and Temperature
at Selected Post-Closure Time Divisions

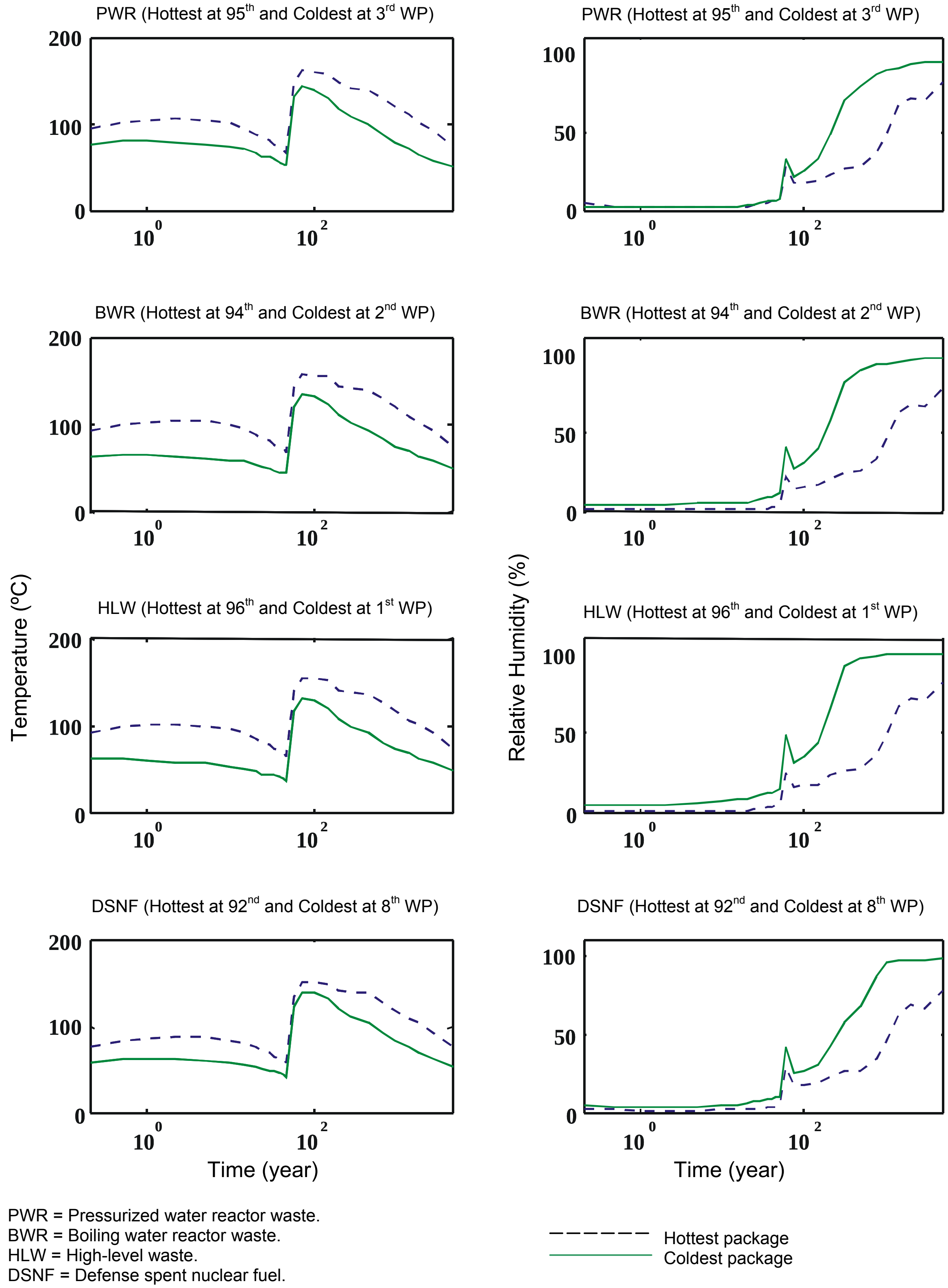


PWR = Pressurized water reactor waste.
BWR = Boiling water reactor waste.
HLW = High-level waste.
DSNF = Defense spent nuclear fuel.
WP = Waste package.

Note: Drift axial dispersion coefficient = 0.004 $m^2$/s; hottest and coldest packages are represented by dashed and solid lines respectively.

Figure 2-20
Waste Package Surface Temperature and Relative Humidity versus Time

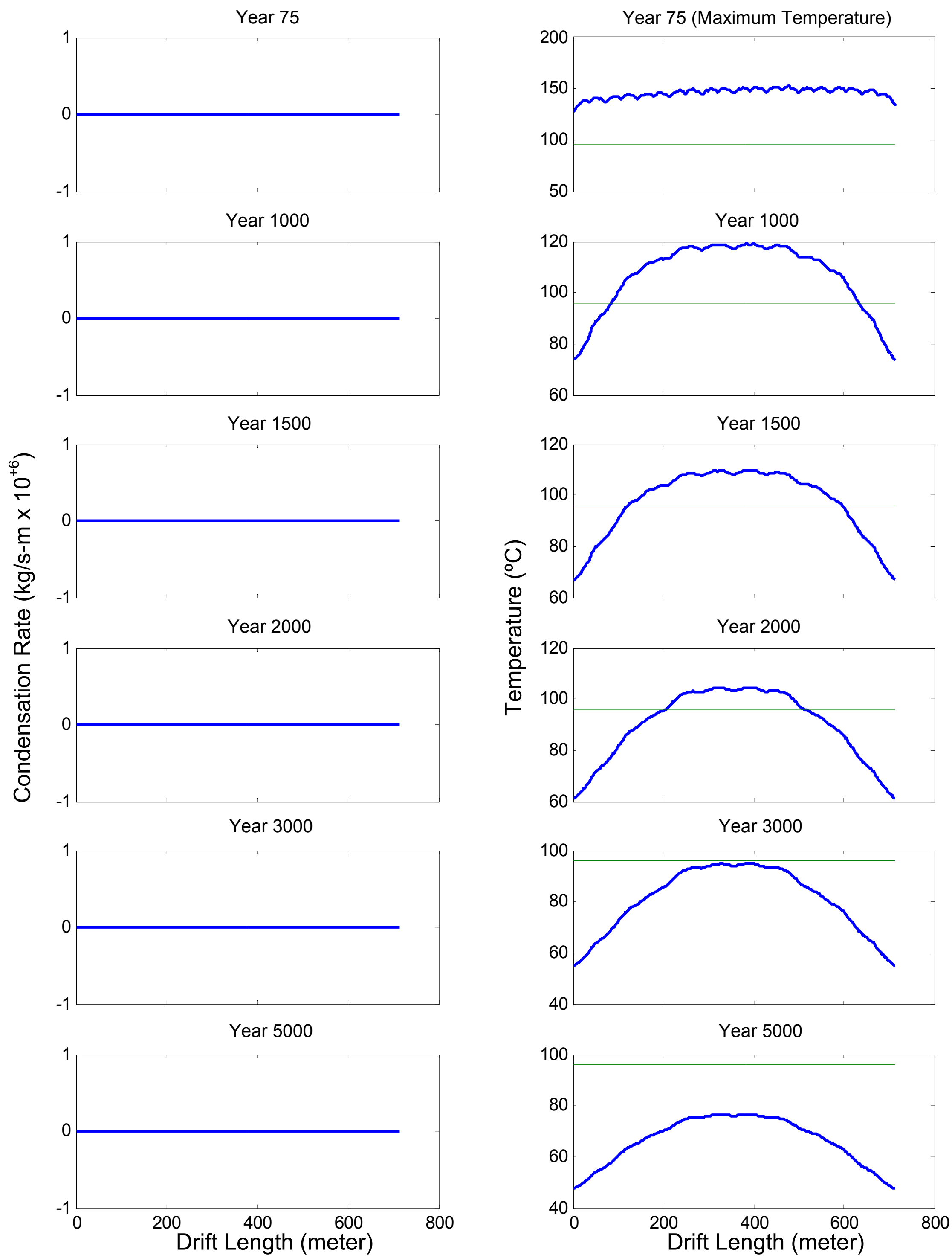


Note: Drift axial dispersion coefficient = 0. 004 $m^2/s$; horizontal line in temperature profiles represents boiling temperature of water at 96 ˚C.

Figure 2-21
Axial Distribution of Drift Centerline Condensation Rate and Temperature at Selected Post-Closure Time Divisions

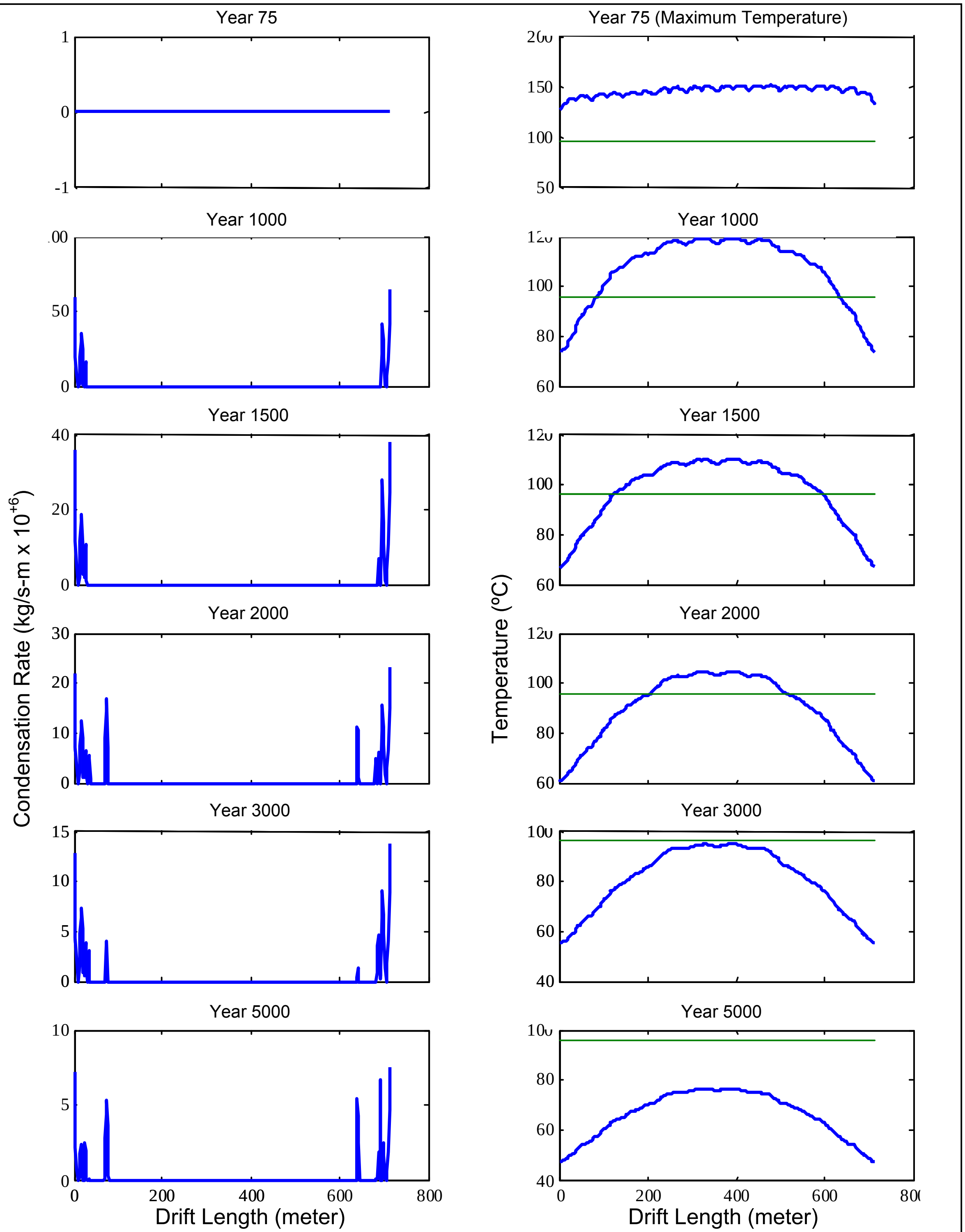


Note: Drift axial dispersion coefficient = 0.004 $m^2/s$; horizontal line in temperature profiles represents boiling temperature of water at 96 °C.

Figure 2-22
Axial Distribution of Drift Wall Condensation Rate and Temperature at Selected Post-Closure Time Divisions

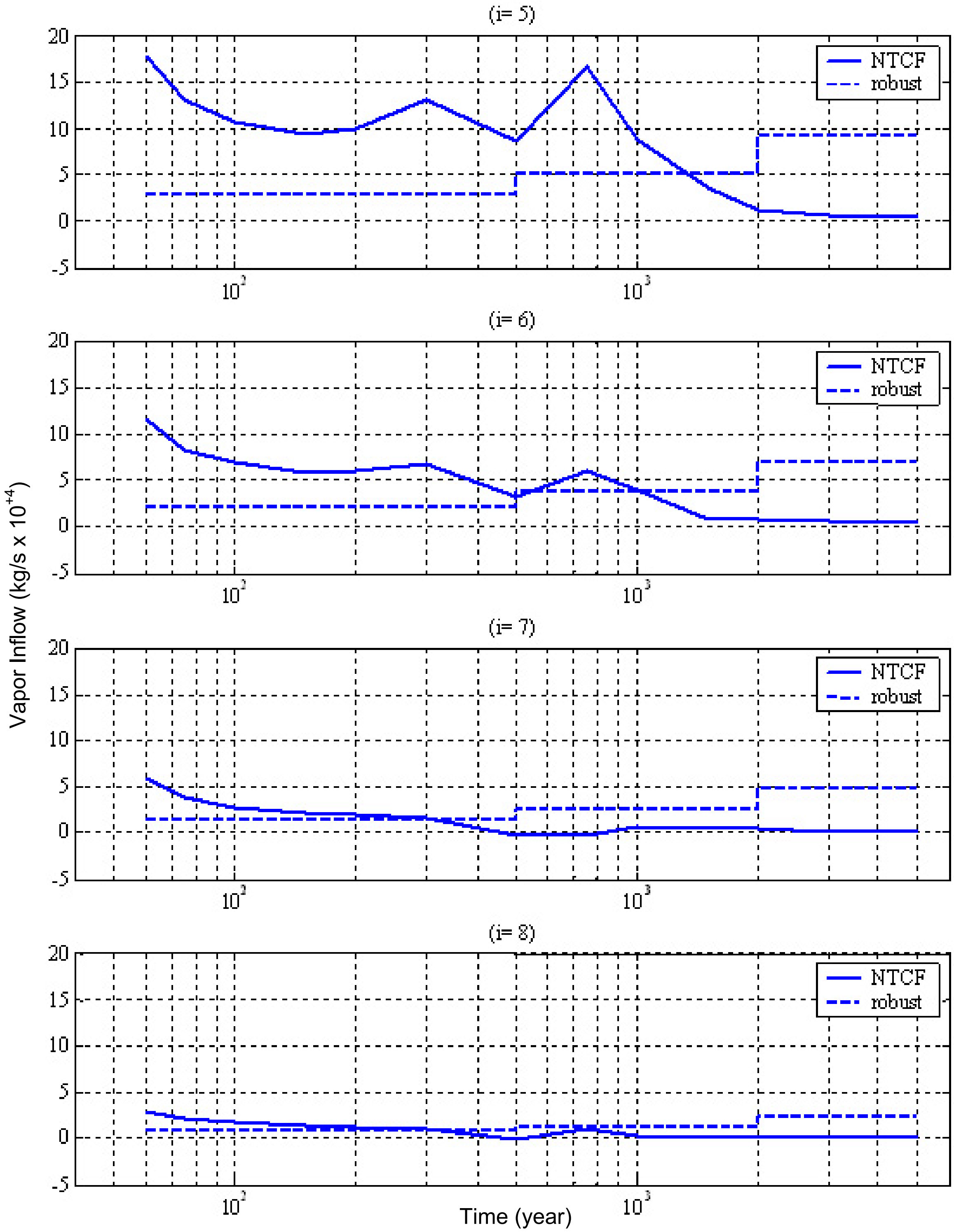


NTCF = Numerical transport code functionalization.
Note: Drift axial dispersion coefficient = 0.004 $m^2$/s.

Figure 2-23
Comparison of Vapor Inflow Rates versus Time for
Robust Moisture Transport and Numerical Transport Code Functionalization Models

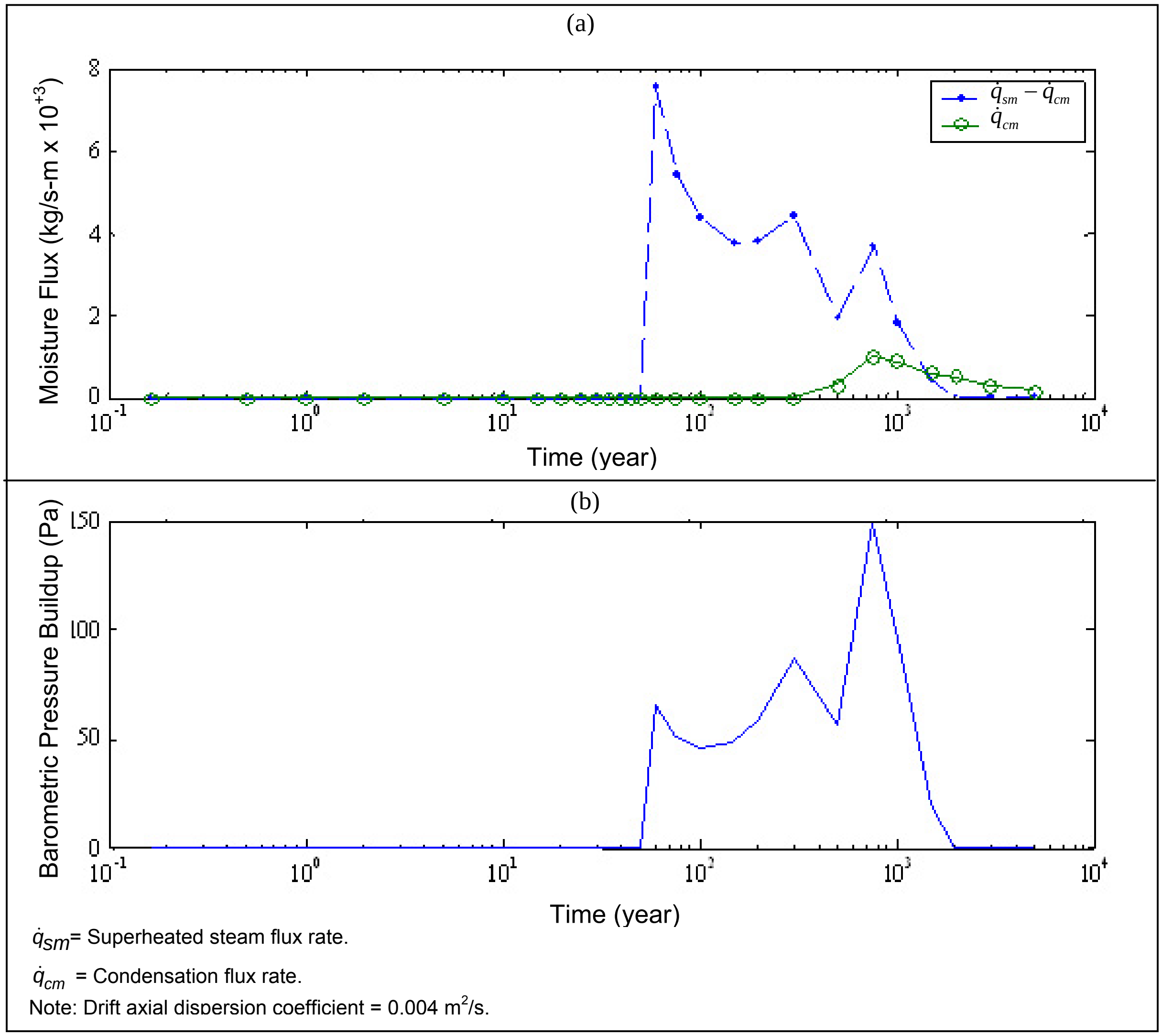


Figure 2-24
Superheated Steam and Condensation Flux Rates in the Emplacement Drift
versus Time from the Computational Fluid Dynamics Solution (a)
and Total Barometric Pressure Buildup in the Drift to Discharge the Excess Steam
into the Unheated Rockmass in the Horizontal Direction (b)

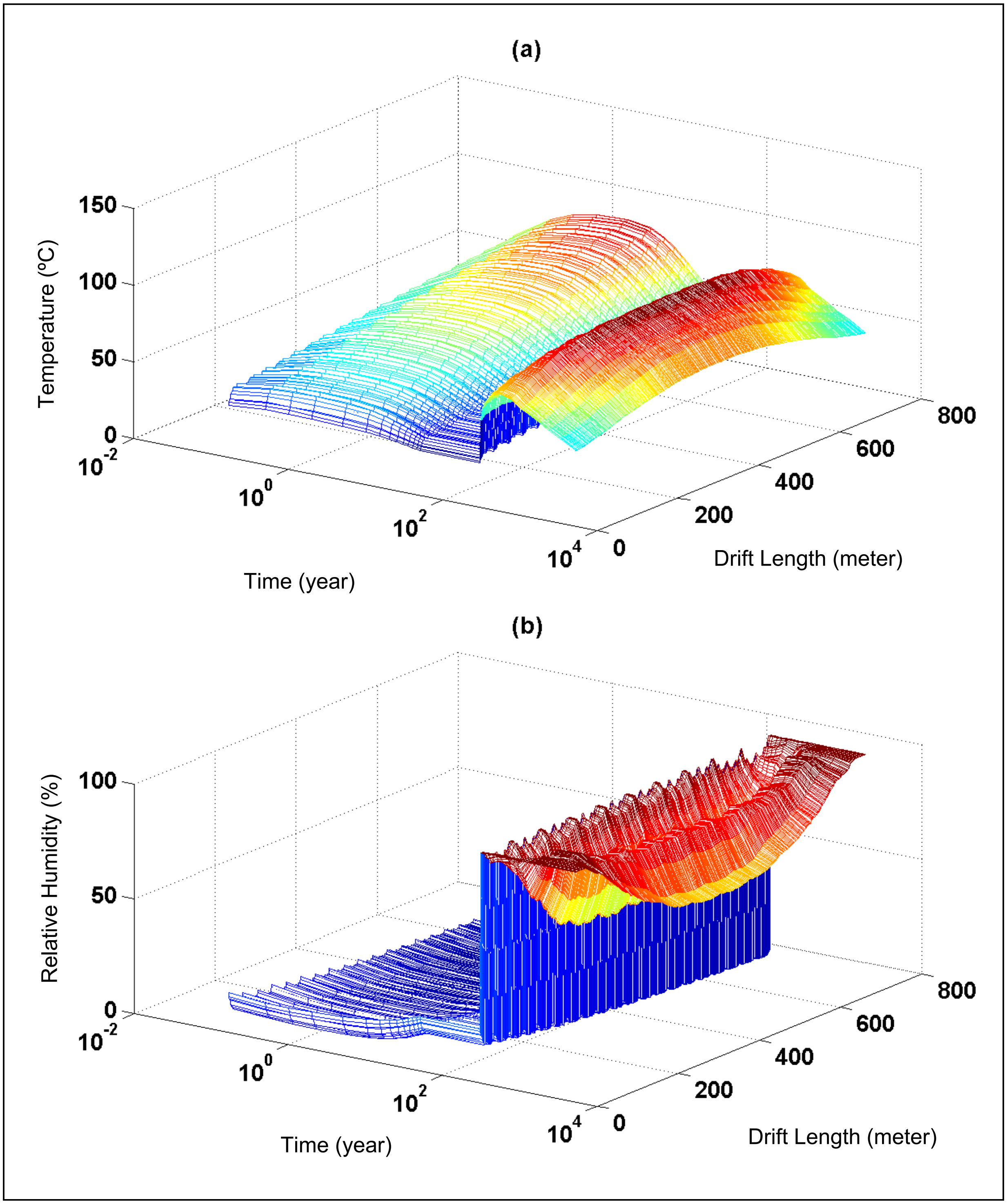


Figure 3-1
Drift Wall Temperature (a)
and Relative Humidity Distributions (b)
in Time and Space with 300-Year Pre-Closure

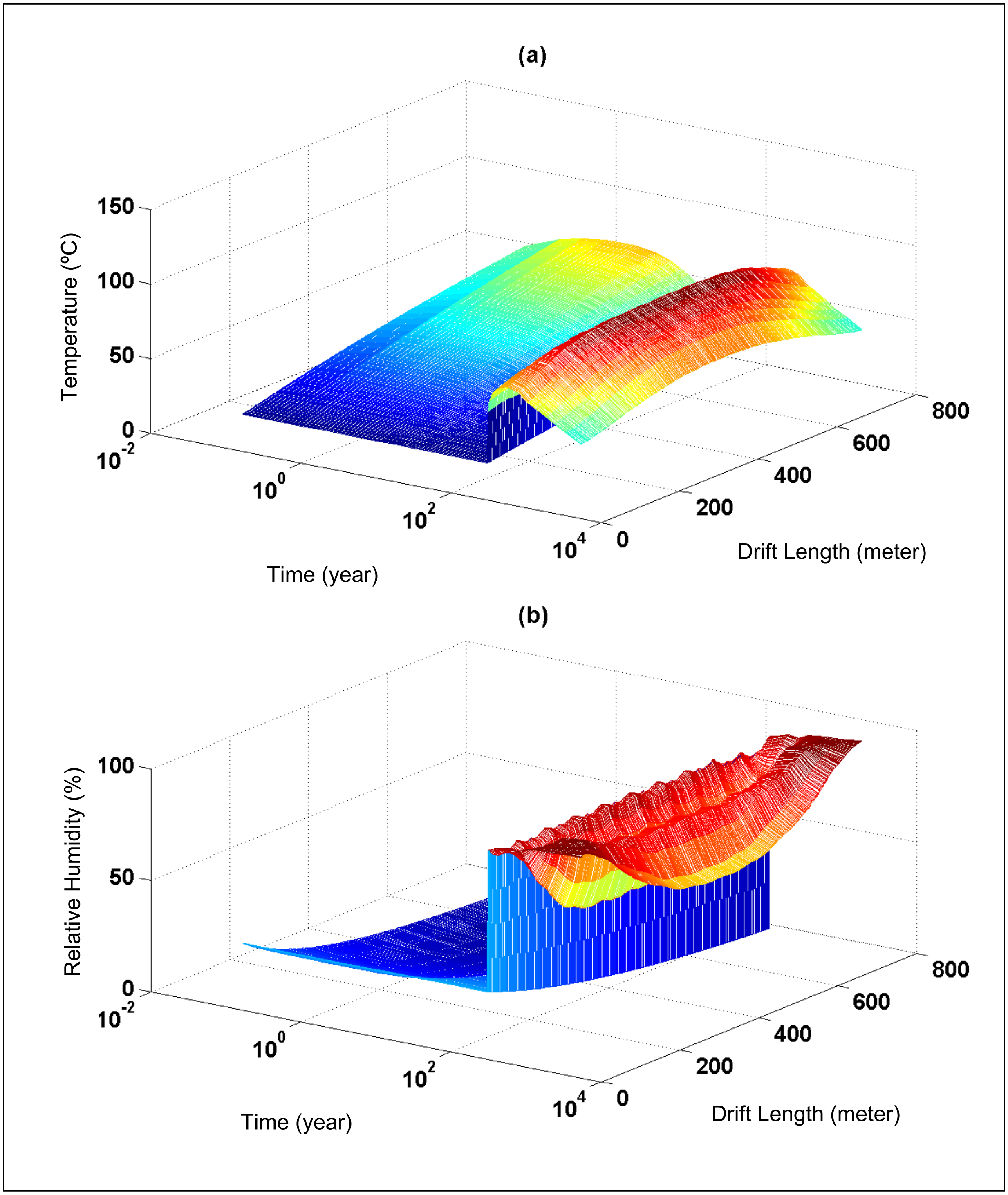


Figure 3-2
Drift Air Temperature (a)
and Relative Humidity Distributions (b)
in Time and Space with 300-Year Pre-Closure

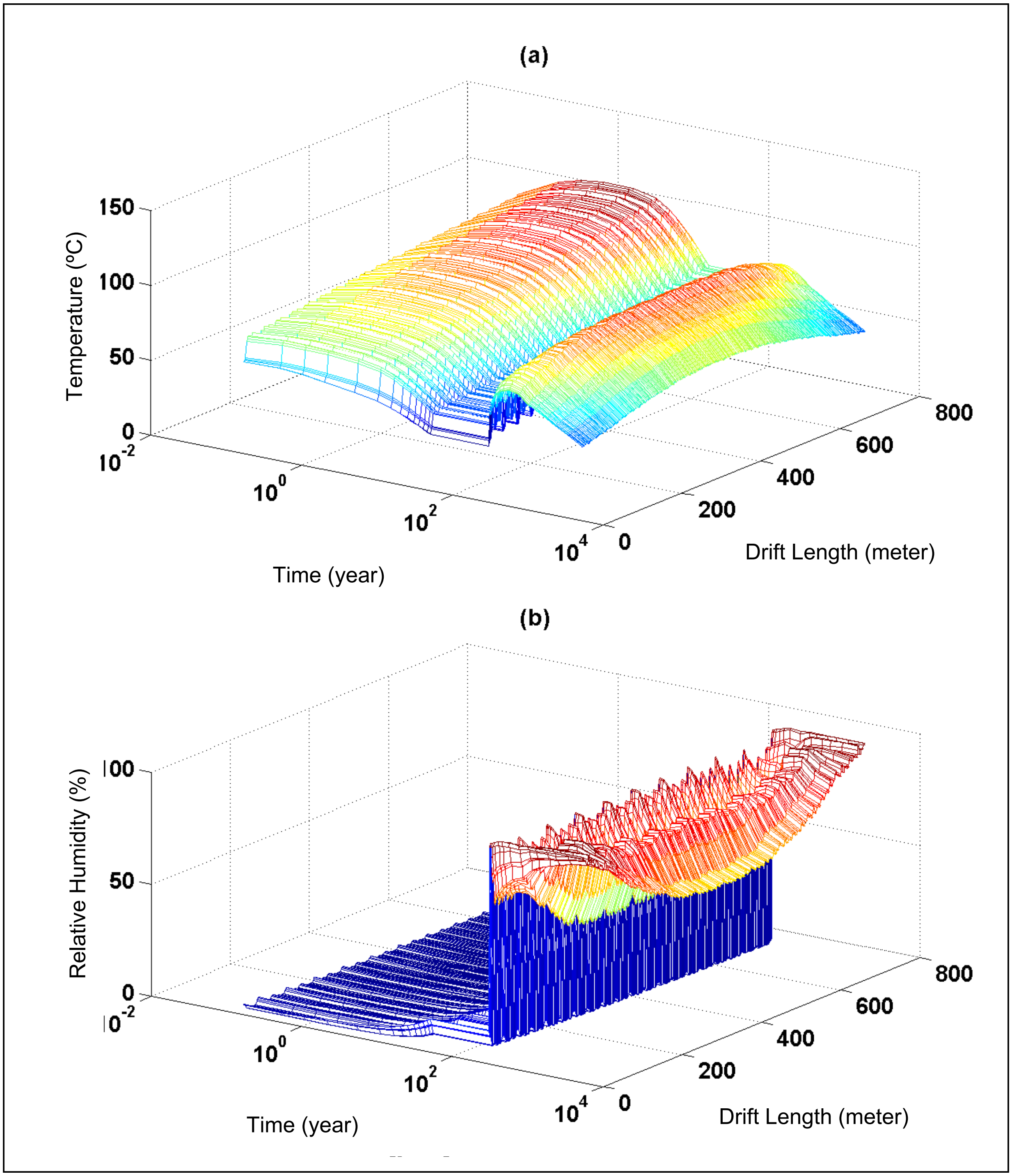


Figure 3-3
Drift Centerline Temperature (a)
and Relative Humidity Distributions (b)
in Time and Space with 300-Year Pre-Closure

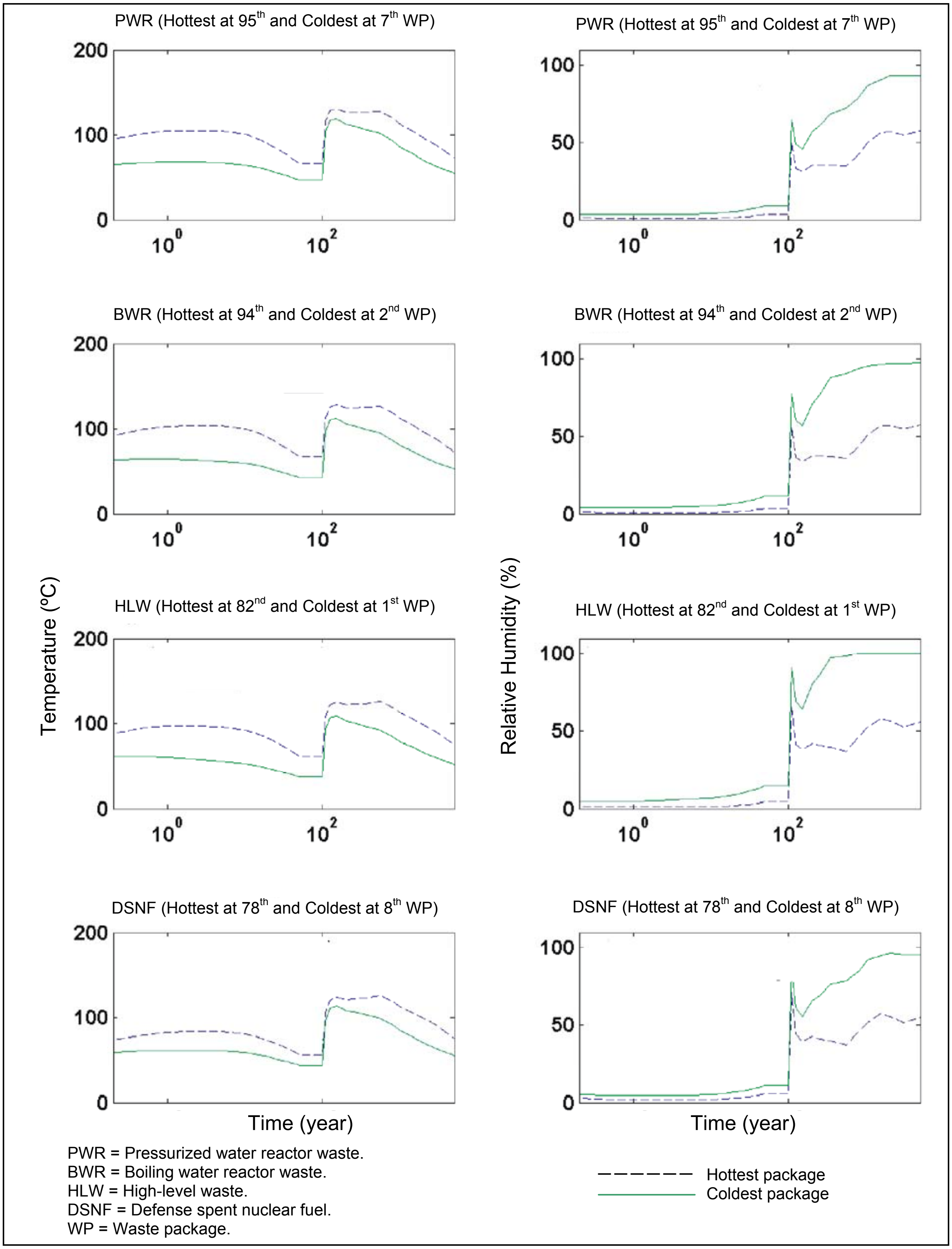


Figure 3-4
Surface Temperature and Relative Humidity versus Time for Hottest and Coldest Waste Package in Each Waste Type, based on 100-Year Pre-Closure Ventilation

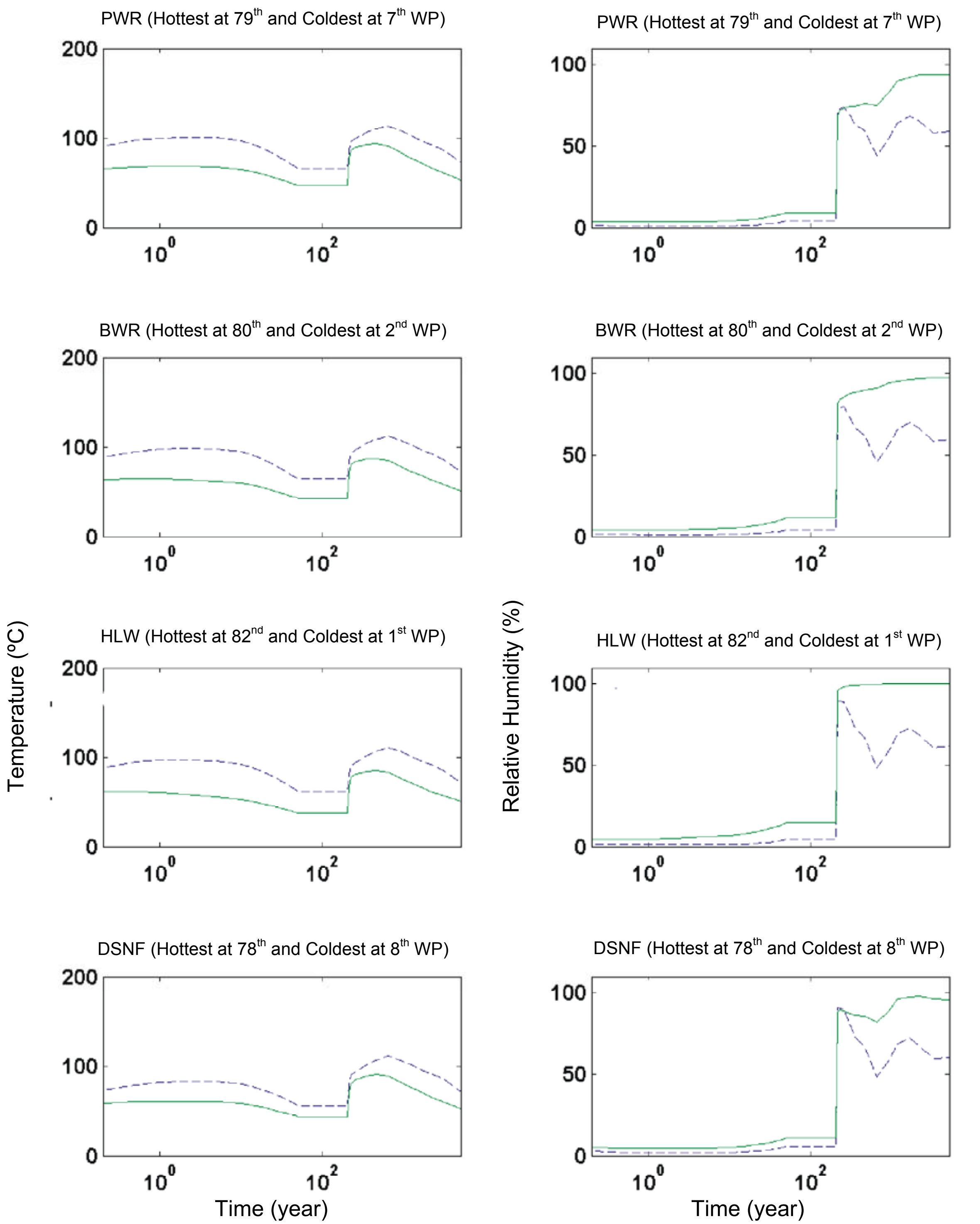


PWR = Pressurized water reactor waste.
BWR = Boiling water reactor waste.
HLW = High-level waste.
DSNF = Defense spent nuclear fuel.
WP = Waste package.

Figure 3-5
Surface Temperature and Relative Humidity versus Time for Hottest and Coldest Waste Package in Each Waste Type, based on 200-Year Pre-Closure Ventilation

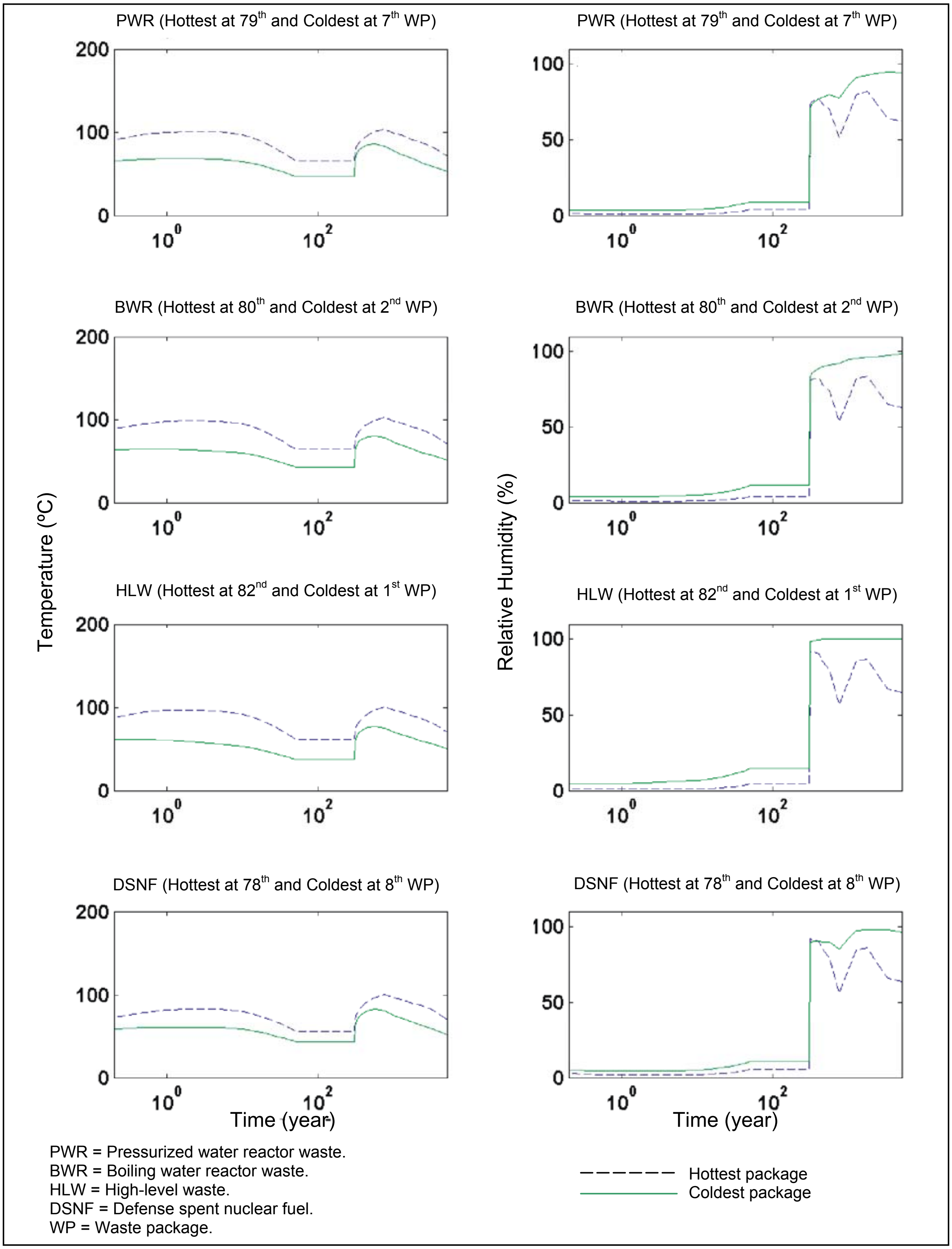


Figure 3-6
Surface Temperature and Relative Humidity versus Time for Hottest and Coldest Waste Package in Each Waste Type, based on 300-Year Pre-Closure Ventilation

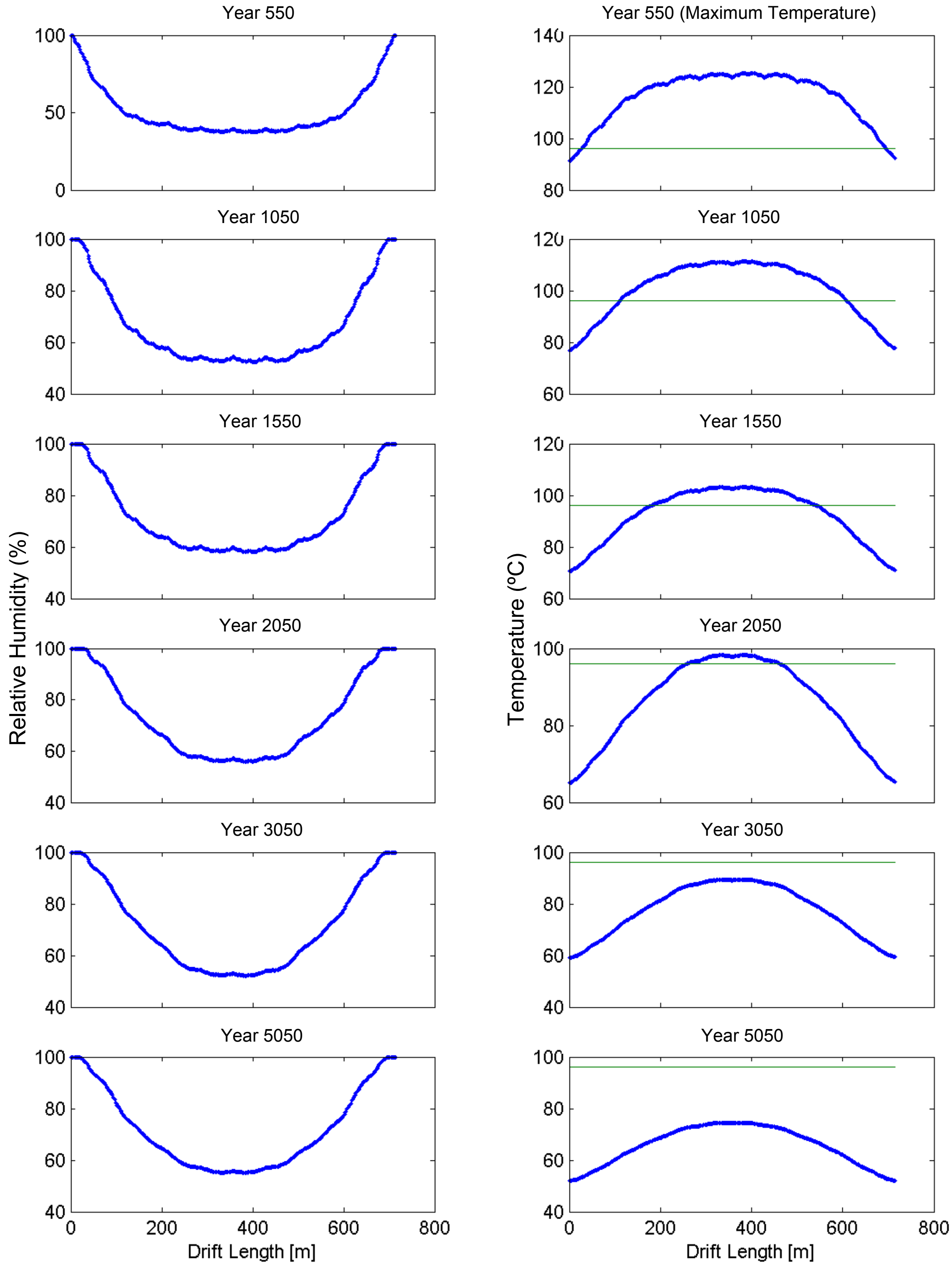


Note: Horizontal line in temperature profiles represents boiling temperature of water at 96 °C.

Figure 3-7
Axial Distribution of Drift Wall Relative Humidity and Temperature
at Selected Time Divisions for 100-Year Pre-Closure Ventilation

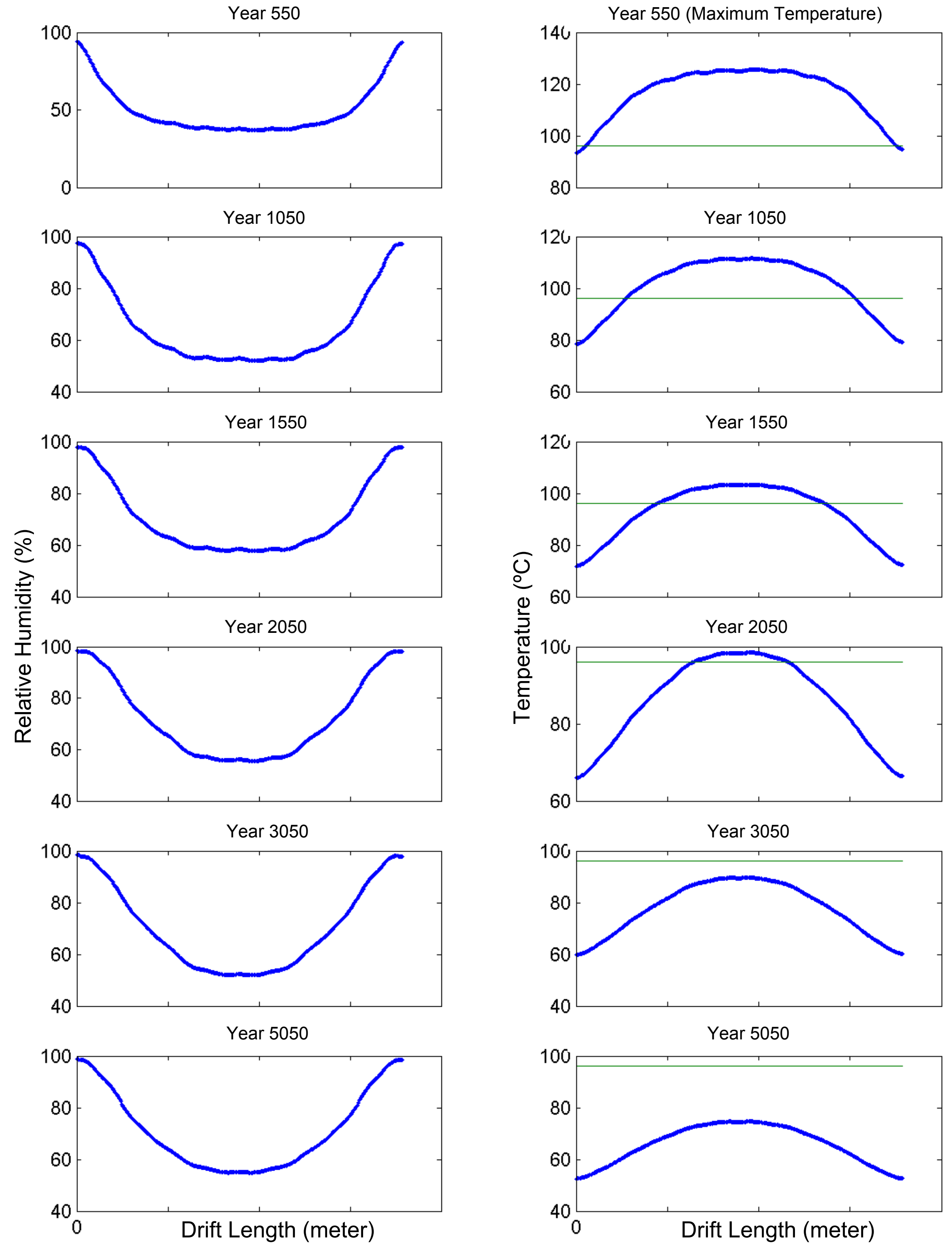


Note: Horizontal line in temperature profiles represents boiling temperature of water at 96 °C.

Figure 3-8
Axial Distribution of Drift Air Relative Humidity and Temperature
at Selected Time Divisions for 100-Year Pre-Closure Ventilation

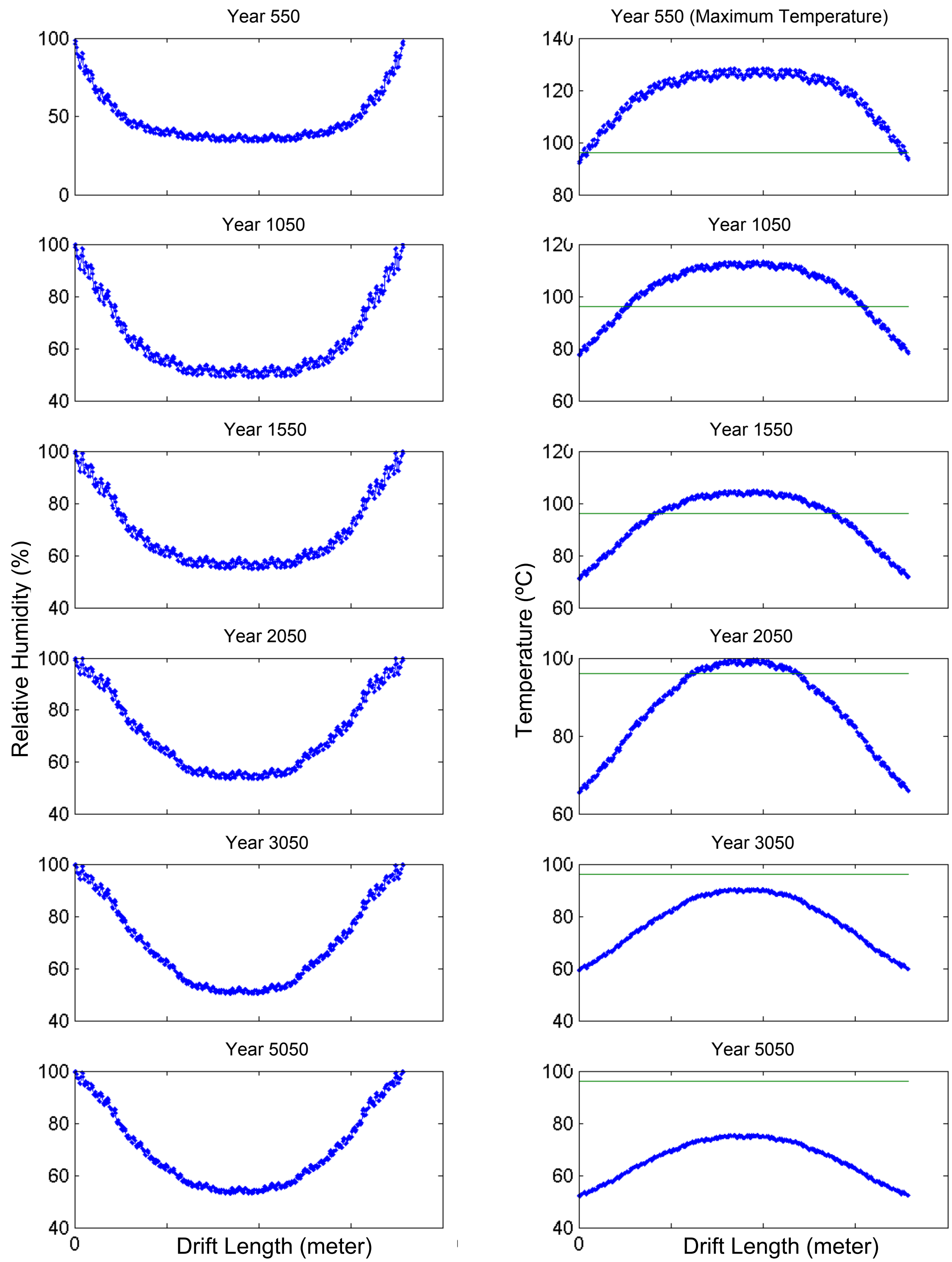


Note: Horizontal line in temperature profiles represents boiling temperature of water at 96 °C.

Figure 3-9
Axial Distribution of Drift Centerline Relative Humidity and Temperature
at Selected Time Divisions for 100-Year Pre-Closure Ventilation

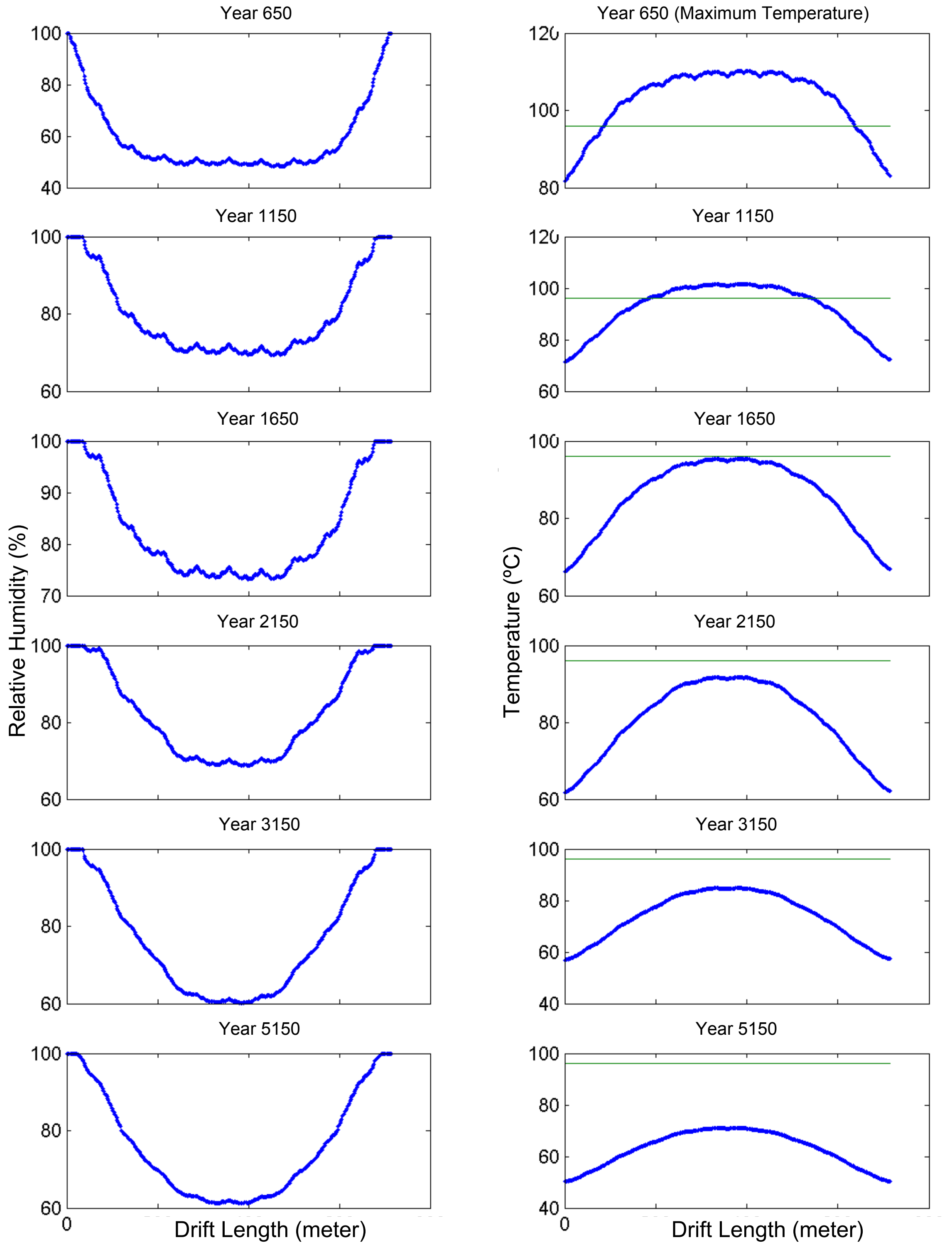


Note: Horizontal line in temperature profiles represents boiling temperature of water at 96 °C.

Figure 3-10
Axial Distribution of Drift Wall Relative Humidity and Temperature
at Selected Time Divisions for 200-Year Pre-Closure Ventilation

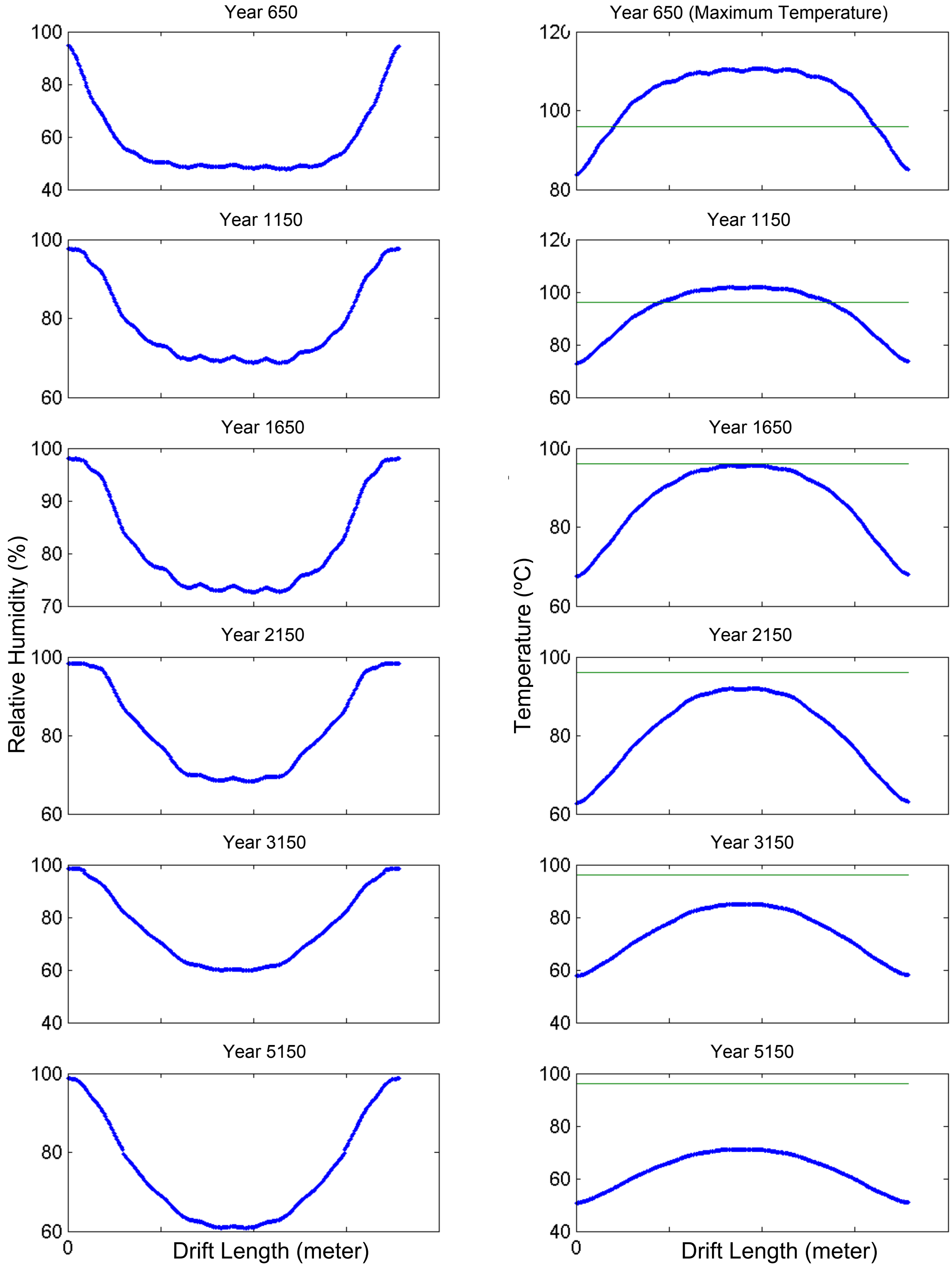


Note: Horizontal line in temperature profiles represents boiling temperature of water at 96 °C.

Figure 3-11
Axial Distribution of Drift Air Relative Humidity and Temperature
at Selected Time Divisions for 200-Year Pre-Closure Ventilation

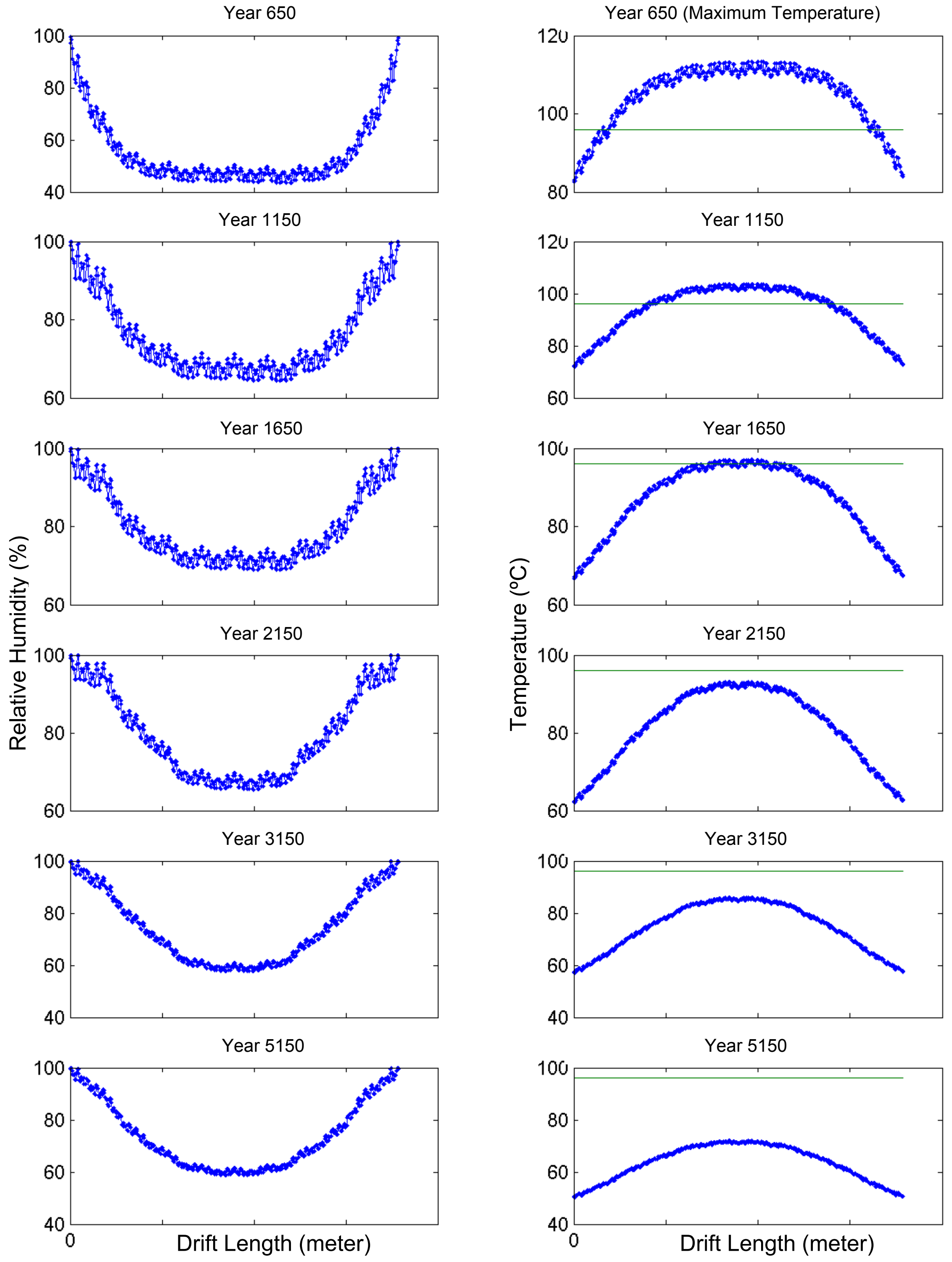


Note: Horizontal line in temperature profiles represents boiling temperature of water at 96 °C.

Figure 3-12
Axial Distribution of Drift Centerline Relative Humidity and Temperature
at Selected Time Divisions for 200-Year Pre-Closure Ventilation

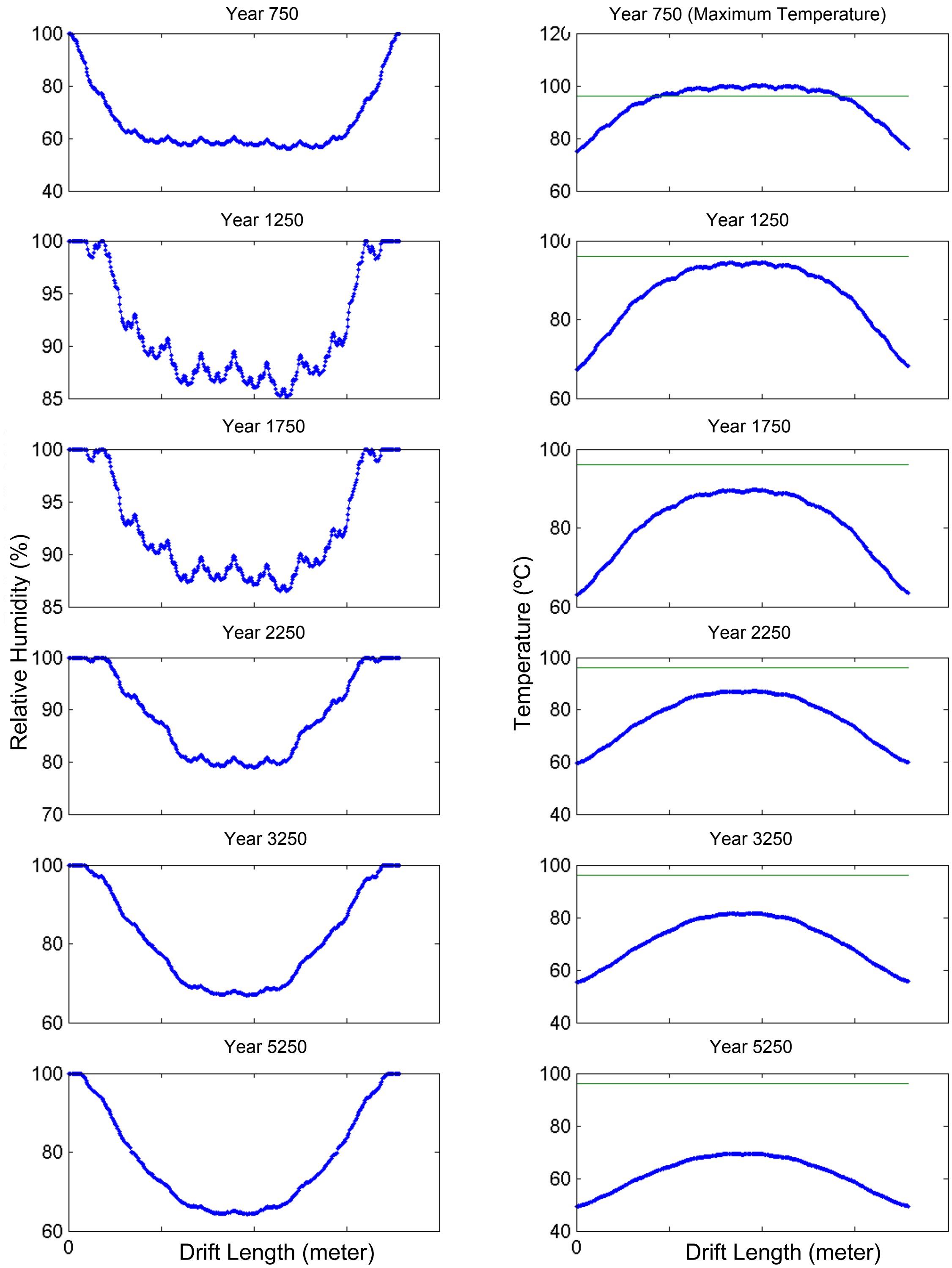


Note: Horizontal line in temperature profiles represents boiling temperature of water at 96 °C.

Figure 3-13
Axial Distribution of Drift Wall Relative Humidity and Temperature
at Selected Time Divisions for 300-Year Pre-Closure Ventilation

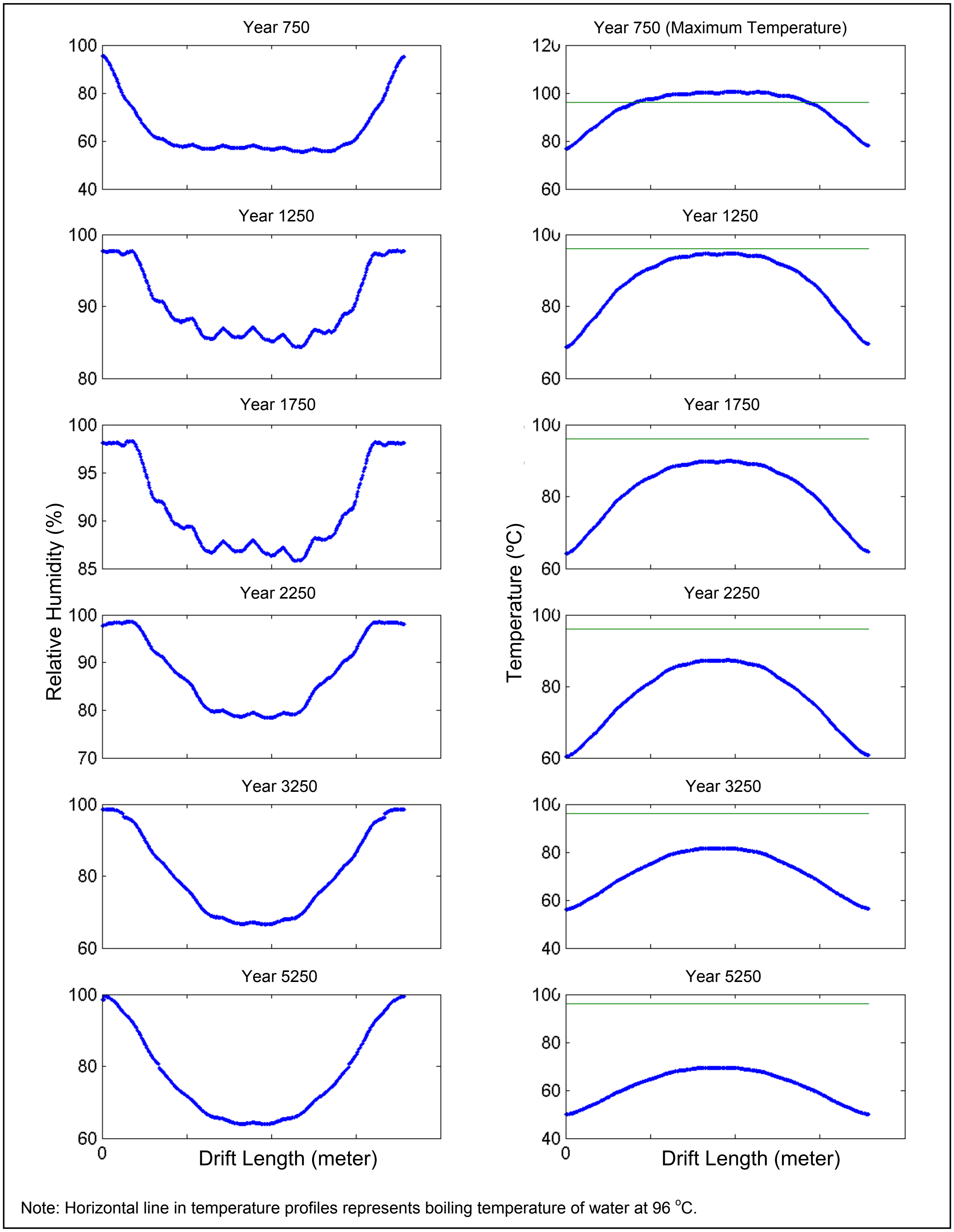


Figure 3-14
Axial Distribution of Drift Air Relative Humidity and Temperature
at Selected Time Divisions for 300-Year Pre-Closure Ventilation

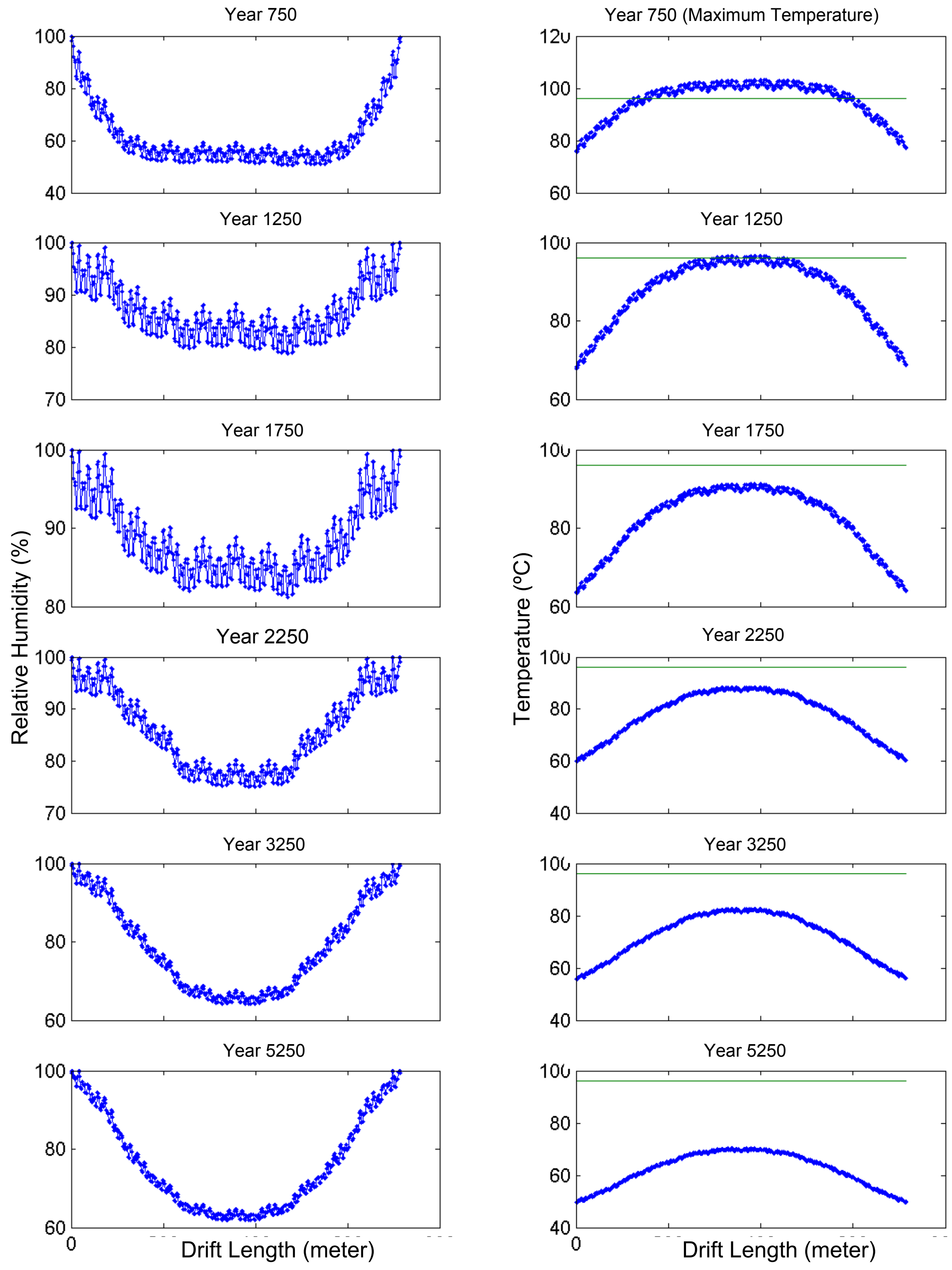


Note: Horizontal line in temperature profiles represents boiling temperature of water at 96 °C.

Figure 3-15
Axial Distribution of Drift Centerline Relative Humidity and Temperature
at Selected Time Divisions for 300-Year Pre-Closure Ventilation

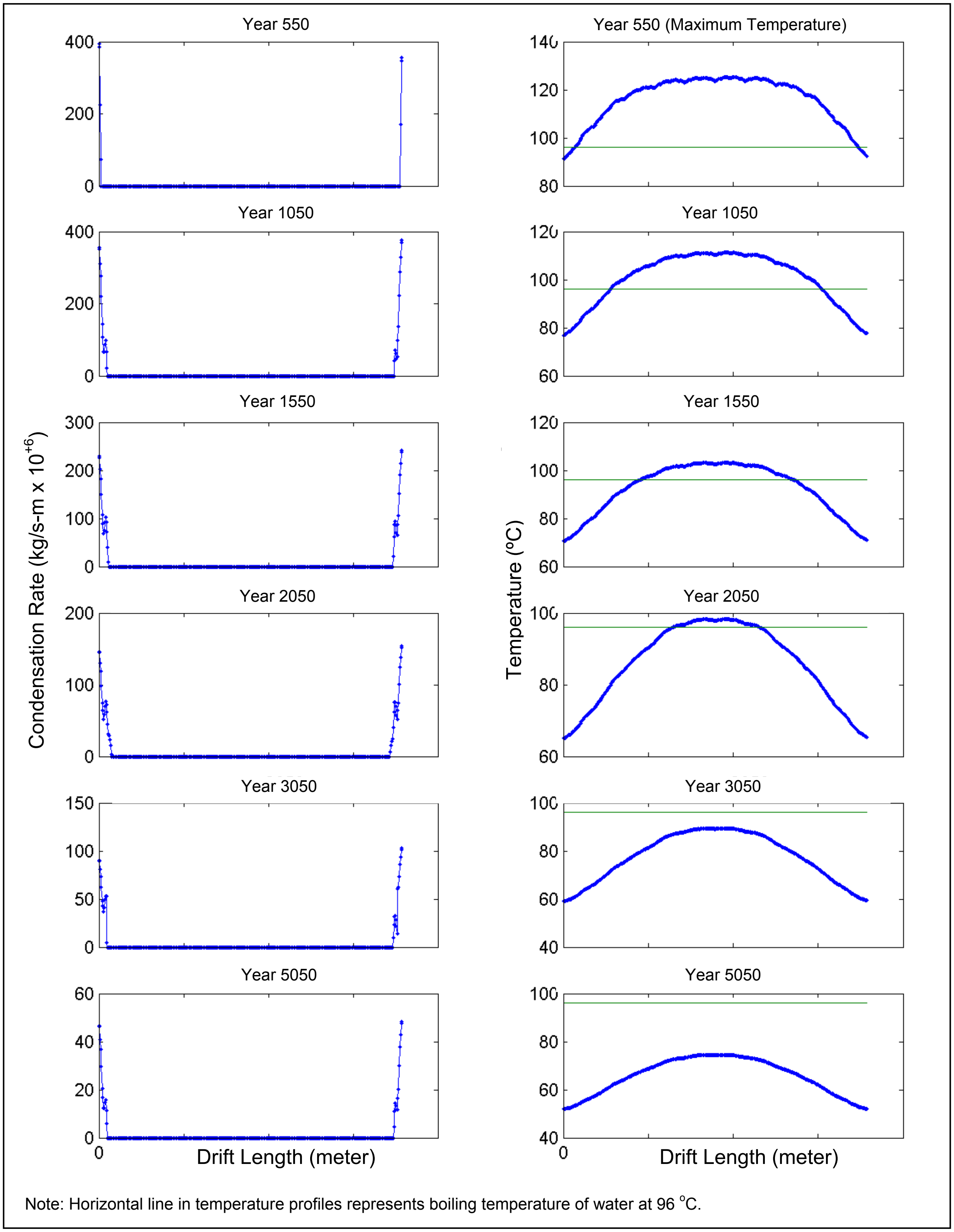


Figure 3-16
Axial Distribution of Drift Wall Condensation Rate and Temperature
at Selected Time Divisions for 100-Year Pre-Closure Ventilation

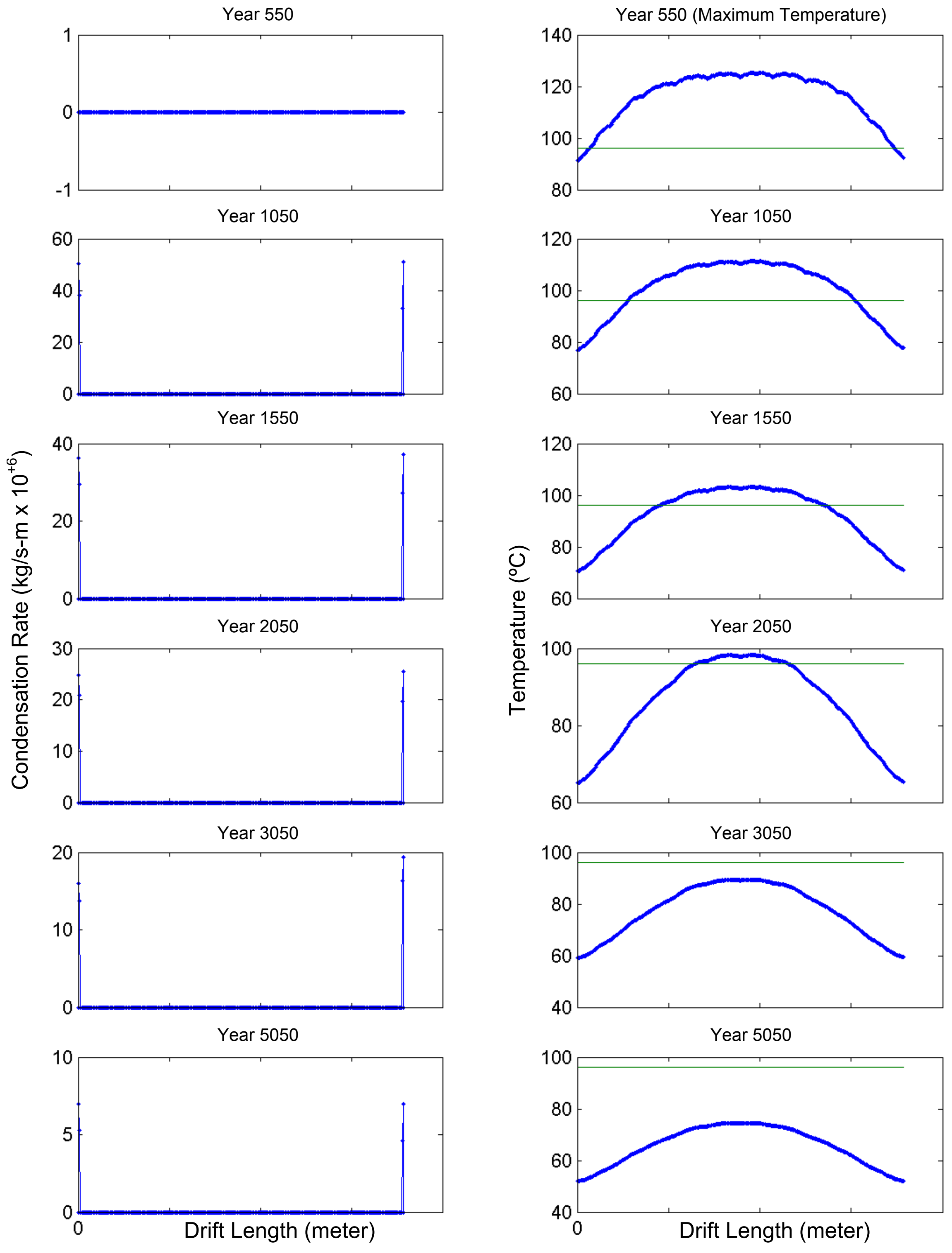


Note: Horizontal line in temperature profiles represents boiling temperature of water at 96 °C.

Figure 3-17
Axial Distribution of Drift Centerline Condensation Rate and Temperature
at Selected Time Divisions for 100-Year Pre-Closure Ventilation

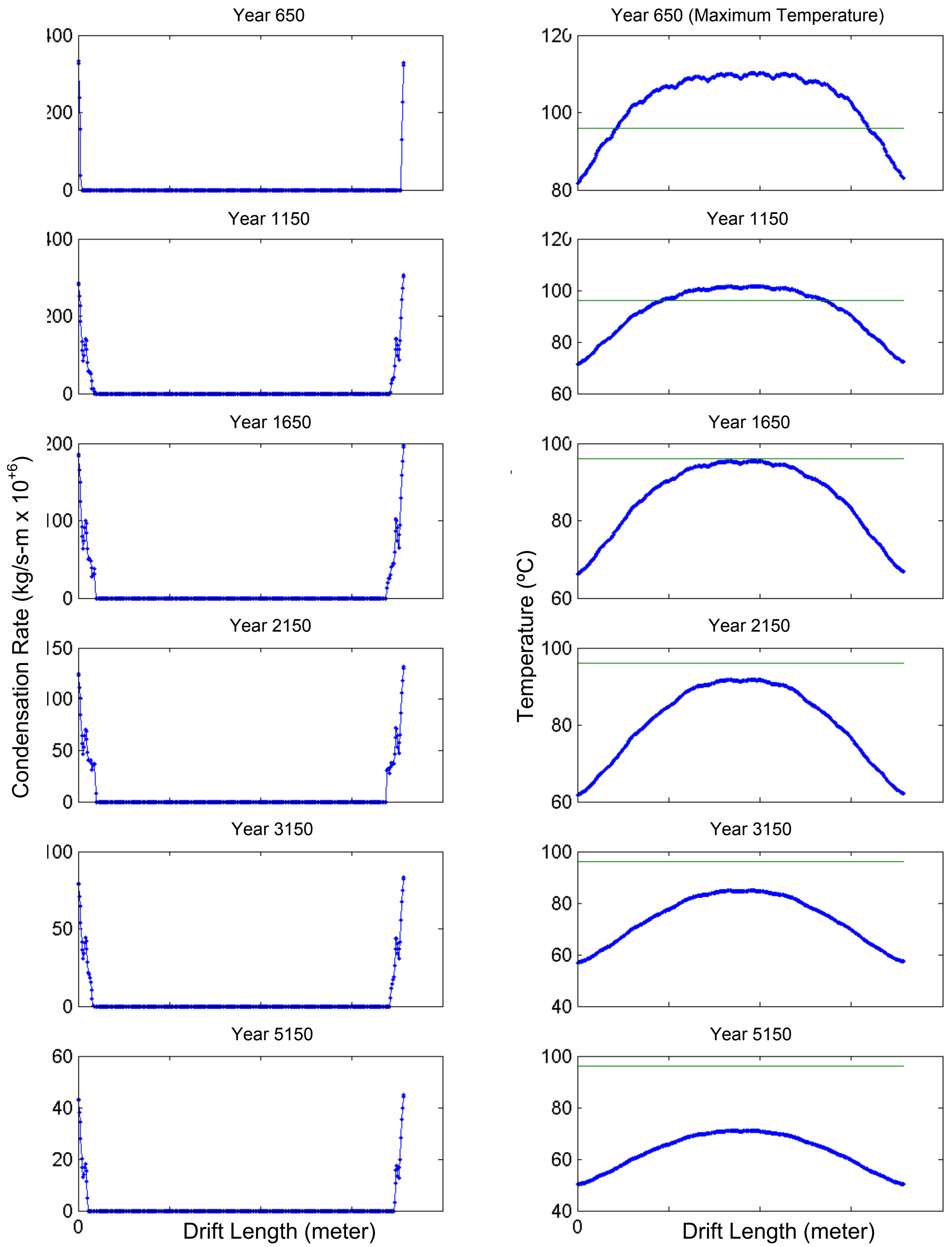


Note: Horizontal line in temperature profiles represents boiling temperature of water at 96 °C.

Figure 3-18
Axial Distribution of Drift Wall Condensation Rate and Temperature
at Selected Time Divisions for 200-Year Pre-Closure Ventilation

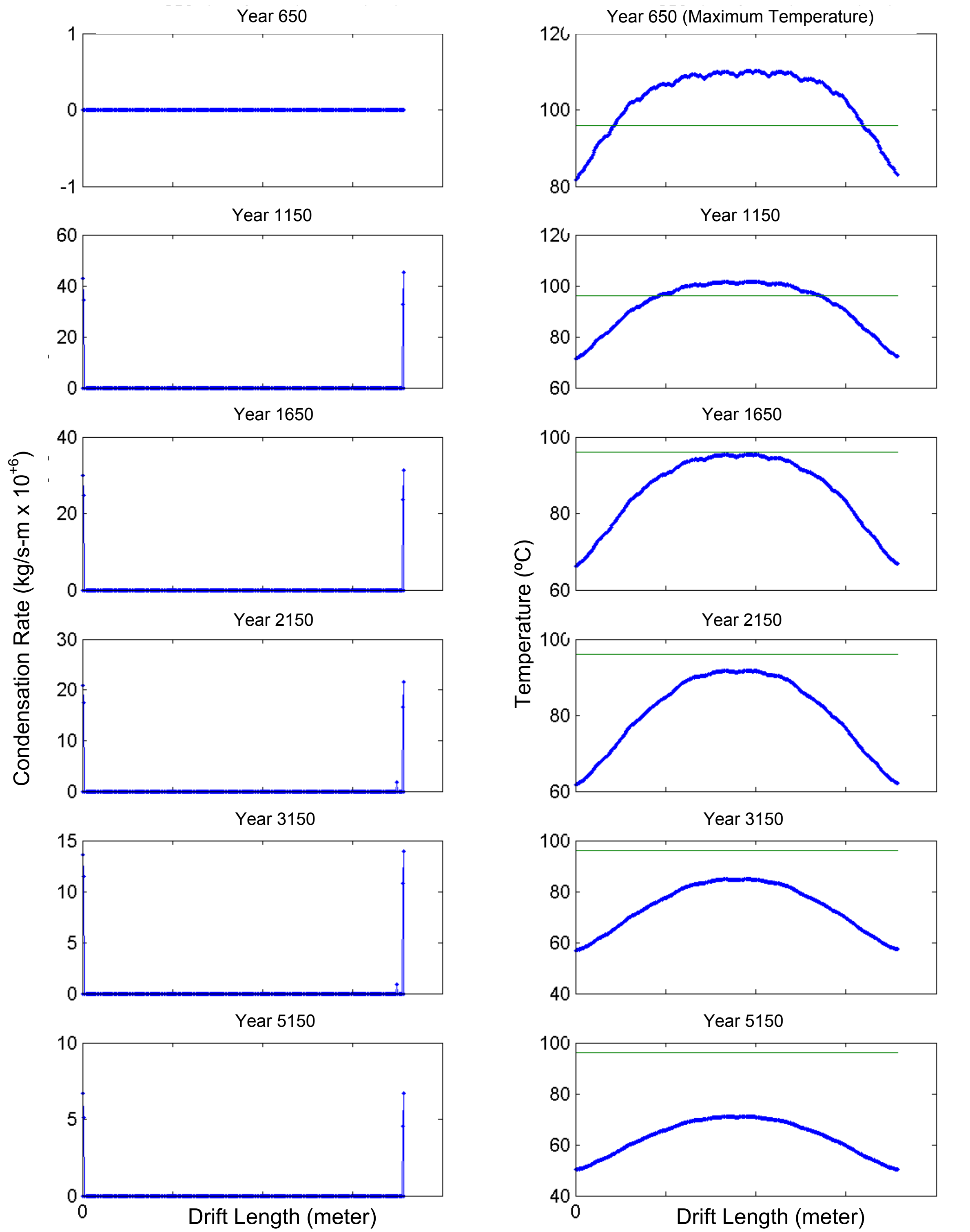


Note: Horizontal line in temperature profiles represents boiling temperature of water at 96 °C.

Figure 3-19
Axial Distribution of Drift Centerline Condensation Rate and Temperature
at Selected Time Divisions for 200-Year Pre-Closure Ventilation

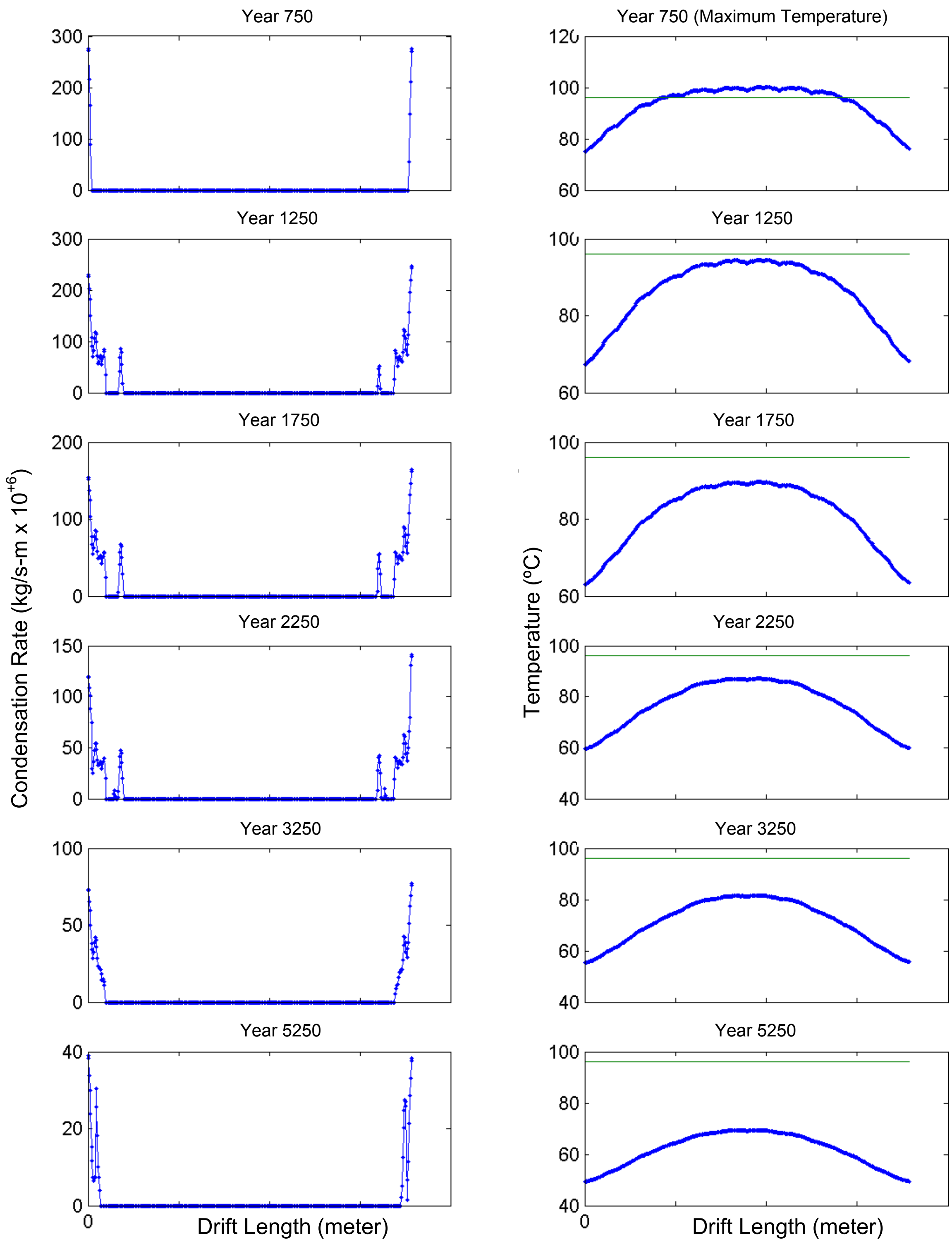


Note: Horizontal line in temperature profiles represents boiling temperature of water at 96 °C.

Figure 3-20
Axial Distribution of Drift Wall Condensation Rate and Temperature
at Selected Time Divisions for 300-Year Pre-Closure Ventilation

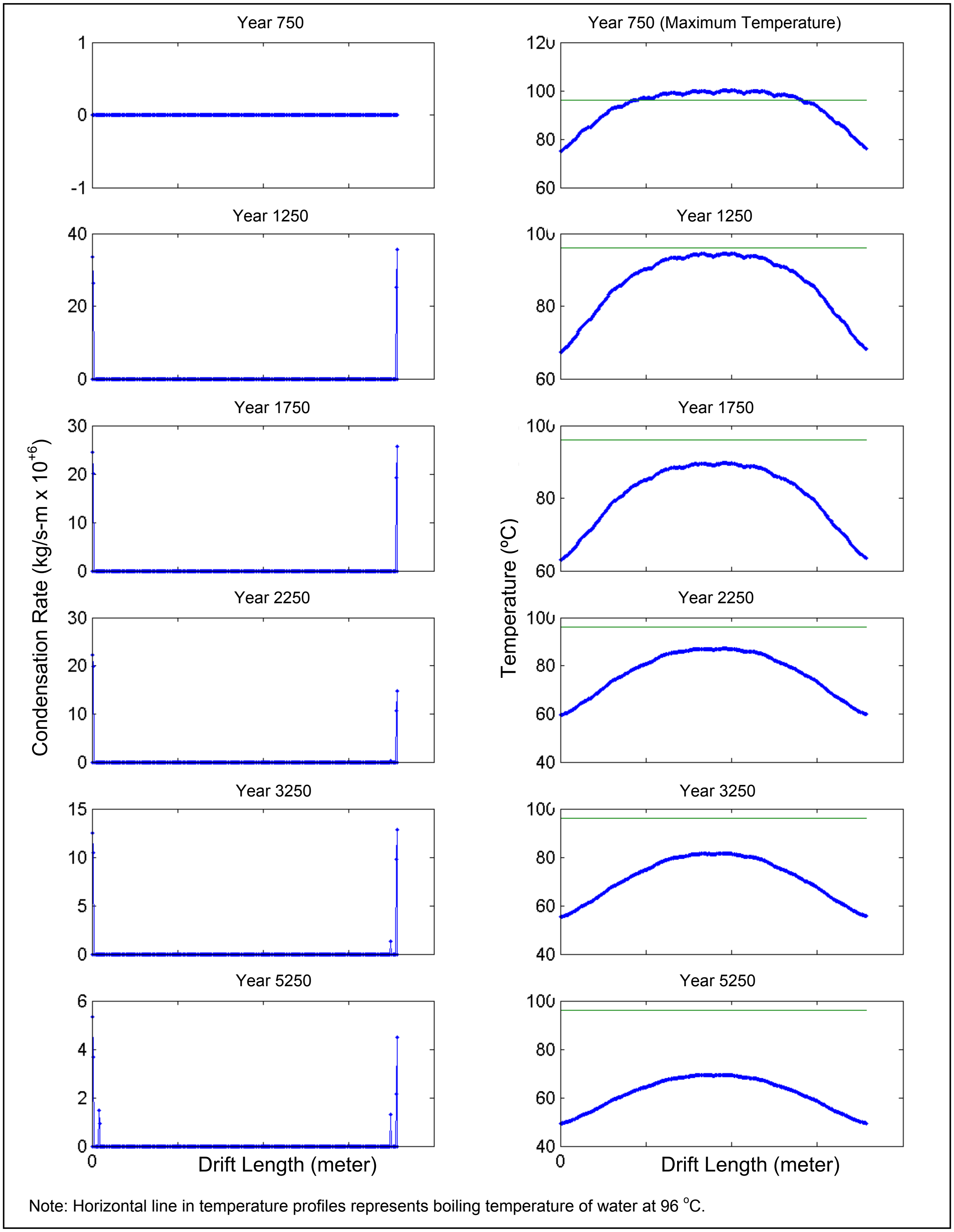


Figure 3-21
Axial Distribution of Drift Centerline Condensation Rate and Temperature
at Selected Time Divisions for 300-Year Pre-Closure Ventilation

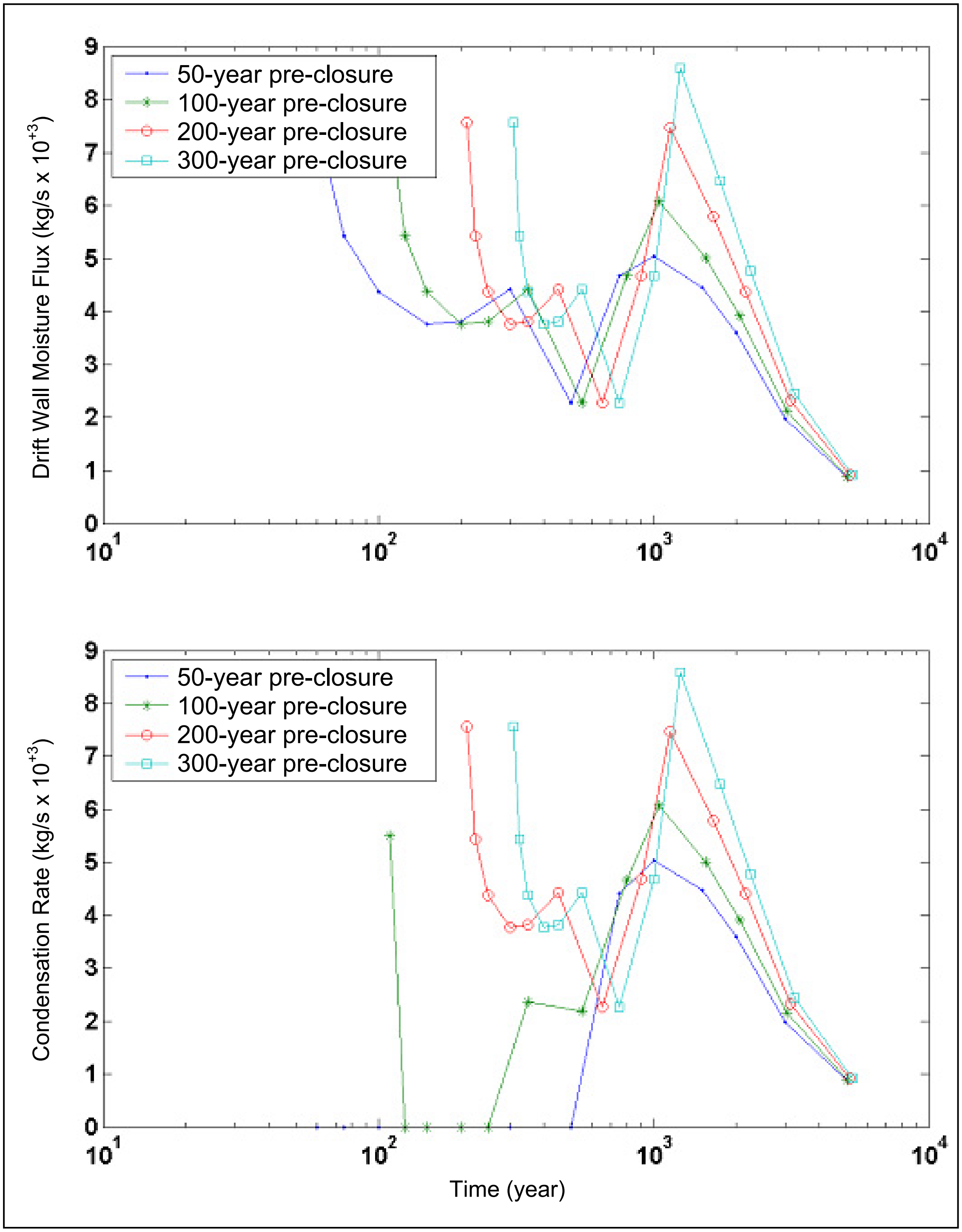


Figure 3-22
Drift Inflow of Moisture and Condensation Rate versus Time for Four Pre-Closure Time Periods

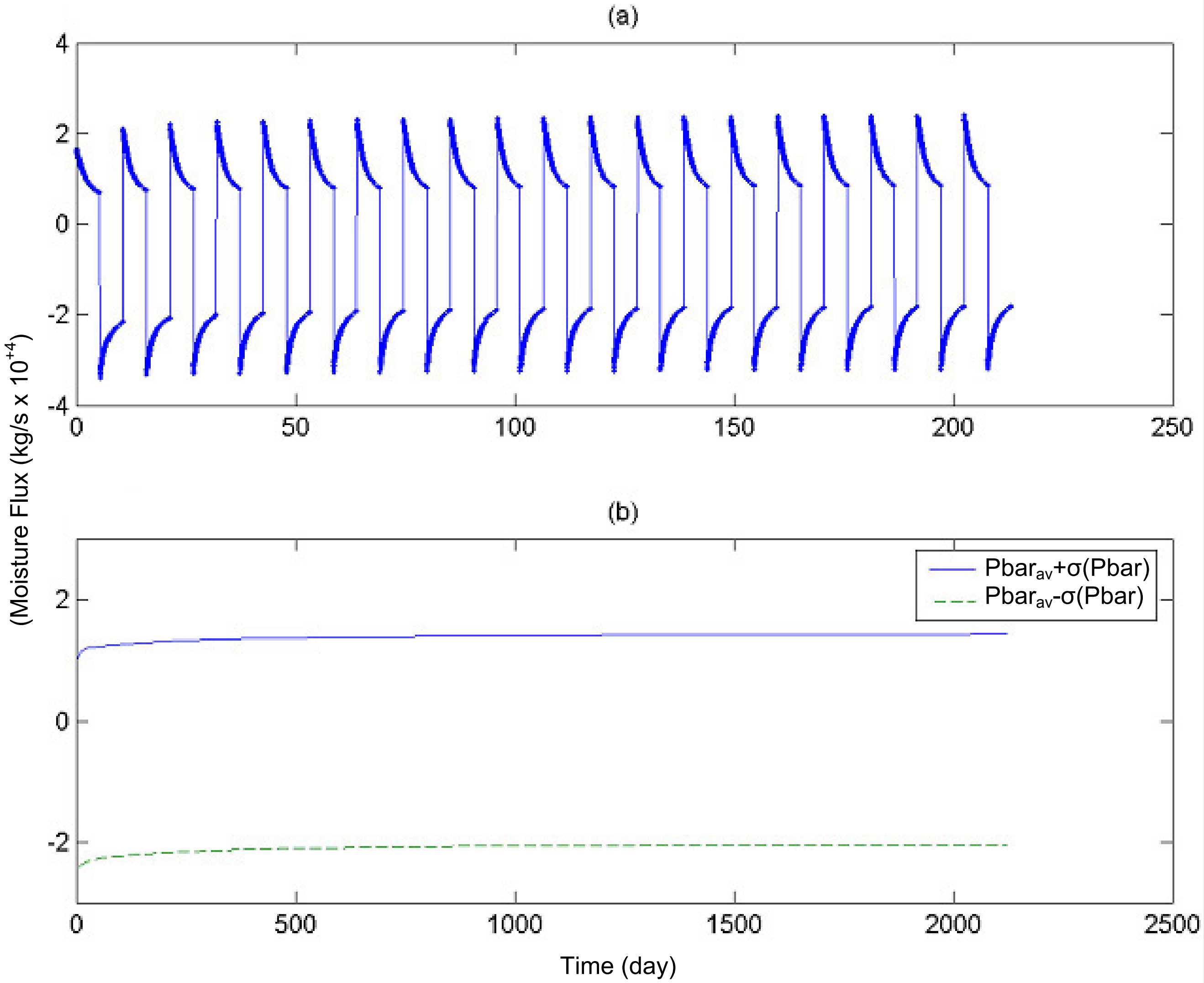


$Pbar_{av}$ = Average barometric pressure.
σ(Pbar) = Standard deviation about average barometric pressure.
Note: 1-meter two-dimensional model after Year 750.

Figure 4-1
Effect of Cyclic Barometric Pressure Variation on Moisture Flux Response of
Flux Variation with Time for the First 20 Cycles (a)
and Weighted Average Flux for Positive and Negative Halves for All 200 Cycles (b)

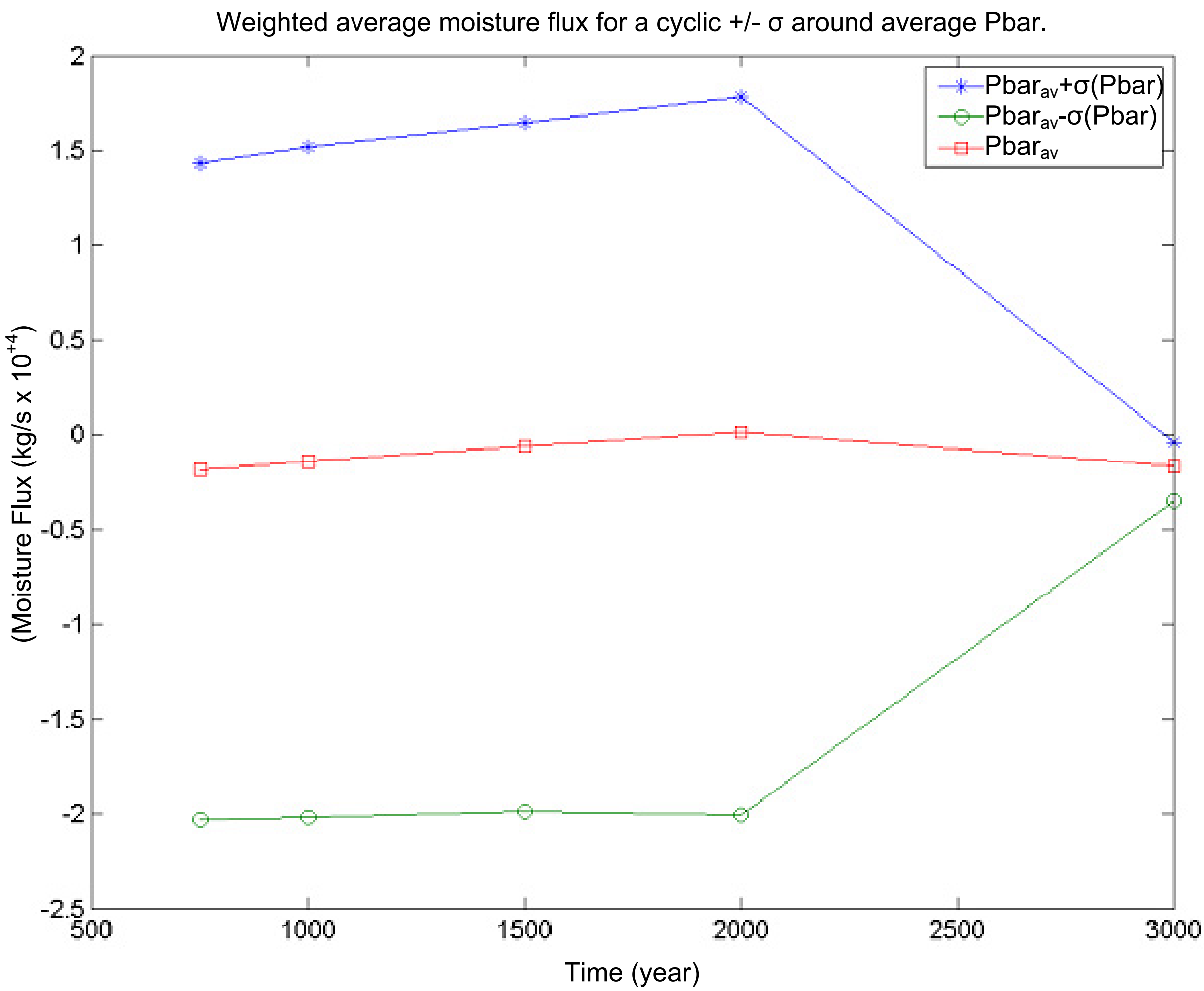


Pbar$_{av}$ = Average barometric pressure.
σ(Pbar) = Standard deviation about average barometric pressure.
Note: 1-meter two-dimensional model after Year 750.

Figure 4-2
Positive and Negative Integral-Averaged Moisture Flux Deviation
as a Function of Cyclic Variation of Barometric Pressure

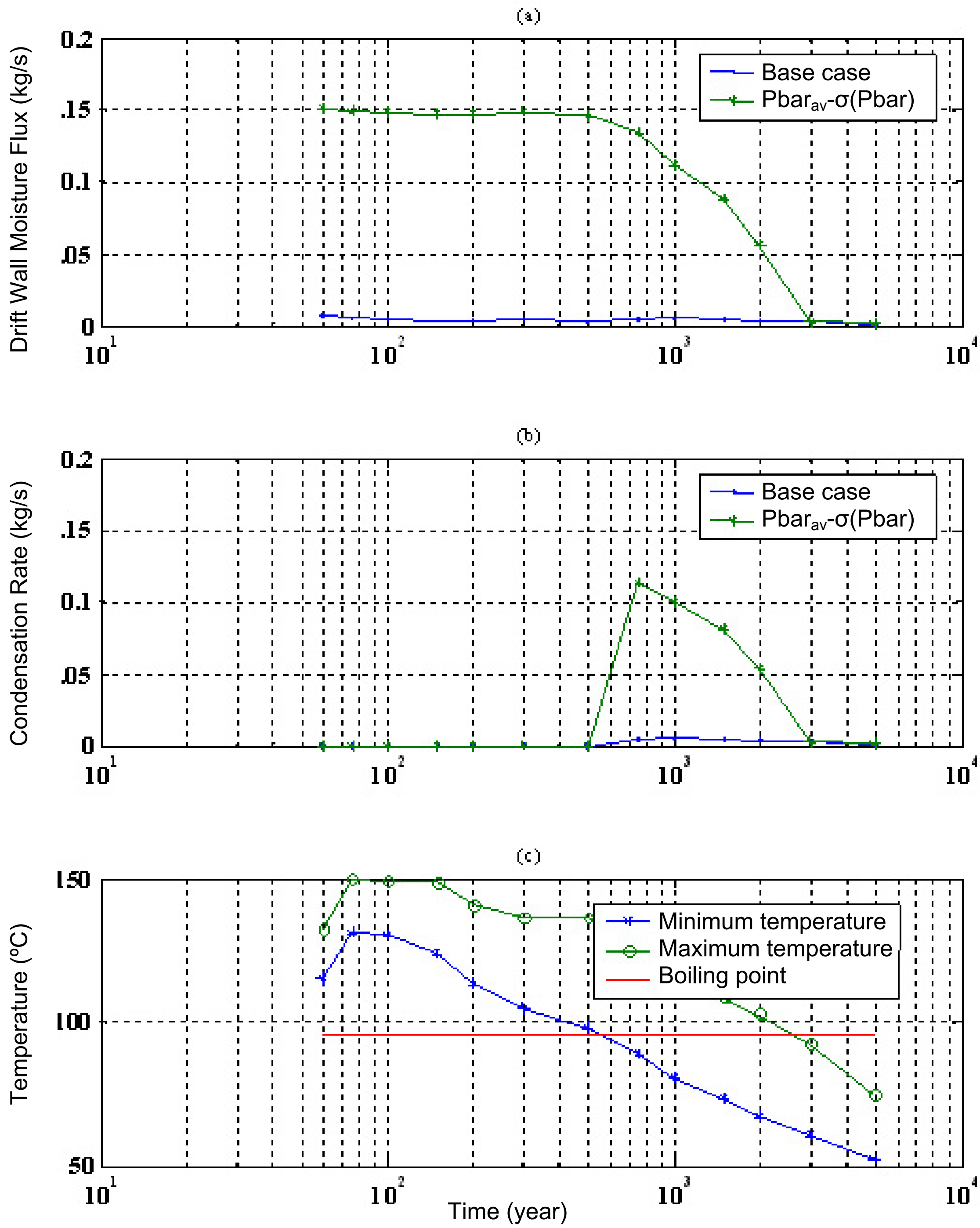


$Pbar_{av}$ = Average barometric pressure.
σ(Pbar) = Standard deviation about average barometric pressure.

Figure 4-3
Effect of Barometric Pressure Fluctuation on Drift Moisture Inflow (a) and Condensation Rate (b) and Maximum and Minimum Temperature (c)

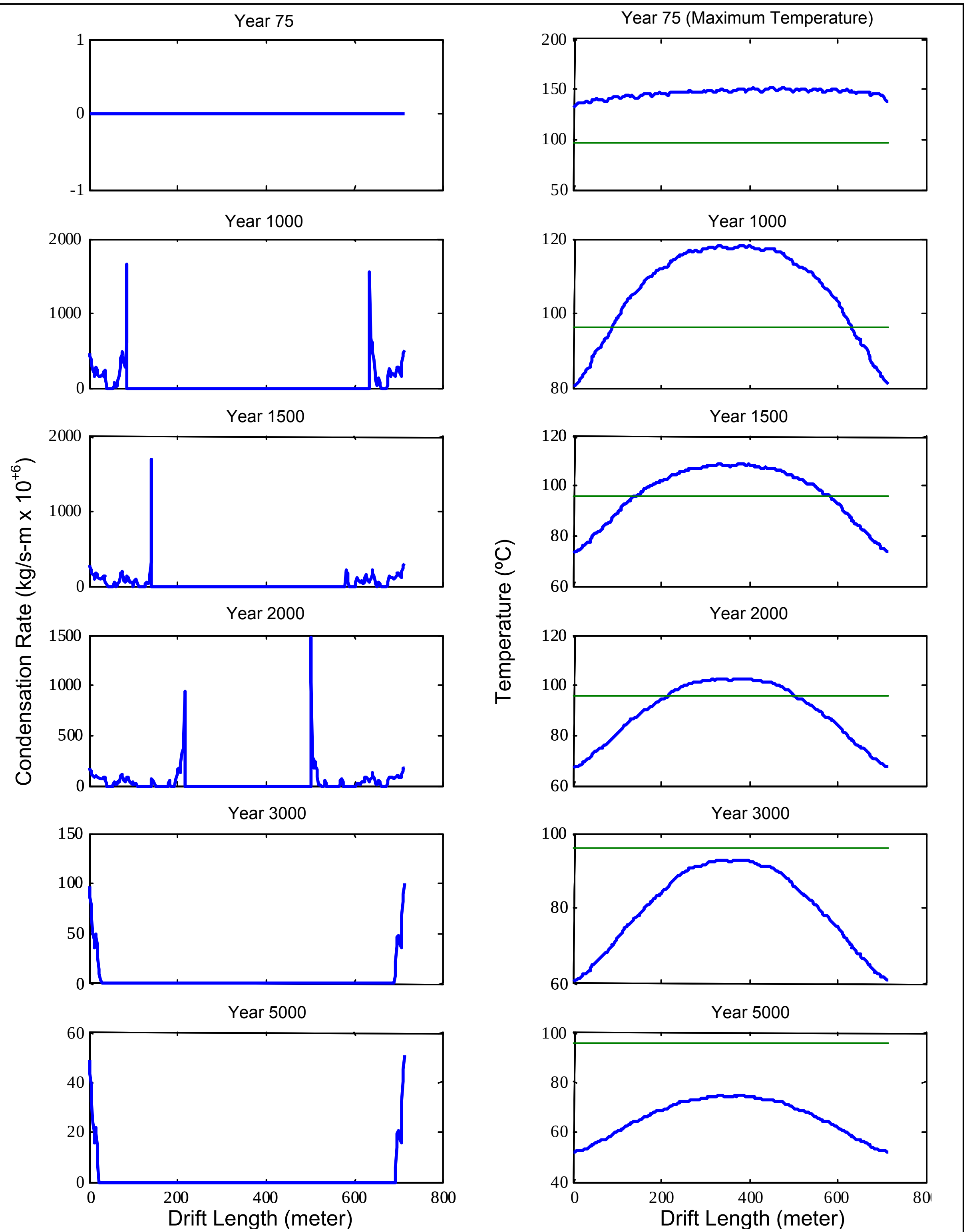


Note: Horizontal line in temperature profiles represents boiling temperature of water at 96 °C.

Figure 4-4
Axial Distribution of Drift Wall Condensation Rate and Temperature
for the Case of $Pbar_{av}$-$\sigma$(Pbar) at Selected Post-Closure Time Divisions

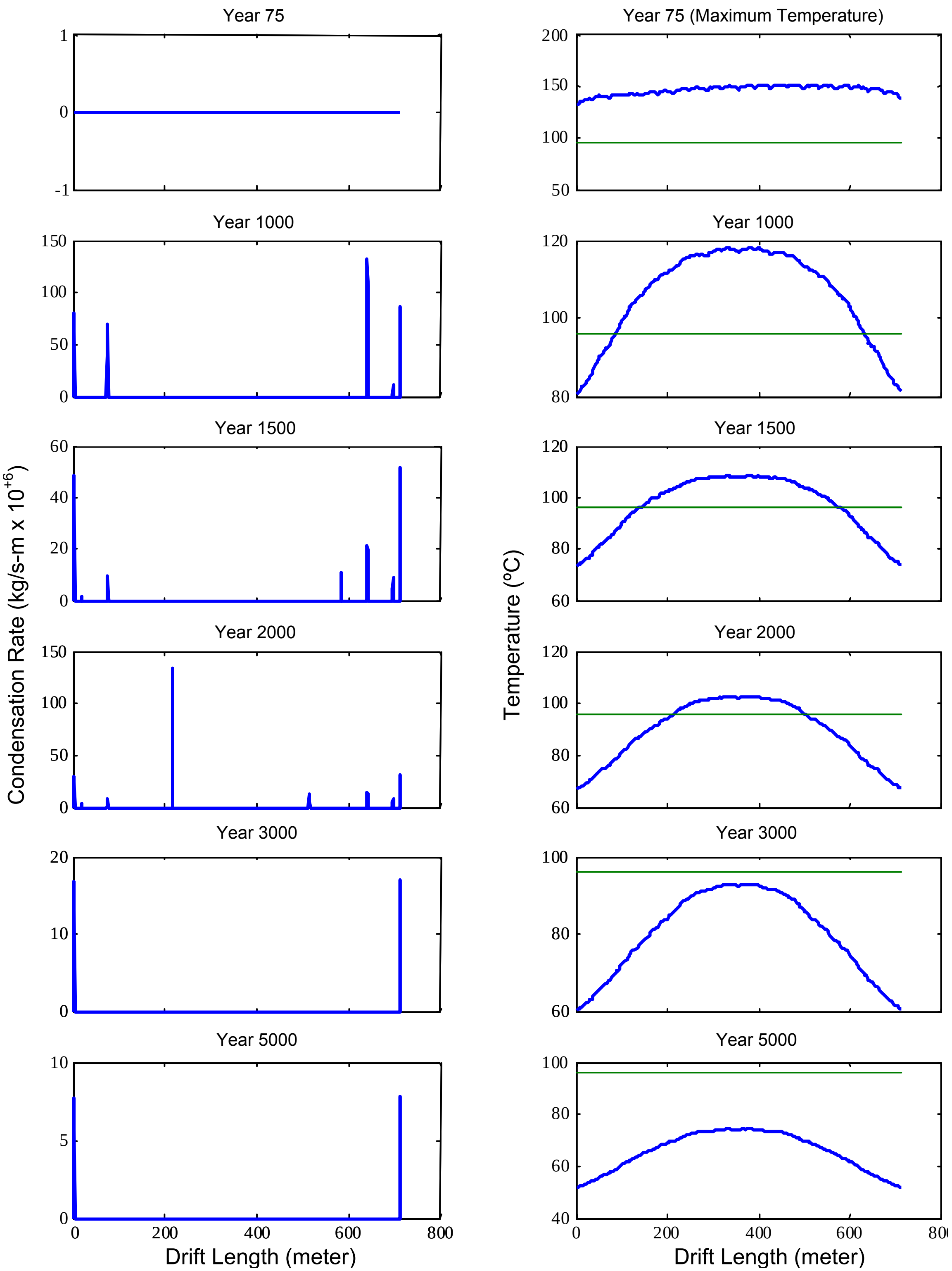


Note: Horizontal line in temperature profiles represents boiling temperature of water at 96 °C.

Figure 4-5
Axial Distribution of Drift Centerline Condensation Rate and Temperature
for the Case of $Pbar_{av}$-σ(Pbar) at Selected Post-Closure Time Divisions

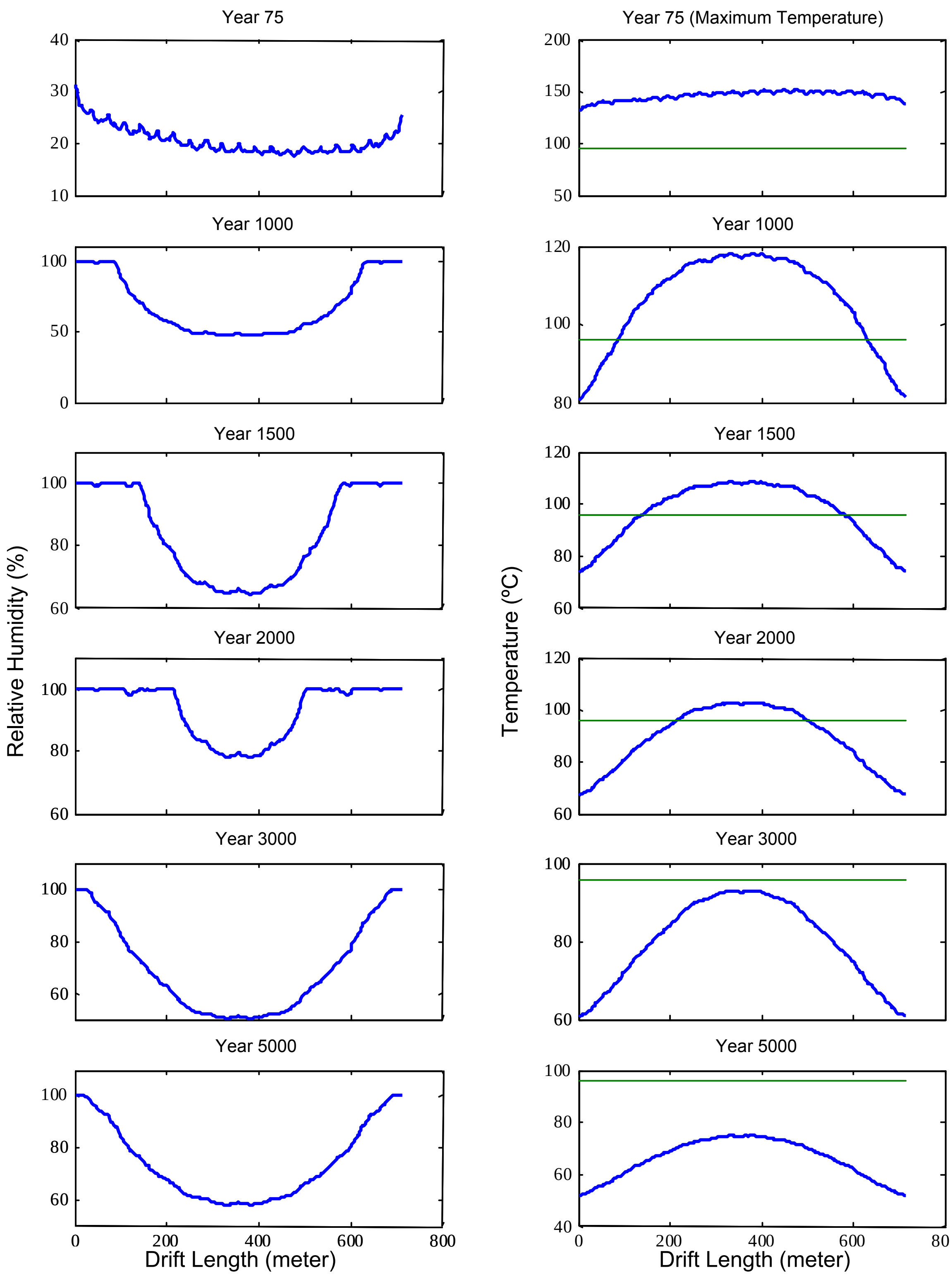


Note: Horizontal line in temperature profiles represents boiling temperature of water at 96 °C.

Figure 4-6
Axial Distribution of Drift Wall Relative Humidity and Temperature
for the Case of $Pbar_{av}$-$\sigma$(Pbar) at Selected Post-Closure Time Divisions

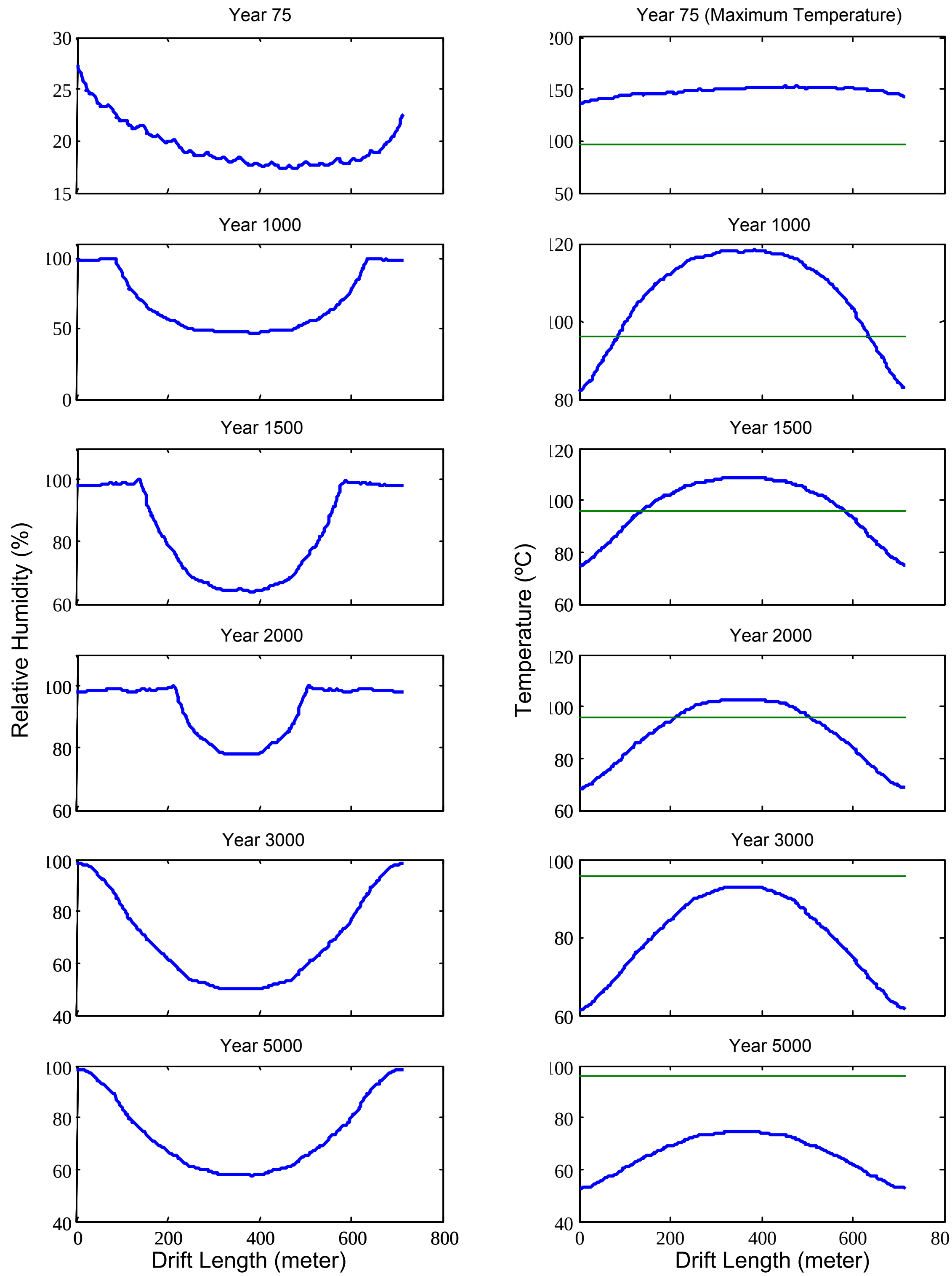


Note: Horizontal line in temperature profiles represents boiling temperature of water at 96 °C.

Figure 4-7
Axial Distribution of Drift Air Relative Humidity and Temperature
for the Case of $Pbar_{av}$-$\sigma$(Pbar) at Selected Post-Closure Time Divisions

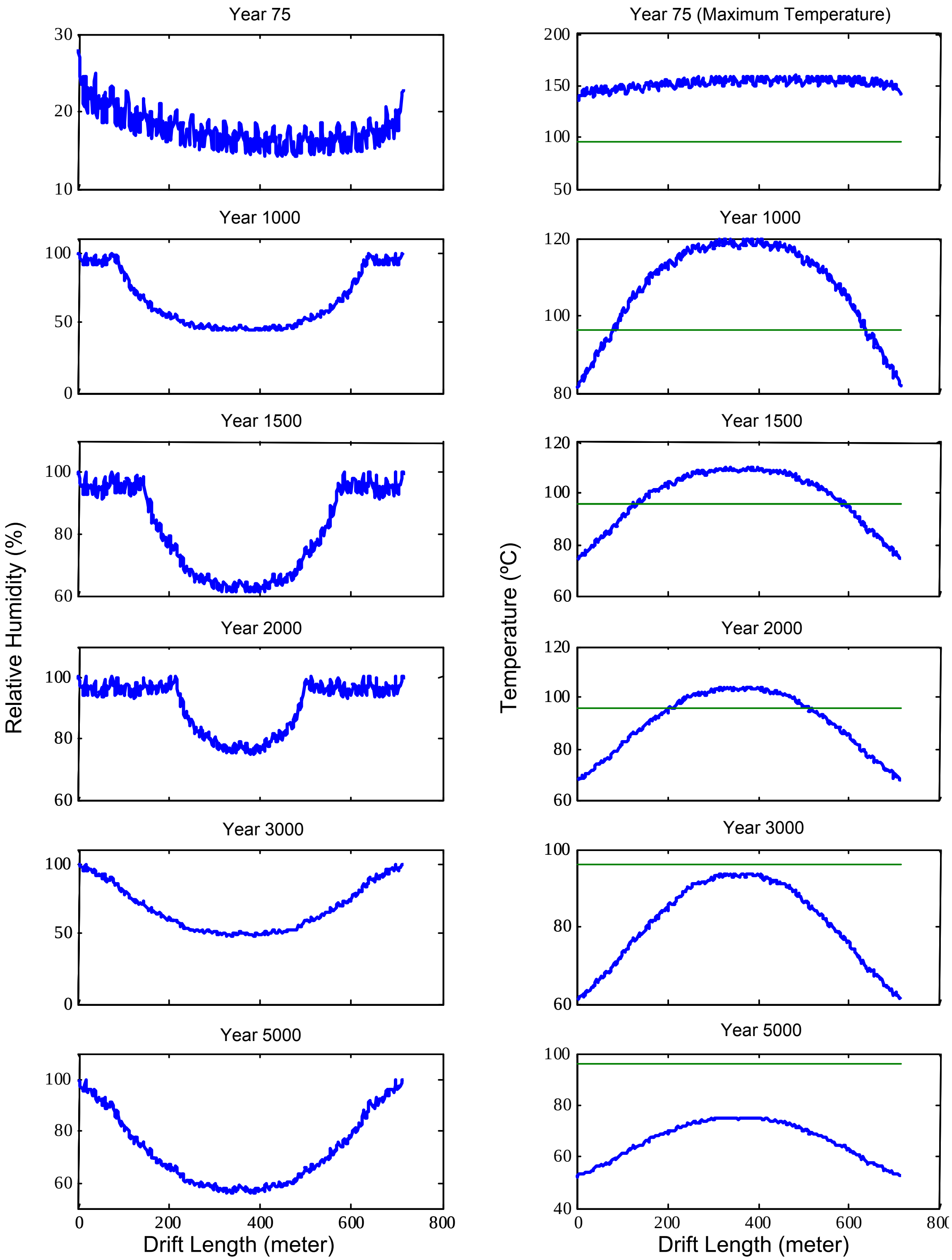


Note: Horizontal line in temperature profiles represents boiling temperature of water at 96 °C.

Figure 4-8
Axial Distribution of Drift Centerline Relative Humidity and Temperature
for the Case of $Pbar_{av}$-$\sigma$(Pbar) at Selected Post-Closure Time Divisions

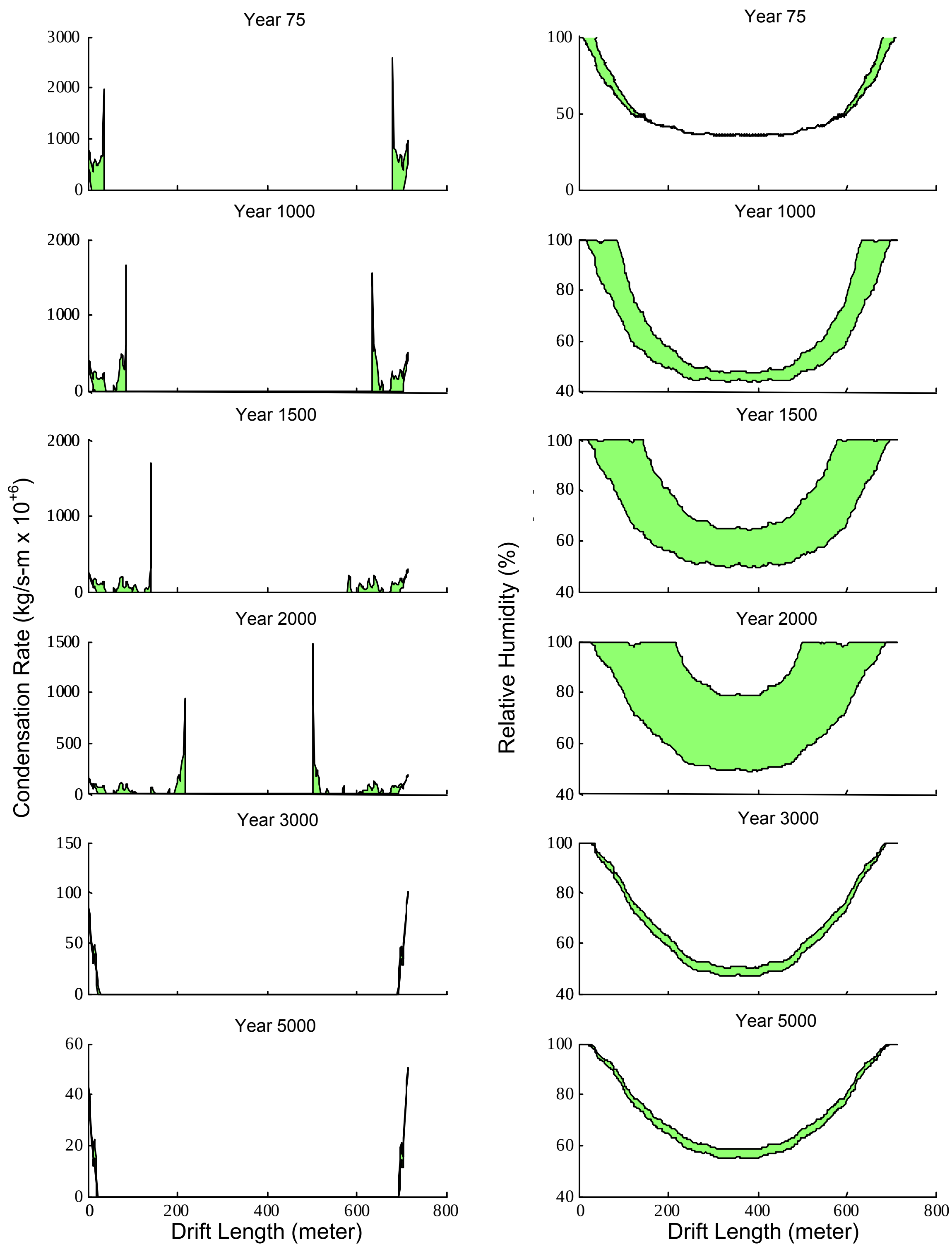


Note: Shaded area represents variation bound between the base case (Lower bound) and case of $Pbar_{av}$-σ(Pbar) (Upper bound).

Figure 4-9
Axial Distribution of Drift Wall Condensation Rate and Relative Humidity at Selected Post-Closure Time Divisions

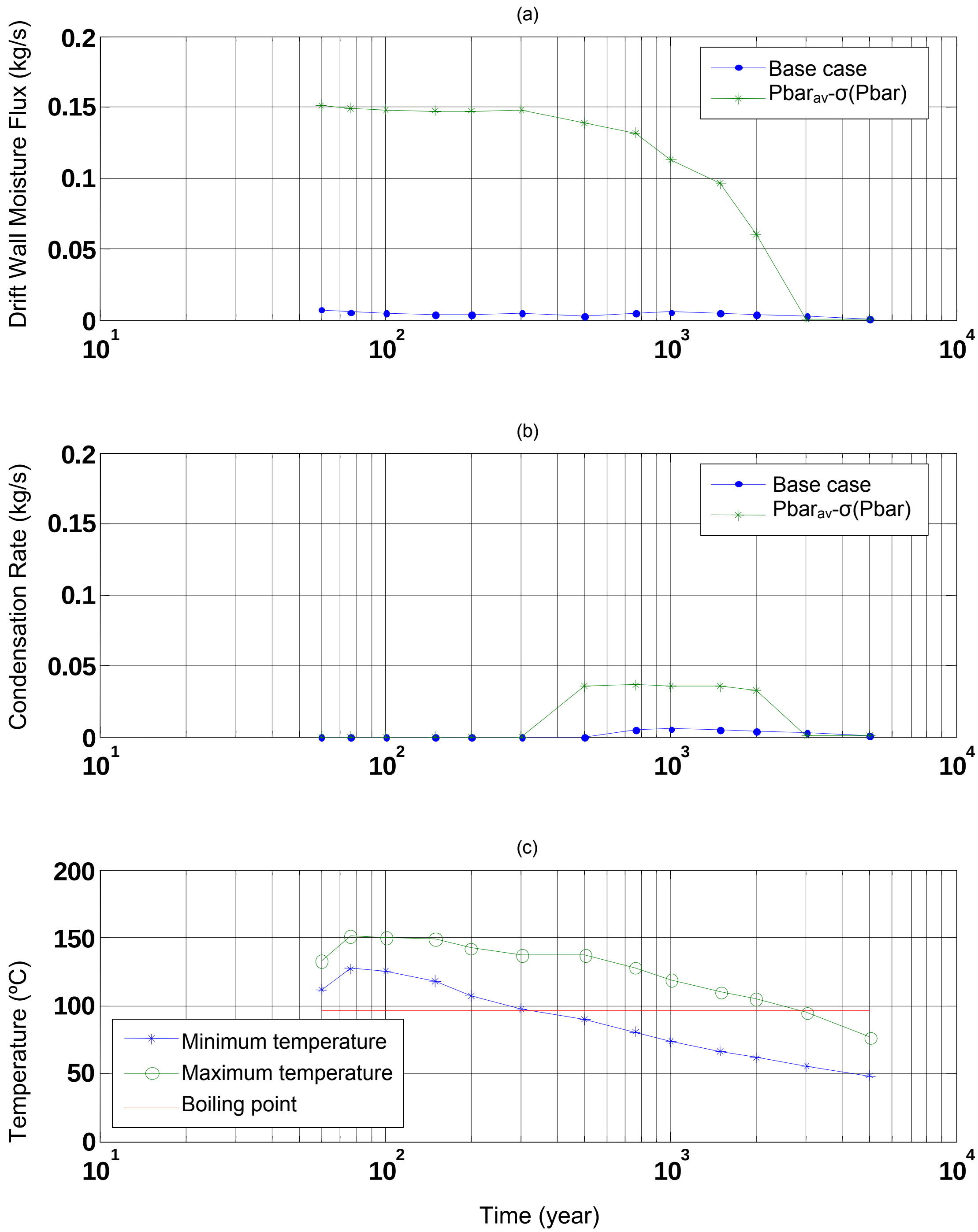


$Pbar_{av}$ = Average barometric pressure.
σ(Pbar) = Standard deviation about average barometric pressure.
Note: Drift axial dispersion coefficient = 0.004 $m^2$/s.

Figure 4-10
Effect of Barometric Pressure Fluctuation on Drift Moisture Inflow (a) and Condensation Rate (b) and Maximum and Minimum Temperature (c)

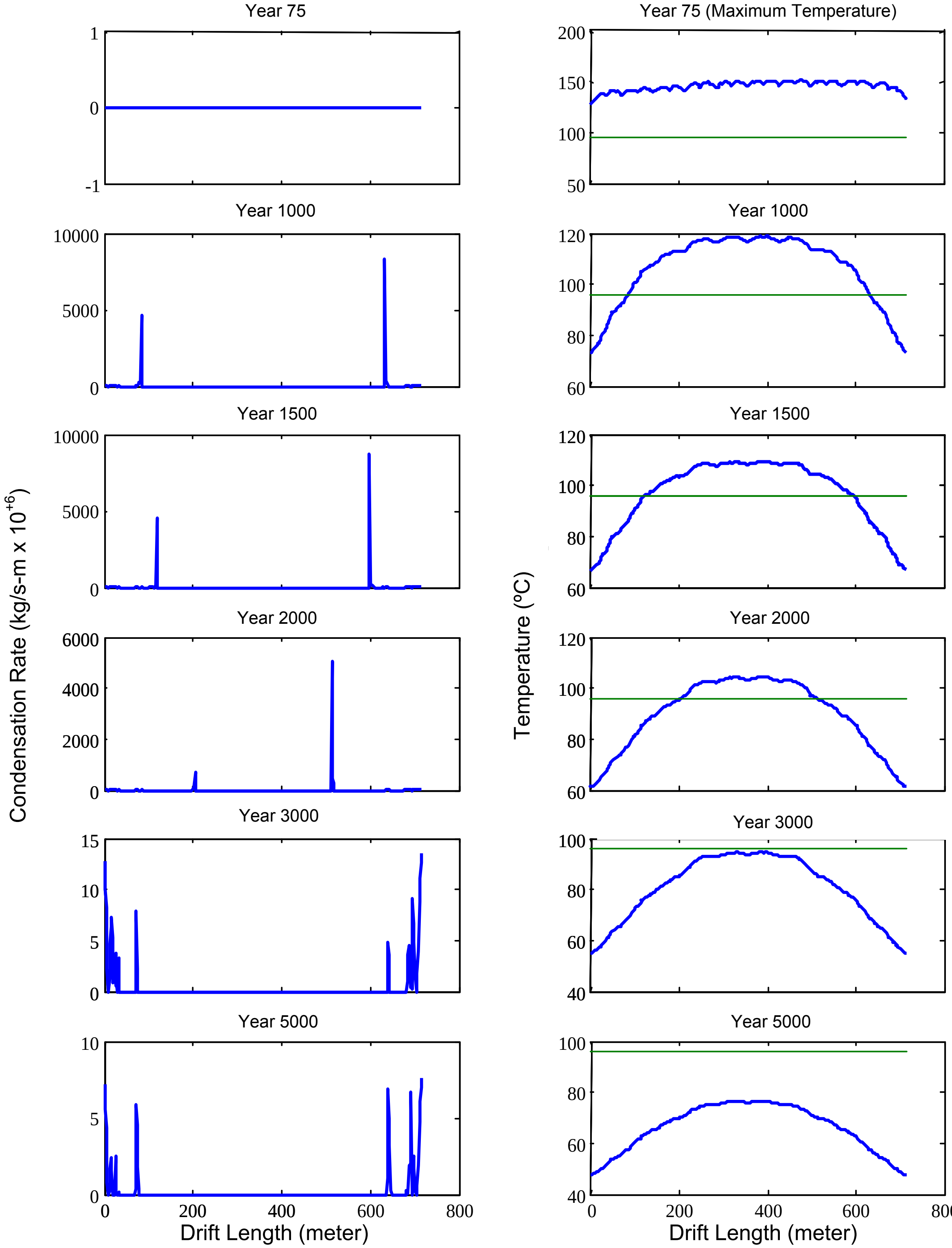


Note: Drift axial dispersion coefficient = 0.004 m$^2$/s; horizontal line in temperature profiles represents boiling temperature of water at 96 $^o$C.

Figure 4-11
Axial Distribution of Drift Wall Condensation Rate and Temperature
for the Case of Pbar$_{av}$-$\sigma$(Pbar) at Selected Post-Closure Time Divisions

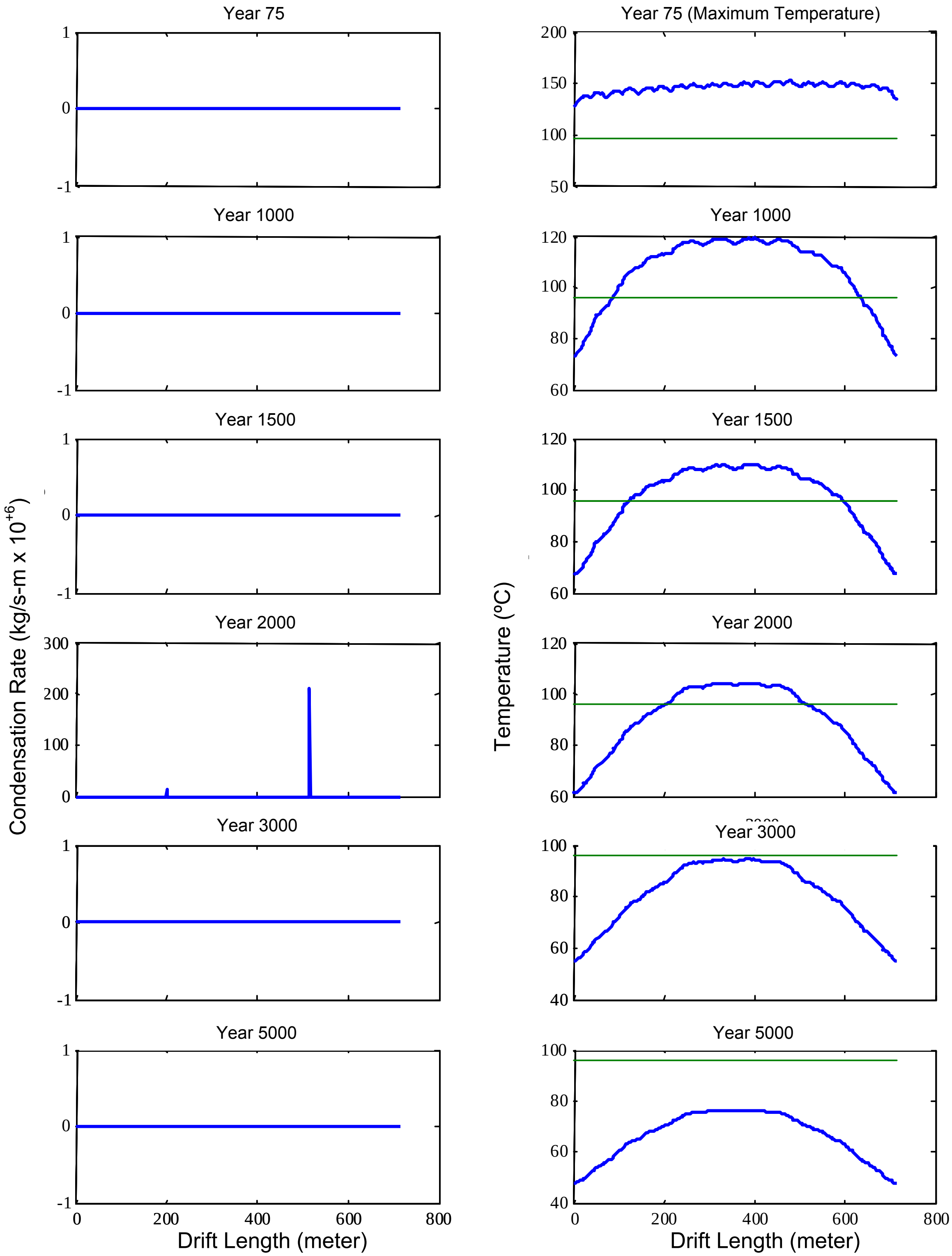


Note: Drift axial dispersion coefficient = 0.004 m$^2$/s; horizontal line in temperature profiles represents boiling temperature of water at 96 °C.

Figure 4-12
Axial Distribution of Drift Centerline Condensation Rate and Temperature for the Case of $Pbar_{av}$-$\sigma$(Pbar) at Selected Post-Closure Time Divisions

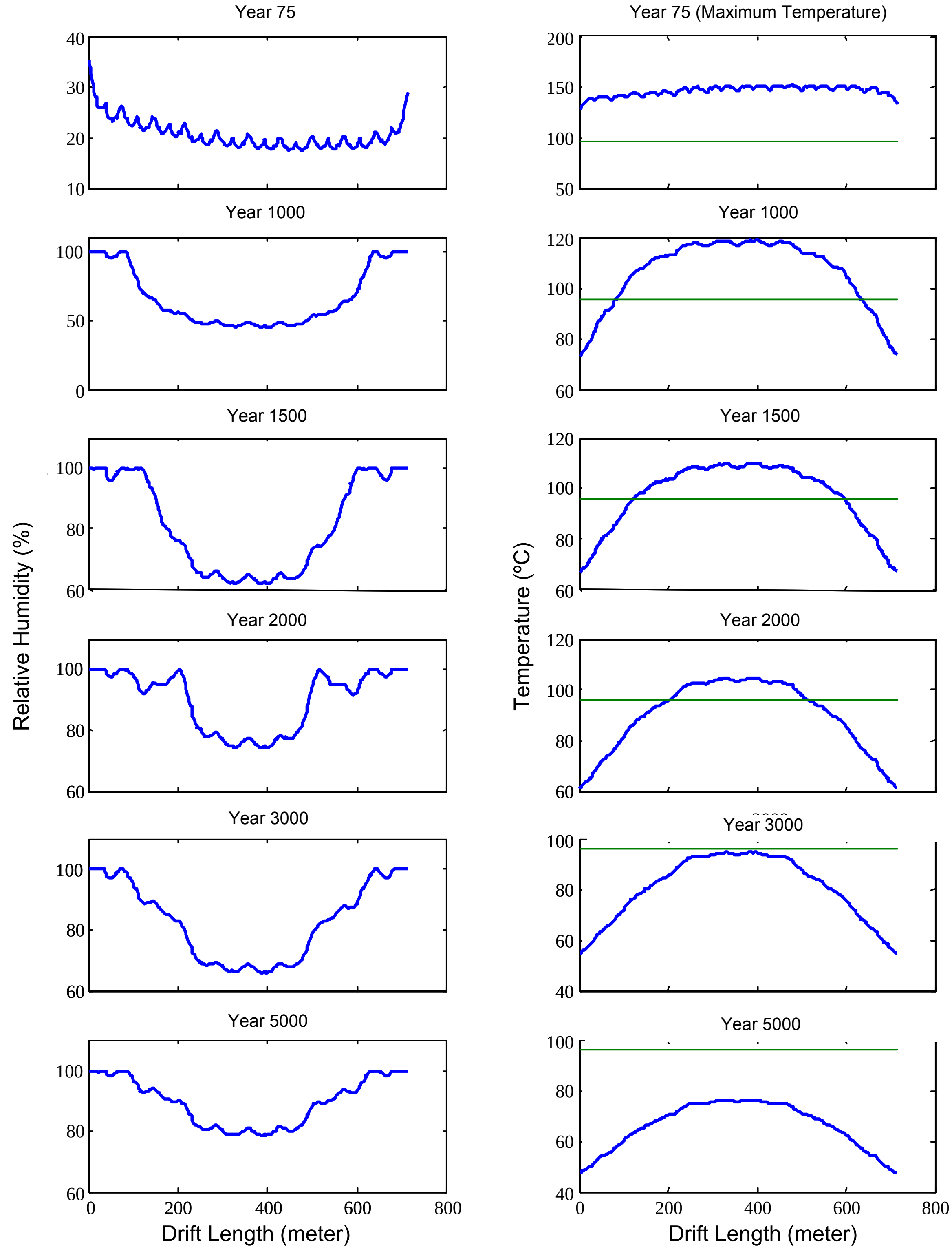


Note: Drift axial dispersion coefficient = 0.004 $m^2/s$; horizontal line in temperature profiles represents boiling temperature of water at 96 °C.

Figure 4-13
Axial Distribution of Drift Wall Relative Humidity and Temperature
for the Case of $Pbar_{av}$-$\sigma$(Pbar) at Selected Post-Closure Time Divisions

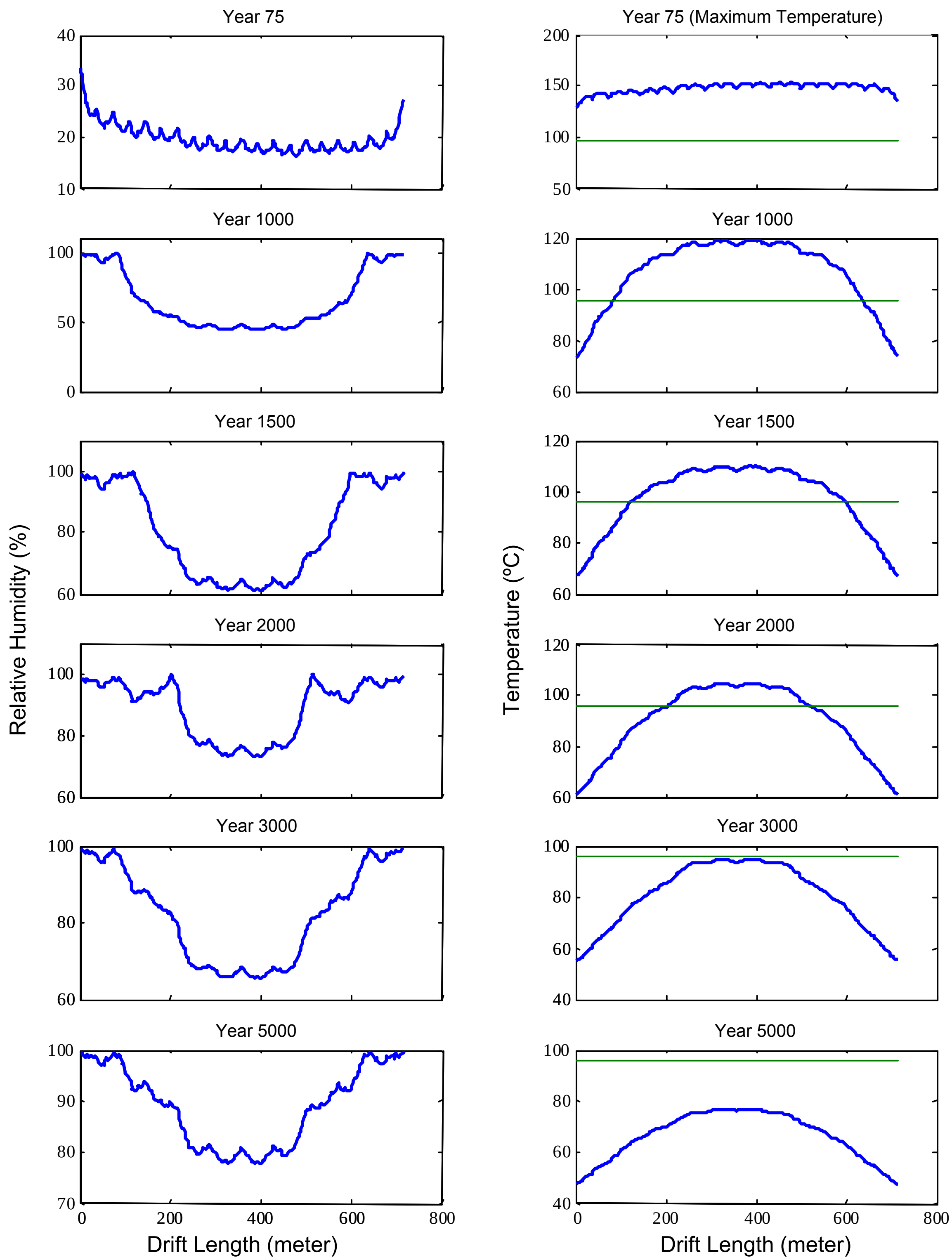


Note: Drift axial dispersion coefficient = 0.004 $m^2/s$; horizontal line in temperature profiles represents boiling temperature of water at 96 °C.

Figure 4-14
Axial Distribution of Drift Air Relative Humidity and Temperature
for the Case of $Pbar_{av}$-$\sigma$(Pbar) at Selected Post-Closure Time Divisions

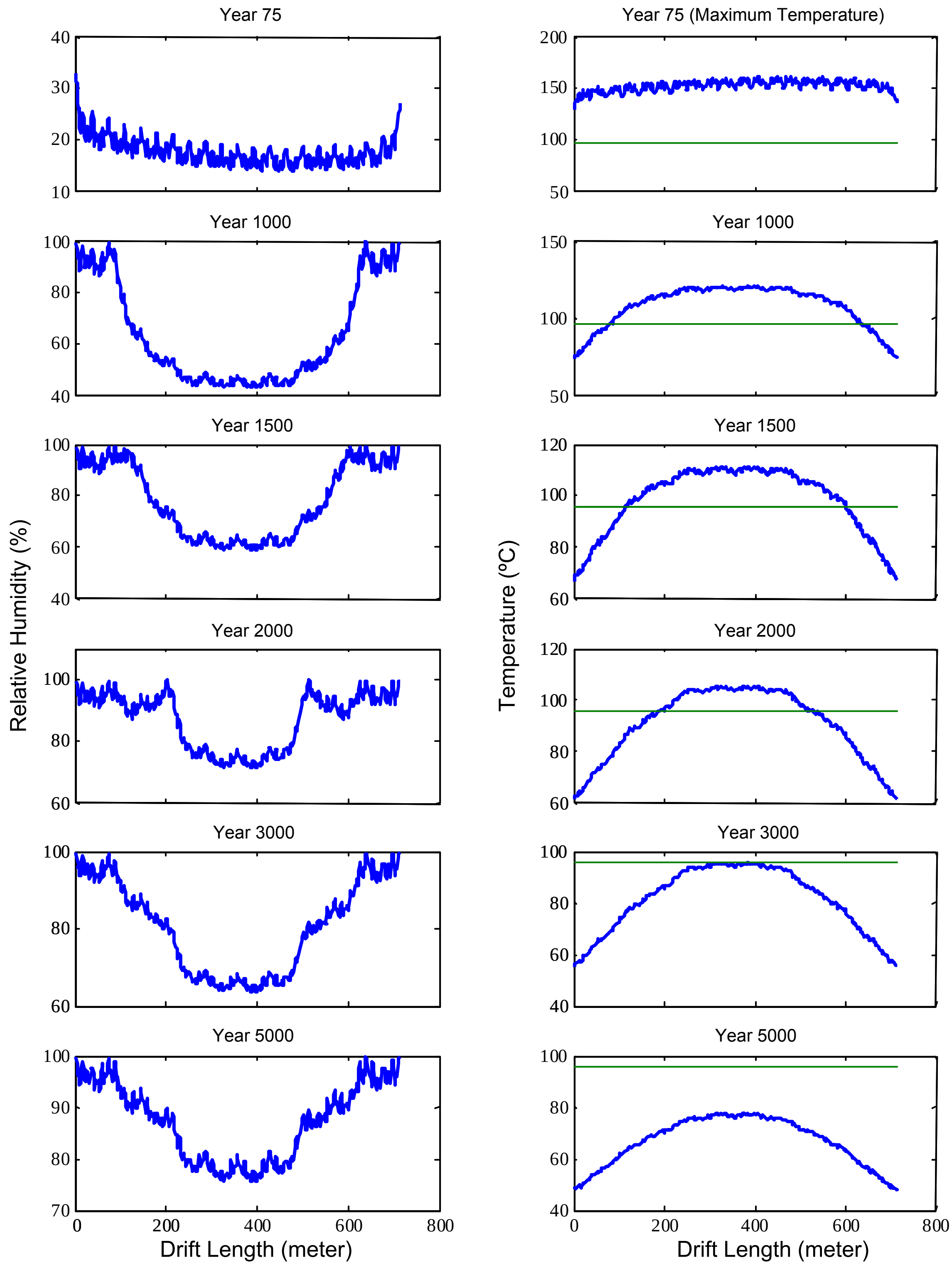


Note: Drift axial dispersion coefficient = 0.004 m$^2$/s; horizontal line in temperature profiles represents boiling temperature of water at 96 °C.

Figure 4-15
Axial Distribution of Drift Centerline Relative Humidity and Temperature for the Case of Pbar$_{av}$-$\sigma$(Pbar) at Selected Post-Closure Time Divisions

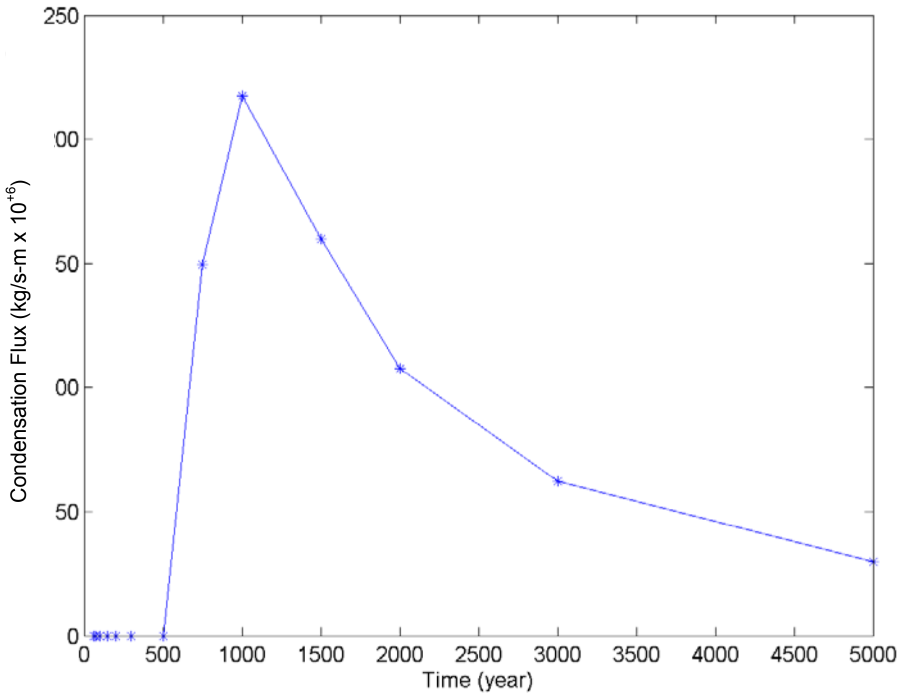


Note: 710.9-meter location with balanced condensation rate.

Figure 5-1
Drift Wall Condensation Rate per Meter of Drift Length

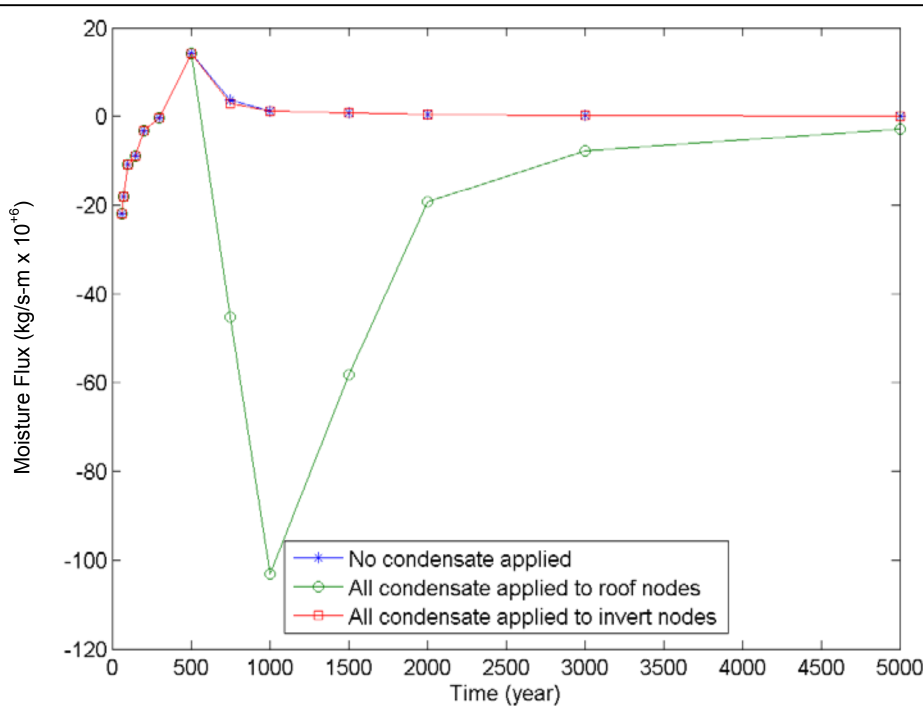


Note: 710.9-meter location with balanced condensation rate.

Figure 5-2
Comparison of Drift Wall Moisture Fluxes

| | | | | | | | | | | | |
|---|---|---|---|---|---|---|---|---|---|---|---|
| 96.02 | 96.12 | 96.19 | 96.23 | 96.24 | 96.25 | 96.25 | 96.26 | 96.27 | 96.27 | 96.28 | 96.28 |
| 96.28 | 96.48 | 96.62 | 96.71 | 96.75 | 96.76 | 96.77 | 96.79 | 96.80 | 96.81 | 96.82 | 96.84 |
| 96.52 | 96.85 | 97.13 | 97.30 | 97.39 | 97.42 | 97.44 | 97.48 | 97.51 | 97.53 | 97.56 | 97.59 |
| 96.69 | 97.15 | 97.57 | 97.85 | 98.02 | 98.07 | 98.11 | 98.19 | 98.25 | 98.28 | 98.33 | 98.39 |
| 96.82 | 97.36 | 97.89 | 98.29 | 98.53 | 98.61 | 98.67 | 98.78 | 98.88 | 98.91 | 98.98 | 99.05 |
| 96.90 | 97.50 | 98.11 | 98.61 | 98.94 | 99.06 | 99.13 | 99.28 | 99.42 | 99.46 | 99.55 | 99.59 |
| 96.95 | 97.57 | 98.22 | 98.77 | 99.15 | 99.29 | 99.38 | 99.55 | 99.71 | 99.75 | 99.84 | 99.85 |
| 96.98 | 97.61 | 98.27 | 98.86 | 99.28 | 99.43 | 99.52 | 99.70 | 99.87 | 99.92 | 99.99 | 100.00 |
| 96.99 | 97.62 | 98.29 | 98.89 | 99.32 | 99.48 | 99.58 | 99.75 | 99.92 | | | |
| 97.00 | 97.64 | 98.31 | 98.92 | 99.37 | 99.53 | 99.63 | 99.80 | 99.96 | | | |
| 97.02 | 97.67 | 98.35 | 98.96 | 99.45 | 99.63 | 99.74 | 99.85 | 99.97 | | | |
| 97.04 | 97.69 | 98.37 | 98.99 | 99.51 | 99.74 | 99.86 | 99.90 | 99.98 | | | |
| 97.06 | 97.72 | 98.39 | 98.99 | 99.53 | 99.89 | 99.99 | 100.00 | 100.00 | | | |
| 97.07 | 97.73 | 98.40 | 98.98 | 99.46 | | | | | | | |
| 97.09 | 97.75 | 98.41 | 98.96 | 99.32 | | | | | | | |
| 97.13 | 97.78 | 98.41 | 98.87 | 99.09 | | | | | | | |
| 97.18 | 97.80 | 98.37 | 98.73 | 98.86 | | | | | | | |
| 97.22 | 97.81 | 98.30 | 98.57 | 98.65 | | | | | | | |
| 97.25 | 97.80 | 98.20 | 98.40 | 98.45 | | | | | | | |
| 97.28 | 97.77 | 98.08 | 98.18 | 98.19 | | | | | | | |
| 97.29 | 97.73 | 97.96 | 97.96 | 97.88 | | | | | | | |
| 97.30 | 97.72 | 97.90 | 97.85 | 97.67 | | | | | | | |
| 97.31 | 97.70 | 97.84 | 97.72 | 97.40 | 97.09 | 96.86 | 96.51 | 96.30 | | | |
| 97.31 | 97.67 | 97.78 | 97.64 | 97.33 | 97.08 | 96.90 | 96.58 | 96.35 | | | |
| 97.32 | 97.64 | 97.70 | 97.52 | 97.22 | 97.06 | 96.94 | 96.69 | 96.42 | 96.27 | 96.00 | 95.67 |
| 97.33 | 97.59 | 97.58 | 97.39 | 97.17 | 97.07 | 97.00 | 96.84 | 96.66 | 96.59 | 96.44 | 96.24 |
| 97.33 | 97.52 | 97.47 | 97.33 | 97.19 | 97.13 | 97.09 | 97.00 | 96.91 | 96.87 | 96.80 | 96.69 |
| 97.34 | 97.46 | 97.42 | 97.33 | 97.26 | 97.23 | 97.21 | 97.17 | 97.12 | 97.10 | 97.07 | 97.02 |
| 97.35 | 97.44 | 97.42 | 97.38 | 97.34 | 97.32 | 97.31 | 97.29 | 97.27 | 97.26 | 97.24 | 97.21 |

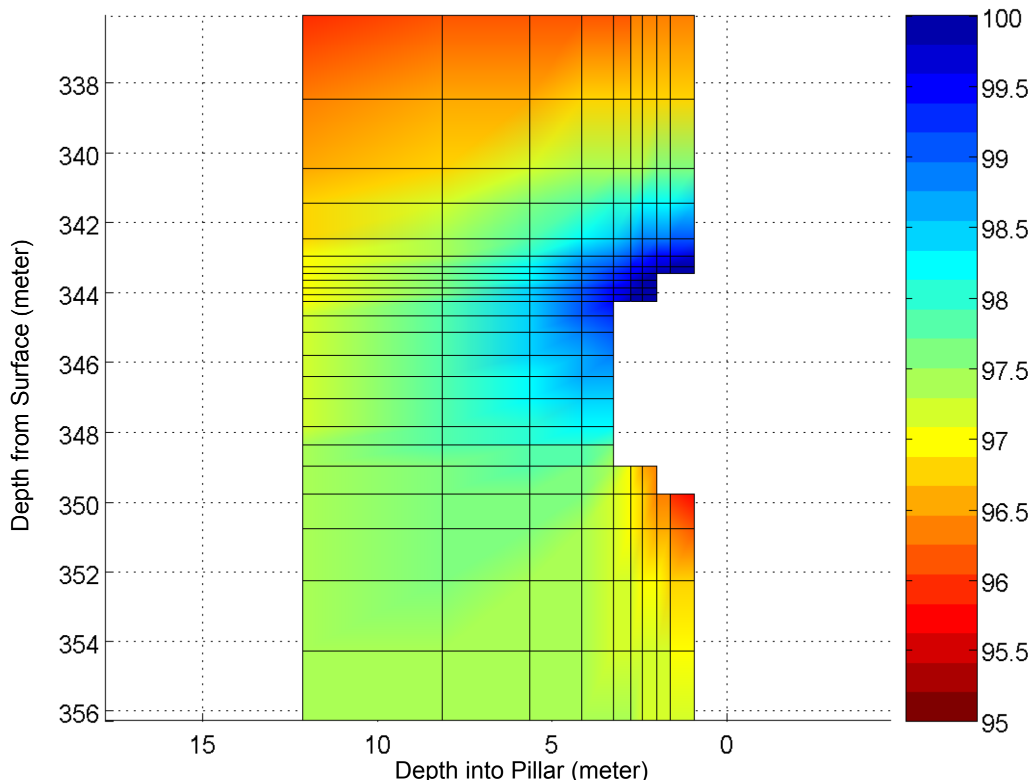


Figure 5-3
Roof Condensation Case: Absolute Rock Matrix Liquid Saturation at Year 5000

| | | | | | | | | | | | |
|---|---|---|---|---|---|---|---|---|---|---|---|
| 0.14 | 0.19 | 0.22 | 0.24 | 0.24 | 0.25 | 0.25 | 0.25 | 0.25 | 0.26 | 0.26 | 0.26 |
| 0.22 | 0.32 | 0.38 | 0.41 | 0.43 | 0.43 | 0.43 | 0.44 | 0.45 | 0.45 | 0.45 | 0.46 |
| 0.31 | 0.47 | 0.58 | 0.64 | 0.67 | 0.68 | 0.69 | 0.70 | 0.71 | 0.71 | 0.72 | 0.72 |
| 0.38 | 0.60 | 0.78 | 0.87 | 0.92 | 0.93 | 0.94 | 0.95 | 0.96 | 0.96 | 0.97 | 0.97 |
| 0.43 | 0.70 | 0.92 | 1.05 | 1.11 | 1.13 | 1.13 | 1.15 | 1.15 | 1.14 | 1.13 | 1.10 |
| 0.47 | 0.77 | 1.03 | 1.20 | 1.27 | 1.28 | 1.29 | 1.30 | 1.28 | 1.26 | 1.22 | 1.10 |
| 0.49 | 0.81 | 1.09 | 1.27 | 1.35 | 1.36 | 1.37 | 1.37 | 1.35 | 1.30 | 1.21 | 1.02 |
| 0.50 | 0.83 | 1.12 | 1.32 | 1.40 | 1.40 | 1.41 | 1.39 | 1.39 | 1.32 | 1.18 | 0.97 |
| 0.51 | 0.84 | 1.13 | 1.33 | 1.41 | 1.42 | 1.41 | 1.39 | 1.40 | | | |
| 0.51 | 0.85 | 1.14 | 1.35 | 1.43 | 1.43 | 1.42 | 1.39 | 1.41 | | | |
| 0.52 | 0.86 | 1.17 | 1.38 | 1.47 | 1.45 | 1.43 | 1.32 | 1.30 | | | |
| 0.53 | 0.88 | 1.18 | 1.40 | 1.51 | 1.48 | 1.44 | 1.22 | 1.17 | | | |
| 0.54 | 0.89 | 1.20 | 1.42 | 1.56 | 1.56 | 1.44 | 1.16 | 1.02 | | | |
| 0.55 | 0.90 | 1.21 | 1.42 | 1.56 | | | | | | | |
| 0.56 | 0.91 | 1.22 | 1.43 | 1.54 | | | | | | | |
| 0.58 | 0.93 | 1.23 | 1.43 | 1.51 | | | | | | | |
| 0.60 | 0.95 | 1.24 | 1.41 | 1.47 | | | | | | | |
| 0.61 | 0.97 | 1.24 | 1.38 | 1.43 | | | | | | | |
| 0.63 | 0.97 | 1.23 | 1.36 | 1.40 | | | | | | | |
| 0.64 | 0.98 | 1.21 | 1.33 | 1.37 | | | | | | | |
| 0.65 | 0.97 | 1.20 | 1.31 | 1.35 | | | | | | | |
| 0.65 | 0.97 | 1.19 | 1.30 | 1.34 | | | | | | | |
| 0.66 | 0.97 | 1.18 | 1.28 | 1.32 | 1.32 | 1.31 | 1.30 | 1.28 | | | |
| 0.66 | 0.96 | 1.16 | 1.27 | 1.30 | 1.30 | 1.29 | 1.28 | 1.27 | | | |
| 0.66 | 0.95 | 1.15 | 1.24 | 1.27 | 1.27 | 1.26 | 1.26 | 1.25 | 1.24 | 1.23 | 1.25 |
| 0.66 | 0.94 | 1.11 | 1.18 | 1.21 | 1.21 | 1.21 | 1.21 | 1.20 | 1.20 | 1.19 | 1.19 |
| 0.66 | 0.91 | 1.05 | 1.12 | 1.13 | 1.14 | 1.14 | 1.14 | 1.14 | 1.14 | 1.14 | 1.13 |
| 0.65 | 0.87 | 0.99 | 1.04 | 1.06 | 1.06 | 1.06 | 1.06 | 1.06 | 1.06 | 1.06 | 1.06 |
| 0.64 | 0.82 | 0.92 | 0.97 | 0.99 | 0.99 | 0.99 | 0.99 | 1.00 | 1.00 | 1.00 | 1.00 |

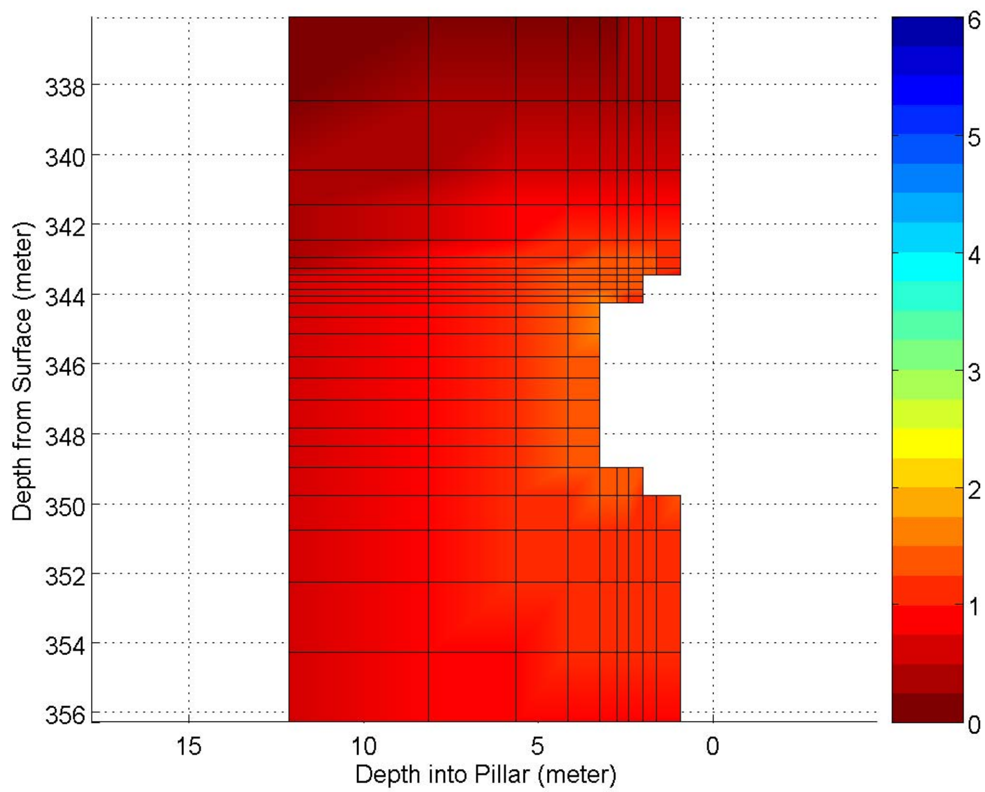


Figure 5-4
Roof Condensation Case: Increase in Rock Matrix Liquid Saturation at Year 5000

| | | | | | | | | | | | |
|---|---|---|---|---|---|---|---|---|---|---|---|
| 4.32 | 4.32 | 4.32 | 4.32 | 4.32 | 4.32 | 4.32 | 4.32 | 4.32 | 4.32 | 4.32 | 4.32 |
| 4.31 | 4.31 | 4.31 | 4.31 | 4.31 | 4.31 | 4.31 | 4.31 | 4.31 | 4.31 | 4.31 | 4.31 |
| 4.31 | 4.30 | 4.30 | 4.30 | 4.30 | 4.30 | 4.30 | 4.30 | 4.30 | 4.30 | 4.30 | 4.30 |
| 4.31 | 4.30 | 4.30 | 4.30 | 4.29 | 4.29 | 4.29 | 4.29 | 4.29 | 4.29 | 4.29 | 4.29 |
| 4.30 | 4.30 | 4.29 | 4.29 | 4.29 | 4.29 | 4.29 | 4.29 | 4.29 | 4.29 | 4.30 | 4.30 |
| 4.30 | 4.30 | 4.29 | 4.29 | 4.29 | 4.29 | 4.29 | 4.32 | 4.38 | 4.42 | 4.49 | 4.55 |
| 4.30 | 4.30 | 4.29 | 4.29 | 4.29 | 4.32 | 4.34 | 4.59 | 5.26 | 5.81 | 6.53 | 7.13 |
| 4.30 | 4.30 | 4.29 | 4.29 | 4.31 | 4.46 | 4.56 | 5.88 | 10.31 | 18.22 | 26.96 | 35.11 |
| 4.30 | 4.30 | 4.29 | 4.29 | 4.33 | 4.54 | 4.67 | 6.11 | 10.41 | | | |
| 4.30 | 4.30 | 4.29 | 4.30 | 4.40 | 4.81 | 5.04 | 6.76 | 10.71 | | | |
| 4.30 | 4.29 | 4.29 | 4.34 | 4.75 | 5.51 | 5.91 | 7.84 | 11.55 | | | |
| 4.30 | 4.29 | 4.29 | 4.56 | 6.14 | 7.89 | 8.96 | 11.53 | 15.14 | | | |
| 4.30 | 4.29 | 4.30 | 5.48 | 12.43 | 25.36 | 32.88 | 42.34 | 48.00 | | | |
| 4.30 | 4.29 | 4.31 | 5.62 | 12.36 | | | | | | | |
| 4.30 | 4.29 | 4.37 | 6.40 | 11.97 | | | | | | | |
| 4.30 | 4.29 | 4.49 | 6.95 | 11.58 | | | | | | | |
| 4.30 | 4.30 | 4.66 | 7.38 | 11.17 | | | | | | | |
| 4.30 | 4.30 | 4.83 | 7.64 | 10.84 | | | | | | | |
| 4.30 | 4.31 | 5.00 | 7.81 | 10.55 | | | | | | | |
| 4.30 | 4.31 | 5.19 | 7.94 | 10.27 | | | | | | | |
| 4.30 | 4.32 | 5.30 | 8.00 | 10.10 | | | | | | | |
| 4.30 | 4.32 | 5.32 | 8.00 | 10.03 | | | | | | | |
| 4.30 | 4.33 | 5.42 | 8.01 | 9.46 | 7.48 | 5.63 | 3.58 | 2.28 | | | |
| 4.30 | 4.34 | 5.44 | 8.00 | 9.41 | 7.49 | 5.71 | 3.65 | 2.31 | | | |
| 4.30 | 4.35 | 5.56 | 7.96 | 8.89 | 7.55 | 6.39 | 4.62 | 3.21 | 2.84 | 1.77 | 0.00 |
| 4.30 | 4.38 | 5.69 | 7.88 | 8.42 | 7.46 | 6.67 | 5.24 | 3.94 | 3.51 | 2.34 | 1.37 |
| 4.30 | 4.42 | 5.84 | 7.75 | 7.97 | 7.29 | 6.77 | 5.66 | 4.57 | 4.13 | 2.99 | 1.79 |
| 4.30 | 4.48 | 5.97 | 7.57 | 7.58 | 7.10 | 6.75 | 5.90 | 5.01 | 4.59 | 3.58 | 2.27 |
| 4.30 | 4.55 | 6.05 | 7.41 | 7.31 | 6.95 | 6.68 | 6.01 | 5.26 | 4.88 | 3.99 | 2.67 |

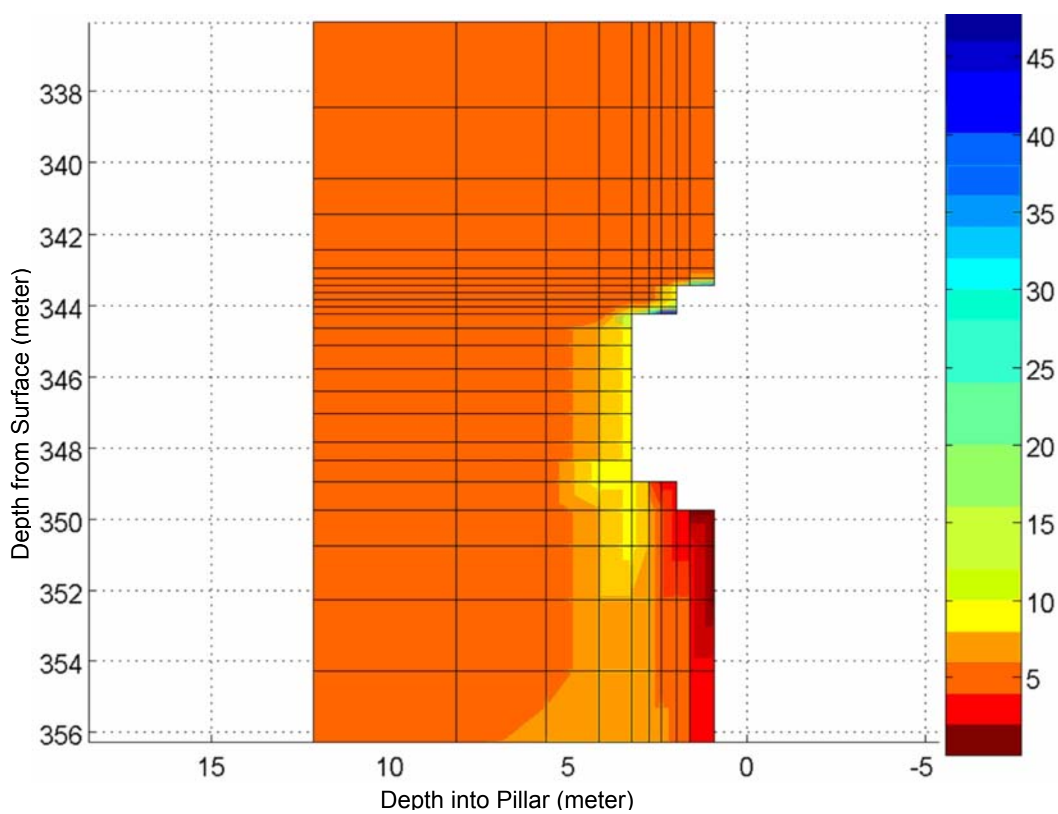


Figure 5-5
Roof Condensation Case: Absolute Rock Fracture Liquid Saturation at Year 5000

| | | | | | | | | | | | |
|---|---|---|---|---|---|---|---|---|---|---|---|
| 0.00 | 0.00 | 0.00 | 0.00 | 0.00 | 0.00 | 0.00 | 0.00 | 0.00 | 0.00 | 0.00 | 0.00 |
| 0.00 | 0.00 | 0.00 | 0.00 | 0.00 | 0.00 | 0.00 | 0.00 | 0.00 | 0.00 | 0.00 | 0.00 |
| 0.00 | 0.00 | 0.00 | 0.00 | 0.00 | 0.00 | 0.00 | 0.00 | 0.00 | 0.00 | 0.00 | 0.00 |
| 0.00 | 0.00 | 0.00 | 0.00 | 0.00 | 0.00 | 0.00 | 0.00 | 0.00 | 0.00 | 0.00 | 0.00 |
| 0.00 | 0.00 | 0.00 | 0.00 | 0.00 | 0.00 | 0.00 | 0.00 | 0.00 | 0.00 | 0.00 | 0.01 |
| 0.00 | 0.00 | 0.00 | 0.00 | 0.00 | 0.00 | 0.01 | 0.02 | 0.05 | 0.06 | 0.09 | 0.10 |
| 0.00 | 0.00 | 0.00 | 0.00 | 0.01 | 0.03 | 0.05 | 0.21 | 0.51 | 0.67 | 0.88 | 1.09 |
| 0.00 | 0.00 | 0.00 | 0.00 | 0.02 | 0.15 | 0.23 | 1.15 | 3.43 | 7.10 | 10.96 | 14.37 |
| 0.00 | 0.00 | 0.00 | 0.00 | 0.03 | 0.21 | 0.32 | 1.30 | 3.55 | | | |
| 0.00 | 0.00 | 0.00 | 0.01 | 0.09 | 0.41 | 0.59 | 1.70 | 3.91 | | | |
| 0.00 | 0.00 | 0.00 | 0.04 | 0.32 | 0.82 | 1.07 | 2.24 | 4.50 | | | |
| 0.00 | 0.00 | 0.00 | 0.22 | 1.11 | 1.92 | 2.47 | 3.95 | 6.22 | | | |
| 0.00 | 0.00 | 0.02 | 0.98 | 4.98 | 11.61 | 15.33 | 19.86 | 22.57 | | | |
| 0.00 | 0.00 | 0.02 | 1.08 | 4.94 | | | | | | | |
| 0.00 | 0.00 | 0.08 | 1.63 | 4.72 | | | | | | | |
| 0.00 | 0.00 | 0.18 | 1.98 | 4.51 | | | | | | | |
| 0.00 | 0.00 | 0.34 | 2.23 | 4.30 | | | | | | | |
| 0.00 | 0.01 | 0.48 | 2.36 | 4.13 | | | | | | | |
| 0.00 | 0.01 | 0.63 | 2.45 | 3.98 | | | | | | | |
| 0.00 | 0.02 | 0.78 | 2.51 | 3.83 | | | | | | | |
| 0.00 | 0.03 | 0.87 | 2.53 | 3.75 | | | | | | | |
| 0.00 | 0.03 | 0.88 | 2.53 | 3.71 | | | | | | | |
| 0.00 | 0.04 | 0.96 | 2.53 | 3.43 | 2.49 | 1.92 | 1.27 | 0.84 | | | |
| 0.00 | 0.04 | 0.97 | 2.53 | 3.41 | 2.50 | 1.97 | 1.32 | 0.87 | | | |
| 0.00 | 0.06 | 1.07 | 2.50 | 3.15 | 2.55 | 2.17 | 1.69 | 1.23 | 1.11 | 0.99 | 0.00 |
| 0.00 | 0.08 | 1.16 | 2.46 | 2.91 | 2.50 | 2.24 | 1.89 | 1.52 | 1.34 | 0.90 | 1.37 |
| 0.00 | 0.12 | 1.26 | 2.38 | 2.67 | 2.41 | 2.24 | 1.99 | 1.72 | 1.55 | 1.18 | 0.72 |
| 0.00 | 0.18 | 1.35 | 2.29 | 2.46 | 2.29 | 2.19 | 2.01 | 1.82 | 1.69 | 1.42 | 0.90 |
| 0.00 | 0.23 | 1.40 | 2.20 | 2.30 | 2.20 | 2.13 | 2.00 | 1.86 | 1.75 | 1.56 | 1.09 |

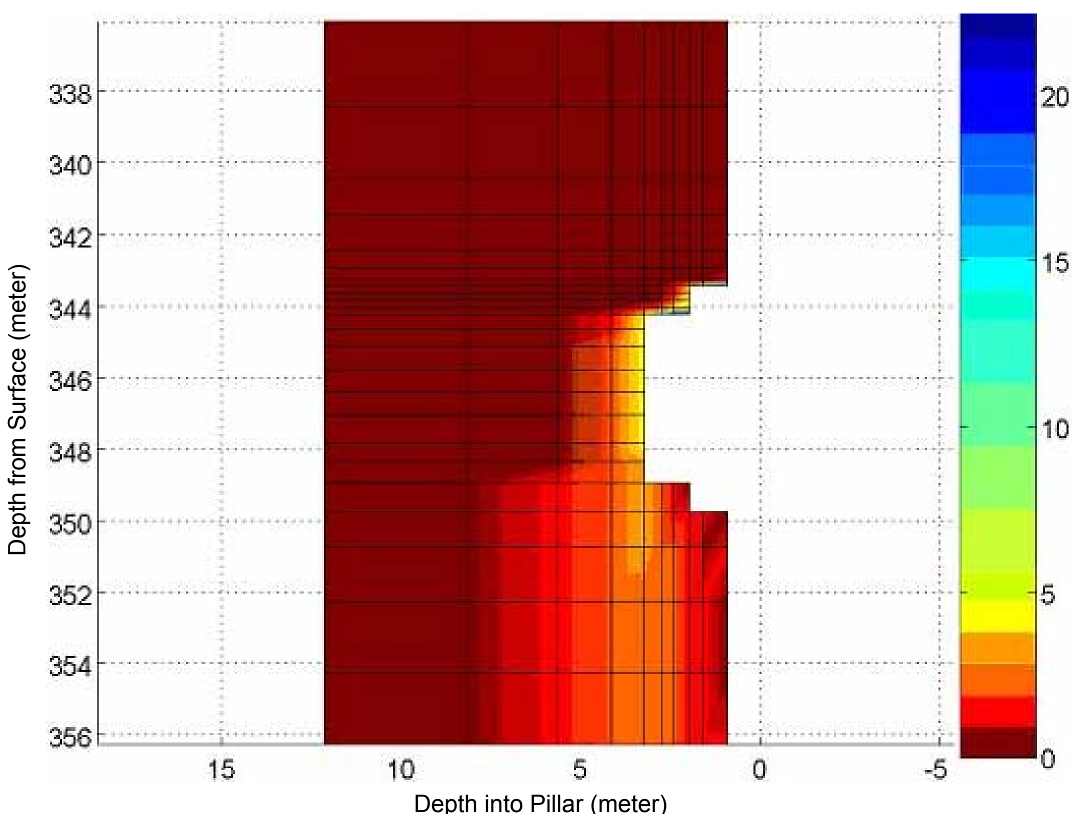


Figure 5-6
Roof Condensation Case: Increase in Rock Fracture Liquid Saturation at Year 5000

| | | | | | | | | | | | |
|---|---|---|---|---|---|---|---|---|---|---|---|
| 95.93 | 95.99 | 96.03 | 96.05 | 96.06 | 96.07 | 96.07 | 96.07 | 96.08 | 96.08 | 96.08 | 96.08 |
| 96.14 | 96.26 | 96.35 | 96.40 | 96.42 | 96.43 | 96.44 | 96.45 | 96.46 | 96.47 | 96.47 | 96.48 |
| 96.35 | 96.55 | 96.71 | 96.81 | 96.87 | 96.89 | 96.90 | 96.93 | 96.96 | 96.97 | 96.99 | 97.01 |
| 96.50 | 96.77 | 97.02 | 97.20 | 97.31 | 97.35 | 97.37 | 97.43 | 97.48 | 97.50 | 97.54 | 97.60 |
| 96.62 | 96.94 | 97.25 | 97.50 | 97.67 | 97.73 | 97.77 | 97.85 | 97.94 | 97.98 | 98.05 | 98.14 |
| 96.71 | 97.07 | 97.43 | 97.73 | 97.96 | 98.04 | 98.10 | 98.23 | 98.36 | 98.42 | 98.53 | 98.68 |
| 96.76 | 97.14 | 97.52 | 97.85 | 98.11 | 98.22 | 98.29 | 98.44 | 98.59 | 98.67 | 98.82 | 99.00 |
| 96.79 | 97.19 | 97.57 | 97.92 | 98.21 | 98.33 | 98.41 | 98.57 | 98.72 | 98.82 | 99.00 | 99.19 |
| 96.81 | 97.21 | 97.59 | 97.94 | 98.24 | 98.37 | 98.46 | 98.62 | 98.76 | | | |
| 96.82 | 97.23 | 97.62 | 97.97 | 98.28 | 98.41 | 98.51 | 98.68 | 98.80 | | | |
| 96.85 | 97.26 | 97.66 | 98.01 | 98.34 | 98.50 | 98.61 | 98.80 | 98.90 | | | |
| 96.87 | 97.30 | 97.69 | 98.04 | 98.38 | 98.59 | 98.73 | 98.94 | 99.04 | | | |
| 96.90 | 97.33 | 97.73 | 98.07 | 98.39 | 98.67 | 98.85 | 99.09 | 99.20 | | | |
| 96.92 | 97.35 | 97.75 | 98.08 | 98.36 | | | | | | | |
| 96.94 | 97.39 | 97.78 | 98.09 | 98.29 | | | | | | | |
| 97.00 | 97.47 | 97.86 | 98.12 | 98.23 | | | | | | | |
| 97.08 | 97.56 | 97.95 | 98.16 | 98.23 | | | | | | | |
| 97.17 | 97.67 | 98.06 | 98.26 | 98.31 | | | | | | | |
| 97.25 | 97.79 | 98.20 | 98.40 | 98.45 | | | | | | | |
| 97.35 | 97.92 | 98.37 | 98.63 | 98.71 | | | | | | | |
| 97.43 | 98.04 | 98.54 | 98.90 | 99.10 | | | | | | | |
| 97.47 | 98.09 | 98.61 | 99.02 | 99.32 | | | | | | | |
| 97.51 | 98.14 | 98.69 | 99.15 | 99.56 | 99.77 | 99.89 | 99.89 | 99.78 | | | |
| 97.55 | 98.19 | 98.75 | 99.21 | 99.57 | 99.74 | 99.83 | 99.87 | 99.84 | | | |
| 97.61 | 98.27 | 98.84 | 99.29 | 99.59 | 99.69 | 99.75 | 99.83 | 99.91 | 99.91 | 99.91 | 99.91 |
| 97.72 | 98.39 | 98.95 | 99.34 | 99.56 | 99.63 | 99.67 | 99.75 | 99.81 | 99.82 | 99.84 | 99.84 |
| 97.85 | 98.52 | 99.03 | 99.34 | 99.50 | 99.55 | 99.59 | 99.65 | 99.70 | 99.72 | 99.75 | 99.77 |
| 98.01 | 98.64 | 99.07 | 99.31 | 99.43 | 99.47 | 99.49 | 99.54 | 99.58 | 99.60 | 99.63 | 99.66 |
| 98.13 | 98.71 | 99.07 | 99.26 | 99.35 | 99.38 | 99.40 | 99.44 | 99.47 | 99.49 | 99.51 | 99.54 |

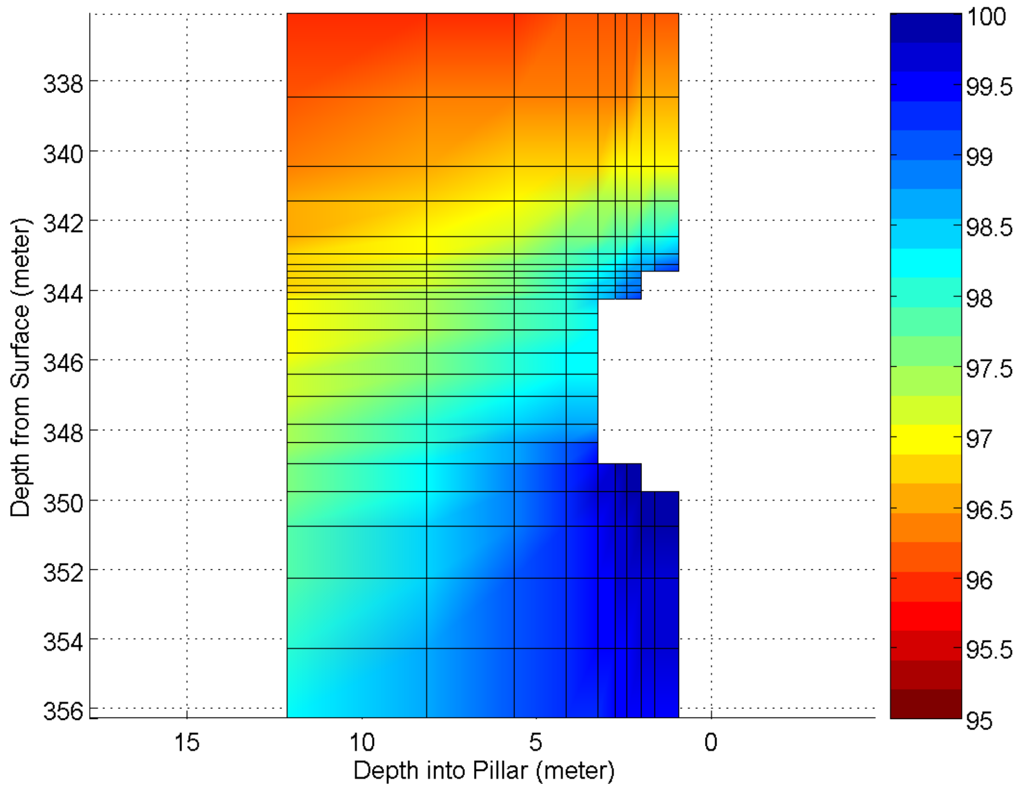


Figure 5-7
Invert Condensation Case: Absolute Rock Matrix Liquid Saturation at Year 5000

| | | | | | | | | | | | |
|---|---|---|---|---|---|---|---|---|---|---|---|
| 0.05 | 0.06 | 0.06 | 0.06 | 0.06 | 0.06 | 0.06 | 0.06 | 0.06 | 0.06 | 0.06 | 0.06 |
| 0.09 | 0.10 | 0.10 | 0.10 | 0.10 | 0.10 | 0.10 | 0.10 | 0.10 | 0.10 | 0.10 | 0.10 |
| 0.14 | 0.16 | 0.16 | 0.16 | 0.16 | 0.15 | 0.15 | 0.15 | 0.15 | 0.15 | 0.15 | 0.15 |
| 0.19 | 0.23 | 0.23 | 0.22 | 0.21 | 0.20 | 0.20 | 0.19 | 0.19 | 0.19 | 0.18 | 0.18 |
| 0.23 | 0.29 | 0.29 | 0.27 | 0.25 | 0.24 | 0.23 | 0.22 | 0.21 | 0.21 | 0.20 | 0.19 |
| 0.28 | 0.35 | 0.35 | 0.32 | 0.28 | 0.27 | 0.26 | 0.24 | 0.22 | 0.22 | 0.20 | 0.18 |
| 0.30 | 0.39 | 0.39 | 0.35 | 0.31 | 0.29 | 0.28 | 0.25 | 0.23 | 0.22 | 0.20 | 0.17 |
| 0.32 | 0.41 | 0.42 | 0.38 | 0.33 | 0.30 | 0.29 | 0.26 | 0.23 | 0.22 | 0.19 | 0.16 |
| 0.33 | 0.42 | 0.43 | 0.39 | 0.33 | 0.31 | 0.29 | 0.26 | 0.24 | | | |
| 0.33 | 0.43 | 0.45 | 0.40 | 0.34 | 0.31 | 0.30 | 0.26 | 0.24 | | | |
| 0.35 | 0.46 | 0.47 | 0.43 | 0.36 | 0.33 | 0.30 | 0.26 | 0.24 | | | |
| 0.37 | 0.48 | 0.50 | 0.46 | 0.39 | 0.34 | 0.31 | 0.26 | 0.23 | | | |
| 0.38 | 0.51 | 0.54 | 0.50 | 0.42 | 0.35 | 0.30 | 0.25 | 0.22 | | | |
| 0.39 | 0.52 | 0.56 | 0.52 | 0.45 | | | | | | | |
| 0.41 | 0.55 | 0.59 | 0.56 | 0.52 | | | | | | | |
| 0.45 | 0.62 | 0.68 | 0.67 | 0.65 | | | | | | | |
| 0.50 | 0.71 | 0.82 | 0.84 | 0.83 | | | | | | | |
| 0.56 | 0.83 | 1.00 | 1.07 | 1.09 | | | | | | | |
| 0.63 | 0.96 | 1.22 | 1.36 | 1.41 | | | | | | | |
| 0.72 | 1.13 | 1.50 | 1.78 | 1.89 | | | | | | | |
| 0.79 | 1.28 | 1.78 | 2.26 | 2.57 | | | | | | | |
| 0.82 | 1.34 | 1.89 | 2.46 | 2.99 | | | | | | | |
| 0.86 | 1.41 | 2.03 | 2.71 | 3.48 | 4.00 | 4.34 | 4.68 | 4.77 | | | |
| 0.90 | 1.48 | 2.14 | 2.84 | 3.54 | 3.96 | 4.23 | 4.56 | 4.76 | | | |
| 0.95 | 1.58 | 2.28 | 3.01 | 3.63 | 3.89 | 4.07 | 4.40 | 4.73 | 4.87 | 5.13 | 5.49 |
| 1.05 | 1.74 | 2.48 | 3.13 | 3.60 | 3.76 | 3.88 | 4.12 | 4.34 | 4.43 | 4.59 | 4.80 |
| 1.18 | 1.91 | 2.61 | 3.13 | 3.45 | 3.56 | 3.63 | 3.79 | 3.93 | 3.98 | 4.08 | 4.22 |
| 1.32 | 2.04 | 2.63 | 3.01 | 3.22 | 3.29 | 3.34 | 3.44 | 3.53 | 3.56 | 3.62 | 3.71 |
| 1.42 | 2.09 | 2.57 | 2.85 | 3.00 | 3.04 | 3.08 | 3.14 | 3.20 | 3.23 | 3.27 | 3.33 |

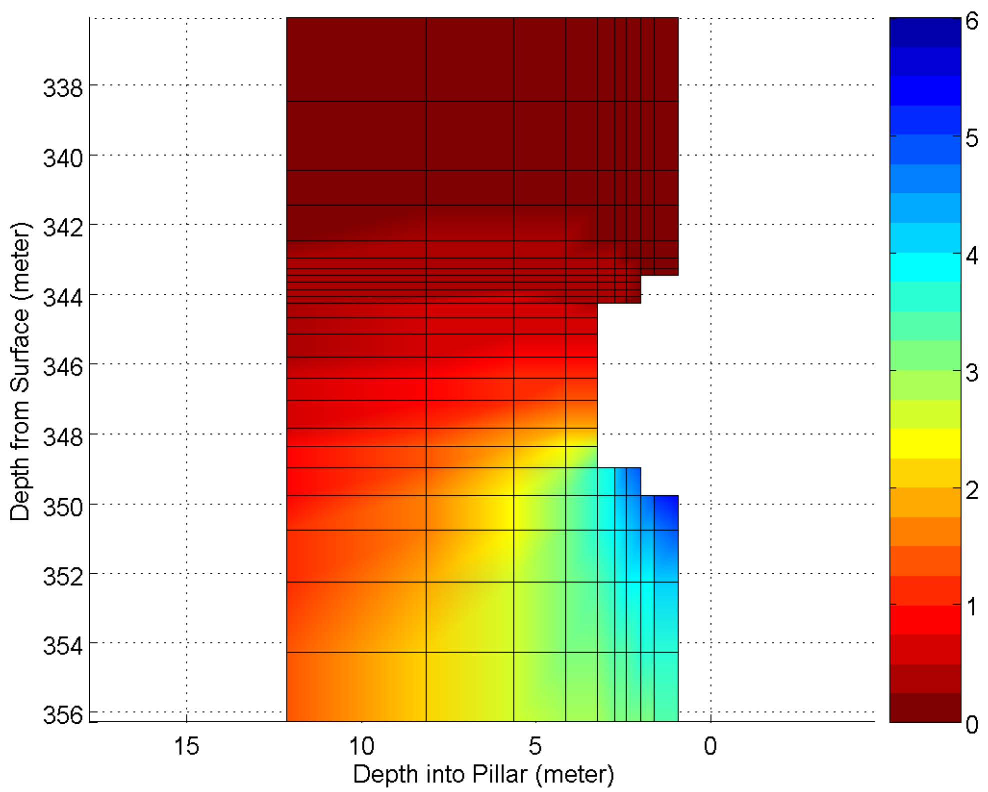


Figure 5-8
Invert Condensation Case: Increase in Rock Matrix Liquid Saturation at Year 5000.

| | | | | | | | | | | | |
|---|---|---|---|---|---|---|---|---|---|---|---|
| 4.32 | 4.32 | 4.32 | 4.32 | 4.32 | 4.32 | 4.32 | 4.32 | 4.32 | 4.32 | 4.32 | 4.32 |
| 4.31 | 4.31 | 4.31 | 4.31 | 4.31 | 4.31 | 4.31 | 4.31 | 4.31 | 4.31 | 4.31 | 4.31 |
| 4.31 | 4.30 | 4.30 | 4.30 | 4.30 | 4.30 | 4.30 | 4.30 | 4.30 | 4.30 | 4.30 | 4.30 |
| 4.31 | 4.30 | 4.30 | 4.29 | 4.29 | 4.29 | 4.29 | 4.29 | 4.29 | 4.29 | 4.29 | 4.29 |
| 4.30 | 4.30 | 4.29 | 4.29 | 4.29 | 4.29 | 4.29 | 4.29 | 4.29 | 4.29 | 4.29 | 4.29 |
| 4.30 | 4.30 | 4.29 | 4.29 | 4.29 | 4.29 | 4.29 | 4.29 | 4.33 | 4.36 | 4.41 | 4.45 |
| 4.30 | 4.29 | 4.29 | 4.29 | 4.28 | 4.29 | 4.30 | 4.37 | 4.75 | 5.14 | 5.65 | 6.04 |
| 4.30 | 4.29 | 4.29 | 4.28 | 4.29 | 4.31 | 4.33 | 4.73 | 6.89 | 11.13 | 16.01 | 20.75 |
| 4.30 | 4.29 | 4.29 | 4.29 | 4.29 | 4.33 | 4.36 | 4.81 | 6.86 | | | |
| 4.30 | 4.29 | 4.29 | 4.29 | 4.31 | 4.40 | 4.45 | 5.06 | 6.81 | | | |
| 4.30 | 4.29 | 4.29 | 4.29 | 4.43 | 4.69 | 4.85 | 5.59 | 7.05 | | | |
| 4.30 | 4.29 | 4.29 | 4.33 | 5.03 | 5.97 | 6.50 | 7.58 | 8.93 | | | |
| 4.30 | 4.29 | 4.29 | 4.50 | 7.46 | 13.76 | 17.57 | 22.51 | 25.46 | | | |
| 4.30 | 4.29 | 4.29 | 4.54 | 7.43 | | | | | | | |
| 4.30 | 4.29 | 4.29 | 4.77 | 7.26 | | | | | | | |
| 4.30 | 4.29 | 4.31 | 4.98 | 7.07 | | | | | | | |
| 4.30 | 4.29 | 4.33 | 5.16 | 6.87 | | | | | | | |
| 4.30 | 4.29 | 4.35 | 5.28 | 6.71 | | | | | | | |
| 4.30 | 4.29 | 4.38 | 5.37 | 6.58 | | | | | | | |
| 4.30 | 4.29 | 4.41 | 5.44 | 6.44 | | | | | | | |
| 4.30 | 4.29 | 4.44 | 5.47 | 6.37 | | | | | | | |
| 4.30 | 4.29 | 4.44 | 5.47 | 6.35 | | | | | | | |
| 4.30 | 4.29 | 4.46 | 5.50 | 6.26 | 6.15 | 6.07 | 5.91 | 3.96 | | | |
| 4.30 | 4.29 | 4.47 | 5.50 | 6.25 | 6.15 | 6.07 | 5.95 | 4.20 | | | |
| 4.30 | 4.29 | 4.50 | 5.52 | 6.17 | 6.14 | 6.12 | 6.22 | 7.02 | 7.00 | 6.98 | 6.98 |
| 4.29 | 4.30 | 4.54 | 5.54 | 6.10 | 6.15 | 6.18 | 6.36 | 6.87 | 6.91 | 6.98 | 7.01 |
| 4.29 | 4.30 | 4.60 | 5.56 | 6.06 | 6.16 | 6.23 | 6.44 | 6.77 | 6.84 | 6.95 | 7.01 |
| 4.30 | 4.31 | 4.67 | 5.57 | 6.04 | 6.17 | 6.26 | 6.47 | 6.72 | 6.79 | 6.92 | 7.00 |
| 4.30 | 4.32 | 4.74 | 5.59 | 6.03 | 6.18 | 6.27 | 6.48 | 6.68 | 6.76 | 6.89 | 7.00 |

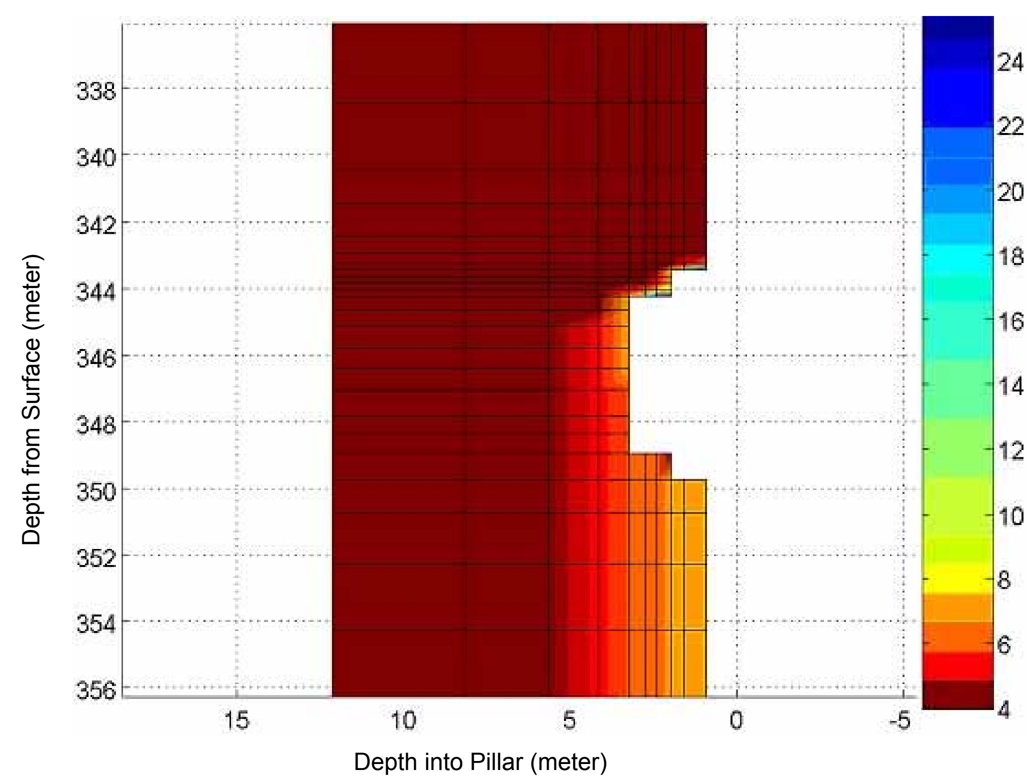


Figure 5-9
Invert Condensation Case: Absolute Rock Fracture Liquid Saturation at Year 5000

| | | | | | | | | | | | |
|---|---|---|---|---|---|---|---|---|---|---|---|
| 0.00 | 0.00 | 0.00 | 0.00 | 0.00 | 0.00 | 0.00 | 0.00 | 0.00 | 0.00 | 0.00 | 0.00 |
| 0.00 | 0.00 | 0.00 | 0.00 | 0.00 | 0.00 | 0.00 | 0.00 | 0.00 | 0.00 | 0.00 | 0.00 |
| 0.00 | 0.00 | 0.00 | 0.00 | 0.00 | 0.00 | 0.00 | 0.00 | 0.00 | 0.00 | 0.00 | 0.00 |
| 0.00 | 0.00 | 0.00 | 0.00 | 0.00 | 0.00 | 0.00 | 0.00 | 0.00 | 0.00 | 0.00 | 0.00 |
| 0.00 | 0.00 | 0.00 | 0.00 | 0.00 | 0.00 | 0.00 | 0.00 | 0.00 | 0.00 | 0.00 | 0.00 |
| 0.00 | 0.00 | 0.00 | 0.00 | 0.00 | 0.00 | 0.00 | 0.00 | 0.00 | 0.00 | 0.00 | 0.00 |
| 0.00 | 0.00 | 0.00 | 0.00 | 0.00 | 0.00 | 0.00 | 0.00 | 0.00 | 0.00 | 0.00 | 0.00 |
| 0.00 | 0.00 | 0.00 | 0.00 | 0.00 | 0.00 | 0.00 | 0.00 | 0.00 | 0.01 | 0.01 | 0.01 |
| 0.00 | 0.00 | 0.00 | 0.00 | 0.00 | 0.00 | 0.00 | 0.00 | 0.00 | | | |
| 0.00 | 0.00 | 0.00 | 0.00 | 0.00 | 0.00 | 0.00 | 0.00 | 0.00 | | | |
| 0.00 | 0.00 | 0.00 | 0.00 | 0.00 | 0.00 | 0.00 | 0.00 | 0.00 | | | |
| 0.00 | 0.00 | 0.00 | 0.00 | 0.00 | 0.00 | 0.00 | 0.00 | 0.01 | | | |
| 0.00 | 0.00 | 0.00 | 0.00 | 0.01 | 0.01 | 0.02 | 0.03 | 0.03 | | | |
| 0.00 | 0.00 | 0.00 | 0.00 | 0.01 | | | | | | | |
| 0.00 | 0.00 | 0.00 | 0.00 | 0.01 | | | | | | | |
| 0.00 | 0.00 | 0.00 | 0.00 | 0.01 | | | | | | | |
| 0.00 | 0.00 | 0.00 | 0.00 | 0.01 | | | | | | | |
| 0.00 | 0.00 | 0.00 | 0.00 | 0.01 | | | | | | | |
| 0.00 | 0.00 | 0.00 | 0.00 | 0.01 | | | | | | | |
| 0.00 | 0.00 | 0.00 | 0.00 | 0.01 | | | | | | | |
| 0.00 | 0.00 | 0.00 | 0.00 | 0.01 | | | | | | | |
| 0.00 | 0.00 | 0.00 | 0.01 | 0.04 | | | | | | | |
| 0.00 | 0.00 | 0.00 | 0.02 | 0.23 | 1.15 | 2.36 | 3.60 | 2.52 | | | |
| 0.00 | 0.00 | 0.00 | 0.03 | 0.25 | 1.15 | 2.33 | 3.61 | 2.76 | | | |
| 0.00 | 0.00 | 0.01 | 0.06 | 0.43 | 1.14 | 1.91 | 3.29 | 5.04 | 5.27 | 6.20 | 6.98 |
| 0.00 | 0.00 | 0.01 | 0.11 | 0.59 | 1.19 | 1.75 | 3.01 | 4.45 | 4.74 | 5.54 | 7.01 |
| 0.00 | 0.00 | 0.03 | 0.19 | 0.76 | 1.27 | 1.70 | 2.77 | 3.92 | 4.27 | 5.15 | 5.94 |
| 0.00 | 0.00 | 0.06 | 0.29 | 0.92 | 1.36 | 1.71 | 2.58 | 3.53 | 3.89 | 4.76 | 5.63 |
| 0.00 | 0.01 | 0.09 | 0.39 | 1.03 | 1.43 | 1.72 | 2.47 | 3.28 | 3.63 | 4.46 | 5.42 |

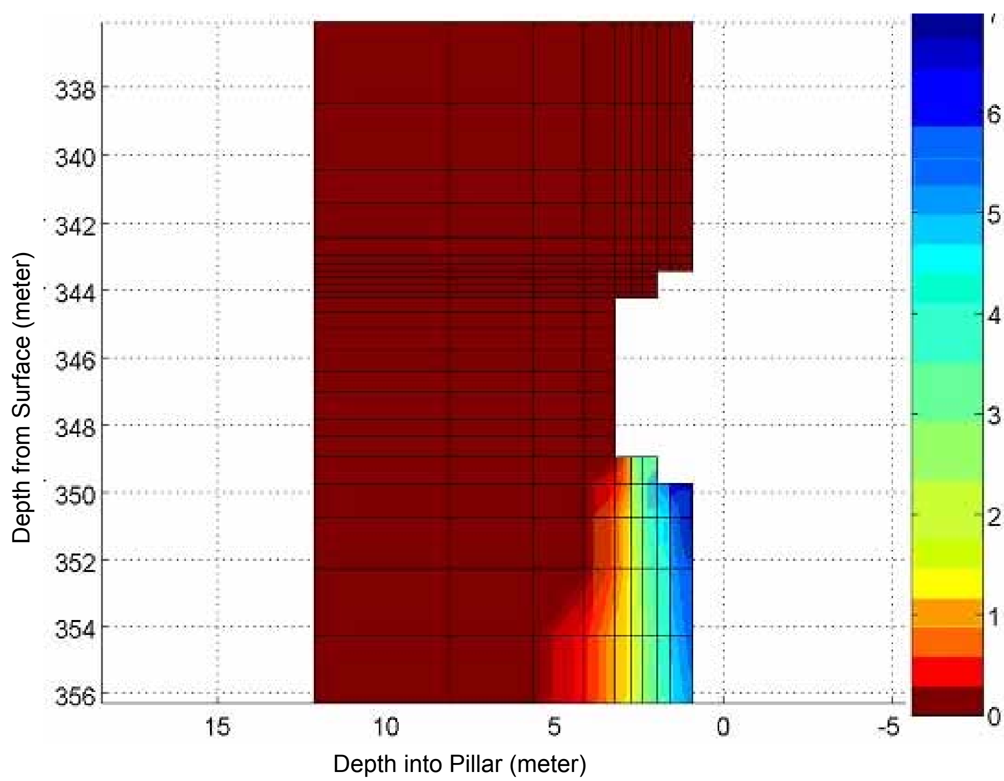


Figure 5-10
Invert Condensation Case: Increase in Rock Fracture Liquid Saturation at Year 5000

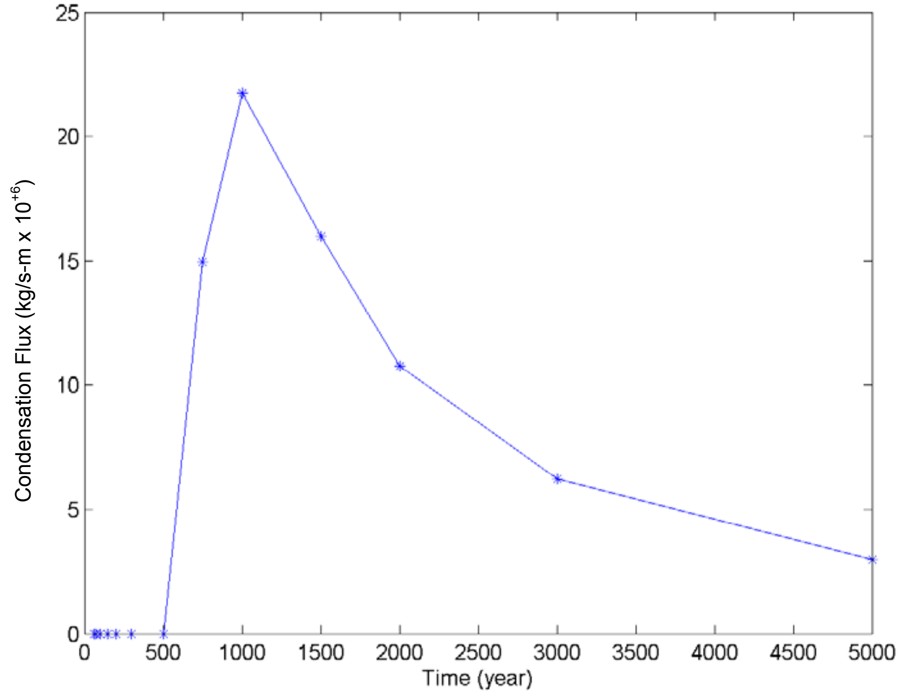


Note: 710.9-meter location with reduced condensation rate.

Figure 5-11
Drift Wall Condensation Rate per Meter of Drift Length

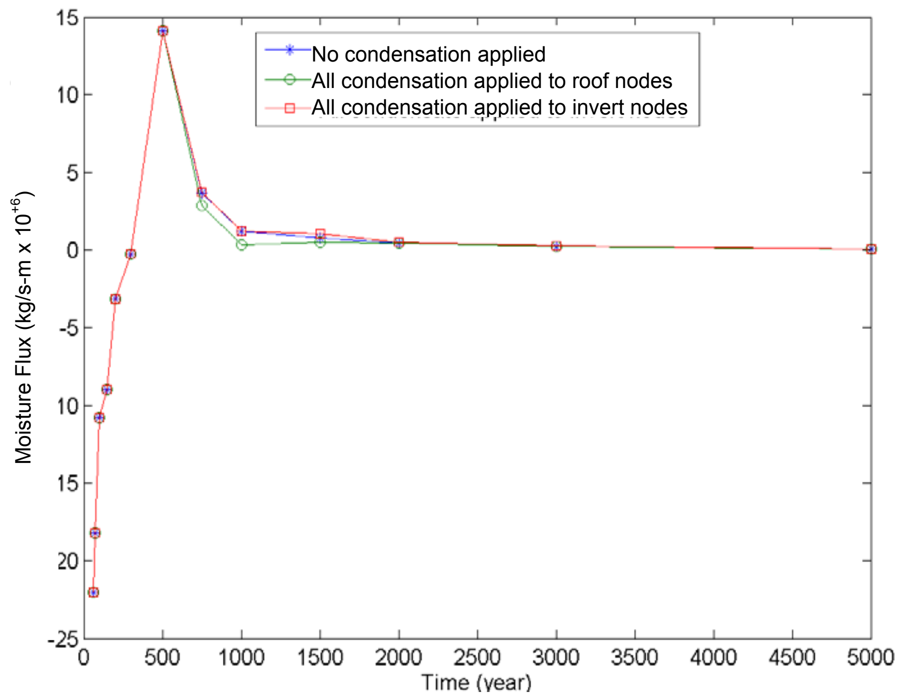


Note: 710.9-meter location with reduced condensation rate.

Figure 5-12
Comparison of Drift Wall Moisture Fluxes for Reduced Condensation Rate

| | | | | | | | | | | | |
|---|---|---|---|---|---|---|---|---|---|---|---|
| 96.00 | 96.10 | 96.16 | 96.19 | 96.21 | 96.22 | 96.22 | 96.23 | 96.23 | 96.24 | 96.24 | 96.25 |
| 96.24 | 96.43 | 96.57 | 96.65 | 96.69 | 96.71 | 96.71 | 96.73 | 96.75 | 96.76 | 96.77 | 96.78 |
| 96.47 | 96.78 | 97.05 | 97.21 | 97.30 | 97.33 | 97.35 | 97.39 | 97.43 | 97.45 | 97.47 | 97.51 |
| 96.63 | 97.06 | 97.46 | 97.74 | 97.91 | 97.96 | 98.00 | 98.08 | 98.15 | 98.18 | 98.23 | 98.29 |
| 96.74 | 97.25 | 97.76 | 98.15 | 98.40 | 98.48 | 98.54 | 98.65 | 98.76 | 98.80 | 98.87 | 98.96 |
| 96.82 | 97.37 | 97.96 | 98.45 | 98.79 | 98.91 | 98.98 | 99.14 | 99.29 | 99.35 | 99.44 | 99.52 |
| 96.86 | 97.43 | 98.05 | 98.60 | 98.99 | 99.13 | 99.22 | 99.40 | 99.57 | 99.64 | 99.75 | 99.80 |
| 96.89 | 97.47 | 98.10 | 98.68 | 99.11 | 99.27 | 99.37 | 99.56 | 99.74 | 99.81 | 99.91 | 99.92 |
| 96.90 | 97.48 | 98.12 | 98.70 | 99.15 | 99.32 | 99.43 | 99.61 | 99.79 | | | |
| 96.91 | 97.50 | 98.14 | 98.73 | 99.20 | 99.37 | 99.49 | 99.67 | 99.85 | | | |
| 96.93 | 97.52 | 98.17 | 98.77 | 99.27 | 99.48 | 99.61 | 99.76 | 99.87 | | | |
| 96.95 | 97.54 | 98.19 | 98.79 | 99.32 | 99.59 | 99.75 | 99.85 | 99.89 | | | |
| 96.96 | 97.56 | 98.20 | 98.79 | 99.32 | 99.71 | 99.90 | 99.93 | 99.94 | | | |
| 96.97 | 97.57 | 98.21 | 98.77 | 99.25 | | | | | | | |
| 96.99 | 97.59 | 98.21 | 98.74 | 99.09 | | | | | | | |
| 97.02 | 97.61 | 98.20 | 98.64 | 98.85 | | | | | | | |
| 97.06 | 97.63 | 98.15 | 98.49 | 98.61 | | | | | | | |
| 97.10 | 97.63 | 98.07 | 98.31 | 98.38 | | | | | | | |
| 97.12 | 97.61 | 97.96 | 98.13 | 98.16 | | | | | | | |
| 97.15 | 97.57 | 97.83 | 97.90 | 97.89 | | | | | | | |
| 97.16 | 97.53 | 97.70 | 97.66 | 97.56 | | | | | | | |
| 97.16 | 97.51 | 97.64 | 97.55 | 97.35 | | | | | | | |
| 97.17 | 97.49 | 97.57 | 97.42 | 97.07 | 96.76 | 96.52 | 96.17 | 95.96 | | | |
| 97.17 | 97.46 | 97.51 | 97.33 | 96.99 | 96.74 | 96.56 | 96.24 | 96.01 | | | |
| 97.17 | 97.43 | 97.43 | 97.20 | 96.89 | 96.72 | 96.61 | 96.35 | 96.08 | 95.93 | 95.66 | 95.28 |
| 97.18 | 97.37 | 97.30 | 97.07 | 96.84 | 96.73 | 96.66 | 96.50 | 96.33 | 96.25 | 96.10 | 95.89 |
| 97.18 | 97.29 | 97.19 | 97.01 | 96.86 | 96.80 | 96.76 | 96.67 | 96.57 | 96.53 | 96.46 | 96.35 |
| 97.17 | 97.23 | 97.13 | 97.02 | 96.93 | 96.90 | 96.88 | 96.83 | 96.79 | 96.77 | 96.74 | 96.69 |
| 97.18 | 97.20 | 97.13 | 97.06 | 97.02 | 97.00 | 96.99 | 96.96 | 96.94 | 96.93 | 96.91 | 96.89 |

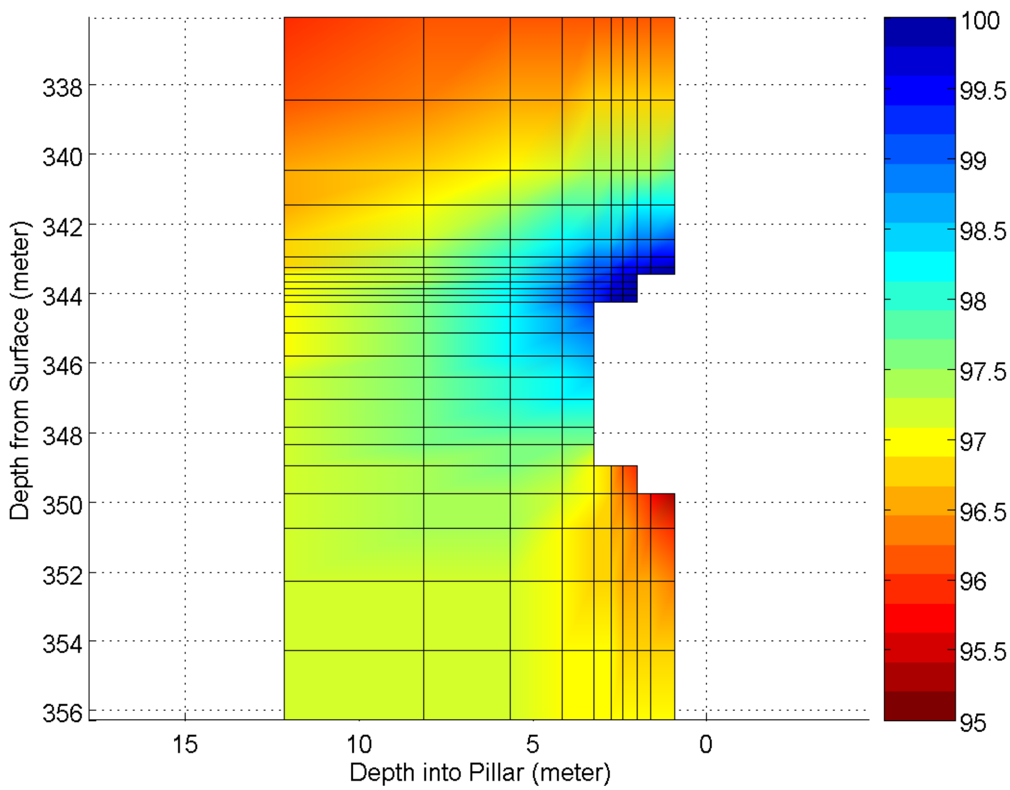


Figure 5-13
Reduced Roof Condensation Case Absolute Rock Matrix Liquid Saturation at Year 5000

| | | | | | | | | | | | |
|---|---|---|---|---|---|---|---|---|---|---|---|
| 0.12 | 0.16 | 0.19 | 0.21 | 0.21 | 0.21 | 0.22 | 0.22 | 0.22 | 0.22 | 0.22 | 0.23 |
| 0.18 | 0.27 | 0.33 | 0.36 | 0.37 | 0.38 | 0.38 | 0.38 | 0.39 | 0.39 | 0.40 | 0.40 |
| 0.26 | 0.40 | 0.50 | 0.56 | 0.59 | 0.60 | 0.60 | 0.61 | 0.62 | 0.63 | 0.63 | 0.64 |
| 0.32 | 0.51 | 0.67 | 0.76 | 0.81 | 0.82 | 0.83 | 0.84 | 0.86 | 0.86 | 0.87 | 0.87 |
| 0.36 | 0.59 | 0.79 | 0.92 | 0.98 | 0.99 | 1.00 | 1.02 | 1.03 | 1.03 | 1.02 | 1.00 |
| 0.39 | 0.65 | 0.88 | 1.04 | 1.11 | 1.13 | 1.15 | 1.16 | 1.16 | 1.14 | 1.12 | 1.03 |
| 0.40 | 0.68 | 0.93 | 1.10 | 1.19 | 1.20 | 1.22 | 1.22 | 1.21 | 1.18 | 1.13 | 0.97 |
| 0.41 | 0.69 | 0.95 | 1.14 | 1.23 | 1.24 | 1.25 | 1.25 | 1.25 | 1.20 | 1.10 | 0.89 |
| 0.42 | 0.70 | 0.96 | 1.15 | 1.24 | 1.26 | 1.26 | 1.25 | 1.27 | | | |
| 0.42 | 0.71 | 0.97 | 1.16 | 1.26 | 1.27 | 1.28 | 1.25 | 1.30 | | | |
| 0.43 | 0.72 | 0.99 | 1.19 | 1.29 | 1.30 | 1.30 | 1.22 | 1.20 | | | |
| 0.44 | 0.73 | 1.00 | 1.20 | 1.33 | 1.33 | 1.32 | 1.17 | 1.08 | | | |
| 0.44 | 0.74 | 1.01 | 1.21 | 1.35 | 1.39 | 1.35 | 1.09 | 0.95 | | | |
| 0.45 | 0.74 | 1.01 | 1.21 | 1.34 | | | | | | | |
| 0.45 | 0.75 | 1.02 | 1.21 | 1.32 | | | | | | | |
| 0.47 | 0.77 | 1.03 | 1.19 | 1.27 | | | | | | | |
| 0.48 | 0.78 | 1.02 | 1.16 | 1.21 | | | | | | | |
| 0.49 | 0.79 | 1.01 | 1.13 | 1.16 | | | | | | | |
| 0.50 | 0.79 | 0.99 | 1.09 | 1.12 | | | | | | | |
| 0.51 | 0.78 | 0.97 | 1.05 | 1.07 | | | | | | | |
| 0.52 | 0.77 | 0.94 | 1.02 | 1.04 | | | | | | | |
| 0.52 | 0.76 | 0.93 | 1.00 | 1.02 | | | | | | | |
| 0.52 | 0.76 | 0.91 | 0.98 | 0.99 | 0.98 | 0.97 | 0.95 | 0.94 | | | |
| 0.52 | 0.75 | 0.90 | 0.96 | 0.97 | 0.96 | 0.95 | 0.94 | 0.93 | | | |
| 0.52 | 0.74 | 0.87 | 0.92 | 0.93 | 0.93 | 0.93 | 0.92 | 0.91 | 0.90 | 0.88 | 0.86 |
| 0.51 | 0.72 | 0.83 | 0.87 | 0.87 | 0.87 | 0.87 | 0.87 | 0.86 | 0.86 | 0.85 | 0.85 |
| 0.50 | 0.68 | 0.77 | 0.80 | 0.80 | 0.80 | 0.80 | 0.80 | 0.80 | 0.80 | 0.80 | 0.80 |
| 0.49 | 0.63 | 0.70 | 0.72 | 0.73 | 0.73 | 0.73 | 0.73 | 0.73 | 0.73 | 0.73 | 0.73 |
| 0.47 | 0.58 | 0.63 | 0.65 | 0.66 | 0.66 | 0.66 | 0.67 | 0.67 | 0.67 | 0.67 | 0.67 |

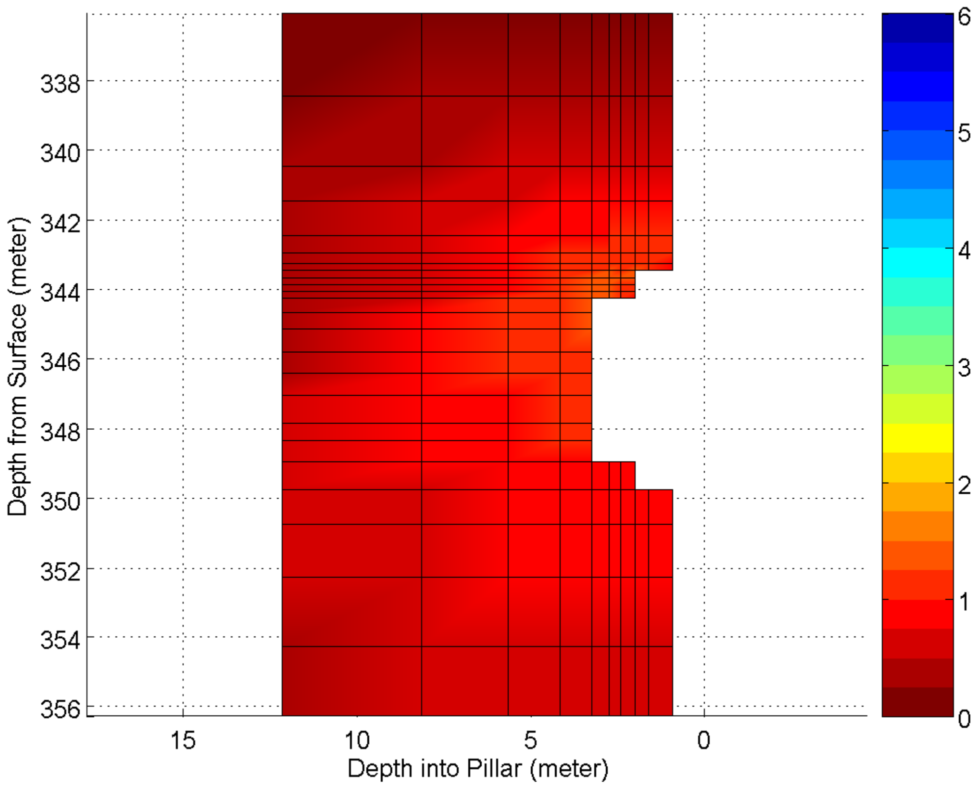


Figure 5-14
Reduced Roof Condensation Case: Increase in Rock Matrix Liquid Saturation at Year 5000

| | | | | | | | | | | | |
|---|---|---|---|---|---|---|---|---|---|---|---|
| 4.32 | 4.32 | 4.32 | 4.32 | 4.32 | 4.32 | 4.32 | 4.32 | 4.32 | 4.32 | 4.32 | 4.32 |
| 4.32 | 4.31 | 4.31 | 4.31 | 4.31 | 4.31 | 4.31 | 4.31 | 4.31 | 4.31 | 4.31 | 4.31 |
| 4.31 | 4.31 | 4.30 | 4.30 | 4.30 | 4.30 | 4.30 | 4.30 | 4.30 | 4.30 | 4.30 | 4.30 |
| 4.31 | 4.30 | 4.30 | 4.30 | 4.29 | 4.29 | 4.29 | 4.29 | 4.29 | 4.29 | 4.29 | 4.29 |
| 4.31 | 4.30 | 4.29 | 4.29 | 4.29 | 4.29 | 4.29 | 4.29 | 4.29 | 4.29 | 4.29 | 4.30 |
| 4.30 | 4.30 | 4.29 | 4.29 | 4.29 | 4.29 | 4.29 | 4.30 | 4.34 | 4.37 | 4.42 | 4.47 |
| 4.30 | 4.30 | 4.29 | 4.29 | 4.29 | 4.30 | 4.30 | 4.40 | 4.83 | 5.24 | 5.78 | 6.20 |
| 4.30 | 4.30 | 4.29 | 4.29 | 4.29 | 4.33 | 4.35 | 4.88 | 7.39 | 12.20 | 17.69 | 23.09 |
| 4.30 | 4.30 | 4.29 | 4.29 | 4.30 | 4.35 | 4.39 | 4.98 | 7.37 | | | |
| 4.30 | 4.30 | 4.29 | 4.29 | 4.32 | 4.44 | 4.52 | 5.29 | 7.33 | | | |
| 4.30 | 4.30 | 4.29 | 4.30 | 4.47 | 4.80 | 4.99 | 5.91 | 7.70 | | | |
| 4.30 | 4.30 | 4.29 | 4.36 | 5.21 | 6.25 | 6.86 | 8.18 | 9.92 | | | |
| 4.30 | 4.29 | 4.29 | 4.61 | 8.21 | 15.56 | 19.99 | 25.81 | 29.34 | | | |
| 4.30 | 4.29 | 4.29 | 4.66 | 8.17 | | | | | | | |
| 4.30 | 4.29 | 4.30 | 4.98 | 7.96 | | | | | | | |
| 4.30 | 4.29 | 4.32 | 5.25 | 7.74 | | | | | | | |
| 4.30 | 4.29 | 4.35 | 5.48 | 7.50 | | | | | | | |
| 4.30 | 4.29 | 4.39 | 5.62 | 7.31 | | | | | | | |
| 4.30 | 4.29 | 4.44 | 5.72 | 7.15 | | | | | | | |
| 4.30 | 4.29 | 4.49 | 5.80 | 6.99 | | | | | | | |
| 4.30 | 4.30 | 4.52 | 5.84 | 6.89 | | | | | | | |
| 4.30 | 4.30 | 4.53 | 5.84 | 6.84 | | | | | | | |
| 4.30 | 4.30 | 4.56 | 5.85 | 6.51 | 5.38 | 4.01 | 2.51 | 1.58 | | | |
| 4.30 | 4.30 | 4.57 | 5.85 | 6.47 | 5.38 | 4.05 | 2.54 | 1.59 | | | |
| 4.30 | 4.30 | 4.61 | 5.83 | 6.17 | 5.38 | 4.56 | 3.20 | 2.17 | 1.94 | 1.24 | 0.00 |
| 4.30 | 4.30 | 4.66 | 5.78 | 5.91 | 5.33 | 4.78 | 3.65 | 2.65 | 2.38 | 1.58 | 0.00 |
| 4.30 | 4.31 | 4.72 | 5.71 | 5.66 | 5.24 | 4.87 | 3.99 | 3.11 | 2.81 | 1.98 | 1.25 |
| 4.30 | 4.32 | 4.78 | 5.61 | 5.46 | 5.14 | 4.88 | 4.21 | 3.47 | 3.17 | 2.38 | 1.52 |
| 4.30 | 4.34 | 4.82 | 5.51 | 5.32 | 5.07 | 4.87 | 4.32 | 3.69 | 3.39 | 2.67 | 1.75 |

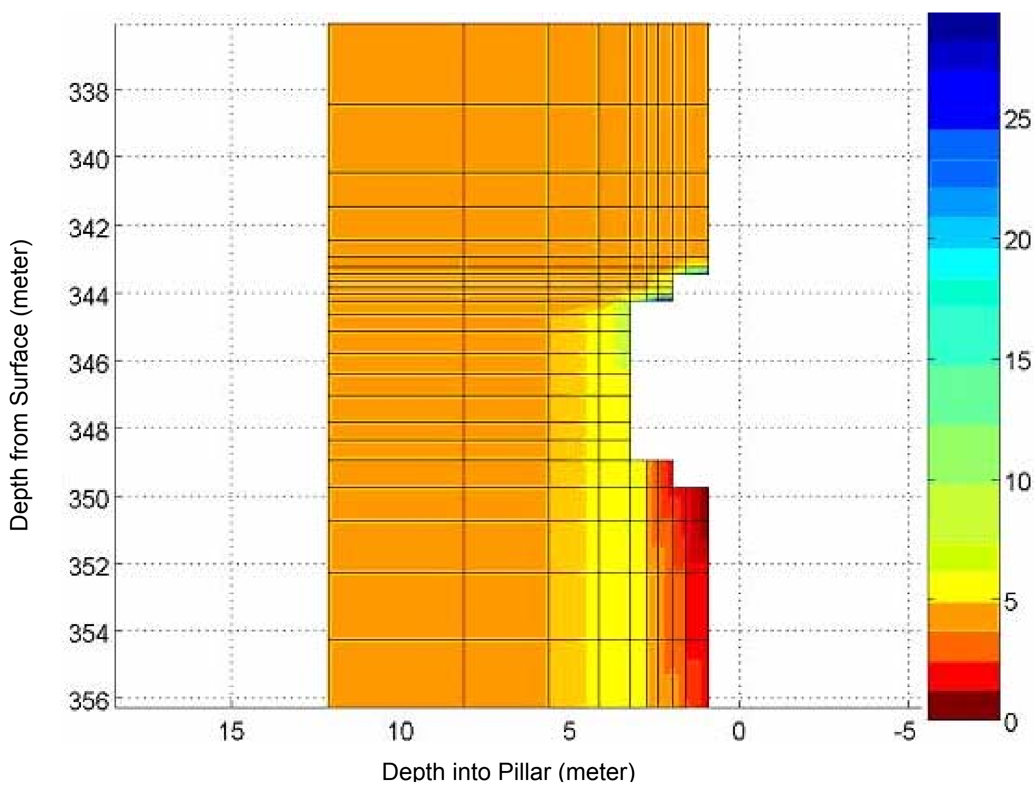


Figure 5-15
Reduced Roof Condensation Case: Absolute Rock Fracture Liquid Saturation at Year 5000

| | | | | | | | | | | | |
|---|---|---|---|---|---|---|---|---|---|---|---|
| 0.00 | 0.00 | 0.00 | 0.00 | 0.00 | 0.00 | 0.00 | 0.00 | 0.00 | 0.00 | 0.00 | 0.00 |
| 0.00 | 0.00 | 0.00 | 0.00 | 0.00 | 0.00 | 0.00 | 0.00 | 0.00 | 0.00 | 0.00 | 0.00 |
| 0.00 | 0.00 | 0.00 | 0.00 | 0.00 | 0.00 | 0.00 | 0.00 | 0.00 | 0.00 | 0.00 | 0.00 |
| 0.00 | 0.00 | 0.00 | 0.00 | 0.00 | 0.00 | 0.00 | 0.00 | 0.00 | 0.00 | 0.00 | 0.00 |
| 0.00 | 0.00 | 0.00 | 0.00 | 0.00 | 0.00 | 0.00 | 0.00 | 0.00 | 0.00 | 0.00 | 0.00 |
| 0.00 | 0.00 | 0.00 | 0.00 | 0.00 | 0.00 | 0.00 | 0.00 | 0.01 | 0.01 | 0.01 | 0.02 |
| 0.00 | 0.00 | 0.00 | 0.00 | 0.00 | 0.00 | 0.01 | 0.03 | 0.08 | 0.11 | 0.14 | 0.16 |
| 0.00 | 0.00 | 0.00 | 0.00 | 0.00 | 0.01 | 0.02 | 0.15 | 0.50 | 1.07 | 1.69 | 2.35 |
| 0.00 | 0.00 | 0.00 | 0.00 | 0.00 | 0.02 | 0.03 | 0.17 | 0.51 | | | |
| 0.00 | 0.00 | 0.00 | 0.00 | 0.01 | 0.04 | 0.06 | 0.23 | 0.53 | | | |
| 0.00 | 0.00 | 0.00 | 0.01 | 0.04 | 0.11 | 0.14 | 0.31 | 0.65 | | | |
| 0.00 | 0.00 | 0.00 | 0.02 | 0.18 | 0.28 | 0.37 | 0.60 | 0.99 | | | |
| 0.00 | 0.00 | 0.00 | 0.11 | 0.76 | 1.81 | 2.43 | 3.33 | 3.91 | | | |
| 0.00 | 0.00 | 0.00 | 0.12 | 0.75 | | | | | | | |
| 0.00 | 0.00 | 0.01 | 0.21 | 0.71 | | | | | | | |
| 0.00 | 0.00 | 0.01 | 0.27 | 0.67 | | | | | | | |
| 0.00 | 0.00 | 0.03 | 0.32 | 0.63 | | | | | | | |
| 0.00 | 0.00 | 0.04 | 0.34 | 0.60 | | | | | | | |
| 0.00 | 0.00 | 0.06 | 0.36 | 0.57 | | | | | | | |
| 0.00 | 0.00 | 0.08 | 0.37 | 0.55 | | | | | | | |
| 0.00 | 0.00 | 0.09 | 0.37 | 0.53 | | | | | | | |
| 0.00 | 0.00 | 0.09 | 0.37 | 0.53 | | | | | | | |
| 0.00 | 0.00 | 0.10 | 0.37 | 0.48 | 0.38 | 0.31 | 0.19 | 0.14 | | | |
| 0.00 | 0.00 | 0.10 | 0.37 | 0.47 | 0.38 | 0.31 | 0.20 | 0.15 | | | |
| 0.00 | 0.01 | 0.12 | 0.37 | 0.43 | 0.38 | 0.35 | 0.26 | 0.19 | 0.21 | 0.46 | 0.00 |
| 0.00 | 0.01 | 0.13 | 0.36 | 0.39 | 0.37 | 0.35 | 0.30 | 0.23 | 0.21 | 0.14 | 0.00 |
| 0.00 | 0.01 | 0.15 | 0.34 | 0.36 | 0.35 | 0.35 | 0.31 | 0.27 | 0.24 | 0.18 | 0.18 |
| 0.00 | 0.01 | 0.16 | 0.32 | 0.34 | 0.33 | 0.33 | 0.31 | 0.28 | 0.26 | 0.21 | 0.14 |
| 0.00 | 0.02 | 0.17 | 0.31 | 0.32 | 0.32 | 0.32 | 0.31 | 0.29 | 0.27 | 0.24 | 0.17 |

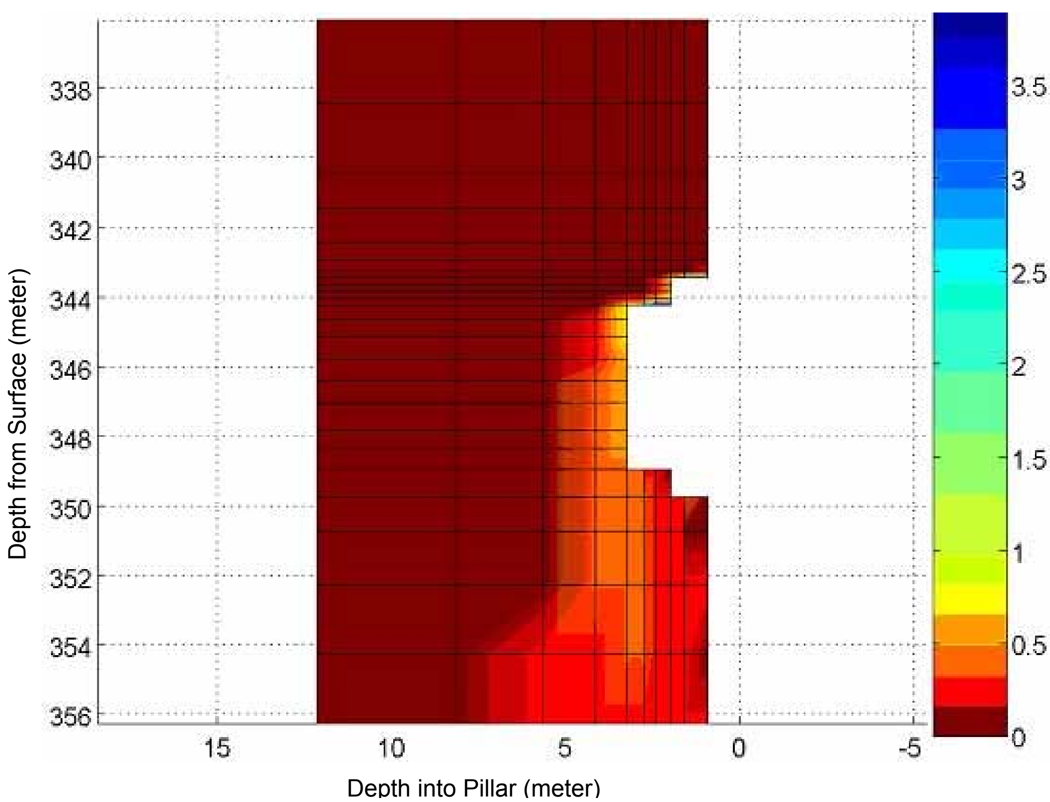


Figure 5-16
Reduced Roof Condensation Case: Increase in Rock Fracture Liquid Saturation at Year 5000

| | | | | | | | | | | | |
|---|---|---|---|---|---|---|---|---|---|---|---|
| 95.92 | 95.98 | 96.02 | 96.04 | 96.05 | 96.05 | 96.06 | 96.06 | 96.07 | 96.07 | 96.07 | 96.07 |
| 96.13 | 96.25 | 96.33 | 96.38 | 96.41 | 96.42 | 96.42 | 96.43 | 96.44 | 96.45 | 96.46 | 96.47 |
| 96.33 | 96.52 | 96.68 | 96.79 | 96.85 | 96.87 | 96.88 | 96.91 | 96.93 | 96.94 | 96.96 | 96.99 |
| 96.47 | 96.74 | 96.98 | 97.16 | 97.28 | 97.31 | 97.34 | 97.40 | 97.45 | 97.47 | 97.51 | 97.57 |
| 96.58 | 96.90 | 97.21 | 97.46 | 97.63 | 97.69 | 97.73 | 97.82 | 97.91 | 97.95 | 98.02 | 98.11 |
| 96.67 | 97.02 | 97.38 | 97.69 | 97.91 | 98.00 | 98.06 | 98.19 | 98.32 | 98.39 | 98.50 | 98.65 |
| 96.72 | 97.09 | 97.46 | 97.80 | 98.07 | 98.17 | 98.25 | 98.40 | 98.55 | 98.64 | 98.79 | 98.97 |
| 96.75 | 97.13 | 97.51 | 97.86 | 98.16 | 98.28 | 98.36 | 98.53 | 98.68 | 98.79 | 98.98 | 99.17 |
| 96.76 | 97.15 | 97.53 | 97.89 | 98.19 | 98.32 | 98.41 | 98.58 | 98.72 | | | |
| 96.77 | 97.16 | 97.55 | 97.91 | 98.23 | 98.37 | 98.46 | 98.64 | 98.76 | | | |
| 96.80 | 97.20 | 97.59 | 97.95 | 98.29 | 98.46 | 98.57 | 98.76 | 98.87 | | | |
| 96.82 | 97.23 | 97.62 | 97.98 | 98.32 | 98.54 | 98.68 | 98.90 | 99.01 | | | |
| 96.85 | 97.26 | 97.65 | 98.00 | 98.33 | 98.62 | 98.81 | 99.05 | 99.17 | | | |
| 96.86 | 97.28 | 97.67 | 98.00 | 98.29 | | | | | | | |
| 96.88 | 97.31 | 97.70 | 98.01 | 98.22 | | | | | | | |
| 96.94 | 97.38 | 97.76 | 98.02 | 98.14 | | | | | | | |
| 97.01 | 97.46 | 97.83 | 98.05 | 98.11 | | | | | | | |
| 97.09 | 97.56 | 97.93 | 98.11 | 98.16 | | | | | | | |
| 97.16 | 97.66 | 98.03 | 98.22 | 98.27 | | | | | | | |
| 97.25 | 97.77 | 98.18 | 98.41 | 98.48 | | | | | | | |
| 97.33 | 97.87 | 98.32 | 98.64 | 98.80 | | | | | | | |
| 97.36 | 97.91 | 98.38 | 98.74 | 99.00 | | | | | | | |
| 97.39 | 97.96 | 98.45 | 98.86 | 99.23 | 99.44 | 99.57 | 99.66 | 99.56 | | | |
| 97.43 | 98.01 | 98.51 | 98.92 | 99.26 | 99.43 | 99.54 | 99.65 | 99.65 | | | |
| 97.48 | 98.07 | 98.59 | 99.01 | 99.31 | 99.43 | 99.50 | 99.64 | 99.77 | 99.77 | 99.77 | 99.77 |
| 97.58 | 98.19 | 98.70 | 99.08 | 99.31 | 99.39 | 99.44 | 99.54 | 99.62 | 99.64 | 99.67 | 99.71 |
| 97.70 | 98.31 | 98.78 | 99.09 | 99.26 | 99.32 | 99.35 | 99.42 | 99.49 | 99.51 | 99.55 | 99.59 |
| 97.84 | 98.41 | 98.82 | 99.06 | 99.18 | 99.22 | 99.25 | 99.30 | 99.35 | 99.37 | 99.40 | 99.44 |
| 97.96 | 98.48 | 98.82 | 99.00 | 99.10 | 99.13 | 99.15 | 99.19 | 99.22 | 99.24 | 99.26 | 99.30 |

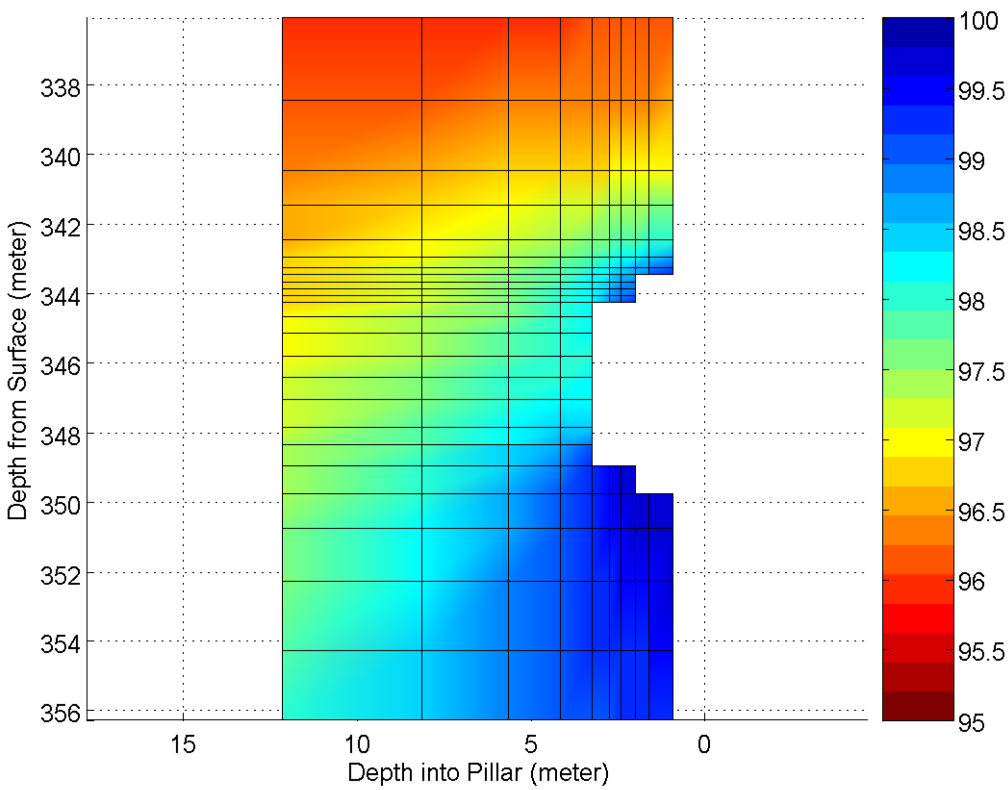


Figure 5-17
Reduced Invert Condensation Case: Absolute Rock Matrix Liquid Saturation at Year 5000

| | | | | | | | | | | | |
|---|---|---|---|---|---|---|---|---|---|---|---|
| 0.04 | 0.05 | 0.05 | 0.05 | 0.05 | 0.05 | 0.05 | 0.05 | 0.05 | 0.05 | 0.05 | 0.05 |
| 0.07 | 0.09 | 0.09 | 0.09 | 0.09 | 0.09 | 0.09 | 0.09 | 0.09 | 0.09 | 0.09 | 0.09 |
| 0.12 | 0.14 | 0.14 | 0.13 | 0.13 | 0.13 | 0.13 | 0.13 | 0.13 | 0.13 | 0.12 | 0.12 |
| 0.16 | 0.19 | 0.19 | 0.18 | 0.17 | 0.17 | 0.17 | 0.16 | 0.16 | 0.16 | 0.15 | 0.15 |
| 0.20 | 0.25 | 0.24 | 0.23 | 0.21 | 0.20 | 0.20 | 0.19 | 0.18 | 0.18 | 0.17 | 0.16 |
| 0.24 | 0.30 | 0.30 | 0.27 | 0.24 | 0.23 | 0.22 | 0.21 | 0.19 | 0.18 | 0.17 | 0.15 |
| 0.26 | 0.33 | 0.33 | 0.30 | 0.26 | 0.25 | 0.24 | 0.22 | 0.20 | 0.18 | 0.17 | 0.15 |
| 0.27 | 0.35 | 0.36 | 0.32 | 0.28 | 0.26 | 0.25 | 0.22 | 0.20 | 0.19 | 0.16 | 0.14 |
| 0.28 | 0.36 | 0.37 | 0.33 | 0.29 | 0.26 | 0.25 | 0.22 | 0.20 | | | |
| 0.29 | 0.37 | 0.38 | 0.34 | 0.29 | 0.27 | 0.25 | 0.22 | 0.21 | | | |
| 0.30 | 0.39 | 0.41 | 0.37 | 0.31 | 0.28 | 0.26 | 0.22 | 0.20 | | | |
| 0.31 | 0.41 | 0.43 | 0.39 | 0.33 | 0.29 | 0.26 | 0.22 | 0.20 | | | |
| 0.33 | 0.44 | 0.46 | 0.43 | 0.36 | 0.30 | 0.26 | 0.21 | 0.19 | | | |
| 0.33 | 0.45 | 0.48 | 0.44 | 0.39 | | | | | | | |
| 0.35 | 0.47 | 0.51 | 0.48 | 0.44 | | | | | | | |
| 0.38 | 0.53 | 0.59 | 0.58 | 0.56 | | | | | | | |
| 0.43 | 0.61 | 0.71 | 0.72 | 0.72 | | | | | | | |
| 0.48 | 0.72 | 0.87 | 0.93 | 0.94 | | | | | | | |
| 0.54 | 0.83 | 1.06 | 1.19 | 1.23 | | | | | | | |
| 0.62 | 0.98 | 1.31 | 1.56 | 1.66 | | | | | | | |
| 0.68 | 1.11 | 1.56 | 1.99 | 2.28 | | | | | | | |
| 0.71 | 1.17 | 1.67 | 2.19 | 2.68 | | | | | | | |
| 0.74 | 1.23 | 1.79 | 2.42 | 3.15 | 3.66 | 4.01 | 4.45 | 4.55 | | | |
| 0.78 | 1.30 | 1.89 | 2.55 | 3.24 | 3.65 | 3.93 | 4.35 | 4.57 | | | |
| 0.82 | 1.38 | 2.03 | 2.73 | 3.36 | 3.64 | 3.82 | 4.21 | 4.59 | 4.73 | 5.00 | 5.35 |
| 0.91 | 1.54 | 2.23 | 2.87 | 3.35 | 3.53 | 3.65 | 3.91 | 4.15 | 4.25 | 4.42 | 4.66 |
| 1.03 | 1.70 | 2.36 | 2.88 | 3.21 | 3.32 | 3.40 | 3.56 | 3.71 | 3.78 | 3.89 | 4.04 |
| 1.15 | 1.82 | 2.39 | 2.76 | 2.98 | 3.05 | 3.10 | 3.20 | 3.29 | 3.33 | 3.40 | 3.49 |
| 1.24 | 1.86 | 2.32 | 2.59 | 2.74 | 2.79 | 2.82 | 2.89 | 2.95 | 2.97 | 3.02 | 3.08 |

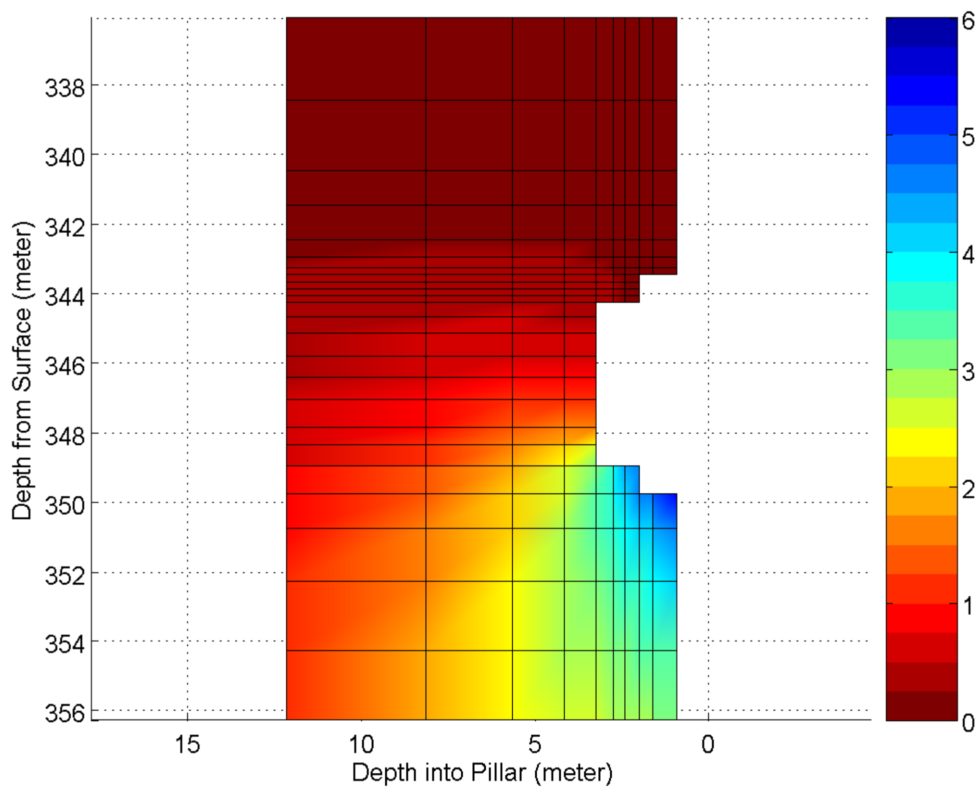


Figure 5-18
Reduced Invert Condensation Case: Increase in Rock Matrix Liquid Saturation at Year 5000

| | | | | | | | | | | | |
|---|---|---|---|---|---|---|---|---|---|---|---|
| 4.32 | 4.32 | 4.32 | 4.32 | 4.32 | 4.32 | 4.32 | 4.32 | 4.32 | 4.32 | 4.32 | 4.32 |
| 4.32 | 4.31 | 4.31 | 4.31 | 4.31 | 4.31 | 4.31 | 4.31 | 4.31 | 4.31 | 4.31 | 4.31 |
| 4.31 | 4.31 | 4.30 | 4.30 | 4.30 | 4.30 | 4.30 | 4.30 | 4.30 | 4.30 | 4.30 | 4.30 |
| 4.31 | 4.30 | 4.30 | 4.30 | 4.29 | 4.29 | 4.29 | 4.29 | 4.29 | 4.29 | 4.29 | 4.29 |
| 4.31 | 4.30 | 4.29 | 4.29 | 4.29 | 4.29 | 4.29 | 4.29 | 4.29 | 4.29 | 4.29 | 4.29 |
| 4.30 | 4.30 | 4.29 | 4.29 | 4.29 | 4.29 | 4.29 | 4.30 | 4.33 | 4.36 | 4.41 | 4.45 |
| 4.30 | 4.30 | 4.29 | 4.29 | 4.29 | 4.29 | 4.30 | 4.37 | 4.75 | 5.14 | 5.65 | 6.04 |
| 4.30 | 4.30 | 4.29 | 4.29 | 4.29 | 4.31 | 4.33 | 4.73 | 6.89 | 11.13 | 16.01 | 20.75 |
| 4.30 | 4.30 | 4.29 | 4.29 | 4.29 | 4.33 | 4.36 | 4.81 | 6.87 | | | |
| 4.30 | 4.30 | 4.29 | 4.29 | 4.31 | 4.40 | 4.46 | 5.06 | 6.81 | | | |
| 4.30 | 4.29 | 4.29 | 4.29 | 4.43 | 4.69 | 4.85 | 5.59 | 7.05 | | | |
| 4.30 | 4.29 | 4.29 | 4.33 | 5.03 | 5.97 | 6.50 | 7.58 | 8.93 | | | |
| 4.30 | 4.29 | 4.29 | 4.50 | 7.46 | 13.76 | 17.57 | 22.50 | 25.46 | | | |
| 4.30 | 4.29 | 4.29 | 4.54 | 7.43 | | | | | | | |
| 4.30 | 4.29 | 4.30 | 4.77 | 7.26 | | | | | | | |
| 4.30 | 4.29 | 4.31 | 4.98 | 7.07 | | | | | | | |
| 4.30 | 4.29 | 4.33 | 5.16 | 6.87 | | | | | | | |
| 4.30 | 4.29 | 4.35 | 5.28 | 6.71 | | | | | | | |
| 4.30 | 4.29 | 4.38 | 5.37 | 6.58 | | | | | | | |
| 4.30 | 4.29 | 4.41 | 5.44 | 6.44 | | | | | | | |
| 4.30 | 4.29 | 4.44 | 5.47 | 6.36 | | | | | | | |
| 4.30 | 4.29 | 4.44 | 5.47 | 6.32 | | | | | | | |
| 4.30 | 4.29 | 4.46 | 5.48 | 6.03 | 5.00 | 3.71 | 2.32 | 1.48 | | | |
| 4.30 | 4.29 | 4.47 | 5.48 | 6.00 | 5.00 | 3.74 | 2.35 | 1.50 | | | |
| 4.30 | 4.30 | 4.50 | 5.46 | 5.75 | 5.01 | 4.23 | 3.00 | 2.74 | 2.84 | 2.99 | 3.04 |
| 4.30 | 4.30 | 4.53 | 5.43 | 5.52 | 4.97 | 4.45 | 3.43 | 2.91 | 2.94 | 2.99 | 3.04 |
| 4.30 | 4.30 | 4.58 | 5.37 | 5.31 | 4.91 | 4.56 | 3.77 | 3.19 | 3.13 | 3.01 | 3.04 |
| 4.30 | 4.31 | 4.62 | 5.29 | 5.14 | 4.84 | 4.60 | 4.00 | 3.46 | 3.34 | 3.09 | 3.05 |
| 4.30 | 4.32 | 4.66 | 5.22 | 5.03 | 4.79 | 4.60 | 4.12 | 3.65 | 3.50 | 3.18 | 3.06 |

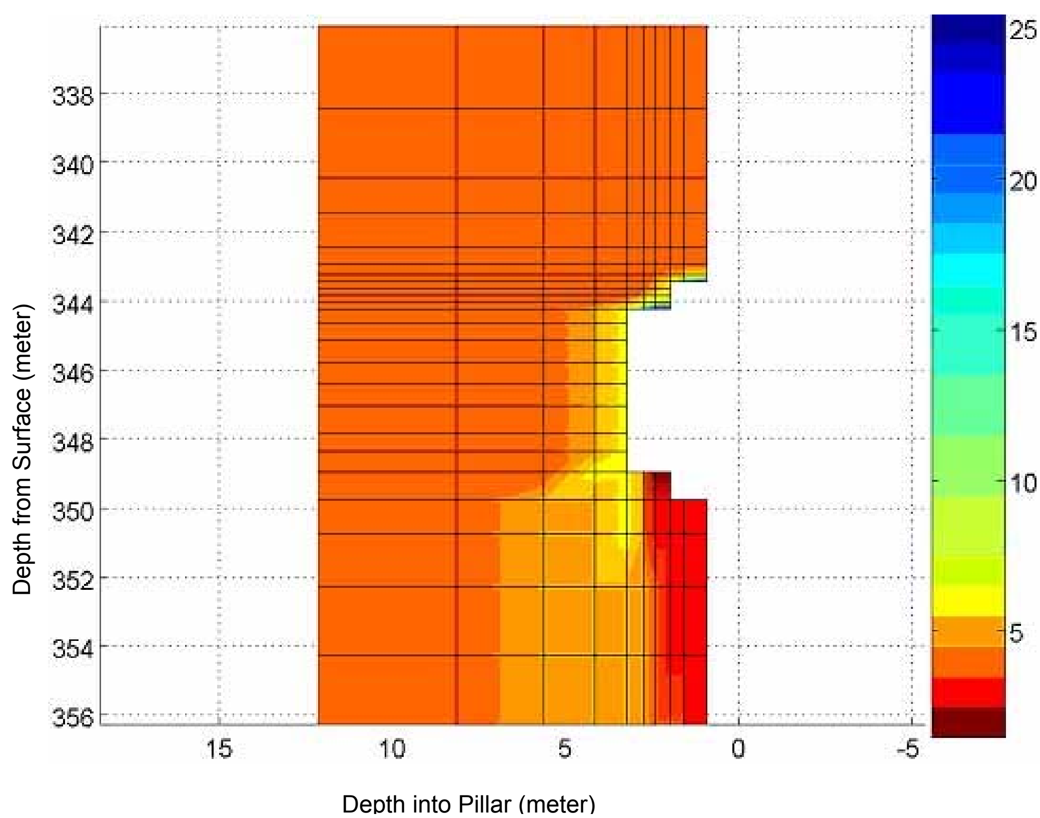


Figure 5-19
Reduced Invert Condensation Case: Absolute Rock Fracture Liquid Saturation at Year 5000

| | | | | | | | | | | | |
|---|---|---|---|---|---|---|---|---|---|---|---|
| 0.00 | 0.00 | 0.00 | 0.00 | 0.00 | 0.00 | 0.00 | 0.00 | 0.00 | 0.00 | 0.00 | 0.00 |
| 0.00 | 0.00 | 0.00 | 0.00 | 0.00 | 0.00 | 0.00 | 0.00 | 0.00 | 0.00 | 0.00 | 0.00 |
| 0.00 | 0.00 | 0.00 | 0.00 | 0.00 | 0.00 | 0.00 | 0.00 | 0.00 | 0.00 | 0.00 | 0.00 |
| 0.00 | 0.00 | 0.00 | 0.00 | 0.00 | 0.00 | 0.00 | 0.00 | 0.00 | 0.00 | 0.00 | 0.00 |
| 0.00 | 0.00 | 0.00 | 0.00 | 0.00 | 0.00 | 0.00 | 0.00 | 0.00 | 0.00 | 0.00 | 0.00 |
| 0.00 | 0.00 | 0.00 | 0.00 | 0.00 | 0.00 | 0.00 | 0.00 | 0.00 | 0.00 | 0.00 | 0.00 |
| 0.00 | 0.00 | 0.00 | 0.00 | 0.00 | 0.00 | 0.00 | 0.00 | 0.00 | 0.00 | 0.00 | 0.00 |
| 0.00 | 0.00 | 0.00 | 0.00 | 0.00 | 0.00 | 0.00 | 0.00 | 0.00 | 0.01 | 0.01 | 0.01 |
| 0.00 | 0.00 | 0.00 | 0.00 | 0.00 | 0.00 | 0.00 | 0.00 | 0.00 | | | |
| 0.00 | 0.00 | 0.00 | 0.00 | 0.00 | 0.00 | 0.00 | 0.00 | 0.00 | | | |
| 0.00 | 0.00 | 0.00 | 0.00 | 0.00 | 0.00 | 0.00 | 0.00 | 0.00 | | | |
| 0.00 | 0.00 | 0.00 | 0.00 | 0.00 | 0.00 | 0.00 | 0.00 | 0.00 | | | |
| 0.00 | 0.00 | 0.00 | 0.00 | 0.01 | 0.01 | 0.02 | 0.02 | 0.03 | | | |
| 0.00 | 0.00 | 0.00 | 0.00 | 0.01 | | | | | | | |
| 0.00 | 0.00 | 0.00 | 0.00 | 0.01 | | | | | | | |
| 0.00 | 0.00 | 0.00 | 0.00 | 0.00 | | | | | | | |
| 0.00 | 0.00 | 0.00 | 0.00 | 0.00 | | | | | | | |
| 0.00 | 0.00 | 0.00 | 0.00 | 0.00 | | | | | | | |
| 0.00 | 0.00 | 0.00 | 0.00 | 0.00 | | | | | | | |
| 0.00 | 0.00 | 0.00 | 0.00 | 0.00 | | | | | | | |
| 0.00 | 0.00 | 0.00 | 0.00 | 0.01 | | | | | | | |
| 0.00 | 0.00 | 0.00 | 0.00 | 0.01 | | | | | | | |
| 0.00 | 0.00 | 0.00 | 0.00 | 0.00 | 0.00 | 0.00 | 0.01 | 0.04 | | | |
| 0.00 | 0.00 | 0.00 | 0.00 | 0.00 | 0.00 | 0.00 | 0.01 | 0.05 | | | |
| 0.00 | 0.00 | 0.00 | 0.00 | 0.01 | 0.01 | 0.01 | 0.06 | 0.77 | 1.11 | 2.21 | 3.04 |
| 0.00 | 0.00 | 0.00 | 0.01 | 0.01 | 0.01 | 0.02 | 0.08 | 0.50 | 0.77 | 1.55 | 3.04 |
| 0.00 | 0.00 | 0.00 | 0.01 | 0.01 | 0.02 | 0.03 | 0.10 | 0.34 | 0.56 | 1.21 | 1.97 |
| 0.00 | 0.00 | 0.01 | 0.01 | 0.02 | 0.03 | 0.05 | 0.10 | 0.27 | 0.44 | 0.93 | 1.67 |
| 0.00 | 0.00 | 0.01 | 0.01 | 0.03 | 0.04 | 0.06 | 0.11 | 0.25 | 0.37 | 0.75 | 1.48 |

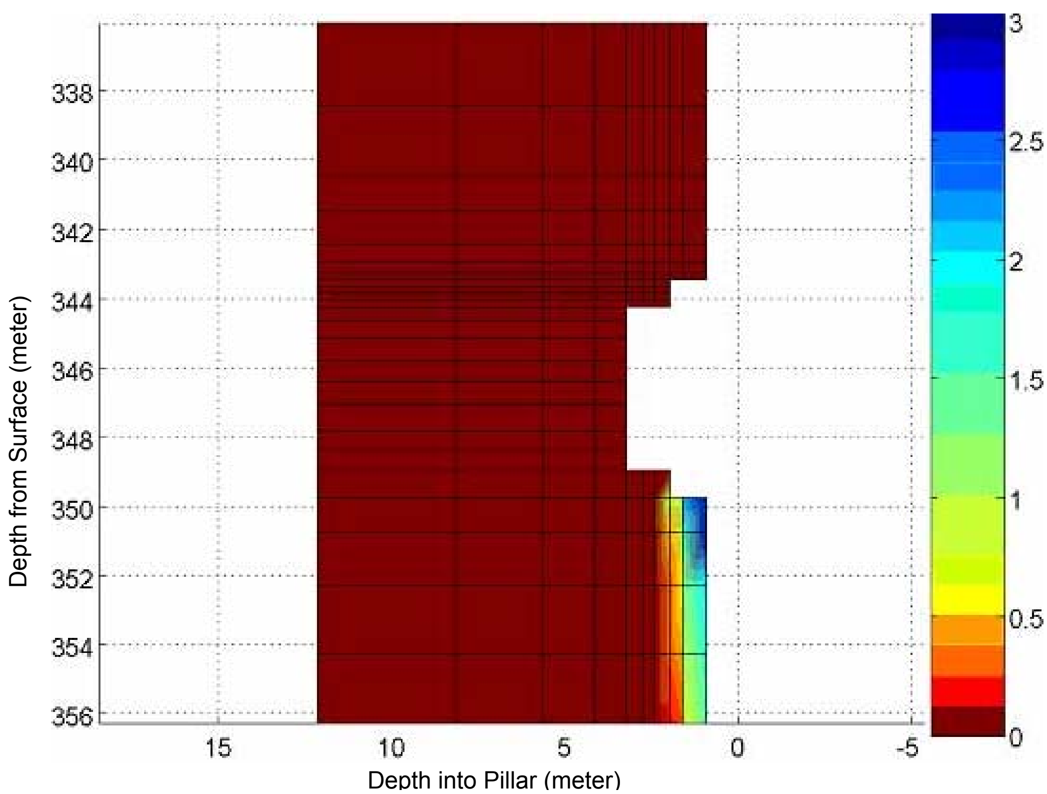


Figure 5-20
Reduced Invert Condensation Case: Increase in Rock Fracture Liquid Saturation at Year 5000

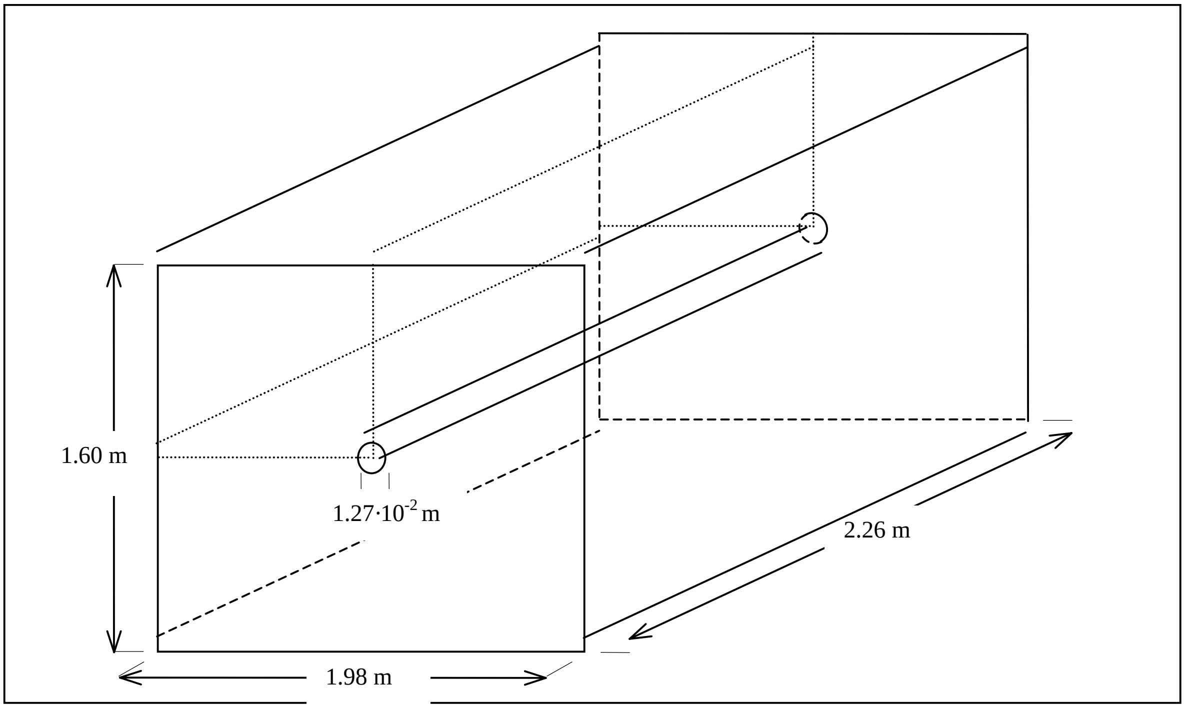


Figure 6-1
Simplified Geometry of Three-Dimensional Welded Tuff Rock

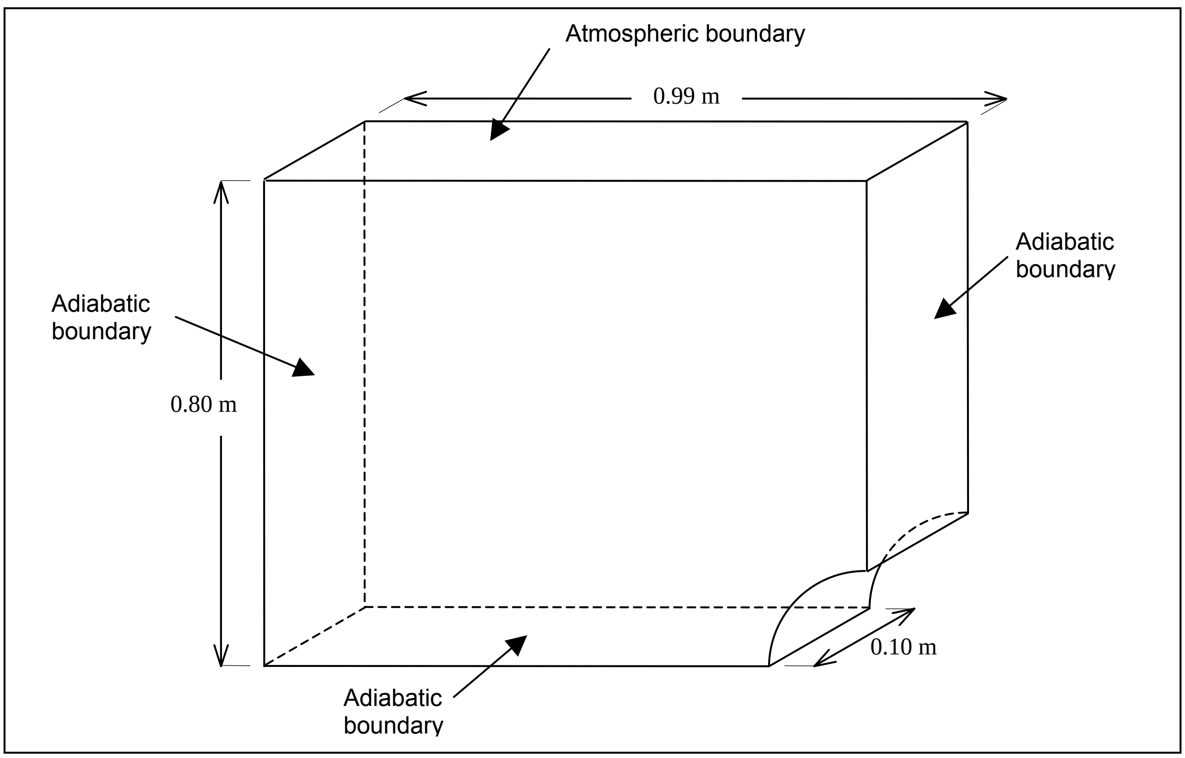


Figure 6-2
Two-Dimensional, One-Fourth Model of Welded Tuff Rock Domain

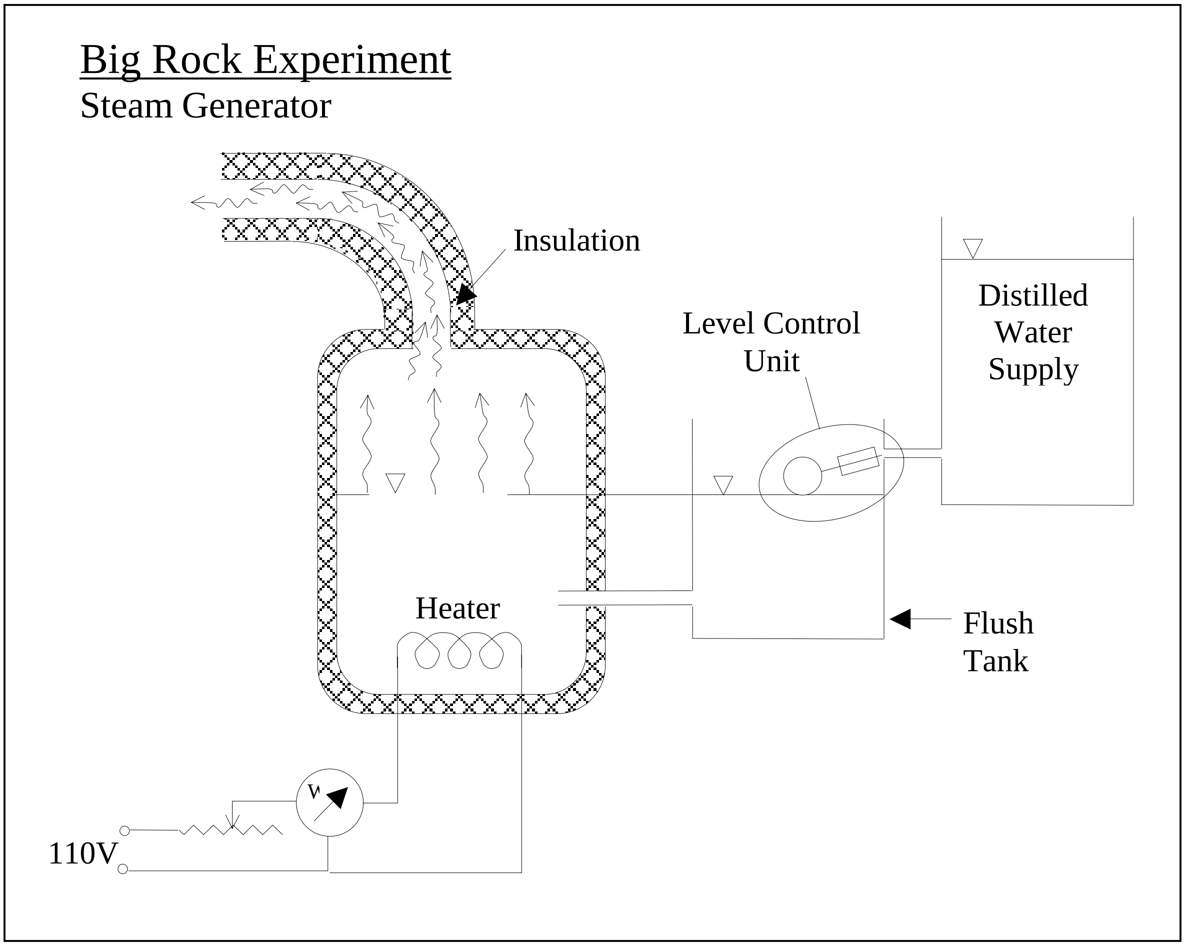


Figure 6-3
Steam Generation Apparatus for Welded Tuff Rock Test
of Moisture Imbibition and Seepage Studies

# Appendix A
# Model Update (Task1)

## CFD Model Configuration

This CFD model configuration is for the post-closure time period.

### model_c11_steam_network2.m

```
%post-closure model configuration with two airlines
%Date: 11/19/03
%Date: 11/02/04 ... added dispersive connection based on dispersion
%coefficients given by S. Webb (2004, ASME).
%Date: 11/09/04 ... added one more airline nodes and airflow loop in each
%section but dispersive between sections.
%Date: 12/16/04 ... replaced the axial dispersive moisture connection with
%directional convective connection in the air lines.
%Date: 01/18/05 ... use a soft approach model configuration in order to
%inject hot steam along the drift toward the edges of the drift.
%
function model_c3_postclosure
%MF3.0
wd='.';  %in test
%configuration macro: prepares CFD model constants of AMR rev01 for Multiflux 2.3
%created on 4/3/01
%This file will be called from cfd_in which prepares Multiflux data files

%!!!!!!!!!!!!!!!
%radiation connections are controlled by non-zero solid angles in the sa matrix
%check ecc ecd edd
%check 3-3 conduction cross section (a7+ainv?)
%kod value?
%!!!!!!!!!!!!!!!

% Definition of lines and nodes
% line 1: containers and gaps - 424 nodes;
% line 2: mixed cold air - 424 nodes;
% line 3: mixed hot air - 424 nodes;
% line 4 liner inside surface - 424 nodes;

dsl=(1.865 0.1 2.6375 2.6375 0.1 2.6525 2.6525 0.1 1.865 1.865 0.1 2.6525...
     2.6525 0.1 2.6375 2.6375 0.1 2.6525 2.6525 0.1 2.785);
dsl=(0.1 dsl(1) repmat((dsl fliplr(dsl)),1,10) dsl(1) 0.1);
LN=length(dsl);
TN=27;  %number of time divisions
LS=(6 LN); %6 lines with 424 segments, entire drift

%NTCF-CFD control table
ctl=dsl*0;
ctl(1:23)=1;
ctl(23+21*0+1:23+21*2)=2;
ctl(23+21*2+1:23+21*5)=3;
ctl(23+21*5+1:23+21*9)=4;
ctl(23+21*9+1:23+21*13)=5;
ctl(23+21*13+1:23+21*16)=6;
ctl(23+21*16+1:23+21*18)=7;
ctl(23+21*18+1:23+21*19+2)=8;


% Container number and container segment indices (zero means no container segment) :
ci=find(dsl~=0.1);
gi=find(dsl==0.1);
nwp=length(gi)-1;
cind=( (1:nwp)' reshape(ci,length(ci)/nwp,nwp)');
(m1  n1)=size(cind);

% Air gap number and indices between containers:
gind=( (1:length(gi))' gi');
(m2  n2)=size(gind);

x=(0 cumsum(dsl));
vf=zeros(TN,LN);
ci=find(dsl~=0.1);
LN=length(dsl);
```

```
d1=1.564;                     %WP diameter
d2=5.52;                      %inner airway diameter

%define connection to NTCF module
%ittg: index vector to relate segments (1,2,..) in NTCF to vector elements in ttg(i)
first=(LS(1)-1)*LN+1;         %first element in 5th line
iliner=first:LS(1)*LN;   %nodes indices on drift surface
igap=gind(:,2:size(gind,2));

%define connection to previous and next sections
%define sources
%iheat: index vector to relate elements of qheat (1,2,...) to CFD nodes
iheat=1:LN;  %nodes of active heat source
%ivapor: index vector to relate elements of moisture network source nodes
ivapor=4*LN+1:5*LN;
ittg=4*LN+1:5*LN;
ippg=4*LN+1:5*LN;
iliner=4*LN+1:5*LN;
iair1=LN+1:2*LN;
iair2=2*LN+1:3*LN;
iair3=3*LN+1:4*LN;
isteam=5*LN+1:6*LN; %steam line
iair=(iair1 iair2 iair3);
%iain: index vector to define intake air elements in ttg(i)
iain=(iair1(1);iair2(1);iair3(1));                               %nodes: first element of
second line
%iaout: index vector to define outflow air elements to connect to next section iain
%case of even LN: exit at  iair2
iaout=(iair1(LN);iair2(LN);iair3(LN));              %nodes: last element of second line

iwin=(iheat(1) iliner(1));    %nodes: surface input prehistory index
iwout=(iheat(LN)  iliner(LN));%nodes: surface output prehistory index



vfactors=0;         %set to 1 if recalculation is needed
if vfactors
    na=20;  %angular divisions
    nl=30;
    for i=ci
        jj=i-7:i+7;
        jj=jj(find(jj>0 & jj<=LN));
        for j=jj
            fcd(find(ci==i),j)=vf_cyl(dsl(i),d1,dsl(j),d2,abs(x(j)-x(i)),na,nl);
        end
    end

    for i=1:LN-1
        j=i+1;
        fdd(i)=vf_ring(dsl(i),dsl(j),d2,x(j)-x(i));
    end

    (m n)=size(cind);
    for i=1:m-1
        i1=max(cind(i,1+find(cind(i,2:n))));
        i2=min(cind(i+1,1+find(cind(i+1,2:n))));
        fcc(i)=vf_disk(d1,d1,sum(dsl(i1+1:i2-1)));
    end
    mwrite(('cfd_d/fcc.dat'), fcc);
    mwrite(('cfd_d/fcd.dat'), fcd);
    mwrite(('cfd_d/fdd.dat'), fdd);
end


%load MULTIFLUX 1.0 fcc fcd fdd solid angle matrices:
fcc=mread((wd '/cfd_d/fcc.dat'));
fdd=mread((wd '/cfd_d/fdd.dat'));
fcd=mread((wd '/cfd_d/fcd.dat'));

%and arrange fcc, fcd, fdd into MULTIFLUX 2.0 sa matrix:
sa=zeros(LS(1)*LN);
```

```
for i=1:m1-1
   i1=max(cind(i,2),cind(i,3));
   i2=cind(i+1,2);
   sa(i1,i2)=fcc(1,i);  %connect WP to WP
end
i2=0;

for i=1:length(ci)
    for j=find(fcd(i,:))
        sa(ci(i),iliner(j))=fcd(i,j); %connect WP to liner
    end
end


for i=1:LN-1
   i1=iliner(i);
   i2=i1+1;
   sa(i1,i2)=fdd(1,i); %connect liner to liner
end


%input data preparation


%This file will be called from model_in which prepares multiflux data files
%input data preparation
pbconst=88720; %user-defined barometric pressure
lew=0.000634;          %Lewis number
kcon=2.02;             %conductivity of wall rock
kvap=1e-10;            %vapor permeability for generator resistance
ainv=0.0;              %invert cross section
arock=(25.5^2-5.5^2)*pi/4;  %rock cross section for axial conduction, 6/17/04
d1=1.564;                     %WP diameter
d2=5.52;                      %inner airway diameter
ct=0.01;                      %wall rock thickness
rgvf=200;                     %RGV wall rock resistance multiplier
rho=2540;                     %rho for wall rock
cp=900;                       %cp for wall rock
keff=10;                      %container inside conduction
cpw=435.25;                   %cp for WP
rcpc=rho*cp;           %rho*cp for concrete
a1=d1*pi;                     %container circumference
a2=d1^2*pi/4;                 %container end surface
a5=d2*pi;                     %drift circumference
a6=d2^2*pi/4;                 %drift cross section
a7=((d2+2*ct)^2-d2^2)*pi/4;   %concrete liner cross section
a8=(a6-a2-ainv);                                      %open cross section
dh=4*a8/(a1+a5);                                      %drift hydraulic diameter
kod=0.025/dh;                 %relative drift surface roughness
hi=1.89;                              %inner surface heat transport coefficient
ho=1.89;                              %outer surface heat transport coefficient

%post-closure
hi=1.85;                              %inner surface heat transport coefficient
ho=1.85;                              %outer surface heat transport coefficient
RpRv=0.62197;           %Rp/Rv
cpa=1050;                %constant Cp
%lewm=1.117*RpRv./cp;    %modified Lewis number
lewm=1.117./cpa;    %modified Lewis number, RpRv is used in m_100 code

%Dm=0.004;        %axial dispersion coefficient, (S. Webb, 2004 ASME), use lowest value, 11/3/04
Dm=0.1;        %axial dispersion coefficient with temperature tilt, (S. Webb, 2004 ASME), use
lowest value, 12/15/04
Kh=Dm/lew;       %equivalent conductivity based on axial dispersion of moisture, 11/3/04

%Thermal leading edge distances:
led=dsl*0+5.5+0.1+1/2*5.5; %AMR model assumption


LN=size(dsl,2);  %conversion
kconc=kcon; %conversion
```

```
e1=0.8;   %example
e2=0.95;  %example
sbc=5.669e-8;  %Stephan-Boltzman constant

cfd_in=( LN sbc e1 e2 d1 d2 ct kconc keff ainv kod rgvf );


%!!!!!!!!!!!!!!!!!!!!!!!

%additional derived radiation constants, using Holman, p. 402, Eq. (8-40)
ecc=1/(1/e1+1/e1-1);                                %container end to container end, 2-body,
fi12=1
ecd=1/(1/e1+d1/d2*(1/e2-1));     %container to drift wall, 2-body, fi12=1
edd=1/(1/e2+1/e2-1);                         %drift wall to drift wall, 2-body, fi12=1



vffa=();  % vffa table: air flow model
vffag=();  % vffag table: air flow model
duca=();  % duca table: air flow model
ducag=();  % ducag table: air flow model

% Definition of connections between nodes of lines - heat
frc=(); % frc table: free convection
foc=();        % foc table: forced convection
moc=();        % moc table: maximum convection
coc=();        % coc table: controlled convection, capacitive
cod=(); % cod table: conduction
rad=();        % rad table: radiation
duc=();        % direct user connection -- not needed for this case; used to be hcc
vcc=();        % differential CFD -- not needed for this case
vccd=();       % differential CFD -- not needed for this case
% Definition of generators
frcg=();       % frcg table: free convection
focg=();       % focg table: forced convection
mocg=();       % mocg table: maximum convection
cocg=();       % cocg table: controlled convection, capacitive
codg=();       % codg table: conduction
radg=();       % radg table: radiation
ducg=();       % direct user connection -- not needed for this case; used to be hcc
vccg=();       % differential CFD -- not needed for this case
steam=();   %steam flow table
% Definition of connections between nodes of lines - moisture
frcm=();       % frcm table: free convection
focm=();       % focm table: forced convection
mocm=();       % mocm table: maximum convection
cocm=();       % cocm table: controlled convection, capacitive
codm=();       % codm table: conduction
ducm=();       % direct user connection -- not needed for this case; used to be hcc
% Definition of generators
frcmg=(); % frcmg table: free convection
focmg=(); % focmg table: forced convection
mocmg=(); % mocmg table: maximum convection
cocmg=(); % cocmg table: controlled convection, capacitive
codmg=(); % codmg table: conduction
ducmg=(); % direct user connection -- not needed for this case; used to be hcc
steamg=();   %steam flow table

%air flow model configuration
%(c i j ai aj dhi dhj L H kod fma);
%%axial flow
% for i=1:LN-1
%     i1=i+LN;    %first air line
%     i2=i+1;
%    vffa=(vffa; 910 i1 i2 a8/3 a8/3 0 0 0 0 0 1/3);
%    vffa=(vffa; 911 i1 i2 0 0 0 0 0 0 0 1);
%     i1=i+2*LN;  %2nd air line
%     i2=i+1;
%    vffa=(vffa; 910 i1 i2 a8/3 a8/3 0 0 0 0 0 1/3);
%    vffa=(vffa; 911 i1 i2 0 0 0 0 0 0 0 1);
%     i1=i+3*LN;  %3rd air line
```

```
%     i2=i+1;
%    vffa=(vffa; 910 i1 i2 a8/3 a8/3 0 0 0 0 0 1/3);
%    vffa=(vffa; 911 i1 i2 0 0 0 0 0 0 0 1);
% end

%section loop
vw=2.0;  %vertical flow width
%fm=0.2;    %assumed vertical air flow rate in cross section
fm=0.2/5;    %assumed vertical air flow rate in cross section, use 1 fifth, 1/18/05
for i=ci    %for WP sections
    i1=iair1(i);
    i2=iair3(i);
    i3=iair2(i);
   vffa=(vffa; 912 i1 i2 dsl(i)*vw dsl(i)*vw 0 0 0 0 0 fm);
   vffa=(vffa; 912 i2 i3 dsl(i)*vw dsl(i)*vw  0 0 0 0 0 fm);
   vffa=(vffa; 912 i3 i1 dsl(i)*vw dsl(i)*vw  0 0 0 0 0 fm);
   vffa=(vffa; 913 i1 i2 0 0 0 0 0 0 0 fm);
   vffa=(vffa; 913 i2 i3 0 0 0 0 0 0 0 fm);
   vffa=(vffa; 913 i3 i1 0 0 0 0 0 0 0 fm);
end

fm_gap=0.01;
for i=gi    %for gap sections
    i1=iair1(i);
    i2=iair3(i);
    i3=iair2(i);
    i4=i;
   vffa=(vffa; 912 i1 i2 dsl(i)*vw dsl(i)*vw  0 0 0 0 0 fm_gap/2);
   vffa=(vffa; 912 i2 i3 dsl(i)*vw dsl(i)*vw  0 0 0 0 0 fm_gap);
   vffa=(vffa; 912 i3 i1 dsl(i)*vw dsl(i)*vw  0 0 0 0 0 fm_gap/2);
   vffa=(vffa; 912 i3 i4 dsl(i)*vw dsl(i)*vw  0 0 0 0 0 fm_gap/2);
   vffa=(vffa; 912 i4 i2 dsl(i)*vw dsl(i)*vw  0 0 0 0 0 fm_gap/2);
   vffa=(vffa; 913 i1 i2 0 0 0 0 0 0 0 fm_gap/2);
   vffa=(vffa; 913 i2 i3 0 0 0 0 0 0 0 fm_gap);
   vffa=(vffa; 913 i3 i1 0 0 0 0 0 0 0 fm_gap/2);
   vffa=(vffa; 913 i3 i4 0 0 0 0 0 0 0 fm_gap/2);
   vffa=(vffa; 913 i4 i2 0 0 0 0 0 0 0 fm_gap/2);
end

% %intake air node, iain
% vffag=(vffag; iain*0+910 iain iain iain*0+a8 iain*0+a8 iain*0 iain*0 iain*0 iain*0 iain*0
iain*0+1/3);
% vffag=(vffag; iain*0+911 iain iain iain*0 iain*0 iain*0 iain*0 iain*0 iain*0 iain*0  iain*0+1);


%1-1 (between nodes on line 1)
% frc table: free convection (within gaps)
%(c i j ai ri ro L m)

% cod table: conduction
%(c i j ai ri ro L k m)
for i=1:m1
   for j=2:n1-1
      i1=cind(i,j);
      i2=cind(i,j+1);
      if i2~=0
         cod=(cod; 500 (i1) (i2) a2 d1/2 d2/2 dsl(i1) keff 1);      %between nodes i1 & i2
         %codm=(codm; 500 (i1) (i2) a2 d1/2 d2/2 dsl(i1) keff*0 1); %moisture unconnected
      end
   end
end
% rad table: radiation
%(c i j ai e vf m)
for i=iheat
   for j=iheat
      if sa(i,j)~=0
         rad=(rad; 600 i j a2 ecc sa(i,j) 1 );
      end
   end
end
```

```
%container end surface to air in the gap
h_gap=2.5;
for i=gi
    if i==1
        i1=i+1;
        i2=i;
        frc=(frc; 100 i1 i2 a2 0 0 0 h_gap);
        frcm=(frcm; 100 i1 i2 a2 0 0 0 h_gap*lewm);
    elseif i==LN
        i1=i-1;
        i2=i;
        frc=(frc; 100 i1 i2 a2 0 0 0 h_gap);
        frcm=(frcm; 100 i1 i2 a2 d1/2 d2/2 dh h_gap*lewm);
    else
        i1=i-1;
        i2=i;
        frc=(frc; 100 i1 i2 a2 0 0 0 h_gap);
        frcm=(frcm; 100 i1 i2 a2 0 0 0 h_gap*lewm);
        i1=i+1;
        i2=i;
        frc=(frc; 100 i1 i2 a2 0 0 0 h_gap);
        frcm=(frcm; 100 i1 i2 a2 0 0 0 h_gap*lewm);
    end
end




%1-2 (between nodes on line 1 and line 2, iair1)
%frc table: user-defined heat transport coefficient
for i=ci
    i1=iheat(i);
    i2=iair1(i);
   frc=(frc; 100 i1 i2 a1*dsl(i) 0 0 0  hi);
   frcm=(frcm; 100 i1 i2 a1*dsl(i) 0 0 0 hi*lewm);
end


%2-2 (between nodes on line 2)
%cod table: axial conduction/dispersion in air nodes, iair1
for i=1:LN-1
    i1=iair1(i);
    i2=i1+1;
   cod=(cod; 500 i1 i2 a8/3 0 0 (dsl(i)+dsl(i+1))/2  Kh 1); %third of the open cross section
   frcm=(frcm; 100 i1 i2 a8/3 0 0 0  Dm/((dsl(i)+dsl(i+1))/2));    %third of the open cross
section
end


%vertical loop controlled-convection connections

for i=ci    %for WP section
    i1=iair1(i);
    i2=iair3(i);
    i3=iair2(i);
   coc=(coc; 400 i1 i2 0 1);
   coc=(coc; 400 i2 i3 0 1);
   coc=(coc; 400 i3 i1 0 1);
   cocm=(cocm; 400 i1 i2 0 1);
   cocm=(cocm; 400 i2 i3 0 1);
   cocm=(cocm; 400 i3 i1 0 1);
end
for i=gi    %for gap section
    i1=iair1(i);
    i2=iair3(i);
    i3=iair2(i);
    i4=i;
   coc=(coc; 400 i1 i2 0 1);
   coc=(coc; 400 i2 i3 0 1);
   coc=(coc; 400 i3 i1 0 1);
   coc=(coc; 400 i4 i2 0 1);
```

```
   coc=(coc; 400 i3 i4 0 1);
   cocm=(cocm; 400 i1 i2 0 1);
   cocm=(cocm; 400 i2 i3 0 1);
   cocm=(cocm; 400 i3 i1 0 1);
   cocm=(cocm; 400 i4 i2 0 1);
   cocm=(cocm; 400 i3 i4 0 1);
end


%3-3 (between nodes on line 3, iair2)
%cod table: axial conduction/dispersion in air nodes
for i=1:LN-1
    i1=iair2(i);
    i2=i1+1;
   cod=(cod; 500 i1 i2 a8/3 0 0 ((dsl(i)+dsl(i+1))/2)  Kh 1);      %half of the open cross
section
   frcm=(frcm; 100 i1 i2 a8/3 0 0 0  Dm/((dsl(i)+dsl(i+1))/2));    %third of the open cross
section
end


%4-4 (between nodes on line 4, iair3)
%cod table: axial conduction/dispersion in air nodes
for i=1:LN-1
    i1=iair3(i);
    i2=i1+1;
   cod=(cod; 500 i1 i2 a8/3 0 0 ((dsl(i)+dsl(i+1))/2)  Kh 1);      %half of the open cross
section
   frcm=(frcm; 100 i1 i2 a8/3 0 0 0  Dm/((dsl(i)+dsl(i+1))/2));    %third of the open cross
section
end


%4-5 (between nodes on line 4 and line 5, iair3 and liner), 20% rock surface
%frc table: user-defined heat transport coefficient
for i=1:LN
    i1=iliner(i);
    i2=iair3(i);
   frc=(frc; 100 i1 i2 a5*dsl(i)*0.20 0 0 0 hi);
   frcm=(frcm; 100 i1 i2 a5*dsl(i)*0.20 0 0 0 hi*lewm);
end
%3-5 (between nodes on line 3 and line 5, iair2 and liner), 80% rock surface
%frc table: user-defined heat transport coefficient
for i=1:LN
   i1=iliner(i);
   i2=iair2(i);
   frc=(frc; 100 i1 i2 a5*dsl(i)*0.80 0 0 0 hi);
   frcm=(frcm; 100 i1 i2 a5*dsl(i)*0.80 0 0 0 hi*lewm);
end

%5-5 (between nodes on line 5, liner)

% cod table: conduction
%(c i j ai ri ro L k m)
for i=1:LN-1
   i1=iliner(i);
   i2=i1+1;
   cod=(cod; 500 i1 i2 a7+ainv+arock d1/2 d2/2 ((dsl(i)+dsl(i+1))/2) kcon 1 );
   %codm - moisture not connected
end
% rad table: radiation, drift to drift liner
for i=1:LN-1
    i1=iliner(i);
    i2=i1+1;
    rad=(rad; 600 i1 i2 a5*dsl(i) edd sa(i1,i2) 1 );
end


%1-5 (between nodes on line 1 and line 5, WP and liner)
% rad table: radiation
for i=iheat
```

```
   for j=iliner
      if sa(i,j)~=0
         rad=(rad; 600 i j a1*dsl(i)+a2  ecd sa(i,j) 1 );
      end
   end
end


%creat team table for line 6
i=(1:LN)';
rhoa=1.02;
% IR=i*0+1e-3*rhoa*RpRv;  %modifier is rhoa*RpRv for the modified driving force
hi_steam=1e3;          %steam transport from source to sink PV(source)>PBAR(source)
steam=(steam; i*0+10 iheat' isteam' dsl(i)'*a1 i*0 i*0 i*0  i*0+hi_steam*lewm);
steam=(steam; i*0+10 iair1' isteam' dsl(i)'*(a1+a5)/3 i*0 i*0 i*0 i*0+hi_steam*lewm);
steam=(steam; i*0+10 iair2' isteam' dsl(i)'*(a1+a5)/3 i*0 i*0 i*0 i*0+hi_steam*lewm);
steam=(steam; i*0+10 iair3' isteam' dsl(i)'*(a1+a5)/3 i*0 i*0 i*0 i*0+hi_steam*lewm);
steam=(steam; i*0+10 iliner' isteam' dsl(i)'*a5 i*0 i*0 i*0  i*0+hi_steam*lewm);

%steam transport from steam line to network if PV(steam)>PV(network)
frcm=(frcm; i*0+111 isteam' iheat' dsl(i)'*a1 i*0 i*0 i*0 i*0+hi_steam*lewm);
frcm=(frcm; i*0+111 isteam' iair1' dsl(i)'*(a1+a5)/3 i*0 i*0 i*0 i*0+hi_steam*lewm);
frcm=(frcm; i*0+111 isteam' iair2' dsl(i)'*(a1+a5)/3 i*0 i*0 i*0  i*0+hi_steam*lewm);
frcm=(frcm; i*0+111 isteam' iair3' dsl(i)'*(a1+a5)/3 i*0 i*0 i*0  i*0+hi_steam*lewm);
frcm=(frcm; i*0+111 isteam' iliner' dsl(i)'*a5 i*0 i*0 i*0  i*0+hi_steam*lewm);

%connect the steam line to the iliner in heat network
frc=(frc; i*0+100 isteam' iliner' dsl(i)'*a5 i*0 i*0 i*0  i*0+1.9);
i=(1 LN)';

%frcmg=(frcmg; i*0+100 isteam(i)' isteam(i)' dsl(i)'*a5 i*0 i*0 i*0  i*0+1e-2*lewm);

%steam flow along steam line
hi_steamax=1000;          %steam transport along steam line
i1=isteam(1:LN-1)';
i2=isteam(2:LN)';
frcm=(frcm; i1*0+100 i1 i2 i1*0+a8 i1*0 i1*0 i1*0 i1*0+hi_steamax*lewm);



%generators

%no intake air, 11/5/04
% %intake air point along airline 1
% % controlled convection
% cocg=(cocg; 400 iain iain a8 1);
% cocmg=(cocmg; 400 iain iain a8 1);

%connection across drift wall along line 5, liner
% conduction
for i=iliner
   i1=i;
   codg=(codg; 500 i1 i1 a5*dsl(i-4*LN) d1/2 d2/2 ct kcon 1/200 ); %modification, 10/31/03,
increase resistance
   codmg=(codmg; 500 i1 i1 a5*dsl(i-4*LN) d1/2 d2/2 ct kvap rgvf );
end

%set up generator connection at the beginig and end of steam line
hi_steamax=hi_steamax;
i1=(424*5+1;424*6);
frcmg=(frcmg; i1*0+120 i1 i1 i1*0+a8 i1*0 i1*0 i1*0 i1*0+hi_steamax*lewm);


%line1 steam generator connections, 1/18/05
%condensation enhancement on hi, mhi=10
% mhi=1;
% for i=iheat
%    i1=i;
%    frcmg=(frcmg; 110 i i a1*dsl(i1) 0 0 0 hi*lewm*mhi);
% end
% airline 1 steam generator connections, 1/18/05
```

```
% for i=iair1
%    i1=i-LN;
%    frcmg=(frcmg; 110 i i a1*dsl(i1) 0 0 0 hi*lewm*mhi);
% end
% airline 2 steam generator connections, 1/18/05
% for i=iair2
%    i1=i-LN*2;
%    frcmg=(frcmg; 110 i i a1*dsl(i1) 0 0 0 hi*lewm*mhi);
% end
% airline 3 steam generator connections, 1/18/05
% for i=iair3
%    i1=i-LN*3;
%    frcmg=(frcmg; 110 i i a1*dsl(i1) 0 0 0 hi*lewm*mhi);
% end



%save results
%new
% mwrite((wd '/cfd_d/fma.dat'), fma);
% mwrite((wd '/cfd_d/fmag.dat'), fmag);
mwrite((wd '/cfd_d/vffa.dat'), vffa);    %fixed, davood, 1/14/03, changed
mwrite((wd '/cfd_d/vffag.dat'), vffag);  %fixed, davood, 1/14/03, changed


mwrite((wd '/cfd_d/frc.dat'), frc);
mwrite((wd '/cfd_d/foc.dat'), foc);
mwrite((wd '/cfd_d/moc.dat'), moc);
mwrite((wd '/cfd_d/coc.dat'), coc);
mwrite((wd '/cfd_d/cod.dat'), cod);
mwrite((wd '/cfd_d/rad.dat'), rad);
mwrite((wd '/cfd_d/duc.dat'), duc);
mwrite((wd '/cfd_d/vcc.dat'), vcc);
mwrite((wd '/cfd_d/vccd.dat'), vccd);
mwrite((wd '/cfd_d/steam.dat'), steam);

mwrite((wd '/cfd_d/frcg.dat'), frcg);
mwrite((wd '/cfd_d/focg.dat'), focg);
mwrite((wd '/cfd_d/mocg.dat'), mocg);
mwrite((wd '/cfd_d/cocg.dat'), cocg);
mwrite((wd '/cfd_d/codg.dat'), codg);
mwrite((wd '/cfd_d/radg.dat'), radg);
mwrite((wd '/cfd_d/ducg.dat'), ducg);
mwrite((wd '/cfd_d/vccg.dat'), vccg);

mwrite((wd '/cfd_d/frcm.dat'), frcm);  %fixed, davood, 1/14/03, added
mwrite((wd '/cfd_d/focm.dat'), focm);
mwrite((wd '/cfd_d/mocm.dat'), mocm);
mwrite((wd '/cfd_d/cocm.dat'), cocm);
mwrite((wd '/cfd_d/codm.dat'), codm);
mwrite((wd '/cfd_d/ducm.dat'), ducm);

mwrite((wd '/cfd_d/frcmg.dat'), frcmg);
mwrite((wd '/cfd_d/focmg.dat'), focmg);
mwrite((wd '/cfd_d/mocmg.dat'), mocmg);
mwrite((wd '/cfd_d/cocmg.dat'), cocmg);
mwrite((wd '/cfd_d/codmg.dat'), codmg);
mwrite((wd '/cfd_d/ducmg.dat'), ducmg);
mwrite((wd '/cfd_d/steamg.dat'), steamg);


mwrite((wd '/cfd_d/LS.dat'), LS);
mwrite((wd '/cfd_d/cfd_in.dat'), cfd_in);
mwrite((wd '/cfd_d/ittg.dat'), ittg);
mwrite((wd '/cfd_d/ippg.dat'), ippg);
mwrite((wd '/cfd_d/iain.dat'), iain);
mwrite((wd '/cfd_d/iaout.dat'), iaout);
mwrite((wd '/cfd_d/iheat.dat'), iheat);
mwrite((wd '/cfd_d/ivapor.dat'), ivapor);
mwrite((wd '/cfd_d/iliner.dat'), iliner);
mwrite((wd '/cfd_d/iair.dat'), iair);
```

```
%mwrite((wd '/cfd_d/qmav.dat'), qmav);
mwrite((wd '/cfd_d/iwin.dat'), iwin);
mwrite((wd '/cfd_d/iwout.dat'), iwout);
mwrite((wd '/cfd_d/ctl.dat'), ctl);
```

## *Waste Package Heat Load Table*

The input file cfd_d\qq.dat contains the heat dissipation values of the drift centerline nodes. For the sake of space conservation, the total heat of first sequence of waste packages are listed as a function of time.

| Time (year) | HLW (W) | 44BWR (W) | 21PWR (W) | HLW (W) | 21PWR (W) | 44BWR (W) | 21PWR (W) | DSNF (W) |
|---|---|---|---|---|---|---|---|---|
| 0.167 | 4013.677 | 7125.855 | 11320.265 | 4013.677 | 11320.265 | 7125.855 | 11320.265 | 790.261 |
| 0.500 | 3853.610 | 7088.143 | 11262.276 | 3853.610 | 11262.276 | 7088.143 | 11262.276 | 786.247 |
| 1.000 | 3590.542 | 7013.068 | 11147.086 | 3590.542 | 11147.086 | 7013.068 | 11147.086 | 782.852 |
| 2.000 | 3272.475 | 6891.060 | 10956.960 | 3272.475 | 10956.960 | 6891.060 | 10956.960 | 776.940 |
| 5.000 | 2901.342 | 6644.660 | 10567.935 | 2901.342 | 10567.935 | 6644.660 | 10567.935 | 763.173 |
| 10.000 | 2545.458 | 6207.300 | 9873.465 | 2545.458 | 9873.465 | 6207.300 | 9873.465 | 733.893 |
| 15.000 | 2260.200 | 5670.280 | 9020.340 | 2260.200 | 9020.340 | 5670.280 | 9020.340 | 691.803 |
| 20.000 | 2016.392 | 5164.280 | 8221.710 | 2016.392 | 8221.710 | 5164.280 | 8221.710 | 647.390 |
| 25.000 | 1801.867 | 4719.220 | 7531.965 | 1801.867 | 7531.965 | 4719.220 | 7531.965 | 605.450 |
| 30.000 | 1611.967 | 4324.980 | 6929.003 | 1611.967 | 6929.003 | 4324.980 | 6929.003 | 566.150 |
| 35.000 | 1443.388 | 3979.030 | 6396.600 | 1443.388 | 6396.600 | 3979.030 | 6396.600 | 529.487 |
| 40.000 | 1293.683 | 3673.450 | 5927.670 | 1293.683 | 5927.670 | 3673.450 | 5927.670 | 495.457 |
| 45.000 | 1160.654 | 3399.550 | 5508.143 | 1160.654 | 5508.143 | 3399.550 | 5508.143 | 464.063 |
| 50.000 | 1042.388 | 3155.570 | 5131.980 | 1042.388 | 5131.980 | 3155.570 | 5131.980 | 435.313 |
| 60.000 | 913.987 | 2888.820 | 4723.635 | 913.987 | 4723.635 | 2888.820 | 4723.635 | 403.333 |
| 75.000 | 746.621 | 2535.170 | 4182.570 | 746.621 | 4182.570 | 2535.170 | 4182.570 | 361.657 |
| 100.000 | 546.987 | 2102.980 | 3515.347 | 546.987 | 3515.347 | 2102.980 | 3515.347 | 317.670 |
| 150.000 | 350.304 | 1652.750 | 2806.440 | 350.304 | 2806.440 | 1652.750 | 2806.440 | 282.890 |
| 200.000 | 195.817 | 1262.910 | 2179.643 | 195.817 | 2179.643 | 1262.910 | 2179.643 | 250.703 |
| 300.000 | 103.537 | 982.630 | 1708.455 | 103.537 | 1708.455 | 982.630 | 1708.455 | 218.033 |
| 500.000 | 59.475 | 770.220 | 1334.970 | 59.475 | 1334.970 | 770.220 | 1334.970 | 187.360 |
| 750.000 | 35.796 | 585.970 | 1008.263 | 35.796 | 1008.263 | 585.970 | 1008.263 | 158.557 |
| 1000.000 | 21.508 | 448.140 | 756.420 | 21.508 | 756.420 | 448.140 | 756.420 | 137.327 |
| 1500.000 | 12.867 | 346.500 | 571.043 | 12.867 | 571.043 | 346.500 | 571.043 | 120.547 |
| 2000.000 | 7.000 | 261.910 | 420.892 | 7.000 | 420.892 | 261.910 | 420.892 | 104.803 |
| 3000.000 | 3.438 | 198.000 | 310.223 | 3.438 | 310.223 | 198.000 | 310.223 | 92.360 |
| 5000.000 | 1.967 | 157.520 | 242.025 | 1.967 | 242.025 | 157.520 | 242.025 | 81.613 |

## *Time Vector*

```
 0.167 0.5 1 2 5 10 15 20 25 30 35 40 45 50 60 75 100 150 200 300 500 750
1000 1500 2000 3000 5000
```

## *Intake Air Temperatures*

```
  2.5000000e+001  2.5000000e+001  2.5000000e+001
  2.5000000e+001  2.5000000e+001  2.5000000e+001
  2.5000000e+001  2.5000000e+001  2.5000000e+001
```

```
2.5000000e+001  2.5000000e+001  2.5000000e+001
2.5000000e+001  2.5000000e+001  2.5000000e+001
2.5000000e+001  2.5000000e+001  2.5000000e+001
2.5000000e+001  2.5000000e+001  2.5000000e+001
2.5000000e+001  2.5000000e+001  2.5000000e+001
2.5000000e+001  2.5000000e+001  2.5000000e+001
2.5000000e+001  2.5000000e+001  2.5000000e+001
2.5000000e+001  2.5000000e+001  2.5000000e+001
2.5000000e+001  2.5000000e+001  2.5000000e+001
2.5000000e+001  2.5000000e+001  2.5000000e+001
2.5000000e+001  2.5000000e+001  2.5000000e+001
2.5000000e+001  2.5000000e+001  2.5000000e+001
2.5000000e+001  2.5000000e+001  2.5000000e+001
2.5000000e+001  2.5000000e+001  2.5000000e+001
2.5000000e+001  2.5000000e+001  2.5000000e+001
2.5000000e+001  2.5000000e+001  2.5000000e+001
2.5000000e+001  2.5000000e+001  2.5000000e+001
2.5000000e+001  2.5000000e+001  2.5000000e+001
2.5000000e+001  2.5000000e+001  2.5000000e+001
2.5000000e+001  2.5000000e+001  2.5000000e+001
2.5000000e+001  2.5000000e+001  2.5000000e+001
2.5000000e+001  2.5000000e+001  2.5000000e+001
2.5000000e+001  2.5000000e+001  2.5000000e+001
2.5000000e+001  2.5000000e+001  2.5000000e+001
```

### *Intake Air Vapor Pressures*

```
9.5062540e+002  9.5062540e+002  9.5062540e+002
9.5062540e+002  9.5062540e+002  9.5062540e+002
9.5062540e+002  9.5062540e+002  9.5062540e+002
9.5062540e+002  9.5062540e+002  9.5062540e+002
9.5062540e+002  9.5062540e+002  9.5062540e+002
9.5062540e+002  9.5062540e+002  9.5062540e+002
9.5062540e+002  9.5062540e+002  9.5062540e+002
9.5062540e+002  9.5062540e+002  9.5062540e+002
9.5062540e+002  9.5062540e+002  9.5062540e+002
9.5062540e+002  9.5062540e+002  9.5062540e+002
9.5062540e+002  9.5062540e+002  9.5062540e+002
9.5062540e+002  9.5062540e+002  9.5062540e+002
9.5062540e+002  9.5062540e+002  9.5062540e+002
9.5062540e+002  9.5062540e+002  9.5062540e+002
9.5062540e+002  9.5062540e+002  9.5062540e+002
9.5062540e+002  9.5062540e+002  9.5062540e+002
9.5062540e+002  9.5062540e+002  9.5062540e+002
9.5062540e+002  9.5062540e+002  9.5062540e+002
9.5062540e+002  9.5062540e+002  9.5062540e+002
9.5062540e+002  9.5062540e+002  9.5062540e+002
9.5062540e+002  9.5062540e+002  9.5062540e+002
9.5062540e+002  9.5062540e+002  9.5062540e+002
9.5062540e+002  9.5062540e+002  9.5062540e+002
9.5062540e+002  9.5062540e+002  9.5062540e+002
9.5062540e+002  9.5062540e+002  9.5062540e+002
9.5062540e+002  9.5062540e+002  9.5062540e+002
9.5062540e+002  9.5062540e+002  9.5062540e+002
```

### *Drift Barometric Pressures*

```
8.7801428e+004
8.7779091e+004
8.7771390e+004
8.7767735e+004
8.7766831e+004
8.7771411e+004
8.7779113e+004
8.7787110e+004
8.7794487e+004
8.7801251e+004
8.7807386e+004
8.7812955e+004
8.7818034e+004
8.7822649e+004
8.7583711e+004
8.7587325e+004
8.7593217e+004
8.7604520e+004
8.7615208e+004
8.7634863e+004
8.7668084e+004
8.7700273e+004
8.7724565e+004
8.7757435e+004
8.7778077e+004
8.7801530e+004
8.7831360e+004
```

### *DISAC control parameters*

```
1.000000e+00  1   0.000000e+00  0.000000e+00  2.500000e+01  9.506254e+02
8.906000e+04  1.000000e+00  1.000000e+00  0.000000e+00  0.000000e+00
0.000000e+00  0.0
```

### *NTCF Files*

**File Name: fun_in.dat**

This input file contains the unperturbed vapor pressure for moisture NTCF component. Although the input file is ready for 12500 year simulation, only upto year 5000 was simulated.

```
30  99
23 27
5

0.0 1.670e-01 5.000e-01 1.000e+00 2.000e+00 5.000e+00 1.000e+01 1.500e+01 2.000e+01 2.500e+01
3.000e+01 3.500e+01 4.000e+01 4.500e+01 5.000e+001  6.000e+001  7.500e+001  1.000e+002
1.500e+002  2.000e+002  3.000e+002  5.000e+002  7.500e+002  1.000e+003  1.500e+003  2.000e+003
3.000e+003  5.000e+003  7.500e+003  1.000e+004  1.250e+004

8.906000e+004  8.906000e+004  8.906000e+004  8.906000e+004  8.906000e+004  8.906000e+004
8.906000e+004  8.906000e+004  8.906000e+004  8.906000e+004  8.906000e+004  8.906000e+004
8.906000e+004  8.906000e+004  8.906000e+004  8.906000e+004  8.906000e+004  8.906000e+004
8.906000e+004  8.906000e+004  8.906000e+004  8.906000e+004  8.906000e+004  8.906000e+004
8.906000e+004  8.906000e+004  8.906000e+004  8.906000e+004  8.906000e+004  8.906000e+004

  5.7530423e+001  6.0794807e+001  6.2906507e+001  6.4434905e+001  6.5860988e+001
  6.8322544e+001  7.3402263e+001  7.6853129e+001  7.9278987e+001  8.1109301e+001
  7.2143228e+001  7.8055039e+001  8.2194944e+001  8.5099039e+001  8.6954349e+001
```

```
 7.4016226e+001  8.0416260e+001  8.5004506e+001  8.8232497e+001  8.9975213e+001
 7.4572152e+001  8.1282504e+001  8.6202175e+001  8.9660818e+001  9.1186051e+001
 7.2467131e+001  7.9056176e+001  8.3954285e+001  8.7387129e+001  8.8672644e+001
 6.8923499e+001  7.5118756e+001  7.9762067e+001  8.3005082e+001  8.4105225e+001
 6.5347095e+001  7.1084362e+001  7.5413750e+001  7.8433500e+001  7.9378847e+001
 6.2120202e+001  6.7432146e+001  7.1466330e+001  7.4275730e+001  7.5077541e+001
 5.9215968e+001  6.4150621e+001  6.7917692e+001  7.0533082e+001  7.1205199e+001
 5.6635414e+001  6.1228943e+001  6.4750002e+001  6.7188080e+001  6.7750144e+001
 5.4340372e+001  5.8625561e+001  6.1923733e+001  6.4202377e+001  6.4667659e+001
 5.2278181e+001  5.6289613e+001  5.9385414e+001  6.1516572e+001  6.1895225e+001
 5.0437787e+001  5.4195245e+001  5.7104002e+001  5.9101184e+001  5.9404462e+001
 1.3180479e+002  1.3247543e+002  1.3274138e+002  1.3268133e+002  1.2952613e+002
 1.4899037e+002  1.4876464e+002  1.4827275e+002  1.4673652e+002  1.4052051e+002
 1.4869187e+002  1.4877224e+002  1.4817819e+002  1.4514819e+002  1.3554560e+002
 1.4741769e+002  1.4675958e+002  1.4480554e+002  1.3901387e+002  1.2543972e+002
 1.3980692e+002  1.3858967e+002  1.3564023e+002  1.2806117e+002  1.1215205e+002
 1.3534927e+002  1.3450309e+002  1.2952207e+002  1.1856321e+002  1.0053085e+002
 1.3569213e+002  1.3252732e+002  1.2447121e+002  1.1004918e+002  9.0511964e+001
 1.2572289e+002  1.2177060e+002  1.1359370e+002  9.8335217e+001  8.0294951e+001
 1.1761731e+002  1.1330283e+002  1.0347223e+002  9.0061480e+001  7.4115422e+001
 1.0685630e+002  1.0151054e+002  9.1410714e+001  7.9654492e+001  6.5842469e+001
 9.8355058e+001  9.2765054e+001  8.3575323e+001  7.2743356e+001  6.0122490e+001
 8.6989712e+001  8.1929604e+001  7.3655658e+001  6.3827204e+001  5.3406604e+001
 7.4055850e+001  6.9539033e+001  6.3146498e+001  5.4669600e+001  4.5612823e+001
 6.4714626e+001  6.1266113e+001  5.5756645e+001  4.8185487e+001  4.0404866e+001
 5.8666040e+001  5.5961775e+001  5.1220195e+001  4.4259872e+001  3.7045418e+001
 5.4366515e+001  5.2165774e+001  4.7957215e+001  4.1436548e+001  3.4633210e+001

  9.8786398e+02   9.9671172e+02   9.7304273e+02   9.1157880e+02   8.2231146e+02
  1.0325875e+03   1.0428230e+03   1.0431001e+03   1.0330088e+03   1.0153017e+03
  1.0290833e+03   1.0353630e+03   1.0402673e+03   1.0418019e+03   1.0368457e+03
  1.0234416e+03   1.0333245e+03   1.0338275e+03   1.0293620e+03   1.0257739e+03
  9.9819254e+02   1.0039134e+03   1.0069607e+03   1.0064869e+03   1.0018819e+03
  9.6842292e+02   9.7587658e+02   9.7896596e+02   9.7772635e+02   9.7418946e+02
  9.6260453e+02   9.6521912e+02   9.6637716e+02   9.6566591e+02   9.6323885e+02
  9.5950109e+02   9.5890502e+02   9.5859530e+02   9.5811709e+02   9.5663141e+02
  9.5841597e+02   9.5627275e+02   9.5537458e+02   9.5517669e+02   9.5422089e+02
  9.5408310e+02   9.5296503e+02   9.5245077e+02   9.5253106e+02   9.5268058e+02
  9.5258031e+02   9.5345877e+02   9.5307002e+02   9.5230775e+02   9.5246821e+02
  9.4827408e+02   9.4922107e+02   9.4999784e+02   9.4992224e+02   9.4871438e+02
  9.4543852e+02   9.4758116e+02   9.4954147e+02   9.4970561e+02   9.4729385e+02
  9.4740040e+02   9.4877553e+02   9.5060651e+02   9.5085178e+02   9.4797344e+02
  9.4958807e+03   1.1499043e+04   1.3000333e+04   1.4048397e+04   1.4666905e+04
  9.6378095e+03   1.1675128e+04   1.3202379e+04   1.4268628e+04   1.4897633e+04
  9.9277961e+03   1.2051579e+04   1.3648124e+04   1.4764883e+04   1.5424312e+04
  1.0319523e+04   1.2510184e+04   1.4150347e+04   1.5294053e+04   1.5967732e+04
  1.0748047e+04   1.3024428e+04   1.4724769e+04   1.5908281e+04   1.6604462e+04
  1.1678439e+04   1.4158754e+04   1.6007821e+04   1.7293026e+04   1.8048481e+04
  1.3486456e+04   1.6339094e+04   1.8453862e+04   1.9917822e+04   2.0776410e+04
  2.3622628e+04   2.8260016e+04   3.1582172e+04   3.3826236e+04   3.4368187e+04
  2.6218933e+04   3.1268047e+04   3.4858492e+04   3.7271309e+04   3.3148105e+04
  3.0357906e+04   3.6081696e+04   4.0121207e+04   4.0500088e+04   2.5487712e+04
  3.4272727e+04   4.0657439e+04   4.2742688e+04   3.1885044e+04   1.9652452e+04
  6.0567882e+04   5.0213237e+04   3.5754504e+04   2.3282968e+04   1.4166003e+04
  3.6365330e+04   2.9995958e+04   2.2576012e+04   1.5011129e+04   9.7018456e+03
  2.4232901e+04   2.0438724e+04   1.5493571e+04   1.0393732e+04   7.3512297e+03
  1.8198865e+04   1.5310253e+04   1.1811933e+04   8.0076265e+03   5.9285020e+03
  1.4838733e+04   1.2236555e+04   9.5702763e+03   6.5410363e+03   5.0174915e+03
```

**File Name: fun_in.dat**

This input file contains the perturbed vapor pressure for moisture NTCF component

```
27 99

23 27

5

0 0.167 0.5 1 2 5 10 15 20 25 30 35 40 45 50 60 75 100 150 200 300 500 750 1e+003 1.5e+003 2e+003
3e+003 5e+003
```

```
8.906000e+004  8.906000e+004  8.906000e+004  8.906000e+004  8.906000e+004  8.906000e+004
8.906000e+004  8.906000e+004  8.906000e+004  8.906000e+004  8.906000e+004  8.906000e+004
8.906000e+004  8.906000e+004  8.906000e+004  8.906000e+004  8.906000e+004  8.906000e+004
8.906000e+004  8.906000e+004  8.906000e+004  8.906000e+004  8.906000e+004  8.906000e+004
8.906000e+004  8.906000e+004  8.906000e+004

5.7530423e+001 6.0794807e+001 6.2906507e+001 6.4434905e+001 6.5860988e+001
6.8322544e+001 7.3402263e+001 7.6853129e+001 7.9278987e+001 8.1109301e+001
7.2143228e+001 7.8055039e+001 8.2194944e+001 8.5099039e+001 8.6954349e+001
7.4016226e+001 8.0416260e+001 8.5004506e+001 8.8232497e+001 8.9975213e+001
7.4572152e+001 8.1282504e+001 8.6202175e+001 8.9660818e+001 9.1186051e+001
7.2467131e+001 7.9056176e+001 8.3954285e+001 8.7387129e+001 8.8672644e+001
6.8923499e+001 7.5118756e+001 7.9762067e+001 8.3005082e+001 8.4105225e+001
6.5347095e+001 7.1084362e+001 7.5413750e+001 7.8433500e+001 7.9378847e+001
6.2120202e+001 6.7432146e+001 7.1466330e+001 7.4275730e+001 7.5077541e+001
5.9215968e+001 6.4150621e+001 6.7917692e+001 7.0533082e+001 7.1205199e+001
5.6635414e+001 6.1228943e+001 6.4750002e+001 6.7188080e+001 6.7750144e+001
5.4340372e+001 5.8625561e+001 6.1923733e+001 6.4202377e+001 6.4667659e+001
5.2278181e+001 5.6289613e+001 5.9385414e+001 6.1516572e+001 6.1895225e+001
5.0437787e+001 5.4195245e+001 5.7104002e+001 5.9101184e+001 5.9404462e+001
1.3180479e+002 1.3247543e+002 1.3274138e+002 1.3268133e+002 1.2952613e+002
1.4899037e+002 1.4876464e+002 1.4827275e+002 1.4673652e+002 1.4052051e+002
1.4869187e+002 1.4877224e+002 1.4817819e+002 1.4514819e+002 1.3554560e+002
1.4741769e+002 1.4675958e+002 1.4480554e+002 1.3901387e+002 1.2543972e+002
1.3980692e+002 1.3858967e+002 1.3564023e+002 1.2806117e+002 1.1215205e+002
1.3534927e+002 1.3450309e+002 1.2952207e+002 1.1856321e+002 1.0053085e+002
1.3569213e+002 1.3252732e+002 1.2447121e+002 1.1004918e+002 9.0511964e+001
1.2572289e+002 1.2177060e+002 1.1359370e+002 9.8335217e+001 8.0294951e+001
1.1761731e+002 1.1330283e+002 1.0347223e+002 9.0061480e+001 7.4115422e+001
1.0685630e+002 1.0151054e+002 9.1410714e+001 7.9654492e+001 6.5842469e+001
9.8355058e+001 9.2765054e+001 8.3575323e+001 7.2743356e+001 6.0122490e+001
8.6989712e+001 8.1929604e+001 7.3655658e+001 6.3827204e+001 5.3406604e+001
7.4055850e+001 6.9539033e+001 6.3146498e+001 5.4669600e+001 4.5612823e+001

9.8786398e+002 9.9671172e+002 9.7304273e+002 9.1157880e+002 8.2231146e+002
1.0325875e+003 1.0428230e+003 1.0431001e+003 1.0330088e+003 1.0153017e+003
1.0290833e+003 1.0353630e+003 1.0402673e+003 1.0418019e+003 1.0368457e+003
1.0234416e+003 1.0333245e+003 1.0338275e+003 1.0293620e+003 1.0257739e+003
9.9819254e+002 1.0039134e+003 1.0069607e+003 1.0064869e+003 1.0018819e+003
9.6842292e+002 9.7587658e+002 9.7896596e+002 9.7772635e+002 9.7418946e+002
9.6260453e+002 9.6521912e+002 9.6637716e+002 9.6566591e+002 9.6323885e+002
9.5950109e+002 9.5890502e+002 9.5859530e+002 9.5811709e+002 9.5663141e+002
9.5841597e+002 9.5627275e+002 9.5537458e+002 9.5517669e+002 9.5422089e+002
9.5408310e+002 9.5296503e+002 9.5245077e+002 9.5253106e+002 9.5268058e+002
9.5258031e+002 9.5345877e+002 9.5307002e+002 9.5230775e+002 9.5246821e+002
9.4827408e+002 9.4922107e+002 9.4999784e+002 9.4992224e+002 9.4871438e+002
9.4543852e+002 9.4758116e+002 9.4954147e+002 9.4970561e+002 9.4729385e+002
9.4740040e+002 9.4877553e+002 9.5060651e+002 9.5085178e+002 9.4797344e+002
9.4958807e+003 1.1499043e+004 1.3000333e+004 1.4048397e+004 1.4666905e+004
9.6378095e+003 1.1675128e+004 1.3202379e+004 1.4268628e+004 1.4897633e+004
9.9277961e+003 1.2051579e+004 1.3648124e+004 1.4764883e+004 1.5424312e+004
1.0319523e+004 1.2510184e+004 1.4150347e+004 1.5294053e+004 1.5967732e+004
1.0748047e+004 1.3024428e+004 1.4724769e+004 1.5908281e+004 1.6604462e+004
1.1678439e+004 1.4158754e+004 1.6007821e+004 1.7293026e+004 1.8048481e+004
1.3486456e+004 1.6339094e+004 1.8453862e+004 1.9917822e+004 2.0776410e+004
2.3622628e+004 2.8260016e+004 3.1582172e+004 3.3826236e+004 3.4368187e+004
8.9060000e+004 8.9060000e+004 8.9060000e+004 7.0234825e+004 3.7163828e+004
8.9060000e+004 8.9060000e+004 7.3938171e+004 4.6773455e+004 2.5981862e+004
8.9060000e+004 7.7819041e+004 5.4670452e+004 3.5061317e+004 2.0033469e+004
6.2539347e+004 5.1186759e+004 3.6447704e+004 2.3734372e+004 1.4440650e+004
3.7070372e+004 3.0577512e+004 2.3013710e+004 1.5348670e+004 9.8899426e+003
```

## File Name: nuft_in

```
;; Implicit DKM with active fracture concept (AFC)
;; NBS material properties from 1D drift-scale mean infiltration flux property set assembled by
Ken Lee
;; AML = 56.48 MTU/acre; half drift spacing = 40.5 m;; AML = 85 MTU/acre; half drift spacing =
26.9 m, Modified on 11/22/02 at UNR

;; Modified by dr1 Bahrami on 9/8/00 for MULTIFLUX input
```

```
;; Mesh changed for the tratigrapic unit of ANSYS run

;;      l4c4.col.units

;;      COLUMN INFORMATION (x,y =   170500.828,   233807.766)


;;      unit    thickness (m)
;;      ____    _____________

;;      tcw11      32.900 -> 30.848
;;      tcw12      89.004 -> 83.453
;;      tcw13       4.951 -> 5.490
;;      ptn21       5.947 -> 4.690
;;      ptn22       2.490 -> 0.530
;;      ptn23       2.373 -> 7.050
;;      ptn24       6.533 -> 4.580
;;      ptn25      14.443 -> 14.090
;;      ptn26      15.498 -> 9.690
;;      tsw31       1.992 -> 6.170
;;      tsw32      42.070 -> 46.850
;;      tsw33      88.711 -> 86.659
;;      tsw34      30.254 -> 29.940
;;      tsw35     111.895 -> 106.210
;;      tsw36      27.119 -> 31.793
;;      tsw37      13.594 -> 15.937
;;      tsw38      23.408 -> 23.600
;;      tsw39       3.779 -> 11.270
;;      ch1v       10.166 -> 3.350
;;      ch2v        0.000 -> 0.000
;;      ch3v        0.000 -> 0.000
;;      ch4v        0.000 -> 0.000
;;      ch5v        0.000 -> 0.000
;;      ch1z        0.000 -> 0.000
;;      ch2z       14.414 -> 15.735
;;      ch3z       14.414 -> 15.735
;;      ch4z       14.414 -> 15.735
;;      ch5z       14.414 -> 15.735
;;      ch6        19.629 -> 21.428
;;      pp4         8.086 -> removed
;;      pp3        33.691 -> removed
;;      pp2        14.707 -> removed
;;      pp1        61.055 -> removed
;;      bf3        17.402 -> removed
;;      bf2         0.000 -> removed

;;      repository elevation (m):                                  1073.934
;;      host rock:                                                    tsw35

;;      meters of host rock (tsw35) above repository:                      16.190
;;      meters of host rock (tsw35) below repository:                      90.020

;;      overburden thickness (m):                                       346.230
;;      distance from repository plane to top of chn (m):
;;      distance from repository plane to top of water table (m):     260.340

(usnt
  (title "1.0130000e+01mm_yr,line-load,AML=56mtu_acre,LDTH561Dds_mc-mi")
  (modelname usnt)


  (stepmax 1000000)
        ;; Set initial condition for multiflux functionalization module:
        ;; for initflag = 1 , first time interval, use 1D restart file
        ;; for initflag =0 , after first time interval, use restart file from previous time
interval
        (include "tmp.inc.time")


  (tolerconv (P 5000.)(S 0.005)(X 0.005)(T 0.5))
  ;; absolute NR conv. tolerance
```

```
  (reltolerconv (P 0.005)(S 0.0)(X 0.0)(T 1.e-3))

  (tolerdt (P 2.e4)(S 0.35)(X 0.25)(T 10.))
  (reltolerdt (P 0.1)(S 0.0)(X 0.0)(T 0.0))

  ;; trying with harmonic mean everywhere which means turning off the goemetric before vtough.pkg
  ;;  gets called.
  (diffusion-geo-mean off)
  ;; for imp-DKM do not have this so that it will default to harmonic for fract-matrix
interaction
  ;;(mult-cont-diff-harmonic off)
  ;; following has to come after tolerances
  (rmstolerconv 1e-4)
  (include-pkg "vtough.pkg")

;;
*************************************************************************************************
**
(output
     (include "tmp.inc.fout")       ;; output the fluxes cross wall
     (include "tmp.inc.res")        ;; output the restart file
     (extool (continuum  f) (variables T RH S.liquid)
        (file-ext ".f.ext")(range "*")
        (outtimes (include "tmp.inc.timeout"))
     )
     (extool (continuum  m) (variables T RH S.liquid)
        (file-ext ".m.ext")(range "*")
        (outtimes (include "tmp.inc.timeout"))
     )
) ;; end output
;;
*************************************************************************************************
(rocktab
        (include "dkm-afc-1Dds-mc-mi-00")
        (include "dkm-afc-EBS_Rev20a")
) ;; close rocktab
        ;;(include "modprop_dr-20")  Removed WP material properties
;;
*************************************************************************************************

;;  This srctab is adjusted to allocate percollation to just the fracture.
  (srctab
        (compflux
                (comp water)
                (name infil)
                (range "*.f*:*:2")
                (mult-by-area z)
                (allocate-by-element ("*" 1.0))
                (include "percolation.tab")  ;;cyclic percolation table
                (enthalpy  0.0   6.68E+04  1E+30   6.68E+04 )
        )

        ;; removed WP data (include "LDTH-SDT-0.3Qheat-50y_vent-20")
  ) ;; end srctab

     ;; set boundary conditions
       (bctab
       (atmos
               (range  "at*")
               (basephase gas)
               (tables
                       (T        0.0  1.8700000e+01   1.0e30  1.8700000e+01 )
                       (S.liquid 0.0  0.0    1.0e30  0.0  )
                       (P        0.0  8.4510758e+04   1.0e30  8.4510758e+04 )
                       (X.air    0.0  9.86600578e-01   1.0e30  9.86600578e-01 )
               )
       )

       (gwater
               (range  "wt*")
               (basephase liquid)
```

```
                (tables
                        (T          0  3.2400000e+01      1.0e30   3.2400000e+01)
                        (S.liquid   0  1.0      1.0e30   1.0)
                        (P          0  9.2e4    1.0e30  9.2e4)
                        (X.air      0  1.0e-6   1.0e30  1.0e-6)
                )

;;      SET PHASEFACTOR GAS TO 0, AND LIQUID TO 1 (JOHN)
                (phasefactor
                        (gas      0  0.0   1.0e30  0.0)
                        (liquid   0  1.0   1.0e30  1.0)
                )

        )
        ( include "tmp.inc.tab" )    ;; Set initial conditions for each
                                  ;; section in drift end b.c.
        ) ;; end bctab


;;This is for a unit symmetry cell with a half drift and half pillar
;;between drifts.
  (genmsh
    (anisotropic)
    (down 0. 0. 1.0)
    (coord rect)
    (multi-continua
       (type rocktab)
       (continuum  (name m)
          ;; 56.48 MTU/acre
          ;;(dx 0.570 0.35 0.3310 0.3597 0.3797 0.42 0.3394 0.5 0.9 1.5 2.5 4.0 6.0  9.0
13.3502)
      (dx 0.920  0.6907  1e-5 0.3797 0.42 0.3394 1e-5 0.5 0.9 1.5 2.5 4.0 6.0  9.0 13.3502)
;;Modified for 56.48 MTU heat load AMR case
      (dy 118.485 94.788 71.091 47.394 23.697 1e-5  35.545 106.64 213.27 )
      (dz
       1.00E-30       15.424  15.424  27.195  28.129  ;;      1-5     atm     tcw11   tcw11   tcw12
       tcw12
       28.129  5.490   4.690   0.530   7.050   ;;      6-10    tcw12   tcw13   ptn21   ptn22   ptn23
       4.580   14.090  9.690   6.170   23.425  ;;      11-15   ptn24   ptn25   ptn26   tsw31   tsw32
       23.425  28.047  29.306  29.306  10.148  ;;      16-20   tsw32   tsw33   tsw33   tsw33   tsw34
       13.195  6.597   3.040   3.000   2.400   ;;      21-25   tsw34   tsw34   tsw35   tsw35   tsw35
       2.000   1.000   1.000   0.500   0.300   ;;      26-30   tsw35   tsw35   tsw35   tsw35   tsw35
       0.200   1.00E-05        0.200   0.200   0.200   ;;      31-35   tsw35   tsw35   tsw35   tsw35
       tsw35
       0.200   1.00E-05        0.400   0.474   0.654   ;;      36-40   tsw35   tsw35   tsw35   tsw35
       tsw35
       0.619   0.647   0.786   0.514   1.00E-05        ;;      41-45   tsw35   tsw35   tsw35   tsw35
       tsw35
       0.60599 1.00E-05        0.800   1.000   1.500   ;;      46-50   tsw35   tsw35   tsw35   tsw35
       tsw35
       2.000   2.000   2.500   3.000   4.000   ;;      51-55   tsw35   tsw35   tsw35   tsw35   tsw35
       6.000   10.000  10.000  10.000  10.000  ;;      56-60   tsw35   tsw35   tsw35   tsw35   tsw35
       10.000  7.235   7.235   23.447  8.346   ;;      61-65   tsw35   tsw35   tsw35   tsw36   tsw36
       15.937  23.600  11.270  3.350   15.735  ;;      66-70   tsw37   tsw38   tsw39   ch1v    ch2z
       15.735  15.735  15.735  21.428  1.00E-30        ;;      71-75   ch3z    ch4z    ch5z    ch6
       wt
      )
      (mat
         (atm         atm   1  nx  1  ny   1   1)
         (tcw11     m-tcw11   1  nx  1  ny   2   3)
         (tcw12     m-tcw12   1  nx  1  ny   4   6)
         (tcw13     m-tcw13   1  nx  1  ny   7   7)
         (ptn21     m-ptn21   1  nx  1  ny   8   8)
         (ptn22     m-ptn22   1  nx  1  ny   9   9)
         (ptn23     m-ptn23   1  nx  1  ny  10  10)
         (ptn24     m-ptn24   1  nx  1  ny  11  11)
         (ptn25     m-ptn25   1  nx  1  ny  12  12)
         (ptn26     m-ptn26   1  nx  1  ny  13  13)
         (tsw31     m-tsw31   1  nx  1  ny  14  14)
         (tsw32     m-tsw32   1  nx  1  ny  15  16)
         (tsw33     m-tsw33   1  nx  1  ny  17  19)
```

```
        (tsw34     m-tsw34   1  nx  1  ny  20  22)
        (tsw35     m-tsw35   1  nx  1  ny  23  63)
        (tsw36     m-tsw36   1  nx  1  ny  64  65)
        (tsw37     m-tsw37   1  nx  1  ny  66  66)
        (tsw38     m-tsw38   1  nx  1  ny  67  67)
        (tsw39     m-tsw39   1  nx  1  ny  68  68)
        (ch1v      m-ch1v    1  nx  1  ny  69  69)
        (ch2z      m-ch2z    1  nx  1  ny  70  70)
        (ch3z      m-ch3z    1  nx  1  ny  71  71)
        (ch4z      m-ch4z    1  nx  1  ny  72  72)
        (ch5z      m-ch5z    1  nx  1  ny  73  73)
        (ch6       m-ch6     1  nx  1  ny  74  74)
        (wt     m-bf3   1  nx  1  ny  75  75)
             ;; artificial backfill
        (hstrk      m-tsw35   1  nx  1  ny  25    49)
        (dr1        m-dr      1   3  1  1  32    47)
        (dr1        m-dr      3   7  1  1  37    45)

        (dr2        m-dr      1   3  2  2  32    47)
        (dr2        m-dr      3   7  2  2  37    45)

        (dr3        m-dr      1   3  3  3  32    47)
        (dr3        m-dr      3   7  3  3  37    45)

        (dr4        m-dr      1   3  4  4  32    47)
        (dr4        m-dr      3   7  4  4  37    45)

        (dr5        m-dr      1   3  5  6  32    47)
        (dr5        m-dr      3   7  5  6  37    45)

        (adrift      NULL       1   2  1  5  33    46)
        (adrift      NULL       3   6  1  5  38    44)
     )
      ) ;; end continuum
      (continuum  (name f)
          (flow-area-density ("*.f*" 1.0))
          (LenFirst  ("*.f*" 1.0))    ;; same as y-direction
                                      ;; half-width of matrix block
          (Len  ("*.f*" 1.0))         ;; same as y-direction
                                      ;; half-width of fracture
                                    ;; LenFirst and Len values are doubled here since 50% of
cont-len-fac
                                    ;; is used in rocktab file (Ken Lee)
          ;; 60 MTU/acre
         ;;(dx 0.570 0.35 0.3310 0.3597 0.3797 0.42 0.3394 0.5 0.9 1.5 2.5 4.0 6.0  9.0 13.3502)
      (dx 0.920  0.6907  1e-5 0.3797 0.42 0.3394 1e-5 0.5 0.9 1.5 2.5 4.0 6.0  9.0 13.3502)
;;Modified for 56.48 MTU heat load AMR case
     (dy 118.485 94.788 71.091 47.394 23.697 1e-5  35.545 106.64 213.27 )
     (dz
      1.00E-30       15.424  15.424  27.195  28.129  ;;      1-5     atm     tcw11   tcw11   tcw12
      tcw12
      28.129  5.490   4.690   0.530   7.050   ;;      6-10    tcw12   tcw13   ptn21   ptn22   ptn23
      4.580   14.090  9.690   6.170   23.425  ;;      11-15   ptn24   ptn25   ptn26   tsw31   tsw32
      23.425  28.047  29.306  29.306  10.148  ;;      16-20   tsw32   tsw33   tsw33   tsw33   tsw34
      13.195  6.597   3.040   3.000   2.400   ;;      21-25   tsw34   tsw34   tsw35   tsw35   tsw35
      2.000   1.000   1.000   0.500   0.300   ;;      26-30   tsw35   tsw35   tsw35   tsw35   tsw35
      0.200   1.00E-05        0.200   0.200   0.200   ;;      31-35   tsw35   tsw35   tsw35   tsw35
      tsw35
      0.200   1.00E-05        0.400   0.474   0.654   ;;      36-40   tsw35   tsw35   tsw35   tsw35
      tsw35
      0.619   0.647   0.786   0.514   1.00E-05        ;;      41-45   tsw35   tsw35   tsw35   tsw35
      tsw35
      0.60599 1.00E-05        0.800   1.000   1.500   ;;      46-50   tsw35   tsw35   tsw35   tsw35
      tsw35
      2.000   2.000   2.500   3.000   4.000   ;;      51-55   tsw35   tsw35   tsw35   tsw35   tsw35
      6.000   10.000  10.000  10.000  10.000  ;;      56-60   tsw35   tsw35   tsw35   tsw35   tsw35
      10.000  7.235   7.235   23.447  8.346   ;;      61-65   tsw35   tsw35   tsw35   tsw36   tsw36
      15.937  23.600  11.270  3.350   15.735  ;;      66-70   tsw37   tsw38   tsw39   ch1v    ch2z
      15.735  15.735  15.735  21.428  1.00E-30        ;;      71-75   ch3z    ch4z    ch5z    ch6
      wt
     )
```

```
      (mat
         (atm         atm   1  nx  1  ny   1   1)
         (tcw11     f-tcw11   1  nx  1  ny   2   3)
         (tcw12     f-tcw12   1  nx  1  ny   4   6)
         (tcw13     f-tcw13   1  nx  1  ny   7   7)
         (ptn21     f-ptn21   1  nx  1  ny   8   8)
         (ptn22     f-ptn22   1  nx  1  ny   9   9)
         (ptn23     f-ptn23   1  nx  1  ny  10  10)
         (ptn24     f-ptn24   1  nx  1  ny  11  11)
         (ptn25     f-ptn25   1  nx  1  ny  12  12)
         (ptn26     f-ptn26   1  nx  1  ny  13  13)
         (tsw31     f-tsw31   1  nx  1  ny  14  14)
         (tsw32     f-tsw32   1  nx  1  ny  15  16)
         (tsw33     f-tsw33   1  nx  1  ny  17  19)
         (tsw34     f-tsw34   1  nx  1  ny  20  22)
         (tsw35     f-tsw35   1  nx  1  ny  23  63)
         (tsw36     f-tsw36   1  nx  1  ny  64  65)
         (tsw37     f-tsw37   1  nx  1  ny  66  66)
         (tsw38     f-tsw38   1  nx  1  ny  67  67)
         (tsw39     f-tsw39   1  nx  1  ny  68  68)
         (ch1v      f-ch1v    1  nx  1  ny  69  69)
         (ch2z      f-ch2z    1  nx  1  ny  70  70)
         (ch3z      f-ch3z    1  nx  1  ny  71  71)
         (ch4z      f-ch4z    1  nx  1  ny  72  72)
         (ch5z      f-ch5z    1  nx  1  ny  73  73)
         (ch6       f-ch6     1  nx  1  ny  74  74)
         (wt     f-bf3   1  nx  1  ny  75  75)
          ;; artificial backfill
         (hstrk      f-tsw35   1  nx  1  ny  25  49)
         (dr1        f-dr      1   3  1  1  32    47)
         (dr1        f-dr      3   7  1  1  37    45)

         (dr2        f-dr      1   3  2  2  32    47)
         (dr2        f-dr      3   7  2  2  37    45)

         (dr3        f-dr      1   3  3  3  32    47)
         (dr3        f-dr      3   7  3  3  37    45)

         (dr4        f-dr      1   3  4  4  32    47)
         (dr4        f-dr      3   7  4  4  37    45)

         (dr5        f-dr      1   3  5  6  32    47)
         (dr5        f-dr      3   7  5  6  37    45)

         (adrift      NULL       1   2  1  5  33    46)
         (adrift      NULL       3   6  1  5  38    44)
      )

       ) ;; end continuum
    ) ;; end multi-continua
  ) ;; end genmsh

;; ************************Down stream
weighting****************************************************
    (downstream-mob
         (liquid
             (crange ("ptn*.m#*" "tsw*.m#*") ("ch*v.m#*" "ch*z.m#*"))
         ) ;; end liquid
    ) ;; end downstream-mob


;; ************************ Solver options
***********************************************************
(include "run_control_param_LDTH-v01")

);; end of model input

;; ******************** Done !*************************************************************
```

**Filename: dkm-afc-1Dds-mc-mi-00**

```
(atm
  (cont-len-fac 1.0) (cont-area-fac 2.0)
  (exfac-adv (liquid 1.000e+00) (gas 1.000e+00))
  (solid-density 1.0e+08) (porosity 0.99)
  (Kd        (water 0.0) (air 0.0))
  (KdFactor  (water 0.0) (air 0.0))
  (Cp 1.0e+08)
  (tcond tcondLin (solid 0.17) (liquid 0.17) (gas 0.17))
  (K0 1.0e-8) (K1 1.0e-8) (K2 1.0e-8)
  (tort (gas 1.0) (liquid 0.000e+00))
  (kr (gas    krgLinear (Smax 1.000e+00)(Sr 0.000e+00))
      (liquid krlLinear (Smax 1.000e+00)(Sr 0.000e+00)))
  (pc (liquid  0.0))
  (krMC (liquid  krMCintrinsic) (gas  krMCintrinsic))
) ;;End of the material
(m-tcw11
  (cont-len-fac 1.812e-01) (cont-area-fac 1.560e+00)
  (exfac-adv (liquid 1.000e+00) (gas 1.000e+00))
  (solid-density 3.214E+03) (porosity 2.530e-01)
  (Kd        (water 0.0) (air 0.0))
  (KdFactor  (water 0.0) (air 0.0))
  (Cp 8.570E+02)
  (tcond tcondLin (solid 5.236E-01) (liquid 9.517E-01) (gas 5.236E-01))
  (K0 3.860e-15) (K1 3.860e-15) (K2 3.860e-15)
  (tort (gas 7.000e-01) (liquid 0.000e+00))
  (kr (liquid krlVanGen (Sr 7.000e-02) (m 4.700e-01) (Smax 1.0))
      (gas krgModCorey (Srl 7.000e-02) (m 4.700e-01) (Slmax 1.0)))
  (pc (liquid pcVanGen (Sr 7.000e-02) (m 4.700e-01) (alpha 4.000e-05) (Smax 1.0)))
  (krMC (liquid  krMCintrinsic) (gas  krMCintrinsic))
) ;;End of the material
```

**(SECTION SKIP)**

```
(m-tsw35
  (cont-len-fac 5.274e-02) (cont-area-fac 9.680e+00)
  (exfac-adv (liquid 1.000e+00) (gas 1.000e+00))
  (solid-density 2.891E+03) (porosity 1.310e-01)
  (Kd        (water 0.0) (air 0.0))
  (KdFactor  (water 0.0) (air 0.0))
  (Cp 9.000E+02)
  (tcond tcondLin (solid 1.185E+00) (liquid 1.996E+00) (gas 1.185E+00))
  (K0 3.040e-17) (K1 3.040e-17) (K2 3.040e-17)
  (tort (gas 7.000e-01) (liquid 0.000e+00))
  (kr (liquid krlVanGen (Sr 1.200e-01) (m 2.360e-01) (Smax 1.0))
      (gas krgModCorey (Srl 1.200e-01) (m 2.360e-01) (Slmax 1.0)))
  (pc (liquid pcVanGen (Sr 1.200e-01) (m 2.360e-01) (alpha 6.440e-06) (Smax 1.0)))
  (krMC (liquid  krMCintrinsic) (gas  krMCintrinsic))
) ;;End of the material
```

**(SECTION SKIP)**

```
 (f-bf2
  (cont-len-fac 1.536e-03) (cont-area-fac 1.000e+00)
  (exfac-adv (liquid 1.000e+00) (gas 1.000e+00))
  (solid-density 1.036e+00) (porosity 4.300e-04)
  (Kd        (water 0.0) (air 0.0))
  (KdFactor  (water 0.0) (air 0.0))
  (Cp 6.330e+02)
  (tcond tcondLin (solid 3.182e-04) (liquid 5.848e-04) (gas 3.182e-04))
  (K0 1.300e-14) (K1 1.300e-14) (K2 1.300e-14)
  (tort (gas 7.000e-01) (liquid 0.000e+00))
  (kr (liquid krlVanGen (Sr 1.000e-02) (m 6.080e-01) (Smax 1.0) (gamma 1.000e-01))
      (gas krgModCorey (Srl 1.000e-02) (m 6.080e-01) (Slmax 1.0)))
  (pc (liquid pcVanGen (Sr 1.000e-02) (m 6.080e-01)(alpha 5.420e-04) (Smax 1.0) (gamma 1.000e-
01)))
  (krMC (liquid  krMCactiveFrac (gamma 1.000e-01) (Sr 1.000e-02))
        (gas     krMCactiveFrac (gamma 1.000e-01) (Sr 0.0)))
) ;;End of the material
```

**File Name: dkm-afc-EBS_Rev20a**

```
;; based on Nick's information in nuft-input_noBF.txt
;; copied from  dkm-afc-EBS_Rev10 with 4 modifications
;; 1. dr-up --> dr
;; 2. 4.534 --> 7.2035
;; 3. bfill material is not used.
;; 4. add 2 different invert materials on Tom's email on Feb. 09, 2000.
;;    tcond = 1.52 invert1
;;    tcond = 0.15 invert2 Tom's email on Feb 09, 2000
;; 5. cont-len-fac =0.05 for invert1 and invert2

(lsnf
  (cont-len-fac 1.0e-5) (cont-area-fac 1.0)
;; a small value of connected length is used to minimize thermal disequilibrium between the
fracture and matrix continua
  (exfac-adv (liquid 1.000e+00) (gas 1.000e+00))
  (solid-density 1.5406e+03) (porosity 0.35)
;; because the wp is impermeable, porosity does not affect TH behavior
;; solid-density calculation is on page 31 of Sept. 20
;; because the lsnf properties are applied to both the matrix and fracture continua, which are
each
;; assumed to comprise 50% of the total volume, it is necessary to divide the solid density by
two
;; relative to the calculation on page 31 of Sept. 20
  (Kd       (air 0.0) (water 0.0) )
  (KdFactor (air 0.0) (water 0.0) )
  (Cp 4.88860e+02)
(tcond tcondLin (solid 7.210000)(liquid 7.21000)(gas 7.210000))   ;;@@@;; Changes
;; tcond =1/2 the single continuum value
  (K0 0.000e+00) (K1 0.000e+00) (K2 0.000e+00)
  (tort (gas 1.000e+00) (liquid 0.0))
  (kr (gas    krgLinear (Smax 1.000e+00)(Sr 0.000e+00))
      (liquid krlLinear (Smax 1.000e+00)(Sr 0.000e+00)))
  (pc (liquid  0.0))
  (krMC (liquid  krMCintrinsic) (gas  krMCintrinsic))
)

(m-dr ;;  equivalent Kth for thermal radiation in the drift
  (cont-len-fac 1.0e-5) (cont-area-fac 1.0)
;; a small value of connected length is used to minimize thermal disequilibrium between the
fracture and matrix continua
  (exfac-adv (liquid 1.000e+00) (gas 1.000e+00))
  (solid-density 5.92500e-01)  (porosity 0.495)
;; porosity =1/2 the single continuum value
;; solid-density=1/2 the single continuum value
  (Kd       (air 0.0) (water 0.0))
  (KdFactor (air 0.0) (water 0.0))
  (Cp 1.006e+03)
  (tcond tcondLin  (solid 7.2035) (liquid 7.2035) (gas 7.2035))   ;;@@@;; Changes
;; tcond = 1/2 the single continuum value
  (K0 0.500e-08) (K1 0.500e-08) (K2 0.500e-08)
;; permeability =1/2 the single continuum value
  (tort (gas 1.000e+00) (liquid 0.0))
  (kr (gas    krgLinear (Smax 1.000e+00)(Sr 0.000e+00))
      (liquid krPower (power 1) (Smax 1.000e+00)(Sr 0.000e+00)))
  (pc (liquid 0.0))
  (krMC (liquid  krMCintrinsic) (gas  krMCintrinsic))
  )

(f-dr ;;  equivalent Kth for thermal radiation in the drift
  (cont-len-fac 1.0e-5) (cont-area-fac 1.0)
;; a small value of connected length is used to minimize thermal disequilibrium between the
fracture and matrix continua
  (exfac-adv (liquid 1.000e+00) (gas 1.000e+00))
  (solid-density 5.92500e-01)  (porosity 0.495)
;; porosity =1/2 the single continuum value
;; solid density = 1/2 the single continuum value
  (Kd       (air 0.0) (water 0.0))
```

```
  (KdFactor (air 0.0) (water 0.0))
  (Cp 1.006e+03)
  (tcond tcondLin  (solid 7.2035) (liquid 7.2035) (gas 7.2035))
;; tcond = 1/2 the single continuum value
  (K0 0.500e-08) (K1 0.500e-08) (K2 0.500e-08)
;; permeability =1/2 the single continuum value
  (tort (gas 1.000e+00) (liquid 0.0))
  (kr (gas    krgLinear (Smax 1.000e+00)(Sr 0.000e+00))
      (liquid krPower (power 1) (Smax 1.000e+00)(Sr 0.000e+00)))
  (pc (liquid 0.0))
  (krMC (liquid  krMCintrinsic) (gas  krMCintrinsic))
  )

(m-bfill ;; matrix-continuum backfill
  (cont-len-fac 1.0e-5) (cont-area-fac 1.0)
;; a small value of connected length is used to minimize thermal disequilibrium between the
fracture and matrix continua
  (exfac-adv (liquid 1.000e+00) (gas 1.000e+00))
  (solid-density 1.350e+03)  (porosity 0.205)
;; porosity =1/2 the single continuum value
;; solid density = 1/2 the single continuum value
  (Kd (air 0.0)(water 0.0))
  (KdFactor (water 0.0) (air 0.0))
  (Cp 7.9550e+02)
  (tcond tcondLin (solid 0.16500)(liquid 0.16500)(gas 0.16500))
;; tcond = 1/2 the single continuum value
  (K0 0.715e-11) (K1 0.715e-11) (K2 0.715e-11)
;; permeability =1/2 the single continuum value
  (tort (gas 0.7) (liquid 0.0)) ;;JJN
  (kr (liquid krlVanGen       (Sr 0.024)           (m 0.5) (Smax 1.0))
      (gas krgVanGenMinus     (Sr 0.024) (Sj 0.07) (m 0.5) (Smax 1.0))
   )
  (pc (liquid pcVanGen (alpha 2.7523e-4)(Sr 0.024)(Sj 0.07)(m 0.5)(Smax 1.0)))
  (krMC (liquid  krMCintrinsic) (gas  krMCintrinsic))
)
(f-bfill ;; fracture-continuum backfill
   (cont-len-fac 1.0e-5) (cont-area-fac 1.0)
;; a small value of connected length is used to minimize thermal disequilibrium between the
fracture and matrix continua
   (exfac-adv (liquid 1.000e+00) (gas 1.000e+00))
  (solid-density 1.350e+03)  (porosity 0.205)
;; porosity =1/2 the single continuum value
;; solid density = 1/2 the single continuum value
   (Kd (air 0.0)(water 0.0))
   (KdFactor (water 0.0) (air 0.0))
   (Cp 7.9550e+02)
   (tcond tcondLin (solid 0.16500)(liquid 0.16500)(gas 0.16500))
;; tcond = 1/2 the single continuum value
  (K0 0.715e-11) (K1 0.715e-11) (K2 0.715e-11)
;; permeability =1/2 the single continuum value
   (tort (gas 0.7) (liquid 0.0)) ;;JJN
   (kr (liquid krlVanGen   (Sr 0.024)           (m 0.5) (Smax 1.0))
       (gas krgVanGenMinus (Sr 0.024) (Sj 0.07) (m 0.5) (Smax 1.0))
   )
  (pc (liquid pcVanGen (alpha 2.7523e-4)(Sr 0.024)(Sj 0.07)(m 0.5)(Smax 1.0)))
  (krMC (liquid  krMCintrinsic) (gas  krMCintrinsic))
)
(m-invert1
  (cont-len-fac 0.05) (cont-area-fac 1.0)
;; a small value of connected length is used to minimize thermal disequilibrium between the
fracture and matrix continua
  (exfac-adv (liquid 1.000e+00) (gas 1.000e+00))
  (solid-density 1.2565e+03)  (porosity 0.2725)
;; porosity =1/2 the single continuum value
;; solid density = 1/2 the single continuum value
  (Kd (air 0.0)(water 0.0))
  (KdFactor (water 0.0) (air 0.0))
  (Cp 9.480e+02)
  (tcond tcondLin (solid 0.7600)(liquid 0.7600)(gas 0.7600))  ;;@@@;; 1.52 from Tom's email
;; tcond = 1/2 the single continuum value
  (K0 3.076e-10) (K1 3.076e-10) (K2 3.076e-10)
```

```
;; permeability =1/2 the single continuum value
  (tort (gas 0.7) (liquid 0.0)) ;;JJN
  (kr (liquid krlVanGen   (Sr 0.092) (m 0.6296) (Smax 1.0))
      (gas krgVanGenMinus (Sr 0.092) (Sj 0.1)(m 0.6296) (Smax 1.0))
   )
  (pc (liquid pcVanGen (alpha 1.2232e-3)(Sr 0.092)(Sj 0.1)(m 0.6296)(Smax 1.0)))
  (krMC (liquid  krMCintrinsic) (gas  krMCintrinsic))
)
;;
(f-invert1
  (cont-len-fac 0.05) (cont-area-fac 1.0)
;; a small value of connected length is used to minimize thermal disequilibrium between the
fracture and matrix continua
 (exfac-adv (liquid 1.000e+00) (gas 1.000e+00))
  (solid-density 1.2565e+03)  (porosity 0.2725)
;; porosity =1/2 the single continuum value
;; solid density = 1/2 the single continuum value
   (Kd (air 0.0)(water 0.0))
   (KdFactor (water 0.0) (air 0.0))
   (Cp 9.480e+02)
   (tcond tcondLin (solid 0.7600)(liquid 0.7600)(gas 0.7600))  ;;@@@;; 1.52 from Tom's email
 ;; tcond = 1/2 the single continuum value
  (K0 3.076e-10) (K1 3.076e-10) (K2 3.076e-10)
;; permeability =1/2 the single continuum value
   (tort (gas 0.7) (liquid 0.0)) ;;JJN
   (kr (liquid krlVanGen   (Sr 0.092) (m 0.6296) (Smax 1.0))
       (gas krgVanGenMinus (Sr 0.092) (Sj 0.1)(m 0.6296) (Smax 1.0))
   )
  (pc (liquid pcVanGen (alpha 1.2232e-3)(Sr 0.092)(Sj 0.1)(m 0.6296)(Smax 1.0)))
  (krMC (liquid  krMCintrinsic) (gas  krMCintrinsic))
)
(m-invert2
  (cont-len-fac 0.05) (cont-area-fac 1.0)
;; a small value of connected length is used to minimize thermal disequilibrium between the
fracture and matrix continua
  (exfac-adv (liquid 1.000e+00) (gas 1.000e+00))
  (solid-density 1.2565e+03)  (porosity 0.2725)
;; porosity =1/2 the single continuum value
;; solid density = 1/2 the single continuum value
  (Kd (air 0.0)(water 0.0))
  (KdFactor (water 0.0) (air 0.0))
  (Cp 9.480e+02)
  (tcond tcondLin (solid 0.0750)(liquid 0.0750)(gas 0.0750)) ;;@@@;; 0.15 from Tom's email
;; tcond = 1/2 the single continuum value
  (K0 3.076e-10) (K1 3.076e-10) (K2 3.076e-10)
;; permeability =1/2 the single continuum value
  (tort (gas 0.7) (liquid 0.0)) ;;JJN
  (kr (liquid krlVanGen   (Sr 0.092) (m 0.6296) (Smax 1.0))
      (gas krgVanGenMinus (Sr 0.092) (Sj 0.1)(m 0.6296) (Smax 1.0))
   )
  (pc (liquid pcVanGen (alpha 1.2232e-3)(Sr 0.092)(Sj 0.1)(m 0.6296)(Smax 1.0)))
  (krMC (liquid  krMCintrinsic) (gas  krMCintrinsic))
)
;;
(f-invert2
 (cont-len-fac 0.05) (cont-area-fac 1.0)
;; a small value of connected length is used to minimize thermal disequilibrium between the
fracture and matrix continua
 (exfac-adv (liquid 1.000e+00) (gas 1.000e+00))
  (solid-density 1.2565e+03)  (porosity 0.2725)
;; porosity =1/2 the single continuum value
;; solid density = 1/2 the single continuum value
   (Kd (air 0.0)(water 0.0))
   (KdFactor (water 0.0) (air 0.0))
   (Cp 9.480e+02)
   (tcond tcondLin (solid 0.0750)(liquid 0.0750)(gas 0.0750)) ;;@@@;; 0.15 from Tom's email
;; tcond = 1/2 the single continuum value
  (K0 3.076e-10) (K1 3.076e-10) (K2 3.076e-10)
;; permeability =1/2 the single continuum value
   (tort (gas 0.7) (liquid 0.0)) ;;JJN
   (kr (liquid krlVanGen   (Sr 0.092) (m 0.6296) (Smax 1.0))
```

```
      (gas krgVanGenMinus (Sr 0.092) (Sj 0.1)(m 0.6296) (Smax 1.0))
   )
  (pc (liquid pcVanGen (alpha 1.2232e-3)(Sr 0.092)(Sj 0.1)(m 0.6296)(Smax 1.0)))
  (krMC (liquid  krMCintrinsic) (gas  krMCintrinsic))
)
```

**File Name: run_control_param_LDTH-v01**

```
(linear-solver pcg)
(eisenstat-walker on)
(pcg-parameters  (precond d4) (north 25) (toler 1.e-5)
                 (itermax 200))
(ilu-degree 4)  ;; increase to 2 if you get maximum
                ;; solver iterations exceeded
```

# Appendix B
# Pre-Closure Time Study (Task2)

The following directories contain the model input/output of the pre-closure study. This task was not mention earlier. Each directory ends with a number which identifies the length of pre-closure time.
**Nye_design0_softmethod_varpbar_allpost5_100yrvent**
**Nye_design0_softmethod_varpbar_allpost5_200yrvent**
**Nye_design0_softmethod_varpbar_allpost5_300yrvent**

To establish a case of pre-closure time length the waste package heat generation table was modified. The number of time division were kept as 27 since the NTCF matrix is based on 27 time divisions. For example, the 200 year preclosure was set up as follows:

1- load the cfd_d\qq.dat as waste package heat generation table.
2- Create a new time vector by adding 150 to the base case post-closure time vector which is based on the 50 year pre-closure.
3- Interpolate th qq table along the rows, corresponding to time, as new heat table. Linear interpolation was used.

## Waste Package Heat for 100 year Pre-closure Time

| Time (year) | HLW (W) | 44BWR (W) | 21PWR (W) | HLW (W) | 21PWR (W) | 44BWR (W) | 21PWR (W) | DSNF (W) |
|---|---|---|---|---|---|---|---|---|
| 0.167 | 4013.677 | 7125.855 | 11320.265 | 4013.677 | 11320.265 | 7125.855 | 11320.265 | 790.261 |
| 0.5 | 3853.61 | 7088.143 | 11262.276 | 3853.61 | 11262.276 | 7088.143 | 11262.276 | 786.247 |
| 1 | 3590.542 | 7013.068 | 11147.086 | 3590.542 | 11147.086 | 7013.068 | 11147.086 | 782.852 |
| 2 | 3272.475 | 6891.06 | 10956.96 | 3272.475 | 10956.96 | 6891.06 | 10956.96 | 776.94 |
| 5 | 2901.342 | 6644.66 | 10567.935 | 2901.342 | 10567.935 | 6644.66 | 10567.935 | 763.173 |
| 10 | 2545.458 | 6207.3 | 9873.465 | 2545.458 | 9873.465 | 6207.3 | 9873.465 | 733.893 |
| 15 | 2260.2 | 5670.28 | 9020.34 | 2260.2 | 9020.34 | 5670.28 | 9020.34 | 691.803 |
| 20 | 2016.392 | 5164.28 | 8221.71 | 2016.392 | 8221.71 | 5164.28 | 8221.71 | 647.39 |
| 25 | 1801.867 | 4719.22 | 7531.965 | 1801.867 | 7531.965 | 4719.22 | 7531.965 | 605.45 |
| 30 | 1611.967 | 4324.98 | 6929.003 | 1611.967 | 6929.003 | 4324.98 | 6929.003 | 566.15 |
| 35 | 1443.388 | 3979.03 | 6396.6 | 1443.388 | 6396.6 | 3979.03 | 6396.6 | 529.487 |
| 40 | 1293.683 | 3673.45 | 5927.67 | 1293.683 | 5927.67 | 3673.45 | 5927.67 | 495.457 |
| 45 | 1160.654 | 3399.55 | 5508.143 | 1160.654 | 5508.143 | 3399.55 | 5508.143 | 464.063 |
| 50 | 1042.388 | 3155.57 | 5131.98 | 1042.388 | 5131.98 | 3155.57 | 5131.98 | 435.313 |
| 110 | 507.651 | 2012.934 | 3373.566 | 507.651 | 3373.566 | 2012.934 | 3373.566 | 310.714 |
| 125 | 448.646 | 1877.865 | 3160.894 | 448.646 | 3160.894 | 1877.865 | 3160.894 | 300.28 |
| 150 | 350.304 | 1652.75 | 2806.44 | 350.304 | 2806.44 | 1652.75 | 2806.44 | 282.89 |
| 200 | 195.817 | 1262.91 | 2179.643 | 195.817 | 2179.643 | 1262.91 | 2179.643 | 250.703 |
| 250 | 149.677 | 1122.77 | 1944.049 | 149.677 | 1944.049 | 1122.77 | 1944.049 | 234.368 |
| 350 | 92.522 | 929.528 | 1615.084 | 92.522 | 1615.084 | 929.528 | 1615.084 | 210.365 |
| 550 | 54.739 | 733.37 | 1269.629 | 54.739 | 1269.629 | 733.37 | 1269.629 | 181.599 |
| 800 | 32.938 | 558.404 | 957.894 | 32.938 | 957.894 | 558.404 | 957.894 | 154.311 |
| 1050 | 20.644 | 437.976 | 737.882 | 20.644 | 737.882 | 437.976 | 737.882 | 135.649 |
| 1550 | 12.28 | 338.041 | 556.028 | 12.28 | 556.028 | 338.041 | 556.028 | 118.972 |
| 2050 | 6.822 | 258.714 | 415.359 | 6.822 | 415.359 | 258.714 | 415.359 | 104.181 |
| 3050 | 3.401 | 196.988 | 308.518 | 3.401 | 308.518 | 196.988 | 308.518 | 92.091 |
| 5050 | 1.93 | 156.508 | 240.32 | 1.93 | 240.32 | 156.508 | 240.32 | 81.345 |

## Waste Package Heat for 200 year Pre-closure Time

| Time (year) | HLW (W) | 44BWR (W) | 21PWR (W) | HLW (W) | 21PWR (W) | 44BWR (W) | 21PWR (W) | DSNF (W) |
|---|---|---|---|---|---|---|---|---|
| 0.167 | 4013.677 | 7125.855 | 11320.265 | 4013.677 | 11320.265 | 7125.855 | 11320.265 | 790.261 |
| 0.5 | 3853.61 | 7088.143 | 11262.276 | 3853.61 | 11262.276 | 7088.143 | 11262.276 | 786.247 |
| 1 | 3590.542 | 7013.068 | 11147.086 | 3590.542 | 11147.086 | 7013.068 | 11147.086 | 782.852 |
| 2 | 3272.475 | 6891.06 | 10956.96 | 3272.475 | 10956.96 | 6891.06 | 10956.96 | 776.94 |
| 5 | 2901.342 | 6644.66 | 10567.935 | 2901.342 | 10567.935 | 6644.66 | 10567.935 | 763.173 |
| 10 | 2545.458 | 6207.3 | 9873.465 | 2545.458 | 9873.465 | 6207.3 | 9873.465 | 733.893 |
| 15 | 2260.2 | 5670.28 | 9020.34 | 2260.2 | 9020.34 | 5670.28 | 9020.34 | 691.803 |
| 20 | 2016.392 | 5164.28 | 8221.71 | 2016.392 | 8221.71 | 5164.28 | 8221.71 | 647.39 |
| 25 | 1801.867 | 4719.22 | 7531.965 | 1801.867 | 7531.965 | 4719.22 | 7531.965 | 605.45 |
| 30 | 1611.967 | 4324.98 | 6929.003 | 1611.967 | 6929.003 | 4324.98 | 6929.003 | 566.15 |
| 35 | 1443.388 | 3979.03 | 6396.6 | 1443.388 | 6396.6 | 3979.03 | 6396.6 | 529.487 |
| 40 | 1293.683 | 3673.45 | 5927.67 | 1293.683 | 5927.67 | 3673.45 | 5927.67 | 495.457 |
| 45 | 1160.654 | 3399.55 | 5508.143 | 1160.654 | 5508.143 | 3399.55 | 5508.143 | 464.063 |
| 50 | 1042.388 | 3155.57 | 5131.98 | 1042.388 | 5131.98 | 3155.57 | 5131.98 | 435.313 |
| 210 | 186.589 | 1234.882 | 2132.524 | 186.589 | 2132.524 | 1234.882 | 2132.524 | 247.436 |
| 225 | 172.747 | 1192.84 | 2061.846 | 172.747 | 2061.846 | 1192.84 | 2061.846 | 242.536 |
| 250 | 149.677 | 1122.77 | 1944.049 | 149.677 | 1944.049 | 1122.77 | 1944.049 | 234.368 |
| 300 | 103.537 | 982.63 | 1708.455 | 103.537 | 1708.455 | 982.63 | 1708.455 | 218.033 |
| 350 | 92.522 | 929.528 | 1615.084 | 92.522 | 1615.084 | 929.528 | 1615.084 | 210.365 |
| 450 | 70.491 | 823.322 | 1428.341 | 70.491 | 1428.341 | 823.322 | 1428.341 | 195.028 |
| 650 | 45.267 | 659.67 | 1138.946 | 45.267 | 1138.946 | 659.67 | 1138.946 | 170.078 |
| 900 | 27.223 | 503.272 | 857.157 | 27.223 | 857.157 | 503.272 | 857.157 | 145.819 |
| 1150 | 18.916 | 417.648 | 700.807 | 18.916 | 700.807 | 417.648 | 700.807 | 132.293 |
| 1650 | 11.107 | 321.123 | 525.997 | 11.107 | 525.997 | 321.123 | 525.997 | 115.824 |
| 2150 | 6.466 | 252.324 | 404.292 | 6.466 | 404.292 | 252.324 | 404.292 | 102.937 |
| 3150 | 3.327 | 194.964 | 305.108 | 3.327 | 305.108 | 194.964 | 305.108 | 91.554 |
| 5150 | 1.856 | 154.484 | 236.91 | 1.856 | 236.91 | 154.484 | 236.91 | 80.807 |

## Waste Package Heat for 300 year Pre-closure Time

| Time (year) | HLW (W) | 44BWR (W) | 21PWR (W) | HLW (W) | 21PWR (W) | 44BWR (W) | 21PWR (W) | DSNF (W) |
|---|---|---|---|---|---|---|---|---|
| 0.167 | 4013.677 | 7125.855 | 11320.265 | 4013.677 | 11320.265 | 7125.855 | 11320.265 | 790.261 |
| 0.5 | 3853.61 | 7088.143 | 11262.276 | 3853.61 | 11262.276 | 7088.143 | 11262.276 | 786.247 |
| 1 | 3590.542 | 7013.068 | 11147.086 | 3590.542 | 11147.086 | 7013.068 | 11147.086 | 782.852 |
| 2 | 3272.475 | 6891.06 | 10956.96 | 3272.475 | 10956.96 | 6891.06 | 10956.96 | 776.94 |
| 5 | 2901.342 | 6644.66 | 10567.935 | 2901.342 | 10567.935 | 6644.66 | 10567.935 | 763.173 |
| 10 | 2545.458 | 6207.3 | 9873.465 | 2545.458 | 9873.465 | 6207.3 | 9873.465 | 733.893 |
| 15 | 2260.2 | 5670.28 | 9020.34 | 2260.2 | 9020.34 | 5670.28 | 9020.34 | 691.803 |
| 20 | 2016.392 | 5164.28 | 8221.71 | 2016.392 | 8221.71 | 5164.28 | 8221.71 | 647.39 |
| 25 | 1801.867 | 4719.22 | 7531.965 | 1801.867 | 7531.965 | 4719.22 | 7531.965 | 605.45 |
| 30 | 1611.967 | 4324.98 | 6929.003 | 1611.967 | 6929.003 | 4324.98 | 6929.003 | 566.15 |
| 35 | 1443.388 | 3979.03 | 6396.6 | 1443.388 | 6396.6 | 3979.03 | 6396.6 | 529.487 |
| 40 | 1293.683 | 3673.45 | 5927.67 | 1293.683 | 5927.67 | 3673.45 | 5927.67 | 495.457 |
| 45 | 1160.654 | 3399.55 | 5508.143 | 1160.654 | 5508.143 | 3399.55 | 5508.143 | 464.063 |
| 50 | 1042.388 | 3155.57 | 5131.98 | 1042.388 | 5131.98 | 3155.57 | 5131.98 | 435.313 |
| 310 | 101.334 | 972.01 | 1689.781 | 101.334 | 1689.781 | 972.01 | 1689.781 | 216.5 |
| 325 | 98.03 | 956.079 | 1661.769 | 98.03 | 1661.769 | 956.079 | 1661.769 | 214.199 |
| 350 | 92.522 | 929.528 | 1615.084 | 92.522 | 1615.084 | 929.528 | 1615.084 | 210.365 |
| 400 | 81.506 | 876.425 | 1521.713 | 81.506 | 1521.713 | 876.425 | 1521.713 | 202.697 |
| 450 | 70.491 | 823.322 | 1428.341 | 70.491 | 1428.341 | 823.322 | 1428.341 | 195.028 |
| 550 | 54.739 | 733.37 | 1269.629 | 54.739 | 1269.629 | 733.37 | 1269.629 | 181.599 |
| 750 | 35.796 | 585.97 | 1008.263 | 35.796 | 1008.263 | 585.97 | 1008.263 | 158.557 |
| 1000 | 21.508 | 448.14 | 756.42 | 21.508 | 756.42 | 448.14 | 756.42 | 137.327 |
| 1250 | 17.188 | 397.32 | 663.731 | 17.188 | 663.731 | 397.32 | 663.731 | 128.937 |
| 1750 | 9.933 | 304.205 | 495.967 | 9.933 | 495.967 | 304.205 | 495.967 | 112.675 |
| 2250 | 6.109 | 245.933 | 393.225 | 6.109 | 393.225 | 245.933 | 393.225 | 101.693 |
| 3250 | 3.254 | 192.94 | 301.698 | 3.254 | 301.698 | 192.94 | 301.698 | 91.017 |
| 5250 | 1.783 | 152.46 | 233.5 | 1.783 | 233.5 | 152.46 | 233.5 | 80.27 |

# Appendix C
# Barometric Pressure Pumping Study (Task3)

### *NUFT 2D input file*

This NUFT input file is obtained by modifying the Task 1 NUFT 3D input file as follows:

```
comment the line
;;(dy 118.485 94.788 71.091 47.394 23.697 1e-5  35.545 106.64 213.27 )  ;;3D
mountain-scale
```

Insert the new line:

```
(dy 1.0)  ;;2D -1m  thick slice
```

There are two instances of **dy** which need to be fixed

### *NTCF input file*

## Piecewise-linear drift wall boundary condition from Year 0 to 750

```
22 94

1 22

1

0 0.167 0.5 1 2 5 10 15 20 25 30 35 40 45 50 60 75 100 150 200 300 500 750

8.790200e+004  8.790200e+004  8.790200e+004  8.790200e+004  8.790200e+004  8.790200e+004
8.790200e+004  8.790200e+004  8.790200e+004  8.790200e+004  8.790200e+004  8.790200e+004
8.790200e+004  8.790200e+004  8.790200e+004  8.790200e+004  8.790200e+004  8.790200e+004
8.790200e+004  8.790200e+004  8.790200e+004  8.790200e+004  8.790200e+004

2.4000000e+001
5.5816476e+001
6.5806782e+001
6.9263329e+001
7.0909084e+001
7.1324616e+001
6.9295735e+001
6.5958029e+001
6.2602314e+001
5.9578929e+001
5.6860833e+001
5.4446788e+001
5.2300557e+001
5.0372915e+001
4.8652629e+001
1.3158008e+002
1.4900638e+002
1.4862878e+002
1.4761358e+002
1.3999984e+002
1.3560394e+002
1.3582457e+002
1.2671772e+002

5.0000000e+003
9.8340507e+002
1.0245249e+003
1.0211234e+003
1.0158862e+003
9.9318654e+002
9.6663468e+002
9.6132749e+002
9.5847343e+002
9.5746941e+002
9.5364894e+002
```

```
9.5236234e+002
9.4854155e+002
9.4606864e+002
9.4780615e+002
8.7584710e+004
8.7588320e+004
8.7594220e+004
8.7605520e+004
8.7616210e+004
8.7635860e+004
8.7669080e+004
8.7701270e+004
```

## Piecewise-linear drift wall boundary condition from Year 0 to 1000

```
23 94

1 23

1

0 0.167 0.5 1 2 5 10 15 20 25 30 35 40 45 50 60 75 100 150 200 300 500 750 1000

8.790200e+004  8.790200e+004  8.790200e+004  8.790200e+004  8.790200e+004  8.790200e+004
8.790200e+004  8.790200e+004  8.790200e+004  8.790200e+004  8.790200e+004  8.790200e+004
8.790200e+004  8.790200e+004  8.790200e+004  8.790200e+004  8.790200e+004  8.790200e+004
8.790200e+004  8.790200e+004  8.790200e+004  8.790200e+004  8.790200e+004  8.790200e+004

2.4000000e+001
5.5816476e+001
6.5806782e+001
6.9263329e+001
7.0909084e+001
7.1324616e+001
6.9295735e+001
6.5958029e+001
6.2602314e+001
5.9578929e+001
5.6860833e+001
5.4446788e+001
5.2300557e+001
5.0372915e+001
4.8652629e+001
1.3158008e+002
1.4900638e+002
1.4862878e+002
1.4761358e+002
1.3999984e+002
1.3560394e+002
1.3582457e+002
1.2671772e+002
1.1778659e+002

5.0000000e+003
9.8340507e+002
1.0245249e+003
1.0211234e+003
1.0158862e+003
9.9318654e+002
9.6663468e+002
9.6132749e+002
9.5847343e+002
9.5746941e+002
9.5364894e+002
9.5236234e+002
9.4854155e+002
9.4606864e+002
9.4780615e+002
8.7584710e+004
```

```
8.7588320e+004
8.7594220e+004
8.7605520e+004
8.7616210e+004
8.7635860e+004
8.7669080e+004
8.7701270e+004
8.7725570e+004
```

## Piecewise-linear drift wall boundary condition from Year 0 to 1500

```
24 94

1 24

1

0 0.167 0.5 1 2 5 10 15 20 25 30 35 40 45 50 60 75 100 150 200 300 500 750 1000 1500

8.790200e+004  8.790200e+004  8.790200e+004  8.790200e+004  8.790200e+004  8.790200e+004
8.790200e+004  8.790200e+004  8.790200e+004  8.790200e+004  8.790200e+004  8.790200e+004
8.790200e+004  8.790200e+004  8.790200e+004  8.790200e+004  8.790200e+004  8.790200e+004
8.790200e+004  8.790200e+004  8.790200e+004  8.790200e+004  8.790200e+004  8.790200e+004
8.790200e+004

2.4000000e+001
5.5816476e+001
6.5806782e+001
6.9263329e+001
7.0909084e+001
7.1324616e+001
6.9295735e+001
6.5958029e+001
6.2602314e+001
5.9578929e+001
5.6860833e+001
5.4446788e+001
5.2300557e+001
5.0372915e+001
4.8652629e+001
1.3158008e+002
1.4900638e+002
1.4862878e+002
1.4761358e+002
1.3999984e+002
1.3560394e+002
1.3582457e+002
1.2671772e+002
1.1778659e+002
1.0834571e+002

5.0000000e+003
9.8340507e+002
1.0245249e+003
1.0211234e+003
1.0158862e+003
9.9318654e+002
9.6663468e+002
9.6132749e+002
9.5847343e+002
9.5746941e+002
9.5364894e+002
9.5236234e+002
9.4854155e+002
9.4606864e+002
9.4780615e+002
8.7584710e+004
8.7588320e+004
8.7594220e+004
8.7605520e+004
```

8.7616210e+004
8.7635860e+004
8.7669080e+004
8.7701270e+004
8.7725570e+004
8.7758430e+004

## Piecewise-linear drift wall boundary condition from Year 0 to 2000

25 94

1 25

1

0 0.167 0.5 1 2 5 10 15 20 25 30 35 40 45 50 60 75 100 150 200 300 500 750 1000 1500 2000

```
8.790200e+004  8.790200e+004  8.790200e+004  8.790200e+004  8.790200e+004  8.790200e+004
8.790200e+004  8.790200e+004  8.790200e+004  8.790200e+004  8.790200e+004  8.790200e+004
8.790200e+004  8.790200e+004  8.790200e+004  8.790200e+004  8.790200e+004  8.790200e+004
8.790200e+004  8.790200e+004  8.790200e+004  8.790200e+004  8.790200e+004  8.790200e+004
8.790200e+004  8.790200e+004
```

2.4000000e+001
5.5816476e+001
6.5806782e+001
6.9263329e+001
7.0909084e+001
7.1324616e+001
6.9295735e+001
6.5958029e+001
6.2602314e+001
5.9578929e+001
5.6860833e+001
5.4446788e+001
5.2300557e+001
5.0372915e+001
4.8652629e+001
1.3158008e+002
1.4900638e+002
1.4862878e+002
1.4761358e+002
1.3999984e+002
1.3560394e+002
1.3582457e+002
1.2671772e+002
1.1778659e+002
1.0834571e+002
1.0280547e+002

5.0000000e+003
9.8340507e+002
1.0245249e+003
1.0211234e+003
1.0158862e+003
9.9318654e+002
9.6663468e+002
9.6132749e+002
9.5847343e+002
9.5746941e+002
9.5364894e+002
9.5236234e+002
9.4854155e+002
9.4606864e+002
9.4780615e+002
8.7584710e+004
8.7588320e+004
8.7594220e+004
8.7605520e+004

```
8.7616210e+004
8.7635860e+004
8.7669080e+004
8.7701270e+004
8.7725570e+004
8.7758430e+004
8.7779080e+004
```

## Piecewise-linear drift wall boundary condition from Year 0 to 3000

```
26 94

1 26

1

0 0.167 0.5 1 2 5 10 15 20 25 30 35 40 45 50 60 75 100 150 200 300 500 750 1000 1500 2000 3000

8.790200e+004  8.790200e+004  8.790200e+004  8.790200e+004  8.790200e+004  8.790200e+004
8.790200e+004  8.790200e+004  8.790200e+004  8.790200e+004  8.790200e+004  8.790200e+004
8.790200e+004  8.790200e+004  8.790200e+004  8.790200e+004  8.790200e+004  8.790200e+004
8.790200e+004  8.790200e+004  8.790200e+004  8.790200e+004  8.790200e+004  8.790200e+004
8.790200e+004  8.790200e+004  8.790200e+004

2.4000000e+001
5.5816476e+001
6.5806782e+001
6.9263329e+001
7.0909084e+001
7.1324616e+001
6.9295735e+001
6.5958029e+001
6.2602314e+001
5.9578929e+001
5.6860833e+001
5.4446788e+001
5.2300557e+001
5.0372915e+001
4.8652629e+001
1.3158008e+002
1.4900638e+002
1.4862878e+002
1.4761358e+002
1.3999984e+002
1.3560394e+002
1.3582457e+002
1.2671772e+002
1.1778659e+002
1.0834571e+002
1.0280547e+002
9.2828307e+001

5.0000000e+003
9.8340507e+002
1.0245249e+003
1.0211234e+003
1.0158862e+003
9.9318654e+002
9.6663468e+002
9.6132749e+002
9.5847343e+002
9.5746941e+002
9.5364894e+002
9.5236234e+002
9.4854155e+002
9.4606864e+002
9.4780615e+002
8.7584710e+004
8.7588320e+004
```

```
8.7594220e+004
8.7605520e+004
8.7616210e+004
8.7635860e+004
8.7669080e+004
8.7701270e+004
8.7725570e+004
8.7758430e+004
8.7779080e+004
3.9345694e+004
```

## Drift wall boundary condition after Year 750 with varying barometric pressure

```
40  94
1  40
1

0   0.0145927   0.0291855   0.0437782   0.058371   0.0729637   0.0875565   0.102149   0.116742
0.131335   0.145927   0.16052   0.175113   0.189706   0.204298   0.218891   0.233484   0.248077
0.262669   0.277262   0.291855   0.306448   0.32104   0.335633   0.350226   0.364819   0.379411
0.394004   0.408597   0.42319   0.437782   0.452375   0.466968   0.481561   0.496153   0.510746
0.525339   0.539932   0.554524   0.569117   0.58371

8.8917935e+004   8.6596935e+004   8.8917935e+004   8.6596935e+004   8.8917935e+004
8.6596935e+004   8.8917935e+004   8.6596935e+004   8.8917935e+004   8.6596935e+004
8.8917935e+004   8.6596935e+004   8.8917935e+004   8.6596935e+004   8.8917935e+004
8.6596935e+004   8.8917935e+004   8.6596935e+004   8.8917935e+004   8.6596935e+004
8.8917935e+004   8.6596935e+004   8.8917935e+004   8.6596935e+004   8.8917935e+004
8.6596935e+004   8.8917935e+004   8.6596935e+004   8.8917935e+004   8.6596935e+004
8.8917935e+004   8.6596935e+004   8.8917935e+004   8.6596935e+004   8.8917935e+004
8.6596935e+004   8.8917935e+004   8.6596935e+004   8.8917935e+004   8.6596935e+004


1.2671772e+002
1.2671772e+002
1.2671772e+002
1.2671772e+002
1.2671772e+002
1.2671772e+002
1.2671772e+002
1.2671772e+002
1.2671772e+002
1.2671772e+002
1.2671772e+002
1.2671772e+002
1.2671772e+002
1.2671772e+002
1.2671772e+002
1.2671772e+002
1.2671772e+002
1.2671772e+002
1.2671772e+002
1.2671772e+002
1.2671772e+002
1.2671772e+002
1.2671772e+002
1.2671772e+002
1.2671772e+002
1.2671772e+002
1.2671772e+002
1.2671772e+002
1.2671772e+002
1.2671772e+002
1.2671772e+002
1.2671772e+002
1.2671772e+002
```

```
1.2671772e+002
1.2671772e+002
1.2671772e+002
1.2671772e+002
1.2671772e+002
1.2671772e+002
1.2671772e+002

8.7701270e+004
8.7701270e+004
8.7701270e+004
8.7701270e+004
8.7701270e+004
8.7701270e+004
8.7701270e+004
8.7701270e+004
8.7701270e+004
8.7701270e+004
8.7701270e+004
8.7701270e+004
8.7701270e+004
8.7701270e+004
8.7701270e+004
8.7701270e+004
8.7701270e+004
8.7701270e+004
8.7701270e+004
8.7701270e+004
8.7701270e+004
8.7701270e+004
8.7701270e+004
8.7701270e+004
8.7701270e+004
8.7701270e+004
8.7701270e+004
8.7701270e+004
8.7701270e+004
8.7701270e+004
8.7701270e+004
8.7701270e+004
8.7701270e+004
8.7701270e+004
8.7701270e+004
8.7701270e+004
8.7701270e+004
8.7701270e+004
8.7701270e+004
8.7701270e+004
```

## Drift wall boundary condition after Year 1000 with varying barometric pressure

```
40  94
1  40
1

0   0.0145927   0.0291855   0.0437782   0.058371   0.0729637   0.0875565   0.102149   0.116742
0.131335   0.145927   0.16052   0.175113   0.189706   0.204298   0.218891   0.233484   0.248077
0.262669   0.277262   0.291855   0.306448   0.32104   0.335633   0.350226   0.364819   0.379411
0.394004   0.408597   0.42319   0.437782   0.452375   0.466968   0.481561   0.496153   0.510746
0.525339   0.539932   0.554524   0.569117   0.58371

8.8917935e+004   8.6596935e+004   8.8917935e+004   8.6596935e+004   8.8917935e+004
8.6596935e+004   8.8917935e+004   8.6596935e+004   8.8917935e+004   8.6596935e+004
8.8917935e+004   8.6596935e+004   8.8917935e+004   8.6596935e+004   8.8917935e+004
8.6596935e+004   8.8917935e+004   8.6596935e+004   8.8917935e+004   8.6596935e+004
8.8917935e+004   8.6596935e+004   8.8917935e+004   8.6596935e+004   8.8917935e+004
```

```
8.6596935e+004   8.8917935e+004   8.6596935e+004   8.8917935e+004   8.6596935e+004
8.8917935e+004   8.6596935e+004   8.8917935e+004   8.6596935e+004   8.8917935e+004
8.6596935e+004   8.8917935e+004   8.6596935e+004   8.8917935e+004   8.6596935e+004


1.1778659e+002
1.1778659e+002
1.1778659e+002
1.1778659e+002
1.1778659e+002
1.1778659e+002
1.1778659e+002
1.1778659e+002
1.1778659e+002
1.1778659e+002
1.1778659e+002
1.1778659e+002
1.1778659e+002
1.1778659e+002
1.1778659e+002
1.1778659e+002
1.1778659e+002
1.1778659e+002
1.1778659e+002
1.1778659e+002
1.1778659e+002
1.1778659e+002
1.1778659e+002
1.1778659e+002
1.1778659e+002
1.1778659e+002
1.1778659e+002
1.1778659e+002
1.1778659e+002
1.1778659e+002
1.1778659e+002
1.1778659e+002
1.1778659e+002
1.1778659e+002
1.1778659e+002
1.1778659e+002
1.1778659e+002
1.1778659e+002
1.1778659e+002
1.1778659e+002

8.7725570e+004
8.7725570e+004
8.7725570e+004
8.7725570e+004
8.7725570e+004
8.7725570e+004
8.7725570e+004
8.7725570e+004
8.7725570e+004
8.7725570e+004
8.7725570e+004
8.7725570e+004
8.7725570e+004
8.7725570e+004
8.7725570e+004
8.7725570e+004
8.7725570e+004
8.7725570e+004
8.7725570e+004
8.7725570e+004
8.7725570e+004
8.7725570e+004
8.7725570e+004
8.7725570e+004
8.7725570e+004
```

```
8.7725570e+004
8.7725570e+004
8.7725570e+004
8.7725570e+004
8.7725570e+004
8.7725570e+004
8.7725570e+004
8.7725570e+004
8.7725570e+004
8.7725570e+004
8.7725570e+004
8.7725570e+004
8.7725570e+004
8.7725570e+004
8.7725570e+004
```

## Drift wall boundary condition after Year 1500 with varying barometric pressure

```
40  94
1  40
1

0   0.0145927   0.0291855   0.0437782   0.058371   0.0729637   0.0875565   0.102149   0.116742
0.131335   0.145927   0.16052   0.175113   0.189706   0.204298   0.218891   0.233484   0.248077
0.262669   0.277262   0.291855   0.306448   0.32104   0.335633   0.350226   0.364819   0.379411
0.394004   0.408597   0.42319   0.437782   0.452375   0.466968   0.481561   0.496153   0.510746
0.525339   0.539932   0.554524   0.569117   0.58371

8.8917935e+004   8.6596935e+004   8.8917935e+004   8.6596935e+004   8.8917935e+004
8.6596935e+004   8.8917935e+004   8.6596935e+004   8.8917935e+004   8.6596935e+004
8.8917935e+004   8.6596935e+004   8.8917935e+004   8.6596935e+004   8.8917935e+004
8.6596935e+004   8.8917935e+004   8.6596935e+004   8.8917935e+004   8.6596935e+004
8.8917935e+004   8.6596935e+004   8.8917935e+004   8.6596935e+004   8.8917935e+004
8.6596935e+004   8.8917935e+004   8.6596935e+004   8.8917935e+004   8.6596935e+004
8.8917935e+004   8.6596935e+004   8.8917935e+004   8.6596935e+004   8.8917935e+004
8.6596935e+004   8.8917935e+004   8.6596935e+004   8.8917935e+004   8.6596935e+004


1.0834571e+002
1.0834571e+002
1.0834571e+002
1.0834571e+002
1.0834571e+002
1.0834571e+002
1.0834571e+002
1.0834571e+002
1.0834571e+002
1.0834571e+002
1.0834571e+002
1.0834571e+002
1.0834571e+002
1.0834571e+002
1.0834571e+002
1.0834571e+002
1.0834571e+002
1.0834571e+002
1.0834571e+002
1.0834571e+002
1.0834571e+002
1.0834571e+002
1.0834571e+002
1.0834571e+002
1.0834571e+002
1.0834571e+002
1.0834571e+002
1.0834571e+002
1.0834571e+002
```

```
1.0834571e+002
1.0834571e+002
1.0834571e+002
1.0834571e+002
1.0834571e+002
1.0834571e+002
1.0834571e+002
1.0834571e+002
1.0834571e+002
1.0834571e+002
1.0834571e+002

8.7758430e+004
8.7758430e+004
8.7758430e+004
8.7758430e+004
8.7758430e+004
8.7758430e+004
8.7758430e+004
8.7758430e+004
8.7758430e+004
8.7758430e+004
8.7758430e+004
8.7758430e+004
8.7758430e+004
8.7758430e+004
8.7758430e+004
8.7758430e+004
8.7758430e+004
8.7758430e+004
8.7758430e+004
8.7758430e+004
8.7758430e+004
8.7758430e+004
8.7758430e+004
8.7758430e+004
8.7758430e+004
8.7758430e+004
8.7758430e+004
8.7758430e+004
8.7758430e+004
8.7758430e+004
8.7758430e+004
8.7758430e+004
8.7758430e+004
8.7758430e+004
8.7758430e+004
8.7758430e+004
8.7758430e+004
8.7758430e+004
8.7758430e+004
8.7758430e+004
```

## Drift wall boundary condition after Year 2000 with varying barometric pressure

```
40  94
1  40
1

0   0.0145927   0.0291855   0.0437782   0.058371   0.0729637   0.0875565   0.102149   0.116742
0.131335   0.145927   0.16052   0.175113   0.189706   0.204298   0.218891   0.233484   0.248077
0.262669   0.277262   0.291855   0.306448   0.32104   0.335633   0.350226   0.364819   0.379411
0.394004   0.408597   0.42319   0.437782   0.452375   0.466968   0.481561   0.496153   0.510746
0.525339   0.539932   0.554524   0.569117   0.58371

8.8917935e+004   8.6596935e+004   8.8917935e+004   8.6596935e+004   8.8917935e+004
8.6596935e+004   8.8917935e+004   8.6596935e+004   8.8917935e+004   8.6596935e+004
```

```
8.8917935e+004   8.6596935e+004   8.8917935e+004   8.6596935e+004   8.8917935e+004
8.6596935e+004   8.8917935e+004   8.6596935e+004   8.8917935e+004   8.6596935e+004
8.8917935e+004   8.6596935e+004   8.8917935e+004   8.6596935e+004   8.8917935e+004
8.6596935e+004   8.8917935e+004   8.6596935e+004   8.8917935e+004   8.6596935e+004
8.8917935e+004   8.6596935e+004   8.8917935e+004   8.6596935e+004   8.8917935e+004
8.6596935e+004   8.8917935e+004   8.6596935e+004   8.8917935e+004   8.6596935e+004

1.0280547e+002
1.0280547e+002
1.0280547e+002
1.0280547e+002
1.0280547e+002
1.0280547e+002
1.0280547e+002
1.0280547e+002
1.0280547e+002
1.0280547e+002
1.0280547e+002
1.0280547e+002
1.0280547e+002
1.0280547e+002
1.0280547e+002
1.0280547e+002
1.0280547e+002
1.0280547e+002
1.0280547e+002
1.0280547e+002
1.0280547e+002
1.0280547e+002
1.0280547e+002
1.0280547e+002
1.0280547e+002
1.0280547e+002
1.0280547e+002
1.0280547e+002
1.0280547e+002
1.0280547e+002
1.0280547e+002
1.0280547e+002
1.0280547e+002
1.0280547e+002
1.0280547e+002
1.0280547e+002
1.0280547e+002
1.0280547e+002
1.0280547e+002
1.0280547e+002

8.7779080e+004
8.7779080e+004
8.7779080e+004
8.7779080e+004
8.7779080e+004
8.7779080e+004
8.7779080e+004
8.7779080e+004
8.7779080e+004
8.7779080e+004
8.7779080e+004
8.7779080e+004
8.7779080e+004
8.7779080e+004
8.7779080e+004
8.7779080e+004
8.7779080e+004
8.7779080e+004
8.7779080e+004
8.7779080e+004
8.7779080e+004
8.7779080e+004
8.7779080e+004
```

```
8.7779080e+004
8.7779080e+004
8.7779080e+004
8.7779080e+004
8.7779080e+004
8.7779080e+004
8.7779080e+004
8.7779080e+004
8.7779080e+004
8.7779080e+004
8.7779080e+004
8.7779080e+004
8.7779080e+004
8.7779080e+004
8.7779080e+004
8.7779080e+004
8.7779080e+004
```

## Drift wall boundary condition after Year 3000 with varying barometric pressure

```
40  94
1  40
1

0   0.0145927   0.0291855   0.0437782   0.058371   0.0729637   0.0875565   0.102149   0.116742
0.131335   0.145927   0.16052   0.175113   0.189706   0.204298   0.218891   0.233484   0.248077
0.262669   0.277262   0.291855   0.306448   0.32104   0.335633   0.350226   0.364819   0.379411
0.394004   0.408597   0.42319   0.437782   0.452375   0.466968   0.481561   0.496153   0.510746
0.525339   0.539932   0.554524   0.569117   0.58371

8.8917935e+004   8.6596935e+004   8.8917935e+004   8.6596935e+004   8.8917935e+004
8.6596935e+004   8.8917935e+004   8.6596935e+004   8.8917935e+004   8.6596935e+004
8.8917935e+004   8.6596935e+004   8.8917935e+004   8.6596935e+004   8.8917935e+004
8.6596935e+004   8.8917935e+004   8.6596935e+004   8.8917935e+004   8.6596935e+004
8.8917935e+004   8.6596935e+004   8.8917935e+004   8.6596935e+004   8.8917935e+004
8.6596935e+004   8.8917935e+004   8.6596935e+004   8.8917935e+004   8.6596935e+004
8.8917935e+004   8.6596935e+004   8.8917935e+004   8.6596935e+004   8.8917935e+004
8.6596935e+004   8.8917935e+004   8.6596935e+004   8.8917935e+004   8.6596935e+004

9.2828307e+001
9.2828307e+001
9.2828307e+001
9.2828307e+001
9.2828307e+001
9.2828307e+001
9.2828307e+001
9.2828307e+001
9.2828307e+001
9.2828307e+001
9.2828307e+001
9.2828307e+001
9.2828307e+001
9.2828307e+001
9.2828307e+001
9.2828307e+001
9.2828307e+001
9.2828307e+001
9.2828307e+001
9.2828307e+001
9.2828307e+001
9.2828307e+001
9.2828307e+001
9.2828307e+001
9.2828307e+001
9.2828307e+001
9.2828307e+001
9.2828307e+001
```

```
9.2828307e+001
9.2828307e+001
9.2828307e+001
9.2828307e+001
9.2828307e+001
9.2828307e+001
9.2828307e+001
9.2828307e+001
9.2828307e+001
9.2828307e+001
9.2828307e+001
9.2828307e+001

3.9345694e+004
3.9345694e+004
3.9345694e+004
3.9345694e+004
3.9345694e+004
3.9345694e+004
3.9345694e+004
3.9345694e+004
3.9345694e+004
3.9345694e+004
3.9345694e+004
3.9345694e+004
3.9345694e+004
3.9345694e+004
3.9345694e+004
3.9345694e+004
3.9345694e+004
3.9345694e+004
3.9345694e+004
3.9345694e+004
3.9345694e+004
3.9345694e+004
3.9345694e+004
3.9345694e+004
3.9345694e+004
3.9345694e+004
3.9345694e+004
3.9345694e+004
3.9345694e+004
3.9345694e+004
3.9345694e+004
3.9345694e+004
3.9345694e+004
3.9345694e+004
3.9345694e+004
3.9345694e+004
3.9345694e+004
3.9345694e+004
3.9345694e+004
3.9345694e+004
```

# Appendix D
# Fate of Condensation Study (Task4)

## NUFT input deck; balanced condensate applied to the roof nodes

File: **nuft_in**

```
;; Implicit DKM with active fracture concept (AFC)
;; NBS material properties from 1D drift-scale mean infiltration flux property set assembled by
Ken Lee
;; AML = 56.48 MTU/acre; half drift spacing = 40.5 m;; AML = 85 MTU/acre; half drift spacing =
26.9 m, Modified on 11/22/02 at UNR

;; Modified by dr1 Bahrami on 9/8/00 for MULTIFLUX input
;; Mesh changed for the tratigrapic unit of ANSYS run

;;      l4c4.col.units

;;      COLUMN INFORMATION (x,y =   170500.828,   233807.766)


;;      unit    thickness (m)
;;      ____    _____________

;;      tcw11      32.900 -> 30.848
;;      tcw12      89.004 -> 83.453
;;      tcw13       4.951 -> 5.490
;;      ptn21       5.947 -> 4.690
;;      ptn22       2.490 -> 0.530
;;      ptn23       2.373 -> 7.050
;;      ptn24       6.533 -> 4.580
;;      ptn25      14.443 -> 14.090
;;      ptn26      15.498 -> 9.690
;;      tsw31       1.992 -> 6.170
;;      tsw32      42.070 -> 46.850
;;      tsw33      88.711 -> 86.659
;;      tsw34      30.254 -> 29.940
;;      tsw35     111.895 -> 106.210
;;      tsw36      27.119 -> 31.793
;;      tsw37      13.594 -> 15.937
;;      tsw38      23.408 -> 23.600
;;      tsw39       3.779 -> 11.270
;;      ch1v       10.166 -> 3.350
;;      ch2v        0.000 -> 0.000
;;      ch3v        0.000 -> 0.000
;;      ch4v        0.000 -> 0.000
;;      ch5v        0.000 -> 0.000
;;      ch1z        0.000 -> 0.000
;;      ch2z       14.414 -> 15.735
;;      ch3z       14.414 -> 15.735
;;      ch4z       14.414 -> 15.735
;;      ch5z       14.414 -> 15.735
;;      ch6        19.629 -> 21.428
;;      pp4         8.086 -> removed
;;      pp3        33.691 -> removed
;;      pp2        14.707 -> removed
;;      pp1        61.055 -> removed
;;      bf3        17.402 -> removed
;;      bf2         0.000 -> removed

;;      repository elevation (m):                                    1073.934
;;      host rock:                                                      tsw35

;;      meters of host rock (tsw35) above repository:                          16.190
;;      meters of host rock (tsw35) below repository:                          90.020

;;      overburden thickness (m):                                          346.230
;;      distance from repository plane to top of chn (m):
;;      distance from repository plane to top of water table (m):     260.340

(usnt
  (title "1.0130000e+01mm_yr,line-load,AML=56mtu_acre,LDTH561Dds_mc-mi")
  (modelname usnt)
```

```
  (stepmax 1000000)
       ;; Set initial condition for multiflux functionalization module:
       ;; for initflag = 1 , first time interval, use 1D restart file
       ;; for initflag =0 , after first time interval, use restart file from previous time
interval
       (include "tmp.inc.time")


  (tolerconv (P 10.0)(S 0.001)(X 0.0001)(T 0.01))
  ;; absolute NR conv. tolerance
  (reltolerconv (P 0.001)(S 0.0)(X 0.0)(T 1.e-3))

  (tolerdt (P 20000)(S 0.25)(X 0.2)(T 10.))
  (reltolerdt (P 0.1)(S 0.0)(X 0.0)(T 0.0))

  ;; trying with harmonic mean everywhere which means turning off the goemetric before vtough.pkg
  ;;  gets called.
  (diffusion-geo-mean off)
  ;; for imp-DKM do not have this so that it will default to harmonic for fract-matrix
interaction
  ;;(mult-cont-diff-harmonic off)
  ;; following has to come after tolerances
  (rmstolerconv 1e-4)
  (include-pkg "vtough.pkg")

;;
***************************************************************************************************
**
(output
     (include "tmp.inc.fout")       ;; output the fluxes cross wall
     (include "tmp.inc.res")        ;; output the restart file
     (extool (continuum  f) (variables T RH S.liquid)
        (file-ext ".f.ext")(range "*")
        (outtimes (include "tmp.inc.timeout"))
     )
     (extool (continuum  m) (variables T RH S.liquid)
        (file-ext ".m.ext")(range "*")
        (outtimes (include "tmp.inc.timeout"))
     )
) ;; end output
;;
***************************************************************************************************
(rocktab
        (include "dkm-afc-1Dds-mc-mi-00")
       (include "dkm-afc-EBS_Rev20a")
) ;; close rocktab
        ;;(include "modprop_dr-20")  Removed WP material properties
;;
***************************************************************************************************

;;  This srctab is adjusted to allocate percollation to just the fracture.
  (srctab
        (compflux
                (comp water)
                (name infil)
                (range "*.f*:*:2")
                (mult-by-area z)
                (allocate-by-element ("*" 1.0))
                (include "percolation.tab")  ;;cyclic percolation table
                (enthalpy  0.0   6.68E+04  1E+30   6.68E+04 )
        )
        (compflux
                (comp water)
                (name condensate)
                (range "cond_h*")
                (mult-by-area z )
                (allocate-by-element ("cond_h*" 1.0))
                (table (include "condensate.tab"))  ;;drift condensate table
                (enthalpy  (include "enthalpy.tab") )
        )
```

```
        (compflux
                (comp water)
                (name condensate)
                (range "cond_v*")
                (mult-by-area x )
                (allocate-by-element ("cond_v*" 1.0))
                (table (include "condensate.tab"))  ;;drift condensate table
                (enthalpy  (include "enthalpy.tab") )
        )

        ;; removed WP data (include "LDTH-SDT-0.3Qheat-50y_vent-20")
  ) ;; end srctab

     ;; set boundary conditions
        (bctab
        (atmos
                (range  "at*")
                (basephase gas)
                (tables
                        (T        0.0  1.8700000e+01   1.0e30  1.8700000e+01 )
                        (S.liquid 0.0  0.0    1.0e30  0.0  )
                        (P        0.0  8.4510758e+04   1.0e30  8.4510758e+04 )
                        (X.air    0.0  9.86600578e-01   1.0e30  9.86600578e-01 )
                )
        )

        (gwater
                (range  "wt*")
                (basephase liquid)
                (tables
                        (T          0  3.2400000e+01      1.0e30   3.2400000e+01)
                        (S.liquid   0  1.0      1.0e30   1.0)
                        (P          0  9.2e4    1.0e30  9.2e4)
                        (X.air      0  1.0e-6   1.0e30  1.0e-6)
                )

;;      SET PHASEFACTOR GAS TO 0, AND LIQUID TO 1 (JOHN)
                (phasefactor
                        (gas      0  0.0   1.0e30  0.0)
                        (liquid   0  1.0   1.0e30  1.0)
                )

        )
        ( include "tmp.inc.tab" )    ;; Set initial conditions for each
                                  ;; section in drift end b.c.
        ) ;; end bctab


;;This is for a unit symmetry cell with a half drift and half pillar
;;between drifts.
  (genmsh
    (anisotropic)
    (down 0. 0. 1.0)
    (coord rect)
    (multi-continua
       (type rocktab)
       (continuum  (name m)
          ;; 56.48 MTU/acre
           ;;(dx 0.570 0.35 0.3310 0.3597 0.3797 0.42 0.3394 0.5 0.9 1.5 2.5 4.0 6.0  9.0
13.3502)
      (dx 0.920  0.6907  1e-5 0.3797 0.42 0.3394 1e-5 0.5 0.9 1.5 2.5 4.0 6.0  9.0 13.3502)
;;Modified for 56.48 MTU heat load AMR case
      ;;(dy 118.485 94.788 71.091 47.394 23.697 1e-5  35.545 106.64 213.27 )  ;;3D mountain-scale
      (dy 1.0)  ;;2D -1m  thich slice
      (dz
       1.00E-30       15.424  15.424  27.195  28.129  ;;      1-5     atm     tcw11   tcw11   tcw12
       tcw12
       28.129  5.490   4.690   0.530   7.050   ;;      6-10    tcw12   tcw13   ptn21   ptn22   ptn23
       4.580   14.090  9.690   6.170   23.425  ;;      11-15   ptn24   ptn25   ptn26   tsw31   tsw32
       23.425  28.047  29.306  29.306  10.148  ;;      16-20   tsw32   tsw33   tsw33   tsw33   tsw34
```

```
  13.195 6.597  3.040  3.000  2.400  ;;     21-25  tsw34  tsw34  tsw35  tsw35  tsw35
  2.000  1.000  1.000  0.500  0.300  ;;     26-30  tsw35  tsw35  tsw35  tsw35  tsw35
  0.200  1.00E-05      0.200  0.200  0.200  ;;     31-35  tsw35  tsw35  tsw35  tsw35
  tsw35
  0.200  1.00E-05      0.400  0.474  0.654  ;;     36-40  tsw35  tsw35  tsw35  tsw35
  tsw35
  0.619  0.647  0.786  0.514  1.00E-05      ;;     41-45  tsw35  tsw35  tsw35  tsw35
  tsw35
  0.60599 1.00E-05     0.800  1.000  1.500  ;;     46-50  tsw35  tsw35  tsw35  tsw35
  tsw35
  2.000  2.000  2.500  3.000  4.000  ;;     51-55  tsw35  tsw35  tsw35  tsw35  tsw35
  6.000  10.000 10.000 10.000 10.000 ;;     56-60  tsw35  tsw35  tsw35  tsw35  tsw35
  10.000 7.235  7.235  23.447 8.346  ;;     61-65  tsw35  tsw35  tsw35  tsw36  tsw36
  15.937 23.600 11.270 3.350  15.735 ;;     66-70  tsw37  tsw38  tsw39  ch1v   ch2z
  15.735 15.735 15.735 21.428 1.00E-30      ;;     71-75  ch3z   ch4z   ch5z   ch6
  wt
 )
 (mat
   (atm        atm   1  nx  1  ny   1   1)
   (tcw11     m-tcw11   1  nx  1  ny   2   3)
   (tcw12     m-tcw12   1  nx  1  ny   4   6)
   (tcw13     m-tcw13   1  nx  1  ny   7   7)
   (ptn21     m-ptn21   1  nx  1  ny   8   8)
   (ptn22     m-ptn22   1  nx  1  ny   9   9)
   (ptn23     m-ptn23   1  nx  1  ny  10  10)
   (ptn24     m-ptn24   1  nx  1  ny  11  11)
   (ptn25     m-ptn25   1  nx  1  ny  12  12)
   (ptn26     m-ptn26   1  nx  1  ny  13  13)
   (tsw31     m-tsw31   1  nx  1  ny  14  14)
   (tsw32     m-tsw32   1  nx  1  ny  15  16)
   (tsw33     m-tsw33   1  nx  1  ny  17  19)
   (tsw34     m-tsw34   1  nx  1  ny  20  22)
   (tsw35     m-tsw35   1  nx  1  ny  23  63)
   (tsw36     m-tsw36   1  nx  1  ny  64  65)
   (tsw37     m-tsw37   1  nx  1  ny  66  66)
   (tsw38     m-tsw38   1  nx  1  ny  67  67)
   (tsw39     m-tsw39   1  nx  1  ny  68  68)
   (ch1v      m-ch1v    1  nx  1  ny  69  69)
   (ch2z      m-ch2z    1  nx  1  ny  70  70)
   (ch3z      m-ch3z    1  nx  1  ny  71  71)
   (ch4z      m-ch4z    1  nx  1  ny  72  72)
   (ch5z      m-ch5z    1  nx  1  ny  73  73)
   (ch6       m-ch6     1  nx  1  ny  74  74)
   (wt     m-bf3   1  nx  1  ny  75  75)
        ;; artificial backfill
   (hstrk      m-tsw35   1  nx  1  ny  25    49)


   ;;only roof matrix surfaces are involved in condensation process, 7/27/04
  ;;comment out next three lines to apply condensate to the invert nodes
   (cond_h       m-tsw35     1   4  1  ny  31    31) ;;horizontal surface
   (cond_v       m-tsw35     4   4  1  ny  31    36) ;;vertical surface
   (cond_h       m-tsw35     4   6  1  ny  36    36) ;;horizontal surface

   ;;only invert matrix surfaces are involved in condensation process, 8/9/04
  ;;uncomment next three lines to apply condensate to the invert nodes
   ;;(cond_h       m-tsw35     1   3  1  ny  48    48) ;;horizontal surface
   ;;(cond_v       m-tsw35     4   4  1  ny  47    48) ;;vertical surface
   ;;(cond_h       m-tsw35     4   6  1  ny  46    46) ;;horizontal surface


   (dr1        m-dr      1   3  1  ny  32    47)
   (dr1        m-dr      3   7  1  ny  37    45)

   (adrift      NULL       1   2  1  ny  33    46)
   (adrift      NULL       3   6  1  ny  38    44)
)
  ) ;; end continuum
  (continuum  (name f)
     (flow-area-density ("*.f*" 1.0))
     (LenFirst  ("*.f*" 1.0))    ;; same as y-direction
```

```
                                  ;; half-width of matrix block
           (Len  ("*.f*" 1.0))        ;; same as y-direction
                                  ;; half-width of fracture
                                ;; LenFirst and Len values are doubled here since 50% of
cont-len-fac
                                ;; is used in rocktab file (Ken Lee)
           ;; 60 MTU/acre
          ;;(dx 0.570 0.35 0.3310 0.3597 0.3797 0.42 0.3394 0.5 0.9 1.5 2.5 4.0 6.0  9.0 13.3502)
       (dx 0.920  0.6907  1e-5 0.3797 0.42 0.3394 1e-5 0.5 0.9 1.5 2.5 4.0 6.0  9.0 13.3502)
;;Modified for 56.48 MTU heat load AMR case
      ;;(dy 118.485 94.788 71.091 47.394 23.697 1e-5  35.545 106.64 213.27 )  ;;3D mountain-scale
      (dy 1.0)  ;;2D -1m  thich slice
      (dz
       1.00E-30       15.424  15.424  27.195  28.129  ;;     1-5    atm    tcw11  tcw11  tcw12
       tcw12
       28.129  5.490   4.690   0.530   7.050   ;;     6-10   tcw12  tcw13  ptn21  ptn22  ptn23
       4.580   14.090  9.690   6.170   23.425  ;;     11-15  ptn24  ptn25  ptn26  tsw31  tsw32
       23.425  28.047  29.306  29.306  10.148  ;;     16-20  tsw32  tsw33  tsw33  tsw33  tsw34
       13.195  6.597   3.040   3.000   2.400   ;;     21-25  tsw34  tsw34  tsw35  tsw35  tsw35
       2.000   1.000   1.000   0.500   0.300   ;;     26-30  tsw35  tsw35  tsw35  tsw35  tsw35
       0.200   1.00E-05        0.200   0.200   0.200   ;;     31-35  tsw35  tsw35  tsw35  tsw35
       tsw35
       0.200   1.00E-05        0.400   0.474   0.654   ;;     36-40  tsw35  tsw35  tsw35  tsw35
       tsw35
       0.619   0.647   0.786   0.514   1.00E-05        ;;     41-45  tsw35  tsw35  tsw35  tsw35
       tsw35
       0.60599 1.00E-05        0.800   1.000   1.500   ;;     46-50  tsw35  tsw35  tsw35  tsw35
       tsw35
       2.000   2.000   2.500   3.000   4.000   ;;     51-55  tsw35  tsw35  tsw35  tsw35  tsw35
       6.000   10.000  10.000  10.000  10.000  ;;     56-60  tsw35  tsw35  tsw35  tsw35  tsw35
       10.000  7.235   7.235   23.447  8.346   ;;     61-65  tsw35  tsw35  tsw35  tsw36  tsw36
       15.937  23.600  11.270  3.350   15.735  ;;     66-70  tsw37  tsw38  tsw39  ch1v   ch2z
       15.735  15.735  15.735  21.428  1.00E-30        ;;     71-75  ch3z   ch4z   ch5z   ch6
       wt
      )
      (mat
         (atm        atm   1  nx  1  ny   1   1)
         (tcw11     f-tcw11   1  nx  1  ny   2   3)
         (tcw12     f-tcw12   1  nx  1  ny   4   6)
         (tcw13     f-tcw13   1  nx  1  ny   7   7)
         (ptn21     f-ptn21   1  nx  1  ny   8   8)
         (ptn22     f-ptn22   1  nx  1  ny   9   9)
         (ptn23     f-ptn23   1  nx  1  ny  10  10)
         (ptn24     f-ptn24   1  nx  1  ny  11  11)
         (ptn25     f-ptn25   1  nx  1  ny  12  12)
         (ptn26     f-ptn26   1  nx  1  ny  13  13)
         (tsw31     f-tsw31   1  nx  1  ny  14  14)
         (tsw32     f-tsw32   1  nx  1  ny  15  16)
         (tsw33     f-tsw33   1  nx  1  ny  17  19)
         (tsw34     f-tsw34   1  nx  1  ny  20  22)
         (tsw35     f-tsw35   1  nx  1  ny  23  63)
         (tsw36     f-tsw36   1  nx  1  ny  64  65)
         (tsw37     f-tsw37   1  nx  1  ny  66  66)
         (tsw38     f-tsw38   1  nx  1  ny  67  67)
         (tsw39     f-tsw39   1  nx  1  ny  68  68)
         (ch1v      f-ch1v    1  nx  1  ny  69  69)
         (ch2z      f-ch2z    1  nx  1  ny  70  70)
         (ch3z      f-ch3z    1  nx  1  ny  71  71)
         (ch4z      f-ch4z    1  nx  1  ny  72  72)
         (ch5z      f-ch5z    1  nx  1  ny  73  73)
         (ch6       f-ch6     1  nx  1  ny  74  74)
         (wt     f-bf3   1  nx  1  ny  75  75)
          ;; artificial backfill
         (hstrk      f-tsw35   1  nx  1  ny  25  49)

         (dr1        f-dr      1   3  1  ny  32    47)
         (dr1        f-dr      3   7  1  ny  37    45)
         (adrift      NULL       1   2  1  ny  33    46)
         (adrift      NULL       3   6  1  ny  38    44)
     )
```

```
      ) ;; end continuum
    ) ;; end multi-continua
  ) ;; end genmsh

;; ************************Down stream
weighting****************************************************
    (downstream-mob
         (liquid
             (crange ("ptn*.m#*" "tsw*.m#*") ("ch*v.m#*" "ch*z.m#*"))
         ) ;; end liquid
    ) ;; end downstream-mob


;; ************************ Solver options
***********************************************************
(include "run_control_param_LDTH-v01")

);; end of model input

;; ******************** Done !*************************************************************
```

Balanced condensate density ( kg/s-m$^2$)

File: **condensate.tab**

```
  0.0000000e+000  0.0000000e+000
  5.2701192e+006  0.0000000e+000
  1.5778800e+007  0.0000000e+000
  3.1557600e+007  0.0000000e+000
  6.3115200e+007  0.0000000e+000
  1.5778800e+008  0.0000000e+000
  3.1557600e+008  0.0000000e+000
  4.7336400e+008  0.0000000e+000
  6.3115200e+008  0.0000000e+000
  7.8894000e+008  0.0000000e+000
  9.4672800e+008  0.0000000e+000
  1.1045160e+009  0.0000000e+000
  1.2623040e+009  0.0000000e+000
  1.4200920e+009  0.0000000e+000
  1.5778800e+009  0.0000000e+000
  1.8934560e+009  0.0000000e+000
  2.3668200e+009  0.0000000e+000
  3.1557600e+009  0.0000000e+000
  4.7336400e+009  0.0000000e+000
  6.3115200e+009  0.0000000e+000
  9.4672800e+009  1.5920170e-006
  1.5778800e+010  1.3763836e-006
  2.3668200e+010  1.1391246e-007
  3.1557600e+010  6.4195478e-007
  4.7336400e+010  1.0702196e-006
  6.3115200e+010  1.3296972e-006
  9.4672800e+010  2.2195752e-006
  1.5778800e+011  2.2585486e-006
  2.3668200e+011  2.2637565e-006
  3.1557600e+011  2.2269588e-006
  3.9447000e+011  2.1965556e-006
```

Reduced condensate density ( kg/s-m$^2$)

File: **condensate.tab**

```
  0.0000000e+000  0.0000000e+000
  5.2701192e+006  0.0000000e+000
  1.5778800e+007  0.0000000e+000
  3.1557600e+007  0.0000000e+000
  6.3115200e+007  0.0000000e+000
  1.5778800e+008  0.0000000e+000
  3.1557600e+008  0.0000000e+000
  4.7336400e+008  0.0000000e+000
  6.3115200e+008  0.0000000e+000
  7.8894000e+008  0.0000000e+000
  9.4672800e+008  0.0000000e+000
  1.1045160e+009  0.0000000e+000
```

```
  1.2623040e+009  0.0000000e+000
  1.4200920e+009  0.0000000e+000
  1.5778800e+009  0.0000000e+000
  1.8934560e+009  0.0000000e+000
  2.3668200e+009  0.0000000e+000
  3.1557600e+009  0.0000000e+000
  4.7336400e+009  0.0000000e+000
  6.3115200e+009  0.0000000e+000
  9.4672800e+009  6.5177289e-007
  1.5778800e+010  5.6349245e-007
  2.3668200e+010  4.6635842e-008
  3.1557600e+010  2.6281675e-007
  4.7336400e+010  4.3814867e-007
  6.3115200e+010  5.4437899e-007
  9.4672800e+010  9.0869569e-007
  1.5778800e+011  9.2465141e-007
  2.3668200e+011  9.2678353e-007
  3.1557600e+011  9.1171853e-007
  3.9447000e+011  8.9927145e-007
```

Zero condensate density ( $kg/s\text{-}m^2$)

File: **condensate.tab**

```
  0.0000000e+000  0.0000000e+000
  5.2701192e+006  0.0000000e+000
  1.5778800e+007  0.0000000e+000
  3.1557600e+007  0.0000000e+000
  6.3115200e+007  0.0000000e+000
  1.5778800e+008  0.0000000e+000
  3.1557600e+008  0.0000000e+000
  4.7336400e+008  0.0000000e+000
  6.3115200e+008  0.0000000e+000
  7.8894000e+008  0.0000000e+000
  9.4672800e+008  0.0000000e+000
  1.1045160e+009  0.0000000e+000
  1.2623040e+009  0.0000000e+000
  1.4200920e+009  0.0000000e+000
  1.5778800e+009  0.0000000e+000
  1.8934560e+009  0.0000000e+000
  2.3668200e+009  0.0000000e+000
  3.1557600e+009  0.0000000e+000
  4.7336400e+009  0.0000000e+000
  6.3115200e+009  0.0000000e+000
  9.4672800e+009  0.0000000e+000
  1.5778800e+010  0.0000000e+000
  2.3668200e+010  0.0000000e+000
  3.1557600e+010  0.0000000e+000
  4.7336400e+010  0.0000000e+000
  6.3115200e+010  0.0000000e+000
  9.4672800e+010  0.0000000e+000
  1.5778800e+011  0.0000000e+000
  2.3668200e+011  0.0000000e+000
  3.1557600e+011  0.0000000e+000
  3.9447000e+011  0.0000000e+000
```

## Piecewise-linear drift wall boundary condition from Year 0 to 12500

File: **fun_in.dat**

```
30  99
1  30
1

0.0 1.670e-01 5.000e-01 1.000e+00 2.000e+00 5.000e+00 1.000e+01 1.500e+01 2.000e+01 2.500e+01
3.000e+01 3.500e+01 4.000e+01 4.500e+01 5.000e+001  6.000e+001  7.500e+001  1.000e+002
1.500e+002  2.000e+002  3.000e+002  5.000e+002  7.500e+002  1.000e+003  1.500e+003  2.000e+003
3.000e+003  5.000e+003  7.500e+003  1.000e+004  1.250e+004

8.7801428e+04   8.7801428e+04   8.7779091e+04   8.7771390e+04   8.7767735e+04   8.7766831e+04
8.7771411e+04   8.7779113e+04   8.7787110e+04   8.7794487e+04   8.7801251e+04   8.7807386e+04
```

```
8.7812955e+04   8.7818034e+04   8.7822649e+04   8.7583711e+04   8.7587325e+04   8.7593217e+04
8.7604520e+04   8.7615208e+04   8.7634863e+04   8.7668084e+04   8.7700273e+04   8.7724565e+04
8.7757435e+04   8.7778077e+04   8.7801530e+04   8.7831360e+04   8.7851721e+04   8.7863578e+04
8.7871124e+04

 2.4000000e+001
 6.5860988e+001
 8.1109301e+001
 8.6954349e+001
 8.9975213e+001
 9.1186051e+001
 8.8672644e+001
 8.4105225e+001
 7.9378847e+001
 7.5077541e+001
 7.1205199e+001
 6.7750144e+001
 6.4667659e+001
 6.1895225e+001
 5.9404462e+001
 1.2204530e+002
 1.3248430e+002
 1.2844940e+002
 1.1864690e+002
 1.0581670e+002
 9.5374150e+001
 8.8202940e+001
 7.9411040e+001
 7.4492160e+001
 7.1032620e+001
 6.6706260e+001
 6.0661580e+001
 5.2629820e+001
 4.5783580e+001
 4.1948210e+001
 3.9038360e+001

 5.0000000e+03
 8.2231146e+02
 1.0153017e+03
 1.0368457e+03
 1.0257739e+03
 1.0018819e+03
 9.7418946e+02
 9.6323885e+02
 9.5663141e+02
 9.5422089e+02
 9.5268058e+02
 9.5246821e+02
 9.4871438e+02
 9.4729385e+02
 9.4797344e+02
 8.8743600e+004
 8.9059850e+004
 8.9060000e+004
 8.9060000e+004
 8.9060000e+004
 8.5930990e+004
 6.5673340e+004
 4.6386710e+004
 3.7815300e+004
 3.2624760e+004
 2.7034210e+004
 2.0564440e+004
 1.3923620e+004
 9.9905250e+003
 8.1893270e+003
 7.0136640e+003
```